WADC TECHNICAL REPORT 55-29
PART IV

HYDRAULIC SERVO CONTROL VALVES
Part IV

RESEARCH ON SERVO VALVES AND SERVO SYSTEMS

BERNARD A. JOHNSON
LESLIE R. AXELROD
PHILLIP A. WEISS

COOK RESEARCH LABORATORIES

AUGUST 1957

WRIGHT AIR DEVELOPMENT CENTER
AIR RESEARCH AND DEVELOPMENT COMMAND
UNITED STATES AIR FORCE
WRIGHT-PATTERSON AIR FORCE BASE, OHIO

FOREWORD

This report, Research on Servo Valves and Servo Systems, was prepared by L. Axelrod, A. D'Andrea, B. Johnson and P. Weiss under the supervision of T. J. Dunsheath, Technical Director of the Automatic Control Systems Section, Cook Research Laboratories, Morton Grove, Illinois, under Air Force Contract No. AF 33(616)-3341, "Hydrau.ic Servo Control Valves". This is the fourth in a series of reports dealing with electrohydraulic servo valves, and the second under the afore-mentioned contract. The first three were titled:

Part I: "A Summary of the Present State of the Art of Electrohydraulic Servo Valves," April 1955

Part II: "An Investigation of a Number of Representative Electrohydraulic Servo Valves," August 1956

Part III: "State of the Art Summary of Electrohydraulic Servo Valves and Applications," December 1956.

This report deals with several studies pertaining to the application of servo valves to aircraft control systems. The work was administered under the direction of the Aeronautical Research Laboratory, WADC, with Mr. R. W. Rautio as supervising Task Scientist. This document is unclassified.
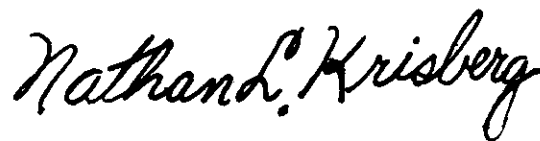
WADC TR 55-29 Pt IV

ABSTRACT

This report deals with the following four investigations:

(1)　　Experimental verification of linearized analysis as applied to electrohydraulic servo valves

(2)　　Investigation of the gain compensation of servo valves

(3)　　Analog study of a typical missile system

(4)　　Test of three new electrohydraulic servo valves.

PUBLICATION REVIEW

This report has been reviewed and is approved.

FOR THE COMMANDER:

NATHAN L. KRISBERG
Colonel, USAF
Chief, Aeronautical Research
　Laboratory
Directorate of Laboratories

TABLE OF CONTENTS

TABLE OF CONTENTS (cont'd)

LIST OF ILLUSTRATIONS

LIST OF ILLUSTRATIONS (cont'd)

LIST OF ILLUSTRATIONS (cont'd)

LIST OF ILLUSTRATIONS (cont'd)

LIST OF ILLUSTRATIONS (cont'd)

LIST OF ILLUSTRATIONS (cont'd)

LIST OF ILLUSTRATIONS (cont'd)

LIST OF ILLUSTRATIONS (cont'd)

LIST OF TABLES

CHAPTER I

INTRODUCTION

A.   Purpose

The work covered in this report was divided into four major tasks. These are as follows:

(1)   Experimental Verification of Linearized Analysis as Applied to Electrohydraulic Servo Valves

(2)   Investigation of Gain Compensation

(3)   Analog Study of a Typical Missile Control System

(4)   Test of Four New Electrohydraulic Servo Valves.

A fifth task, which was completed under this program, involved the formulation of a set of preliminary specifications for the application of electrohydraulic servo valves for missiles. These specifications have been submitted to the Air Force as a separate item and are not included in this report.

The purpose of Task 1 was to investigate experimentally the validity of the linear analysis scheme developed during the previous contract. In this technique, the dynamics of the valve are divided into two parts for analytical purposes, the valve dynamics and the load dynamics. The valve dynamics can be measured experimentally by means of no-load frequency response tests and such data are generally provided by the valve

----

manufacturers. The load dynamics can be theoretically calculated from data available from the static pressure flow curves of the valve and the known load characteristics such as magnitudes of inertia, viscous damping, oil under compression, etc. The specific object of this study was to determine whether the load dynamics as calculated from the above data correspond to the load dynamics as measured experimentally by testing the valve under load, and the degree of accuracy that can be expected.

The object of Task 2 was to determine whether gain compensation of electrohydraulic servo valves is desirable from an over-all standpoint. It had previously been found that gain compensation tended to reduce the no-load response of the valve to some extent and caused the valve to be more susceptible to null shifts. The intended purpose of gain compensation is to maintain the system gain constant over a large range of load pressures, thus permitting the maintenance of system response over a large range of load conditions. In this phase, an electrohydraulic servo system utilizing a gain compensated valve was compared experimentally with a system employing an uncompensated valve under various load conditions to determine the relative merits of gain compensation.

The purpose of Task 3 was to determine whether an electrohydraulic control system could be conveniently simulated on an analog computer and to determine to what extent analog testing could be used to supplant breadboard investigations. The study was performed utilizing the characteristics of a typical high response missile flight control system.

The purpose of Task 4 was to test and evaluate the capabilities of three of the most promising servo valves placed on the market during the last year and a half. The valves selected for test were: Moog 2074, Bendix Pacific HR-9, and Weston Mod 15690-1. In addition, data are presented on the Modified Bell SV-6C valve, which was tested during the last week of the previous contract.

B.   Organization of the Report

Each of the various tasks is included as a separate integral section in this report. Numerous references are made to the three previous reports under this study to minimize duplication. However, for sake of completeness, a few graphs and illustrations which were contained in the previous reports are also included in this report.

Chapter II covers the linearized analysis study while Chapter III takes up the gain compensation investigation. Chapter IV presents the

results of the analog study phase and Chapter V presents an analysis and summary of the test results of the valves tested during the valve test phase. The actual graphs of the experimental data are contained in Appendices I and II.

CHAPTER II

LINEARIZED ANALYSIS

A. Introduction

Because of the rapid growth and development of electrohydraulic servo valves, generalized design data have not been readily available. Many of the valve manufacturers have used different means to describe the performance of their valves, especially from a dynamic standpoint. As a result, control system designers have lacked a method for systematically selecting the proper valve for a given design installation. Quite often, the designer has purchased several valves which appear to meet his static and dynamic requirements and has selected the one which performs best in the actual or simulated system.

The static data available to the designer are flow gain, pressure-flow characteristic curves, hysteresis, quiescent flow, etc.; the dynamic data include the no-load frequency response and phase shift. If it were possible to predict the dynamic contributions of the valve-load combination, enough information would be available to permit direct synthesis of the system without recourse to costly, time-consuming, trial-and-error experimentation.

One of the objects of this study was to develop a method of analysis which is based completely on data that can be obtained in experimental tests of flow control valves and a knowledge of the load and dynamics of the rest of the system.

B. Previous Work

As discussed in greater detail in WADC TR 55-29, Part II, the dynamic contribution of the valve-load combination ("load dynamics") can be expressed as a transfer function relating actuator output to second stage spool displacement. This transfer function was derived under the assumption that the pressure-flow curves could be considered straight

lines over the region of operation. Such an assumption is similar to that made for the small signal analysis of Class A vacuum tube amplifiers, where the static characteristic curves are considered to be parallel, equidistant, straight lines.

As derived therein, the transfer function for an oil-spring-mass system is:

$$\frac{\theta_o}{\theta_i} = \frac{K_1 A / K_3 M}{S^3 + (K_2 / K_3 + B / M)s^2 + \dfrac{(K_2 B + A^2 + K K_3)s}{K_3 M} + \dfrac{K_2 K}{K_3 M}} \qquad (1)*$$

where:

θ_o = actuator displacement (in.)

θ_i = spool displacement (in.)

K_1 = valve gain, $\partial Q / \partial \theta_i / P_L$ = Constant (in^3/ma-sec)

A = area of actuator (in^2)

K_3 = compressibility constant = $K_3' + K_3''$

K_3' = oil compressibility constant = $\dfrac{V_o}{2\beta_o}$ (in^5/lb)

**K_3'' = tubing compressibility constant = $\dfrac{V_t}{2\beta_t}$ (in^5/lb)

---

*In a gain-compensated valve, this relationship relates output position to input differential current because the static relationship between spool position and differential current is not constant, but dependent on flow forces.

**Although this term is customarily neglected, it may contribute as much as 10 per cent to the value of K_3.

V_o = volume of oil on one side of actuator (in^3)

β_o = bulk modulus of oil (lb/in^2)

V_t = volume of tubing on one side of actuator (in^3)

β_t = bulk modulus of tubing (lb/in^2)

K_2 = valve damping coefficient = $C_1 + C_2$ ($in^5/lb\text{-}sec$)

C_1 = slope of valve curves = $\partial Q/\partial P$ ($in^5/lb\text{-}sec$)

C_2 = actuator leakage coefficient ($in^5/lb\text{-}sec$)

B = viscous friction coefficient (lb-sec/in)

K = spring constant (lb/in)

s = Laplacian operator

To simplify the analysis, only an oil-mass load was considered. For this system,

$$\frac{s\theta_o}{\theta_i} = \frac{K_1 A/K_3 M}{s^2 + (K_2/K_3 + B/M)s + \dfrac{(K_2 B + A^2)}{K_3 M}} \tag{2}$$

The denominator of Equation (2) can be compared with the characteristic equation of a second order system:

$$s^2 + 2\zeta\omega_n s + \omega_n^2 = s^2 + \left(\frac{K_2}{K_3} + \frac{B}{M}\right)s + \frac{K_2 B + A^2}{K_3 M} \tag{3}$$

Therefore,

$$2\zeta\omega_n = \frac{K_2}{K_3} + \frac{B}{M} \tag{4}$$

$$\omega_n^2 = \frac{K_2 B + A^2}{K_3 M} \tag{5}$$

Equations (4) and (5) indicate that it should be possible to predict the damping ratio and undamped natural angular velocity (ζ and ω_n) of an oil-mass system by knowing the system parameters (A, B, M and V) and the static characteristics of the valve. The most important static characteristics are K_2, the valve damping, and K_3, the oil compressibility.

Statically, K_2 is the sum of the slope of the pressure-flow curves and the actuator leakage. Dynamically, however, K_2 will vary instantaneously as the point of operation varies with time. By comparing the value of K_2 obtained from dynamic measurements with that obtained statically, it should be possible to find a means of picking one representative value of K_2 from the static curves which will yield the most satisfactory results over the entire range of operation.

A major part of the dynamic test program was devoted to the experimental determination of ζ and ω_n. From a knowledge of those constants, K_2 was calculated and compared with static values.

In the earlier study, it was assumed that B = O. With this assumption, Equations (4) and (5) were solved:

$$K_3 = A^2/M \, \omega_n^2 \tag{6}$$

$$K_2 = \frac{2 \zeta A^2}{M\omega_n} \tag{7}$$

As reported in Part II, very good agreement existed between the dynamic K_3 calculated from Equation (6) and the static K_3 calculated from the equation, $K_3 = V/2\beta$.

However, the dynamic K_2 calculated from Equation (7) was considerably higher than the static K_2 calculated from the slope of the pressure-flow curves, $\dfrac{\partial Q}{\partial P}$.

It was concluded that the nonrigidity of the test stand was partially responsible for the additional damping: forces developed during the load tests were so great that the I-beam supports (two concrete pillars) vibrated with large amplitude and energy was dissipated in the floor.

A more rigid, dynamic test stand was designed as a means of reducing the damping contributed by the I-beam-pillar-floor system. A

description of the new test stand is contained in the next section.

Another limitation of the old test setup was the lack of equipment for measuring load pressure under dynamic conditions. Such information would have been useful in determining the exact extent of the damping forces; it would also have provided valuable data on the range of operating load pressures for any particular valve-load combination.

It was decided to use a larger actuator for the load tests. A larger actuator would also have a longer stroke, permitting measurements to be made at frequencies lower than those previously used.

C.   Experimental Setup

The new dynamic test stand consists of a 60 cubic foot block of re-inforced concrete standing 5 feet high and sunk approximately 2.5 feet into the floor (see Fig. 1). This 8500 pound block has a 400 pound
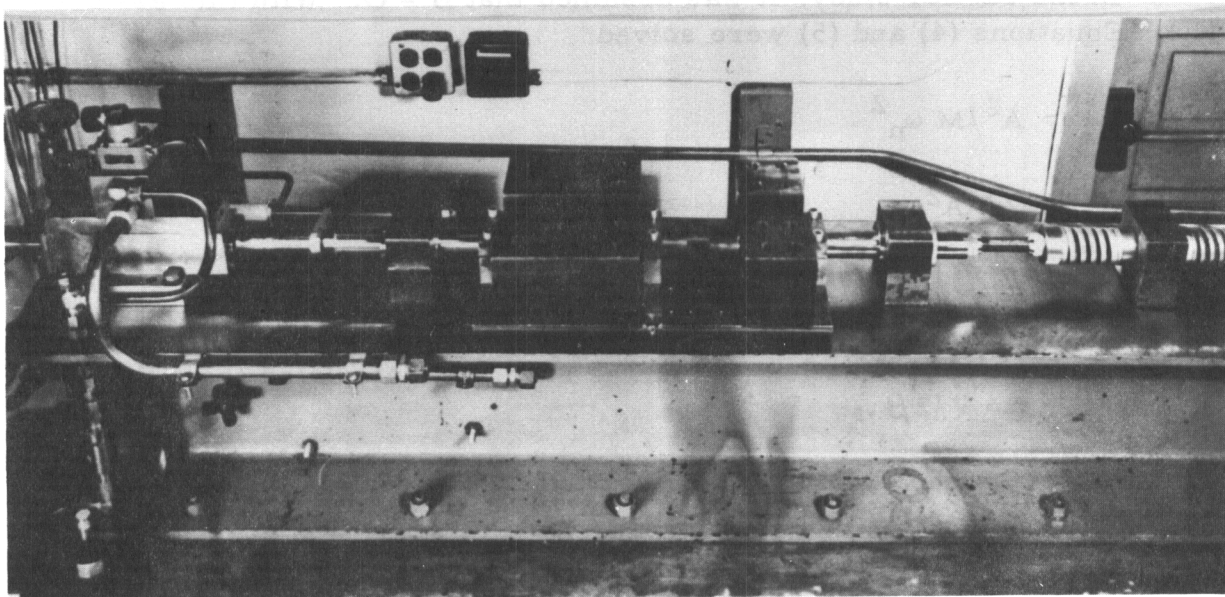
Figure 1. View of New Dynamic Test Stand

10 x 10 steel I-beam embedded in it, with only its top flange exposed. Bolted to the top flange of the embedded I-beam is a 600 pound 12 x 12 steel I-beam. The upper flange of this beam is used as the dynamic test

bed, supporting both the load and the no-load actuators.

The load actuator (see Fig. 2) has a 4 inch stroke and a 0.96 in^2
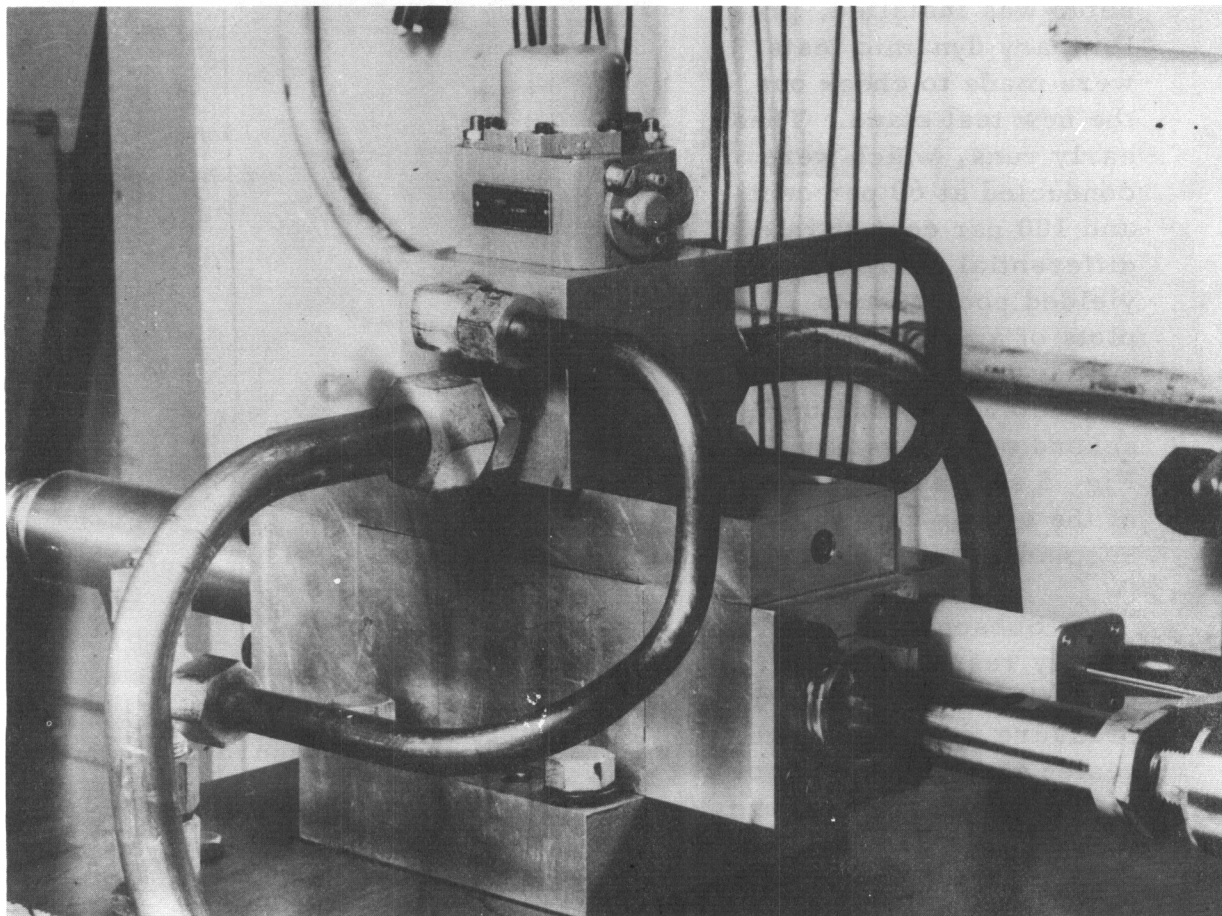
Figure 2. View of New Load Actuator

piston area. Mounted inside the actuator output shaft is a Sanborn 7V4 linear velocity pickoff. Externally mounted is a 4 inch Giannini linear potentiometer used as a positional pickoff. Matched Dynisco pressure transducers rated at 3000 psi are mounted at the actuator load ports (see Fig. 3). A schematic of the pressure transducer circuitry appears in Fig. 4.

D.   Experimental Procedures

1.   Preliminary

After the new test setup was installed, preliminary dynamic tests were made to check out the new test stand. These early runs, which were conducted at 60 per cent and 100 per cent of rated differential current, yielded poor results. The plots of amplitude vs. frequency did not exhibit the characteristic rise of a second order system. As Fig. 5 shows, the peak of the 60 per cent curve seemed to be clipped off.

Subsequent frequency response tests using the newly installed pressure transducers revealed that, for values of

Figure 3.   View of Pressure Transducers

differential current above 20 per cent rated, the load pressure reached approximately 3000 psi well before the resonant frequency and remained at 3000 psi until well after the resonant frequency, exhibiting what will hereafter be termed as pressure saturation.

In order to avoid the nonlinear effects of pressure saturation occurring at the higher input currents, all load tests except one were run at 20 per cent of rated differential current.

The one exception was tests involving the Moog 1402C which exhibited a small amount of pressure saturation at 20 per cent. Figure 6 shows a plot of the load pressure vs. frequency for two input amplitudes of differential current for the Moog 1402C showing that the latter is still pressure saturating at 20 per cent. The tests on the 1402C were conducted at both 20 per cent and 60 per cent rated current.

Figure 4. Schematic of Pressure Transducer Circuitry

DYNAMIC RESPONSE

MOOG 1402 C

60% RATED ΔI

$M = 140.3^{\#}$

$V = 6.68 \text{ IN}^3$
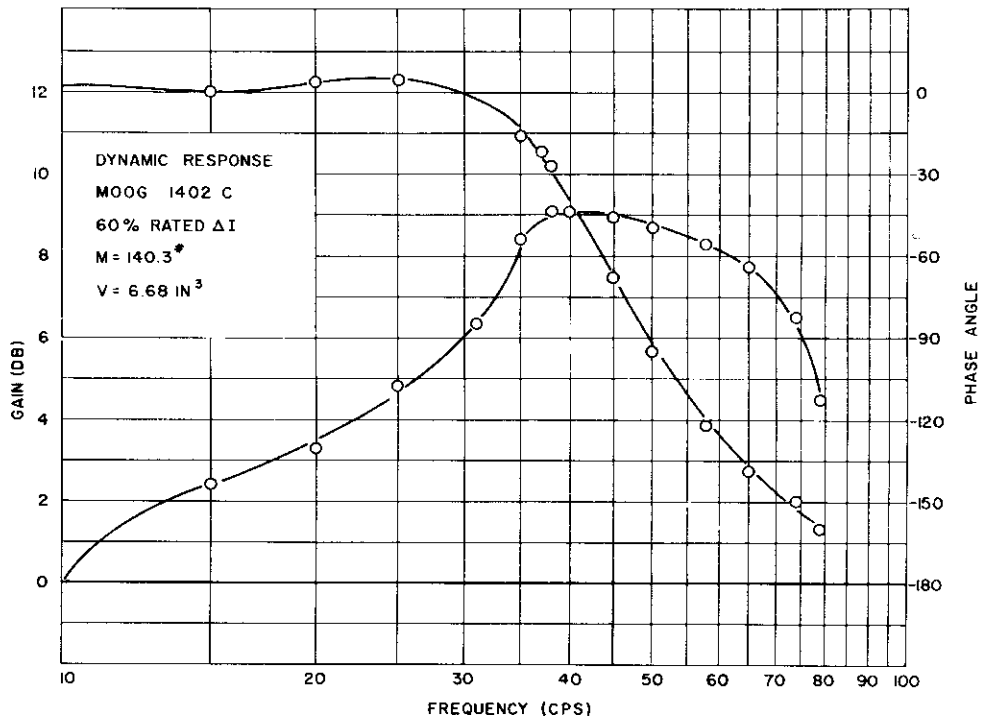
Figure 5. Frequency Response of Moog 1402C Valve - 60 Per Cent Rated Differential Current

LOAD PRESSURE RATIO VS FREQUENCY

MOOG 1402 C

SUPPLY PRESSURE 3000 PSI

RATED DIFF CURRENT 8 MA

WEIGHT = 139.3 LB.

$\text{VOLUME} = 7.15 \text{ IN}^3$

—Δ— 20% RATED DIFF. CURRENT
---O--- 60% RATED DIFF. CURRENT
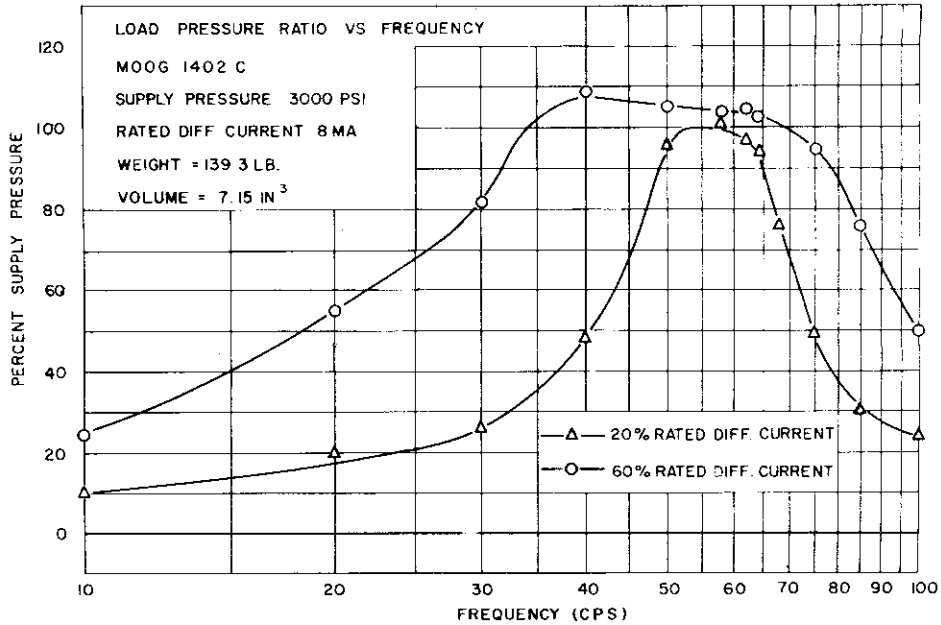
Figure 6. Load Pressure vs. Frequency for Moog 1402C Valve - 20 Per Cent and 60 Per Cent Rated Differential Current

It is desirable to maintain the input amplitude as high as possible (below pressure saturation) to permit operation out of the leakage range of the valve, where the gain is low, and out of the low pressure sensitivity range, where coulomb friction effects become serious.

Other preliminary tests were conducted to determine various load characteristics such as leakage, viscous friction, etc., which could not be determined analytically.

The effective viscous damping coefficient (B) was determined by applying a low frequency sinusoidal input signal to a servo valve-driven actuator, operating unloaded, and measuring the output velocity of the actuator and the differential pressure developed across it. Since the actuator mass (M) is small, the acceleration forces at low frequencies will be small compared with those developed by actuator friction, both viscous and coulomb.

Thus,

$$F = A \, P_{LB} = B \, \dot{\theta} + F_c \tag{8}$$

where A is the actuator area, P_{LB} is the differential pressure on the actuator, $\dot{\theta}$ is the actuator velocity, and F is the applied force on the actuator. The value of A is known; P_L and $\dot{\theta}$ can be measured during the run. B can therefore be computed as follows:

$$B = \frac{A \, P_{LB} - F_c}{\dot{\theta}} \tag{9}$$

The stiction (static friction), F_s, was determined by measuring the pressure necessary to just start the actuator moving in one direction and multiplying this pressure by the actuator area. Thus

$$F_s = A \, P_{L\,s} \tag{10}$$

Figure 7 shows qualitatively how stiction is related to coulomb friction as a function of velocity. It can be seen that at all but the very low frequencies, only coulomb friction (and, of course, viscous damping) will be present.

Experience has shown that coulomb friction is approximately one-fourth the value of stiction. In this case, the measured value of the coulomb friction force, Fc, was sufficiently smaller than the total measured force, P_{LB} A, to justify the latter being considered as pure viscous damping for analytical purposes.
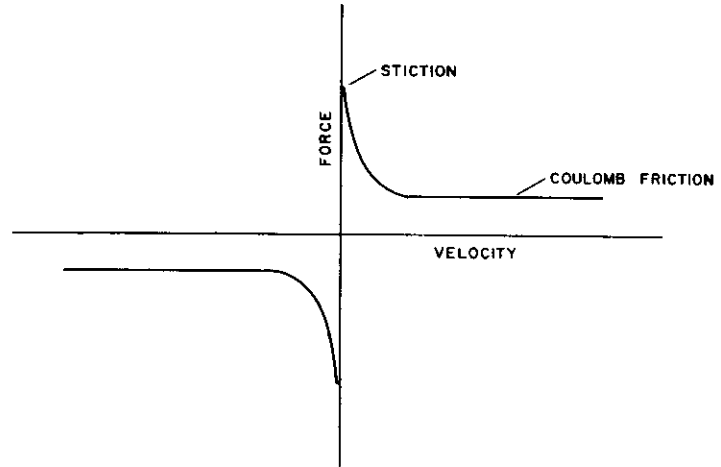
Figure 7. Stiction and Coulomb Friction vs. Velocity

The actuator leakage coefficient, C_2, was determined experimentally by measuring the leakage flow across the actuator piston at various load pressures over the range of 0 to 3000 psi. These flows were divided by the corresponding load pressures. Thus

$$C_2 = Q/ P_L \qquad\qquad (11)$$

A plot of C_2 vs. load pressure was made for the entire pressure range.

Because the density, bulk modulus, and viscosity of the oil are sensitive to temperature changes, it is possible that the natural frequency and damping may also be highly temperature sensitive. To verify this experimentally, the resonant frequency of the oil-mass combination and the velocity amplitude and phase shift at resonance of a particular load combination were measured over the range of temperatures encountered during the frequency response tests, namely 100°F to 150°F.

2.   Dynamic Tests

The actual dynamic tests consisted of frequency response runs in which the maximum input amplitude was held constant and the maximum amplitude and phase of the output velocity were recorded over a frequency range of 10 to 100 cps. The resultant frequency response data contain the combined effect of the no-load characteristics of the valve termed valve dynamics and the valve-load

characteristics termed load dynamics. The load dynamics can be obtained by subtracting the no-load characteristics from the above test results. The resulting data can then be plotted in the form of Bode plots in which the amplitude ratio is plotted in decibels and phase shift in degrees, both as functions of frequency.

The system constants ζ, and ω_n are extracted from the experimental results in the following manner. The Bode plot of the load dynamics is compared with a normalized plot of the frequency response of a second order system (see Fig. 8). The value of ζ is
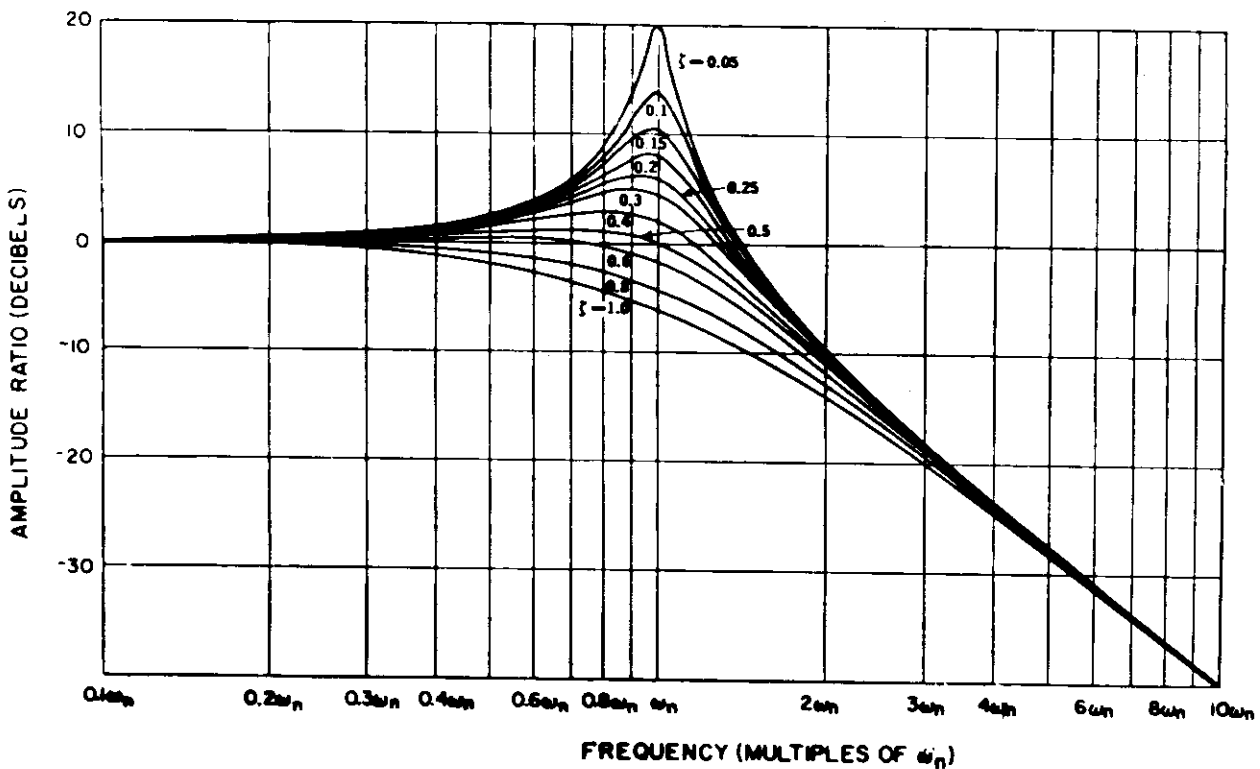
Figure 8. Frequency Response of Second-Order System

obtained by matching the experimental curve with the theoretical second order curve with the same peak amplitude. ω_n is calculated by using the following equation.

$$\omega_n = 2\pi f_n = 2\pi f_r \big/ (1 - 2\zeta^2)^{1/2} \tag{12}$$

where f_r is the resonant frequency obtained from the experimental curves.

As described previously, values for ω_n and ζ can also be obtained by utilizing Equations (4) and (5). It was the purpose of this investigation to compare the results obtained by using these two methods and to determine what points on the static pressure-flow curves should be used for determining K_2.

The tests were conducted utilizing four valves: the Moog 1402X and 1402C and the Cadillac Gage FC-2 and PC-2 valves. Four different mass loads providing two oil-mass natural frequencies were employed with each valve. Thus, one oil-mass natural frequency was obtained by utilizing two combinations of load mass and oil volume, one a large mass and a small oil volume, the other a small mass and a large oil volume. These combinations were employed to assist in pinpointing the cause of discrepancies between theory and practice, if any.

E.   Test Results

1.   Preliminary Tests

a.   Viscous Damping

Two independent runs at different values of differential current were made to determine the viscous damping (B). Each run yielded B = 10 lb/sec in. Since the maximum velocity at 20 per cent rated differential current is about 10 in/sec, the maximum force exerted by viscous damping is about 100 pounds.

b.   Coulomb Friction

The value of stiction was found to be approximately 50 pounds. The value of coulomb friction is about 12.5 pounds. At 20 per cent rated differential current, this is sufficiently less than the viscous damping to be neglected except as it influenced the viscous friction measurements.

c.   Actuator Leakage Coefficient

Figure 9 is a plot of the actuator leakage and the actuator leakage coefficient as functions of load pressure. For all
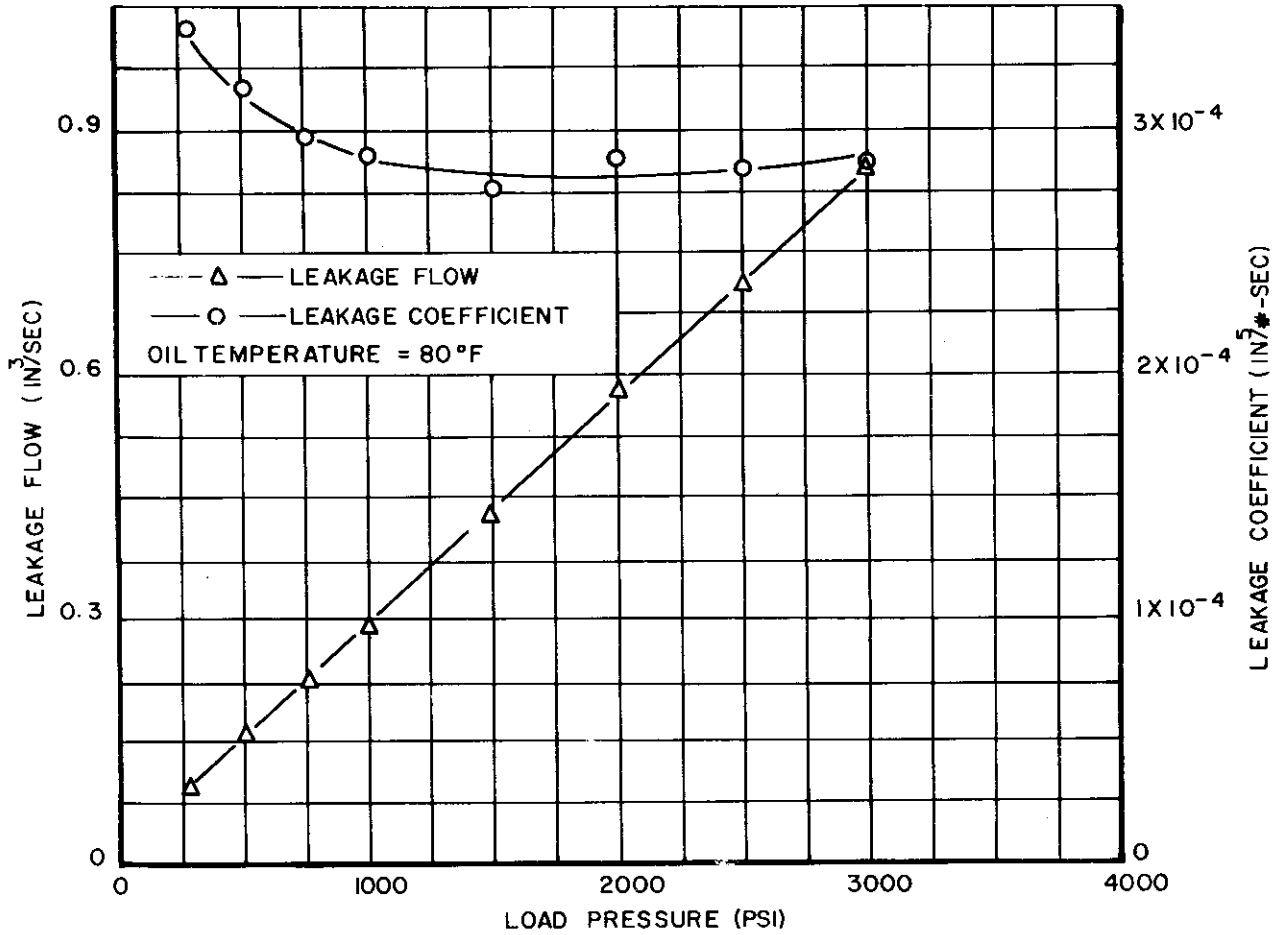
Figure 9. Actuator Leakage and Leakage Coefficient vs. Load Pressure

practical purposes, $C_2 = 2.8 \times 10^{-4}$ in^5/lb-sec over most of the entire range of operation.

d.   Effect of Temperature on Resonance

Figure 10 is a plot of the resonant frequency and the velocity amplitude as functions of inlet oil temperature. As the plot shows, there is a very slight consistent decrease in the velocity amplitude with increasing temperature. The resonant frequency varied by approximately 4 per cent over the temperature range. Theoretically it should vary by approximately 7 per cent. The effect of temperature on phase shift was inconclusive. Phase near resonance was difficult to measure because of its rapid falloff and because of poor waveform.

2. Dynamic Test
Results

The dynamic
test results are pre-
sented in graphical
form in Appendix I.
It will be noticed that
both amplitude and
phase of the load dy-
namics have been
plotted. Values for
ζ can also be obtained
by comparing the res-
onant frequency with
the frequency at 90
degrees which should
occur at the natural
frequency (ω_n) and

Figure 10. Resonant Frequency and
Velocity Amplitude Ratio
vs. Oil Temperature

utilizing Equation (12). However, this technique did not provide as
consistently accurate results as that described previously on page 16.

The damping ratios and natural and resonant frequencies have
been determined from the amplitude curves and are presented in
Tables 1 and 2. In addition, the values for ζ and ω_n as computed
from the static valve characteristics and known load data are pre-
sented. Values for ζ are listed for two values of K_2, one taken at
zero load pressure and one taken at 1000 psi load pressure.

Legend:

$\zeta 1$ Obtained from comparison of load dynamics curve
with the normalized second order curve, Fig. 8

$\zeta 2$ Calculated from Equation (4) with K_2 obtained by
measuring the slope of the pressure-flow curves
at P = O

$\zeta 3$ Calculated from Equation (4) with K_2 obtained by
measuring the slope of the pressure-flow curves
at P = 1000 psi

ω_{n1} Calculated from Equation (12)

ω_{n2} Calculated from Equation (14)

ω_r Measured resonant frequency.

F.   Discussion of Results

1.   Flow Control Valves

It can be seen by examination of Table 1 that very good agreement existed between the values of ω_n obtained experimentally and those obtained analytically. Although similarly numbered runs had the same mass and the same oil volume, the calculated values of ω_n were slightly different because of the variations in oil temperature.

The difference between the experimental and calculated values of ω_n was consistently less than 6 per cent except for Runs 1 and 2 of the Moog 1402X; on these runs, the error was approximately 9 per cent. It is believed that these results are satisfactory for synthesis purposes.

The values of ζ did not agree as closely as did the values of ω_n, the average error being 21 per cent of the calculated value. However, in most applications the damping would have to be increased to a value of 0.6 or more, making small errors in the damping ratio negligible. Furthermore, this damping ratio is of less importance when the complete electrohydraulic servo loop is considered.

Runs 1 and 2 with the Moog 1402C did not exhibit the same agreement between values of ζ as was obtained on other trials. It will be shown in the following paragraphs that this lack of agreement was due to system saturation caused by the low valve damping of the 1402C.

Our work has shown that the transfer function relating load pressure and differential current can be written:

$$\frac{P_L}{\Delta I} = \frac{K_1 S/K_3 + K_1 B/K_3 M}{s^2 + \left(\dfrac{K_2}{K_3} + \dfrac{B}{M}\right) s + \dfrac{K_2 B + A^2}{K_3 M}} \tag{13}$$

TABLE 1 SUMMARY OF RESULTS FLOW CONTROL VALVES

Moog 1402C	ζ_1	ζ_2	ζ_3	ω_{n1}	ω_{n2}	ω_r
Run 1	0.12	0.03	0.05	337	345	333
2	0.10	0.04	0.06	387	409	383
3	0.07	0.05	0.07	350	355	346
4	0.06	0.06	0.07	396	412	395
Moog 1402X						
1	0.14	0.14	0.14	320	350	314
2	0.12	0.13	0.13	383	417	377
3	0.10	0.13	0.13	342	354	339
4	0.10	0.13	0.13	394	405	390
Cadillac FC-2						
1	0.15	0.12	0.15	347	352	339
2	0.10	0.12	0.14	400	414	396
3	0.10	0.12	0.14	346	358	344
4	0.09	0.12	0.13	408	410	405

Run No.	Weight (lb)	Volumes (in^3)		
		Tubing	Manifolds and Cylinder	Total
1	139.3	5.35	2.70	8.05
2	100.2	5.35	2.70	8.05
3	95.9	8.86	2.70	11.56
4	71.4	8.86	2.70	11.56

In this equation, A, B, K_3 and M are functions only of the system, K_1 (valve gain) is a function only of the valve, and K_2 (valve damping) is a function of both the valve (C_1 = slope of pressure-flow curves) and the system (C_2 = actuator leakage coefficient).

The anomalous values of ζ were probably not due to any of the system parameters, because this same system gave satisfactory results with the Moog 1402X and the Cadillac Gage FC-2. Furthermore, comparison of the 1402C and the 1402X shows that they have almost the same valve gain (K_1 = 4 in^3/sec-ma). By a process of elimination, the only factor left is C_1, the slope of the pressure-flow curves. This slope is negative for the fully gain-compensated 1402C and almost zero for the slightly compensated 1402X. Since leakage is a constant and since $K_2 = C_1 + C_2$, K_2 is considerably less for the 1402C than for the 1402X.

For a flow control valve, $K_2 B << A^2$. Therefore, ω_n is essentially independent of the value of K_2.

$$\omega_n = A / (K_3 M)^{1/2} \tag{14}$$

However, ζ is dependent on the value of K_2

$$2 \zeta \omega_n = K_2 / K_3 + B/M \tag{15}$$

Since K_2 is less for the 1402C, it follows that ζ is also less for the 1402C than for 1402X.

Examination of the family of frequency response curves for a second order system with ζ as a parameter shows that, as ζ becomes smaller, the amplitude ratio not only starts to rise sooner but also rises faster and higher.

If these various considerations are applied to Equation (13), it can be seen that for any constant ΔI, P_L will increase faster and reach the supply pressure of 3000 psi at a lower frequency with the 1402C than with the 1402X. This accounts for the clipped off appearance of the load dynamics curve for the 1402C (Fig. 11).

In other words the lower valve damping inherent in a gain-compensated valve results in a faster, higher response. Consequently, load pressure reaches supply pressure before the system is at resonance. The resulting curve has the appearance of a system with a larger ζ than it actually possesses.
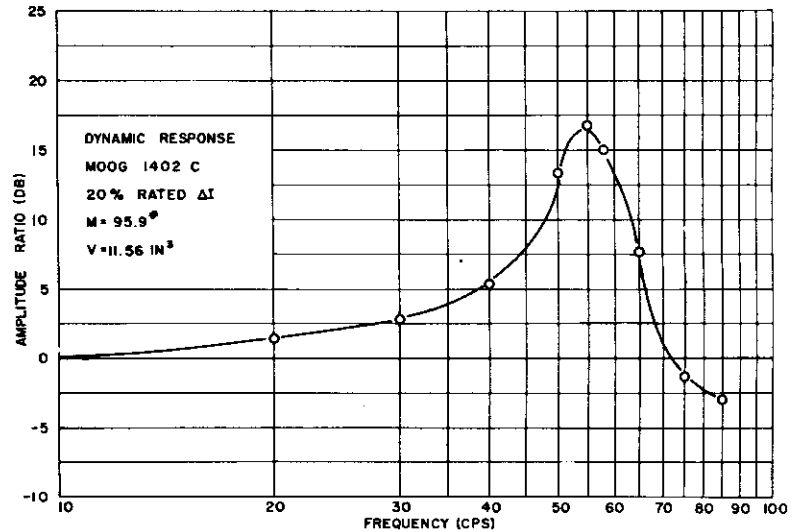
Figure 11. Frequency Response of Moog 1402C Valve - 20 Per Cent Rated Differential Current

Although this discussion explains why the 1402C at 20 per cent rated ΔI experienced system saturation and the 1402X did not, it does not explain why this effect occurred only on Runs 1 and 2. The following explanation will consider this aspect of the problem. If Equation (14) is substituted into Equation (15), we obtain

$$2 \zeta A / (K_3 M)^{1/2} = K_2/K_3 + B/M \tag{16}$$

Solving for ζ, we obtain

$$\zeta = \frac{K_2 (M/K_3)^{1/2} + B(K_3/M)^{1/2}}{2A} \tag{17}$$

It can be seen that if $K_2 (M/K_3)^{1/2} << B (K_3/M)^{1/2}$, ζ will depend only on the second term of the equation. For the 1402C, this inequality is satisfied. Therefore

$$\zeta = B (K_3/M)^{1/2} /2A \tag{18}$$

Now, Runs 1 and 2 were made with larger masses and smaller oil volumes than Runs 3 and 4. Since $K_3 = V/2\beta$, the use of the smaller volume resulted in a smaller value of K_3. Therefore, ζ on Runs 1 and 2 was so much smaller than on Runs 3 and 4 that the saturation effect discussed previously produced anomalous values of ζ .

Run 1 was repeated on the 1402C at 10 per cent rated differential current instead of the usual 20 per cent. The use of half as much differential current resulted in approximately half as much load pressure being developed at any given frequency, reducing the possibility of early system saturation. Because the slope of the pressure-flow curves is decidedly less negative at lower differential currents, the use of reduced differential current also resulted in a larger value of valve damping. As discussed previously, the larger valve damping produces a larger value of ζ ; this larger ζ also contributed to reduction of system saturation.

Figure 12 shows the resulting load dynamics frequency response at 10 per cent ΔI. By comparison with published curves, $\zeta = 0.075$. By calculation based on a K_2 with slope measured at null, $\zeta = 0.067$. The agreement in values of ζ is sufficiently close to verify the analysis presented in this section of the report.

Figure 12. Frequency Response of Moog 1402C - 10 Per Cent Rated Differential Current

The data in Table 1 show that the best point for the measurement of the slopes of the pressure flow curves (C_1), is near zero load pressure.

It is interesting to compare the results of this investigation with those reported in WADC TR 55-29, Part II. The parameters

K_3 and K_2 can be computed from the experimental results utilizing Equations (6) and (7), respectively. Typical values for K_3 and K_2 are 2×10^{-5} in^5/lb and 0.7×10^{-3} in^5/lb-sec, respectively, when utilizing the following data:

$$\zeta = 0.1$$

$$\omega_n = 375 \text{ rad/sec}$$

$$B = 10 \text{ lb sec/in}$$

$$M = 0.25 \text{ lb sec}^2/\text{in}$$

$$A = 0.96 \text{ in}^2$$

This typical K_2 is approximately one-third to one-eighth the value of K_2 reported in Part II. The question naturally arises: since K_2 and K_3 are interrelated by Equations (4) and (5), how could the static and dynamic values of K_3 have shown such good agreement, whereas the values of K_2 did not? This question can be answered by consideration of Equations (4) and (5), which are repeated here for convenience.

$$2 \zeta \omega_n = K_2/K_3 + B/M \tag{19}$$

$$\omega_n^2 = (K_2 B + A^2)/K_3 M \tag{20}$$

First, calculation of the numerator of Equation (5), using typical system values, shows that $K_2 B$ is much less than A^2; actually the error in ω_n^2 resulting from the neglect of $K_2 B$ is approximately 1 per cent. That is,

$$\omega_n^2 \approx A^2/K_3 M \tag{21}$$

or,

$$K_3 = A^2/\omega_n^2 M \tag{22}$$

Since B was assumed zero in the previous report, and since $K_2 B$ actually is negligible in Equation (5), the value of K_3 obtained from Equation (5) will agree with that obtained from Equation (6).

It is this agreement in K_3, whether calculated from Equation (5) or (6), that explains the good results reported in TR 55-29, Part II.

Calculation of the terms in Equation (4) will show that K_2/K_3 is the same order of magnitude as B/M. Therefore, the assumption that $B = 0$ results in a calculated K_2 approximately twice that which was obtained in Equation (7).

As mentioned earlier in this report, system saturation at higher input differential currents resulted in a clipped-off curve. This curve had the approximate appearance of a second order system with a ζ of 0.3 to 0.5. The net result of solving for K_2 from Equation (19), with a value of ζ three to five times too large and with $B = 0$, is a calculated value of K_2 which can be anywhere from 4 to 10 times larger than that expected.

These factors, plus the nonrigidity of the test stand (already discussed), account for the unusually high damping reported in TR 55-29, Part II.

2. Pressure Control Valves

For a pressure-control valve, the values for C_1 and consequently K_2 are very large. Consequently, the approximation that $K_2B << A^2$ is no longer valid and Equation (5), instead of Equation (14), must be used to find ω_n.

It can be seen by examination of Table 2 that very good

TABLE 2 SUMMARY OF RESULTS PRESSURE CONTROL VALVE

Cadillac PC-2	ζ exp	ζ calc	$\omega_{n_{exp}}$	$\omega_{n_{calc}}$	ω_r
Run 2	.15	2.3	580	562	565
3	.10	2.7	556	483	552
4	.09	2.3	600	560	596

Note: Same load conditions as listed in Table 1.

agreement existed between the values of ω_n obtained experimentally and those obtained analytically. The average difference between the two values of ω_n was 7 per cent.

However, the calculated value of ζ indicated overdamping, whereas the experimental values of ζ indicated considerable under-damping. No satisfactory explanation yet exists for the poor correlation between these two values.

Possibly the effect of flow forces on the dynamic characteristics of the second stage spool is not negligible with a pressure-control valve. Another possibility is that the load dynamics cannot be adequately represented by a second order characteristic equation. In any event, further study of pressure-control valves will be necessary to obtain a completely satisfactory method of analysis.

G. Electrical Analog

1. Introduction

In order to increase the understanding of the interrelationships in an electrohydraulic servo system, two electrical analogs are presented. Both analogs, with appropriately chosen electrical parameters, satisfy the three basic equations used in TR 55-29, Part II, to derive Equation (2) of this report. However, as will be seen shortly, the constant-current analog more adequately represents a flow-control valve and the constant-voltage analog is more suitable for representing a pressure-control valve.

The first basic equation satisfied by either analog describes the forces acting on the oil-mass combination:

$$A P_L = M s^2 \theta_o + B s \theta_o \tag{23}$$

The second basic equation relates load flow to valve flow:

$$Q_v = A \theta_o s + C_2 P_L + K_3 s P_L \tag{24}$$

The third basic equation is the equation of a linearized pressure-flow curve:

$$Q_v = K_1 \theta_i - C_1 P_L \tag{25}$$

2. Constant-Current Source

One electrical analog that satisfies Equations (23) to (25) is a parallel network driven by a constant-current generator (Fig. 13).

In this circuit, the electrical parameters have the following hydraulic analogs:

$$E = A P_L \qquad\qquad I = K_1 \theta_1$$

$$R_1 = A/C_1 \qquad\qquad I_1 = C_1 P_L$$

$$C = K_3/A \qquad\qquad I_2 = K_3 s P_L$$

$$R_2 = A/C_2 \qquad\qquad I_3 = C_2 P_L$$

$$L = M/A \qquad\qquad I_4 = A\theta_0 s$$

$$R_3 = B/A \qquad\qquad I_n = Q_v$$

This analog is particularly appropriate for a flow-control valve, where C_1 is very small and consequently R_1 ($= A/C_1$) is very large. In this case, the valve acts very much like a constant-current source.

Application of conventional network analysis leads to:

$$I_4 = \frac{I/LC}{s^2 + \left(\dfrac{1}{R_1 C} + \dfrac{1}{R_2 C} + \dfrac{R_3}{L}\right) s + \dfrac{1}{LC}\left(1 + \dfrac{R_3}{R_1} + \dfrac{R_3}{R_2}\right)} \qquad (26)$$

Substitution of analog equivalents yields the familiar relation:

$$\frac{\theta_0 s}{\theta_i} = \frac{K_1 A/K_3 M}{s^2 + \left(\dfrac{K_2}{K_3} + \dfrac{B}{M}\right) s + \left(\dfrac{K_2 B + A^2}{K_3 M}\right)} \qquad (27)$$

3.   Constant Voltage Source

Another electrical analog can be obtained by using as a driving source the Thevenin's equivalent circuit of the network to the left of terminals 1-1' in Fig. 13. (See Fig. 14.)

In this circuit, the electrical parameters have the following hydraulic analogs:

$$E = K_1 \theta_i \, A/C_1$$

$$E_1 = A \, P_L$$

$$I = Q_v$$

$$I_1 = K_3 s \, P_L$$

$$I_2 = C_2 \, P_L$$

$$I_3 = A\theta_o s$$

(All other parameters have the same hydraulic analogs as in the constant-current circuit.) This analog is especially appropriate for a pressure-control valve, where C_1 is very large and consequently R_1 is very small. In this case the valve acts very much like a constant-voltage source.
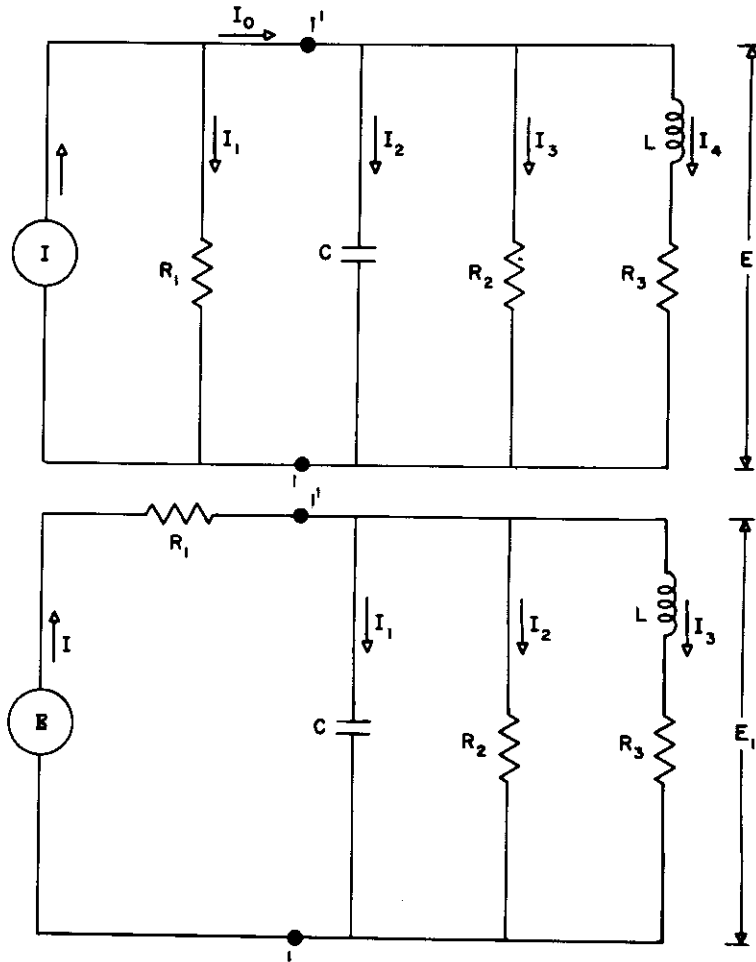
Figure 13.   Constant Current Electrical Analog of Electrohydraulic Servo Valve

Figure 14.   Constant Voltage Electrical Analog of Electrohydraulic Servo Valve

Using conventional network analysis, we obtain:

WADC TR 55-29 Pt IV   28

$$I_3 = \frac{E/R_1 LC}{s^2 + \left(\dfrac{1}{R_1 C} + \dfrac{1}{R_2 C} + \dfrac{R_3}{L}\right)s + \dfrac{1}{LC}\left(1 + \dfrac{R_3}{R_1} + \dfrac{R_3}{R_2}\right)} \tag{28}$$

Substitution of analog equivalents again yields Equation (27). An ordinary servo valve can be adequately represented by either analog. However, in the limiting cases of perfectly horizontal or perfectly vertical pressure-flow curves, it is necessary to use the appropriate electrical analog to obtain physically meaningful relationships.

H.   Conclusions

The following conclusions can be drawn from the linear analysis phase of the valve study:

(1)   The linear analysis approach produces satisfactory results when applied to a flow-control valve

   (a)   The undamped natural angular velocity (ω_n) can be very closely approximated by the relation: $\omega_n = A / (K_3 M)^{1/2}$

   (b)   The damping ratio (ζ) can be fairly well predicted from the relation: $2\zeta\omega_n = \dfrac{K_2}{K_3} + \dfrac{B}{M}$, with the valve damping (K_2) obtained by measuring the slope of the pressure-flow curves at 0 psi.

(2)   The linear analysis approach permits very good calculation of the undamped natural angular velocity (ω_n) of a system using a pressure-control valve, by use of the relation: $\omega_n{}^2 = \dfrac{K_2 B + A^2}{K_3 M}$

However, further study is required to obtain a satisfactory method of predicting the damping ration (ζ).

   Assuming no valve saturation, the over-all relationship between actuator output position and input differential current can be expressed as a fourth order transfer function:

$$\frac{\theta_o}{\Delta I} = \frac{K_1 \, A/K_3 \, M}{s \, (Ts + 1) \left[s^2 + (K_2/K_3 + B/M) \, s + \left(\dfrac{K_2 B + A^2}{K_3 M} \right) \right]}$$

where $1/(Ts + 1)$ is the valve dynamics and the remainder is the load dynamics.

A block diagram of an open-loop electrohydraulic servo system using this transfer function is presented in Fig. 15.
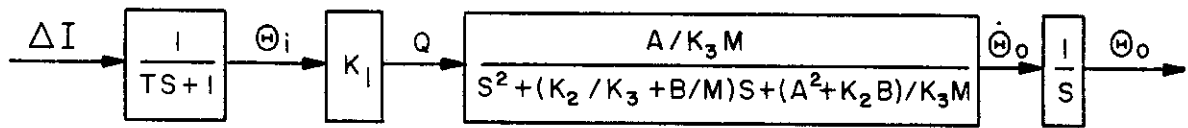
Figure 15. Block Diagram of Electrohydraulic Servo Valve (Open Loop)

CHAPTER III

GAIN COMPENSATION

A   Description

The pressure-flow characteristics of a variable area orifice can be represented by a set of parabolic curves similar to the solid line curves of Fig. 16. The characteristics of a servo valve in which the output spool position is proportional to the input current are similarly shaped, the parameter being differential current and represented by the following relationship:

$$Q = K \, \Delta I \, (P_S - P_L)^{1/2}$$

where Q = output flow

K = constant

ΔI = differential current

P_L = load pressure

P_S = supply pressure (assuming drain pressure equal to zero)

Differentiating Q with respect to ΔI

$$\frac{\partial Q}{\partial \Delta I} = K \, (P_S - P_L)^{1/2}$$
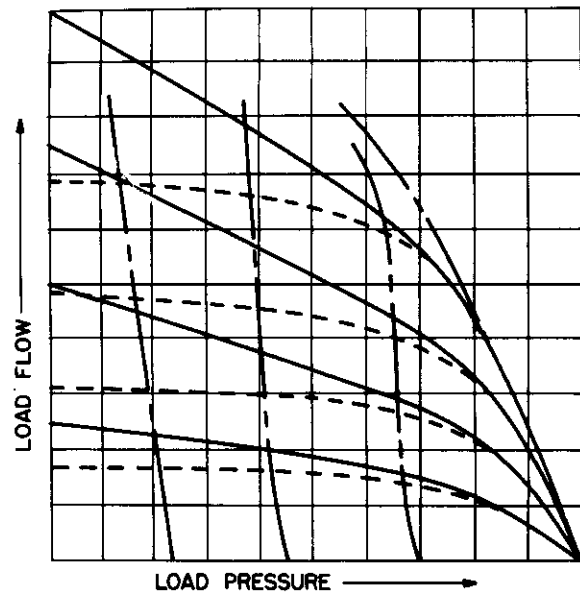
Figure 16. Typical Pressure Flow Curves

Thus, the flow gain of the valve, $\dfrac{\partial Q}{\partial \Delta I}$, varies as the square root of the load pressure.

In many control applications, it is desirable to have a constant gain irrespective of the load variations. This is not possible with a valve with parabolic pressure-flow characteristics as shown above. For instance, the flow gain is down to about 82 per cent of its no-load value when the load pressure is one-third supply pressure and to about 58 per cent of its no-load value at two-thirds supply pressure. At large load pressures, the gain drops off very rapidly until it reaches zero at a load pressure equal to full supply pressure.

The purpose of this particular investigation was to determine whether it is desirable to compensate the valve to maintain constant gain over a wider range of load pressure (see dotted line curve of Fig. 16). However, before considering that problem, a description of how gain compensation is physically accomplished will be presented.

If the gain compensation is to be performed within the valve, it is necessary for the valve to sense the actual flow rate and compensate for the variance in flow at the various load pressures. One method would be to develop a pressure proportional to this flow and feed the pressure back to the first stage, as a force in the opposite sense to the electromagnetic drive input. This has been tried in a number of valves, but to date, considerable difficulty has been experienced in obtaining repeatable results. Apparently the tolerances must be held closer than is possible under the production techniques presently being used in the manufacture of valves.

One technique which has been quite successful is applicable only to valves utilizing spring restrained output stages. This covers all single stage valves and all the Moog type valves.

To see how this compensation works, a conventional flapper nozzle, two-stage valve with a spring restrained output stage (see Fig. 17) will be analyzed. If the steady state forces acting on the valve spool are totaled, the following equation results:

$$A P_1 = K_1 \Delta I = 2 K_2 \theta_S + F_L \tag{1}$$

where P_1 = differential pressure across the spool ends

       A = area of the spool

K_1 = constant

K_2 = spring constant of each spring restraining the spool

ΔI = differential current

θ_S = spool position

F_L = flow forces

The flow forces are defined by the relationship, $F_L = K_3 Q \times (P_S - P_L)^{1/2}$*. Furthermore, according to the Bernoulli relationship

$$Q = K_4 \theta_S (P_S - P_L)^{1/2} \qquad (2)$$

where K_4 includes the combined influence of the orifice area and orifice coefficient and P_L is load pressure.

Figure 17. Typical Two-Stage Flapper Nozzle Spring-Restrained Second Stage Servo Valve

Equating,

$$K_1 \Delta I = \frac{2K_2}{K_4} \frac{Q}{(P_S - P_L)^{1/2}} + K_3 Q (P_S - P_L)^{1/2} \qquad (3)$$

or

$$K_1 \Delta I = \left[K' (P_S - P_L)^{-1/2} + K_3 (P_S - P_L)^{1/2} \right] Q \qquad (4)$$

_____

* "Axial Forces on Control Valve Pistons", by S. Lee, J. F. Blackburn, DACL, MIT.

where

$$K' = \frac{2 K_2}{K_4}$$

In order for Q to be constant over a range of load pressures, the terms within the brackets must be constant or

$$K' (P_S - P_L)^{-1/2} + K_3 (P_S - P_L)^{+1/2} = \text{constant}$$

It is quickly evident that this relation can only be satisfied at a single point. However, by properly selecting the relationship between the constants K' and K_3, the bracketed term of Equation (4) (which represents the impedance of the valve) can be made approximately constant over a wide range of load pressures. Two examples are shown in Figs. 18 and 19 to
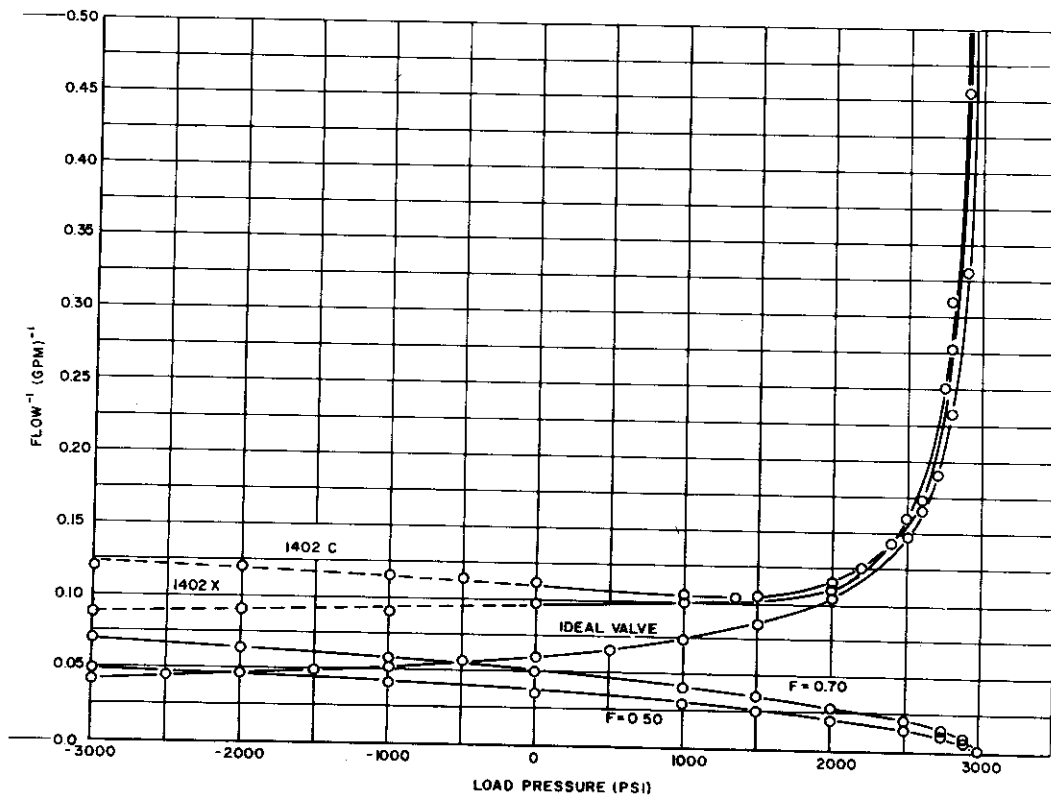
Figure 18. Valve Impedance Curves
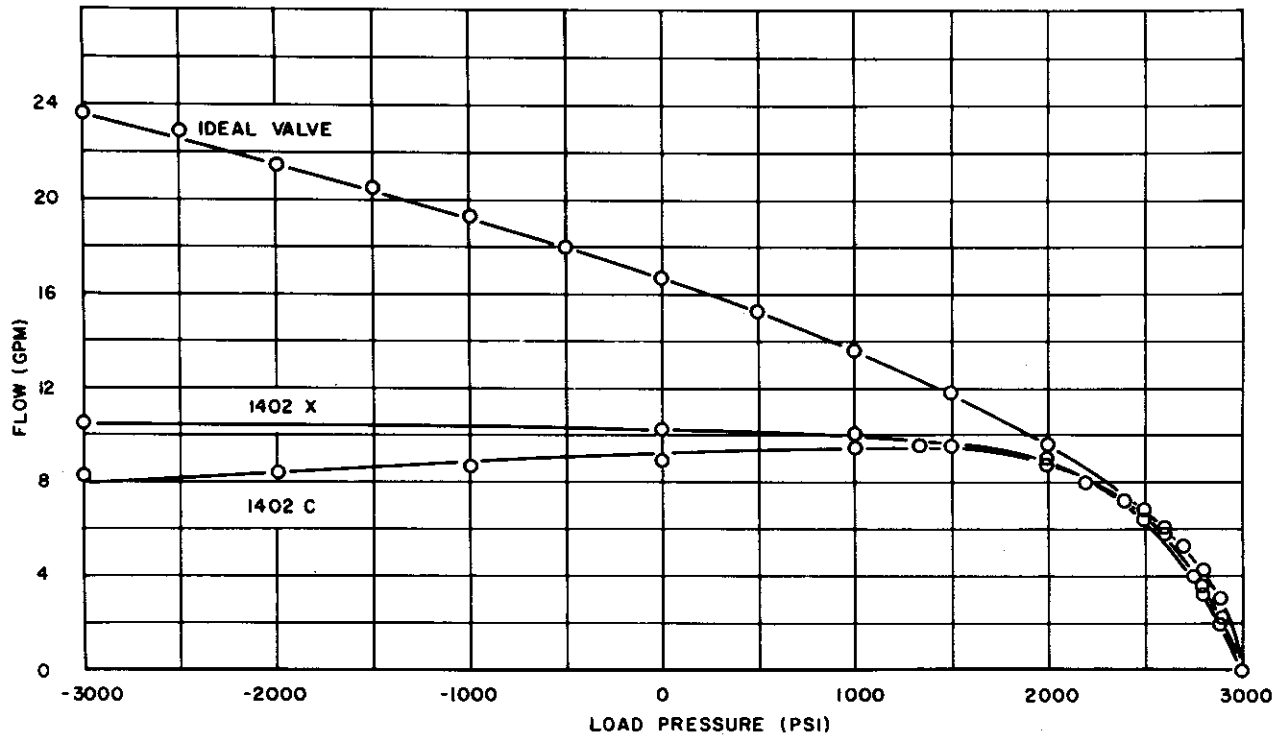
Figure 19. Actual Pressure Flow Curves

illustrate this effect. In Fig. 18 curves are plotted for both the individual
terms in the brackets and the bracketed term itself for two values of gain
compensation. The curves labeled 1402C and 1402X represent the result-
ant curves and very closely describe the pressure flow characteristics of
actual valves. The resultant curve for the 1402C shows slight over-gain
compensation while the 1402X curve is fairly flat to 2000 psi. This is
illustrated more clearly in Fig. 19 where the inverse of these curves, or
the actual pressure-flow characteristics, are plotted. In an actual valve
construction, gain compensation is obtained by reducing the spring constant
of the restraining springs (K_2), decreasing the output from the first stage
(K_1) and possibly increasing the orifice size (K_4) by varying the port size,
depending on the flow desired.

B.   Need for Gain Compensation

A gain compensated valve may be desirable for several reasons.
First, it may be necessary to maintain the actuator shaft speed approxi-
mately constant over a range of loads. One example might be a large
ground based radar antenna driven by a rotary hydraulic motor. Since

these antennas may be quite large, wind gusts can create fairly large loads on the hydraulic motor. By utilizing a gain compensated valve, the speed can be maintained fairly constant over a large range of wind loads. Of course, this can also be accomplished with the use of tachometer feedback but with a considerable amount of added complication since high accuracy in controlling speed in this application is not necessary.

Another application for which a gain compensated valve could be used is flow limiting. This is most often done with a flow-sensitive variable orifice valve in one of the supply, drain or load lines (see TR 55-29, Part III). Another method is to employ a saturating amplifier in conjunction with electrohydraulic servo valve. In this case the servo valve limits at a flow dictated by the amplifier. If the valve is gain compensated, the limiting speed can be maintained constant over a wide range of load pressures and no sacrifice in performance need be made at a particular load condition.

The aforementioned applications for gain compensated valves are realistic. There is no doubt but that the control systems would perform as predicted. However, there has been considerable disagreement as to the need for gain compensated valves to improve the response of hydraulic servos under load.

Because gain compensation requires the reduction of the first stage gain for a particular output flow, response is apt to be lowered when compared with a noncompensated valve. This can be seen by comparing the test results of the Moog 1402C and 1402X valves (see TR 55-29, Part II). While the variance is not great, the 1402X shows a definite superiority in response over the 1402C. Gain compensated valves also appear to be more susceptible to null shifts as discussed in TR 55-29, Part III. These are factors that degrade the servo performance.

As was discussed in the previous chapter, the slope of the pressure-flow characteristics $\dfrac{\partial Q}{\partial P_L}$ also have a considerable effect on the system's performance. When the oil mass natural frequency is outside the valve bandwidth (compressibility is negligible), low values of $\dfrac{\partial Q}{\partial P_L}$ have a stabilizing influence on the system - the transfer function of Equation (2) in Chapter 2 reduces to:

$$\frac{\theta_o}{\theta_i} \approx \frac{K}{S\,(T_S + 1)} \quad \text{, with T directly related to} \quad \frac{\partial Q}{\partial P_L}.$$

On the other hand, when the oil mass natural frequency is inside the valve bandwidth (compressibility is not negligible), low values of $\frac{\partial Q}{\partial P_L}$ have a destabilizing influence - the transfer function reduces to:

$$\frac{\theta_o}{\theta_i} \approx \frac{K'}{S\,(S^2 + 2\,\zeta\,W_n\,S + W_n^2)} \quad , \text{ with } \zeta \text{ directly related}$$

to $\frac{\partial Q}{\partial P_L}$

However, it has been found that the damping inherent in the actuator and load generally masks the damping effect of the valve's pressure-flow characteristics. Moreover, additional load damping in the form of by-pass leakage across the actuator, tachometer feedback, or compensation networks is generally required to augment the damping. Therefore, from an over-all standpoint, it appears that the values of $\frac{\partial Q}{\partial P_L}$ should be as small as possible to take into account cases where the oil mass natural frequency is high. Gain compensation provides these characteristics.

When systems are designed utilizing the maximum power transfer rule, the maximum required flow is selected to occur at a load pressure of two-thirds supply pressure with rated current applied. If the valve is not gain compensated, then the flow at lower load pressures will be correspondingly higher unless provision is included for limiting the maximum flow to this valve.

Since the flow is maximum at low load pressure, the loop gain will also be maximum at low load pressures. Thus, the maximum loop gain must be adjusted to provide stable operation at low load pressures. If the valve is not gain compensated, some degradation in response will have to be accepted at the higher load pressures where the loop gain is reduced. In most cases the loop gain will be sufficiently high so that the amplifier valve combination will saturate for small input signals. Therefore, there will be no conflict between the requirements of the maximum power transfer rule and stability criteria.

Thus, from the above discussion it can be seen that gain compensation has the following theoretical advantages and disadvantages:

Advantages:

(1) Reduces gain variations; response maintained over a wide range of loads

(2) Reduces undesirable damping in certain applications

(3) Provides a means of constant flow limiting

(4) Ideal in applications requiring constant output velocity over a range of loads.

Disadvantages:

(1) Susceptible to null shifts

(2) Reduces valve dynamic response.

C. Experimental Program

1. General

To determine experimentally the desirability of employing gain compensated valves to improve system response under load, a position control system was set up on the hydraulic test stand and tested with both gain-compensated and uncompensated valves. The test system consisted of a typical electrohydraulic control system driving a spring-mass load. The weight of the total mass load was 20 pounds while the combined spring rate of the springs was 6000 pounds per inch. The maximum travel of the actuator was limited to 0.375 inch. The system had an oil-mass resonance of 250 cps and was operated at various gains.

This combination of loads was selected to permit the valves to operate at relatively large load pressures over an extended portion of the total actuator travel. If only a mass load had been employed, the large load pressures would have been reached only during the high accelerations which occur during the terminal movements of the actuator for step inputs or during oil-mass resonance for sinusoidal inputs. Tests were conducted with and without the spring load to determine the effect of extending the load pressure range over large displacements.

Originally, it had been planned to conduct both frequency response and transient tests on the system. However, the former were discontinued when it was found that the servo system was highly amplitude sensitive, making frequency response comparisons difficult. This amplitude sensitivity was partially due to valve gain variations at low amplitudes, to coulomb friction resulting from slight misalignment of the spring supporting structure and to possible transmission lags in the system. In addition, the servo valve amplifier began to saturate at frequencies at the higher end of the bandpass for inputs greater than 1 volt (rms), thus providing a variable loop gain dependent on input amplitude. The variation in gain naturally resulted in a variation in the servo loop resonant frequency. Figure 20 shows a plot of the closed loop resonant
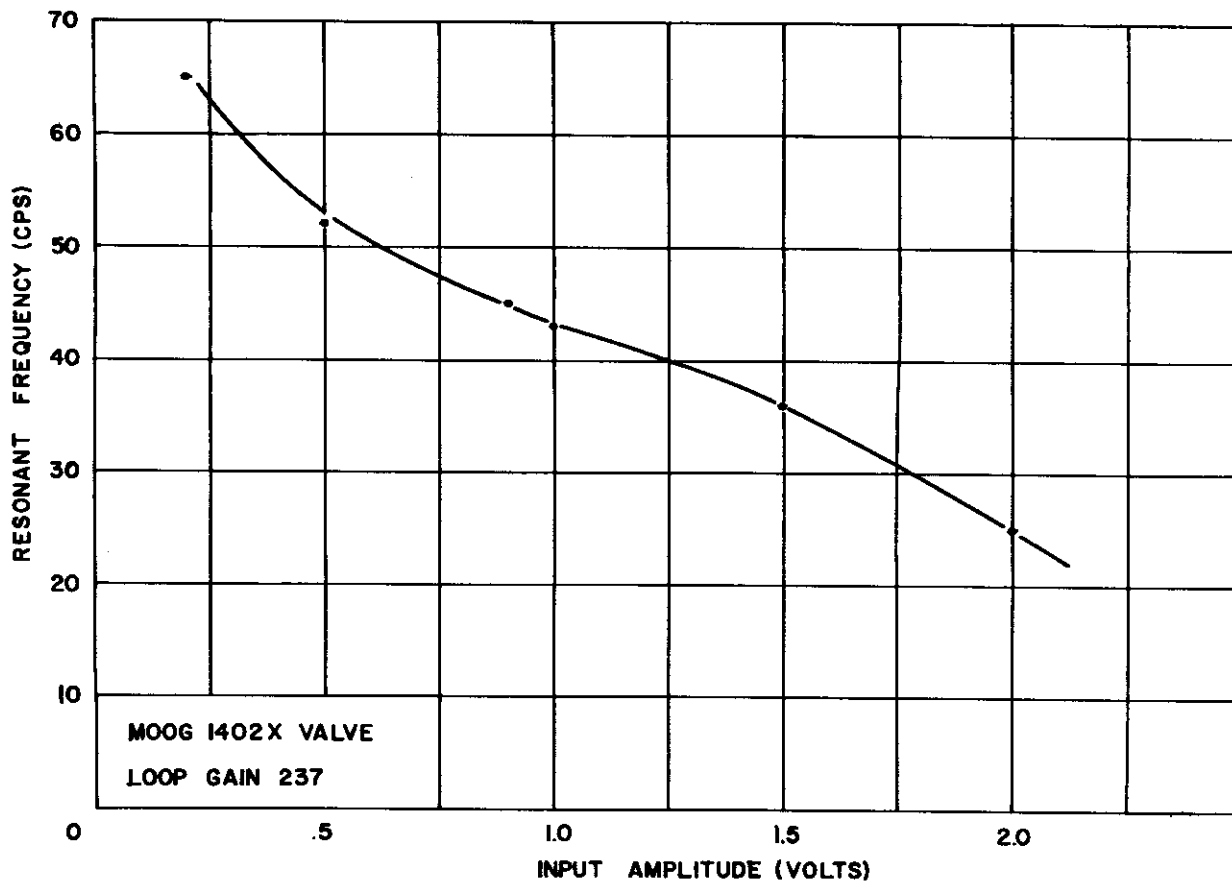

Figure 20. Moog 1402X Resonant Frequency vs. Input Amplitude

frequency vs. input amplitude for the system employing a Moog 1402X valve. The curve represents the average values of several test runs. At some large input amplitudes, the resonant frequency was multivalued, being a different value when approached from the lower frequencies than when approached from higher frequencies. This so-called jump resonance is a natural characteristic of closed-loop systems employing a saturable element such as an amplifier with a limited output driving current.

Since a saturated amplifier introduces a nonlinearity in the system, the small perturbation theory discussed in the previous section cannot be directly applied in the determination of system response for large inputs. The theory is acceptable, however, in ascertaining system stability, since this is of most concern at moderately low inputs which do not saturate the amplifier and which occur at maximum loop gain and minimum valve damping. This case is not of interest in the investigation of gain compensation.

One method of determining response of a system containing one or more nonlinear elements with the frequency response method is to represent the nonlinear element by its describing function. In this technique, the output of the nonlinear element is represented by the fundamental of the Fourier series describing the actual output when a sinusoidal input is applied. The pseudo or equivalent transfer function of the nonlinear element can be represented by a variable gain and phase lag, both of which are functions of the input signal amplitude. Conventional frequency response analysis techniques can then be applied to the composite system as was done in the previous section. It can be shown that the pseudo transfer function of a saturating amplifier can be represented by a variable gain only which is a function of input amplitude; no phase shift normally results from the saturation effect.

Because the frequency response test results have to be analyzed with respect to the describing function approach, a considerable amount of time is required in the interpretation of the test results. Due to the limited amount of time allotted for this phase of the work, it was decided to dispense with the frequency response tests and employ transient tests only. The frequency response approach was applied to a limited extent in the analog study phase and is described in the next section of this report.

The transient tests employed in this phase of the study consisted of the application of square wave inputs of various magnitudes to the control system and the photographic recording of the oscilloscope traces of the feedback voltages representing the resulting actuator piston displacements. All runs were conducted at a square wave repetition frequency of 3 cps. At this low frequency, there was sufficient time for the transients to die out before a change in input occurred.

Three different valves, the Moog 1402X, Moog 1402C and Cadillac FC-2 were employed during the test program.

As described in previous reports, (see WADC TR 55-29, Parts I, II) the 1402X is a standard Moog valve with approximately 10 gpm no-load flow at 3000 psi supply pressure. The 1402C is a gain compensated valve with a maximum flow of about 9 gpm. The FC-2 is a flow control valve with nearly ideal parabolic pressure flow characteristics and a no-load flow of about 7 gpm.

The 1402X and 1402C valves were purchased for previous valve study work intended to investigate experimentally the effect of gain compensation on valve performance. Unfortunately, it was found that the 1402X is also highly gain compensated and does not typify the uncompensated valve. The fact is that the 1402X is relatively highly gain compensated while the 1402C is overly gain compensated, having positive pressure-flow curve slopes at load pressures under 1500 psi. It was for this reason that the Cadillac FC-2 was also included in this test program. The test results thus permit comparison of an uncompensated valve, and valves with moderate and high degrees of gain compensation.

2.   Test Procedures

The test setup for conducting the gain compensation test is shown in block diagram form in Fig. 21.

In this test setup, the Hewlett-Packard oscillator provides square wave inputs to the control system, and the output position, which is measured by the feedback potentiometer, is displayed on a Dumont 404 rack-mounted oscilloscope. The output responses were recorded by means of a Fairchild oscilloscope camera.
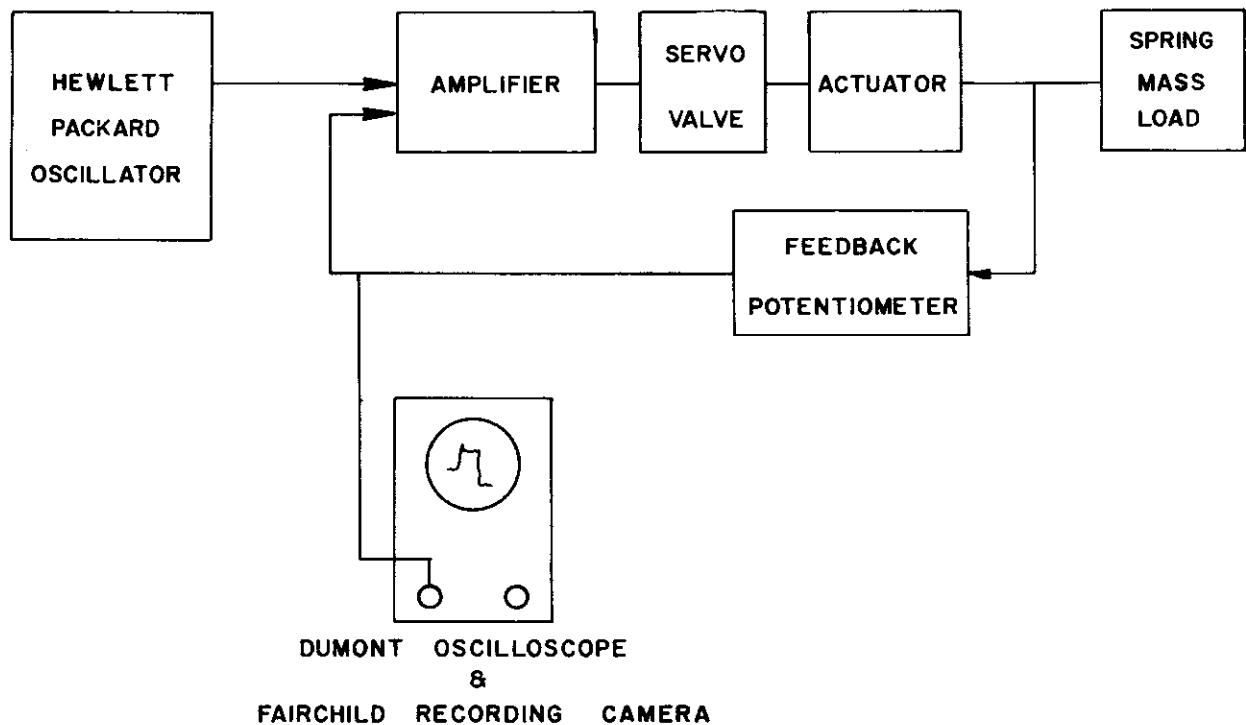
Figure 21. Block Diagram of Gain Compensation Test Setup

The tests were conducted with two input square wave magnitudes of 1.4 and 2.8 volts, adjusted as follows. The Hewlett-Packard generator was switched to sine wave output and the frequency adjusted to 3 cps. The desired square wave output was obtained by adjusting the sine wave amplitude to these magnitudes and then switching the oscillator to square wave output. The resulting square wave has the same amplitude as the sine wave, being 1.4 times the rms value. A 2.0 volt (rms) input corresponds to a differential current of 90 per cent rated, open loop. Thus, neither input saturates the amplifier. Runs were made at loop gains of 190, 237, and 283 sec^{-1}. No additional compensation was employed as each gain provided stable operation without compensation and the object of the tests was to compare responses of the different valves, not obtain optimum response. The loop gains listed, of course, comprise the valve gain. Thus, the lower valve gain of the FC-2 valve as compared with the 1402X valve was compensated for by a high electrical gain to maintain the same loop gain for comparison purposes.

3.   Analysis of Test Results

Figure 22 shows tracings of the system response to a step input for a 20 pound mass load with loop gains of 190 and 283 sec^{-1}, respectively, for all three valves. (Tracings were published rather than the photos because the quality of the photos was not high enough for reproduction.) The response of the system utilizing the 1402X and 1402C are very nearly the same for both inputs. The 1402X tends to provide slightly more oscillatory operation, however, especially for the higher input signal. The FC-2 shows markedly less overshoot at a gain of 190, especially for the 2 volt input signal. At a gain of 283, its response is increased relatively speaking, although it still exhibits lower overshoot amplitudes

Figure 22.   Moog 1402C, 1402V and Cadillac Gage FC-2 Transient Responses with Mass Load-Gains of 283 and 190

in comparison to the other valves. This results from the fact that the no-load response of the FC-2 valve is superior to that of the other two. The gain of the Moog valves could be adjusted for the same overshoot but with a degradation in response.
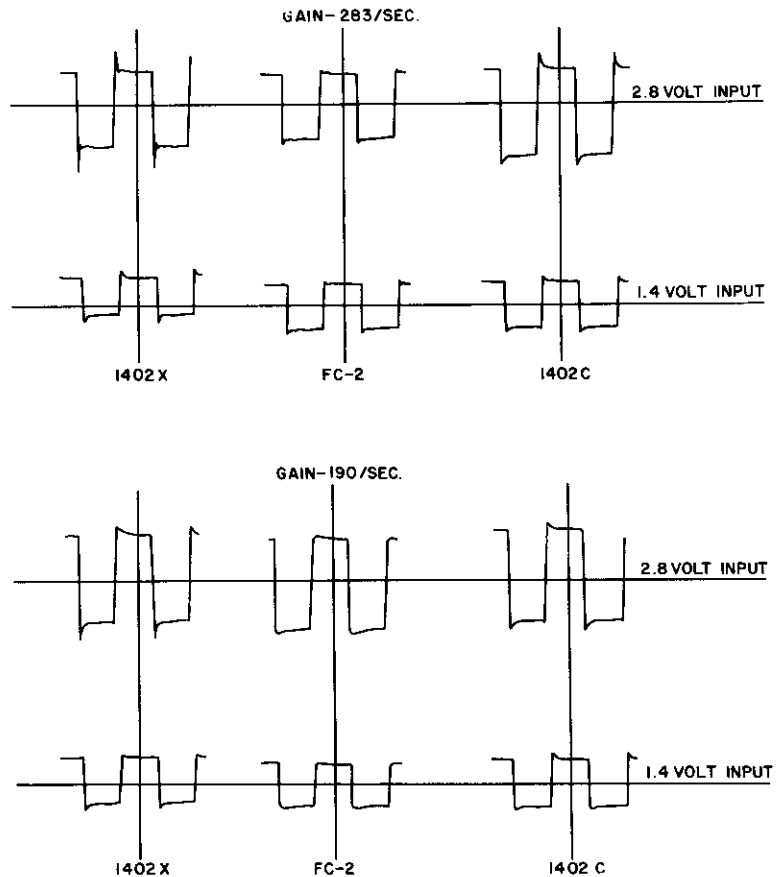
It is interesting to note that at no time did the valves pressure saturate; that is, the load pressure never reached a value of more

than one-third supply pressure. This was also the case during frequency response tests.

Figures 23 and 24 show the response of the system while driving the spring-mass load. The advantage of utilizing gain compensated valves is illustrated quite emphatically by comparing these responses with those of Fig. 22. The addition of the spring has not appreciably affected the response of the gain compensated valve control system, but has reduced the response of the uncompensated valve system appreciably. Once again the responses of the system with the two Moog valves are very nearly the same. No results were printed of the Moog 1402X driving the spring-mass load at loop gains of 190 and 283, as its response was the same as that of the 1402C. The comparison of system performance between the Cadillac Gage valve and the Moog valves with the mass load should not

Figure 23. Moog 1402C and Cadillac Gage FC-2 Transient Responses with Mass Spring Load - Gains of 190 and 237

be taken as a direct comparison of valves' responses. The Moog valves are larger flow valves and therefore, logically, have a poorer response capability. However, under large loads, the response of
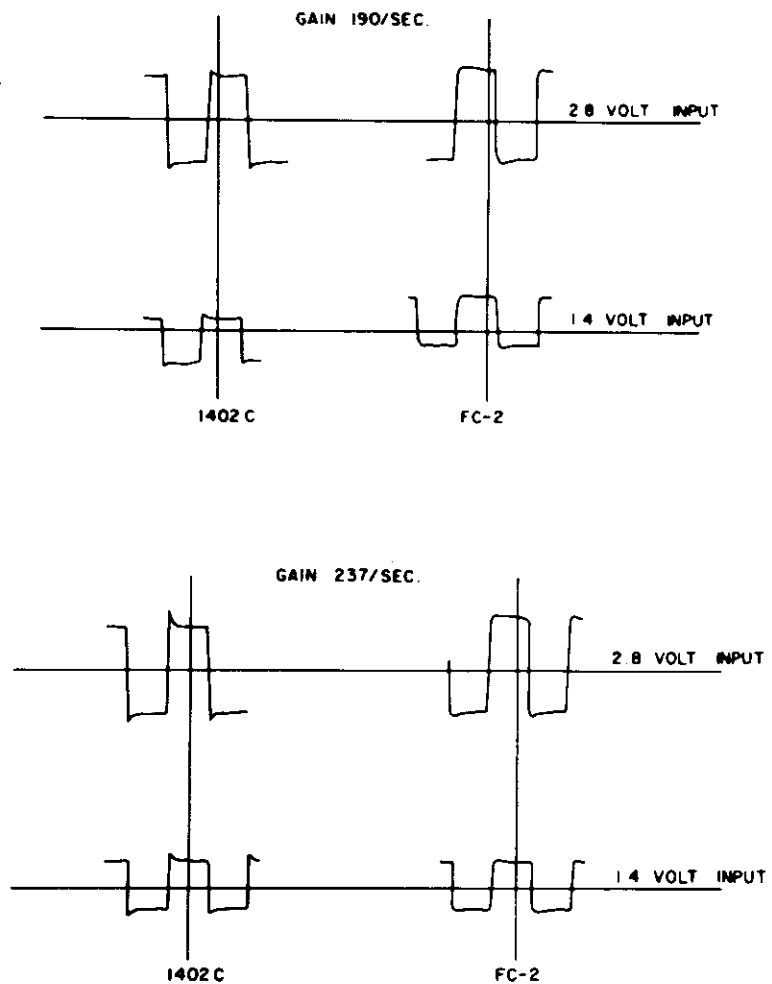
the FC-2 fell off while
that of the Moog
valves remained es-
sentially the same,
showing that when a
system is required
to operate under
large magnitude loads,
the addition of gain
compensation may
more than make up
for the poorer no-
load dynamics.

GAIN 283/SEC.

2.8 VOLT INPUT

1.4 VOLT INPUT

1402 X   FC-2   1402C

On the other
hand, it has been
found that the no-load

Figure 24.   Moog 1402C, 1402X, and
Cadillac Gage FC-2 Tran-
sient Responses with Mass
Spring Load - Gain of 283

responses of the valves were much superior when tested on the pres-
ent test stand than when tested on the old test stand, which was much
less rigid and had about one-fifth the mass. On the old test stand,
the FC-2 valve exhibited considerably higher no-load dynamics than
the two Moog valves. On the present test stand, its superiority is
not nearly as great. It is expected that in an aircraft the valves will
perform more nearly as they did on the old test stand because of the
lack of rigidity, although this is not known for sure. Thus, any deg-
radation in valve performance with the inclusion of gain compensation
may more than offset any improvement that can be gained from the
maintenance of constant gain. Neglecting the null shift consideration,
it can be stated that for two valves of approximately equal dynamic
performance, that which is gain compensated will provide better
performance under load. However, if the uncompensated valve has
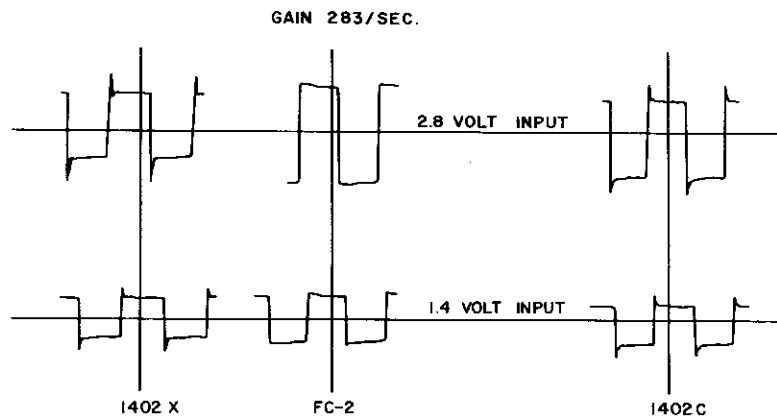much superior dynamic characteristics, then its choice will probably
be a good one.

CHAPTER IV

ANALOG STUDY OF A TYPICAL MISSILE CONTROL SYSTEM

A. Introduction

1. Purpose

The purpose of this phase of the valve study was to determine the feasibility of using analog techniques to supplement or replace some phases of laboratory tests on aircraft electrohydraulic control systems. It would be desirable, for example, to eliminate the necessity of breadboard testing which is highly time consuming, both in manpower and materials. In addition, the utilization of simulation techniques would provide the designer greater flexibility in selecting components and optimum compensation networks, provided that the simulation results can be considered as reliable as actual breadboard tests. It must be remembered, of course, that the latter does not always provide for the final design changes. Final adjustments are often made at the prototype stage, or even the production stage, to obtain the desired control system characteristics while operating in the missile or aircraft. However, no major changes should be necessary in the last two stages of design and test.

Simulation techniques, of course, have been used for some time in the design of dynamic systems of various types. These are often used to determine ball park figures on such items as loop gains, dynamic responses, frequency spectra for compensation networks, etc. As a result, components can be selected and purchased which best meet these requirements. In addition, amplifiers and compensation networks can be selected or built with variable characteristics and the necessary adjustments for optimum performance can be made during the prototype test phase.

One of the problems in performing all this work during the simulation stage is in the difficulty of mechanizing some of the

nonlinear elements of the control system on the computer, or even in describing the dynamic characteristics of the elements mathematically or graphically. For instance, the electrohydraulic servo valve is a conglomeration of nonlinearities, some of which interact on each other. While progress has been made in describing the dynamic performance of the valve utilizing linearized techniques, the results are not adequate to eliminate breadboard testing. Other nonlinearities associated with the system which are simpler to describe and mechanize are amplifier saturation, force or pressure saturation, coulomb friction, threshold, etc.

It was the purpose of this phase of study to introduce some of these nonlinearities in the analog mechanization of the system in an effort to improve the correspondence between the simulation test and breadboard tests and to determine whether a saving in time and effort was realized. Because of the limited amount of nonlinear analog equipment available at the time of the study, it was not possible to consider all the nonlinearities. Those which could be mechanized were the nonlinear pressure-flow characteristics of the valve, amplifier and valve saturation, pressure saturation and coulomb friction.

2. Plan of Attack

To render this investigation as realistic as possible, it was decided to perform the analog study on a typical missile control system. The one selected was representative of those found on high response missiles.

Because of the difficulty of obtaining complete response characteristics on an actual missile control system, it was decided to duplicate the control system in the hydraulics laboratory by matching the general characteristics of the two systems and then using the hydraulics laboratory system as a reference for the analog study. Not only did this facilitate the acquisition of experimental information for comparison purposes, but it also permitted the use of test equipment and procedures of known reliability. The plan of attack was to determine the characteristics of the hydraulics laboratory system, using both experimental transient and frequency response tests and analytical calculations, and then to set up a system on the analog computer which would match these characteristics as closely as possible when tested in the same manner.

B.   Description of System to be Simulated

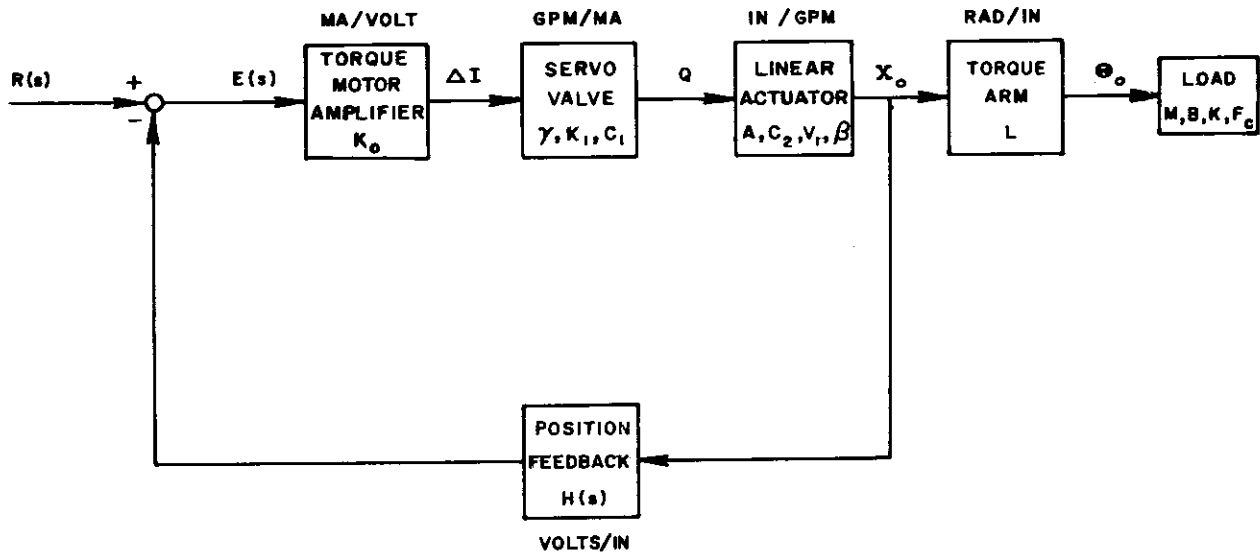A block diagram of the system to be simulated is shown in Fig. 25.

Figure 25.   Block Diagram of System to be Simulated

The significant characteristics of this system are listed below:

(1)   Load mass - 5.18×10^{-2} lb-sec^2/in.   (M)

(2)   Viscous damping - 10 lb-sec/in.   (B)

(3)   Aerodynamic spring rate - 150 lb/in.   (K)

(4)   Coulomb friction - negligible   (Fc)

(5)   Torque arm - 1.5 in.   (L)

(6)   Oil mass resonant frequency - 250 cps   (fr)

(7)   Loop gain - 300 sec^{-1}

(8)   Required closed-loop frequency response

(a)   Ratio of output to input - flat to 20 cps

(b)   Phase lag of output - $2°/cps$

The values listed for the load characteristics are those reflected back to the actuator shaft; it is assumed that the bell crank is perpendicular to the actuator at the null point. It is also assumed that the displacements are sufficiently small, so that variations in the effective torque arm do not affect the system gain or the torque transmitted to the load.

The aerodynamic spring rate is actually nonlinear with respect to control surface displacement; the average value is listed. However, neither the variation in the effective torque arm nor the nonlinearity of the aerodynamic spring will enter into the analog study, as these characteristics are not variable in the hydraulics laboratory simulated system which will be used as the actual reference.

The oil-mass resonance of 250 cps was computed on the basis that the bulk modulus of the oil is approximately 2.2×10^5 at an oil temperature of $120°F$ which was the average temperature maintained during these tests. Actually it varies with temperature, pressure, amount of entrained air, etc.

The closed-loop response requirements are specified for a non-saturating condition. These characteristics are necessarily much poorer if any of the elements in the servo loop saturate. The actual saturation level of the torque motor amplifier was not specified but a value of 125 per cent rated differential current was employed in the laboratory setup.

C.   Description of the Laboratory System

1.   Load

In the laboratory system, the bell crank was eliminated and linear translational loads were applied to the control actuator. A view of the load setup is shown in Fig. 26. The mass of the load shaft plus actuator shaft was 5×10^{-2} lb-sec^2/in. The total spring rate of the two restraining springs was 150 lb/in. The viscous and coulomb friction of the load setup, when properly aligned, was negligible as the shaft was mounted in ball bearing collars.

2.   Actuator

The actuator utilized for this investigation was the load actuator discussed previously in this report (see Fig. 2).

This is a symmetrical, double-acting actuator with an area of 0.96 in^2 and a variable maximum stroke. To obtain the oil-mass resonance of 250 cps, the maximum stroke of 2 inches was used. The total volume of oil under compression, including that in the manifold block between the actuator and the servo valve, was 2.55 in^3. As discussed previously, the actuator has provisions for mounting

Figure 26. View of Load Setup for Reference System

pressure pickoffs to permit the monitoring of the instantaneous load pressure.

The viscous friction of the actuator was approximately 10 lb-sec/in., the same as called for in the specifications. The experimentally measured coulomb friction was 12.5 pounds for sinusoidal tests.

3. Valves

Two servo valves were employed during the simulation, the Moog 1402C and the Cadillac Gage FC-2. Although their rated flows were larger than those customarily found in high response missile systems, the response of these valves was adequate for the simulation of the system specified. The pressure-flow characteristics of the two valves are shown in Figs. 27 and 28. These characteristics are sufficiently unlike to produce different closed-loop responses. The flow gain curves of the two valves are shown in Figs. 29 and 30; their no-load responses are shown in Figs 64 and 69.

4. Summing Amplifier and Compensation

The static characteristics of the amplifier are depicted by the
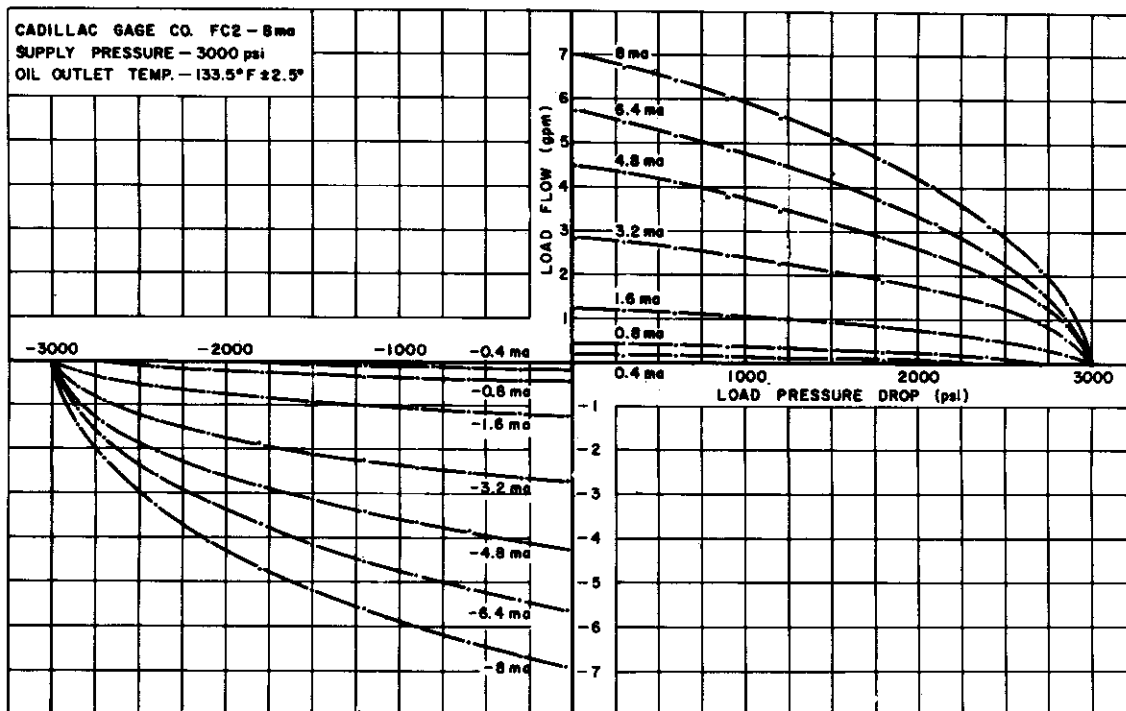
Figure 27.   Pressure-Flow Characteristics for FC-2 Valve
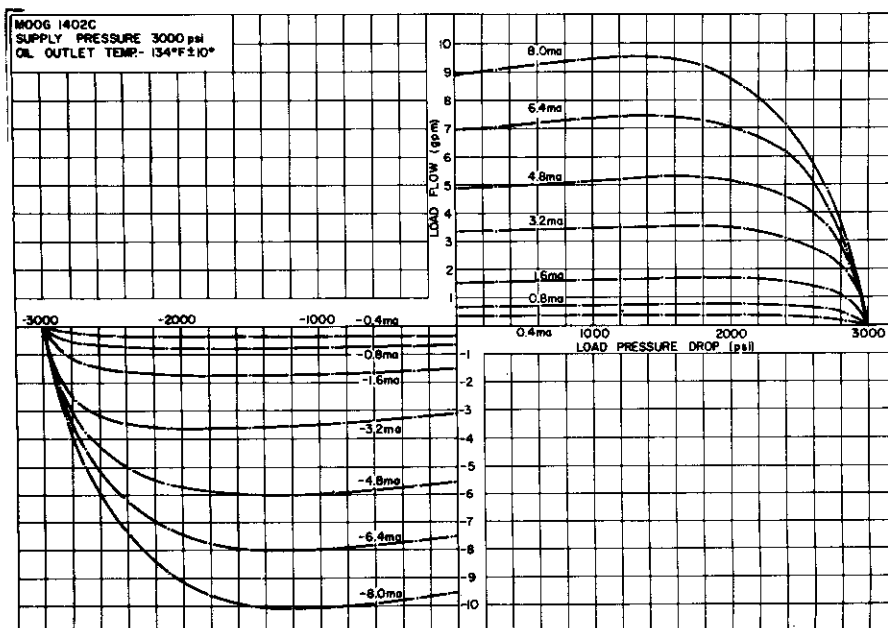

Figure 28.   Pressure-Flow Characteristics for 1402C Valve
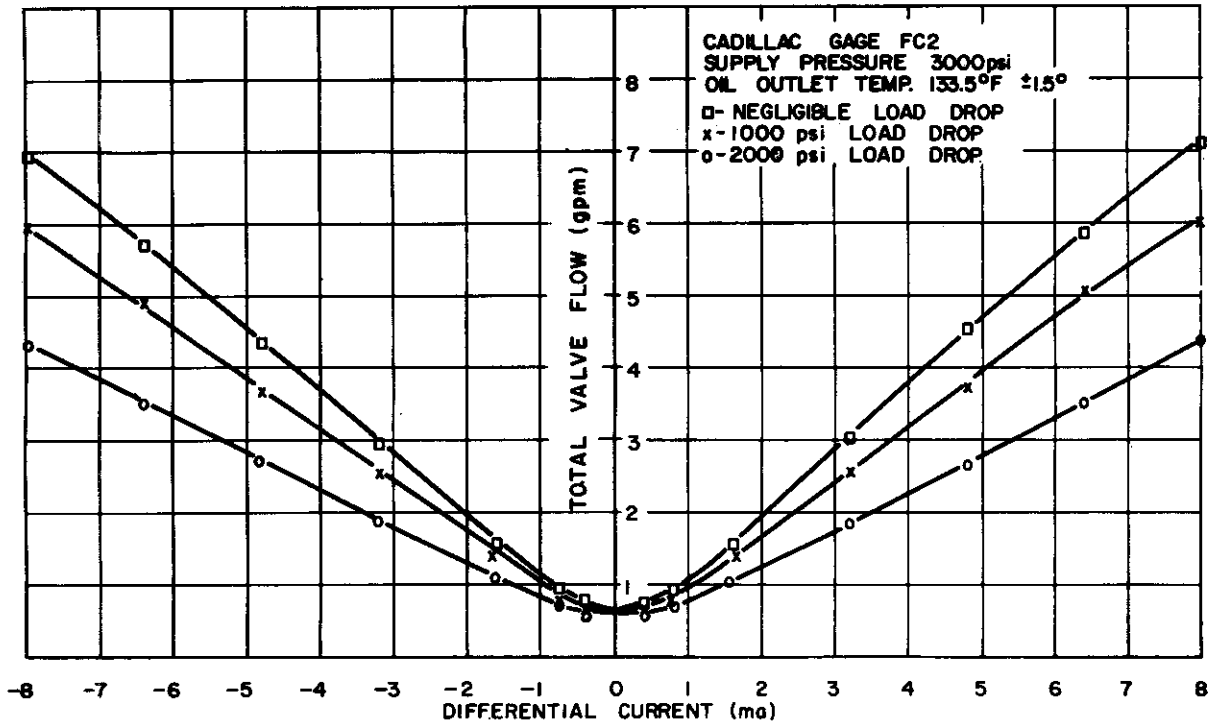
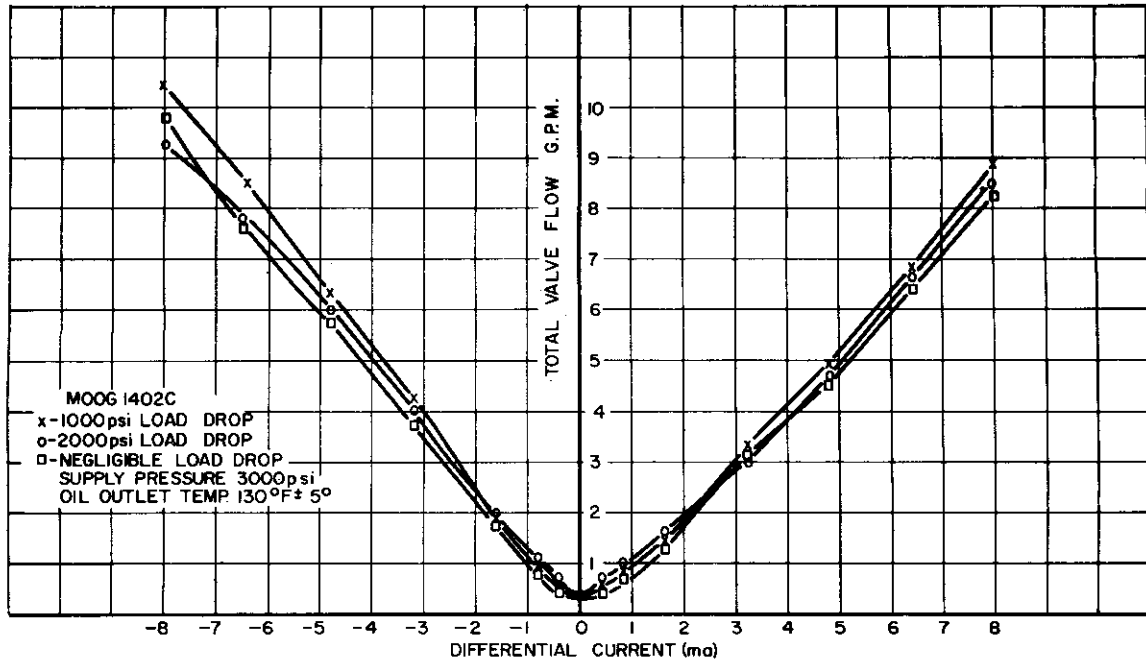Figure 29.   Valve Flow Curves for FC-2 Valve

Figure 30.   Valve Flow Curves for 1402C Valve

differential current vs. input voltage curve of Fig. 31. This curve shows that gain is fairly constant until the output differential current reaches approximately 9 ma; above this value the amplifier exhibits saturation. The dynamic lags of the amplifier can be considered negligible. Compensation networks were not needed to meet the specifications of the system.
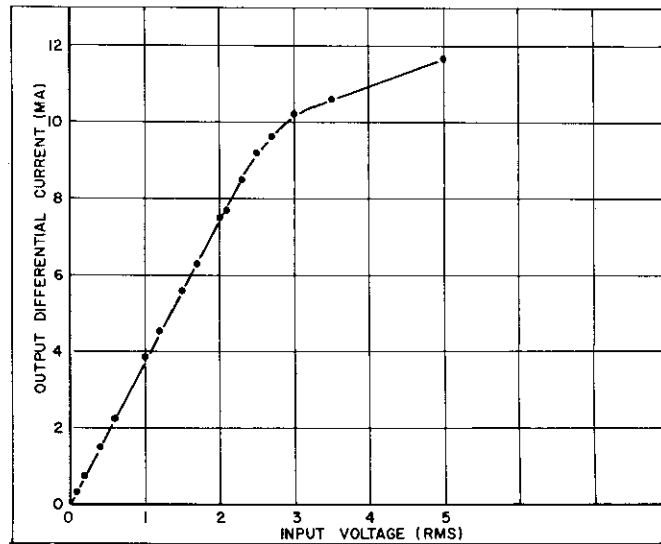
Figure 31. Torque Motor Amplifier Characteristic Curve

5.   Position Feedback Network

The over-all loop was closed with position feedback. The actuator shaft position was sensed by the Giannini linear potentiometer discussed previously in this report. The pickoff voltage, after being attenuated by a Helipot, was fed into the grid of the summing amplifier. By varying the Helipot setting, the loop gain could be varied from zero to 400 sec^{-1}.

D.   Simulation of System Components

1.   Amplifier

Over the linear range of the amplifier, its gain was simulated by a scale-changing (coefficient) circuit. Diode limiting was used to simulate amplifier saturation. The diode cutoff voltage was adjusted so that limiting occurred at the equivalent of 10 ma. No dynamic lag circuit was required (see Fig. 32.)

2.   Position Feedback Network

The position feedback network was simulated by a scale-changing (coefficient) circuit; the magnitude of the scale change could be

ANALOG COMPUTER SETUP OF MISSILE CONTROL SURFACE SERVO SYSTEM

Figure 32. Analog Computer Wiring Diagram

varied over a wide enough range to produce analog loop gains corresponding to system loop gains of zero to 400 sec^{-1} (see Fig. 32).

3. Servo Valve

The servo valve consists of a great number of nonlinearities, the effects of all of which are not completely understood. The valve has one input, differential current, and two outputs, load flow and load pressure. These can be related mathematically if flow is the desired output, as:

$$Q = f(\Delta I, P_L) \qquad (1)$$

Statically, the above relationship can be represented by the pressure-flow curves of the valve with differential current a parameter. For dynamic inputs, lags occur between the differential current and output spool position, which effectively modify the differential current parameter of the pressure-flow curves. Since the spool position does not appear directly in the above equation, the lags must be introduced as appearing between the output differential current of the amplifier and the effective differential current of the pressure flow curves. These lags are described by the no-load frequency response characteristics or valve dynamics.

In this case it is assumed that the no-load dynamic characteristics do not vary under load. This is a good assumption for the FC-2 valve. Its validity has never been proven experimentally for the Moog 1402C, although the good results of the linearized analysis study have added credence to its use.

The no-load frequency response characteristics of the two valves as shown in Fig. 77 cannot be perfectly duplicated by any simple network. In the analog simulation, they were represented by a first order lag whose transfer function is:

$$\frac{\theta_i}{\Delta I} = \frac{1}{Ts + 1} \qquad (2)$$

The value of the time constant was determined by examining the break points and 45 degree phase shift points of the no-load frequency response for various magnitudes of input differential current and picking an average value from which to compute T. Admittedly an approximation, this method yielded reasonably satisfactory

results during the tests.

The pressure-flow curves were generated on a two-channel function generator and a function multiplier. The function generator simulated the shapes of the pressure flow curves for both positive and negative differential current and the function multiplier established the valve flow gain (flow vs. differential current). The purpose of the polarized relay and associated limiting circuitry was to select the correct pressure-flow curve, depending on the sense of the differential current, with minimum dead time. A single function generator channel could have been employed if the pressure inputs to the function generator were switched instead of the outputs.

The above setup provided for a constant flow gain. It can be seen from Figs. 29 and 30 that K_1, the valve gain of the two valves, is constant only over a limited range of differential currents. However, the flow saturation accompanying large inputs was not simulated because amplifier saturation occurred first. The gain reduction at low inputs was accounted for by actually changing the gain of the first-order lag circuit.

The complete simulation of the valve can be seen in Fig. 32.

4. Actuator-Load

Since the actuator and load are intimately related and since they operate on both valve flow and valve load pressure, they will be considered together.

The equations relating valve flow and load pressure, respectively, to the actuator and load can be written as follows:

$$Q_v = C_2 P_L + K_3 \dot{P}_L + A \dot{\theta}_o \tag{3}$$

$$P_L = \frac{F}{A} = \frac{1}{A} \left(M \ddot{\theta}_o + B \dot{\theta}_o + K \theta_o + F_c \frac{\dot{\theta}_o}{|\dot{\theta}_o|} \right) \tag{4}$$

The simulation of these equations is straight forward as shown in Fig. 32.

Equations (1), (2), (3) and (4) were combined and included in a signal flow graph of the over-all control system (see Fig. 33). A block diagram of the over-all system is also included (see Fig. 34).
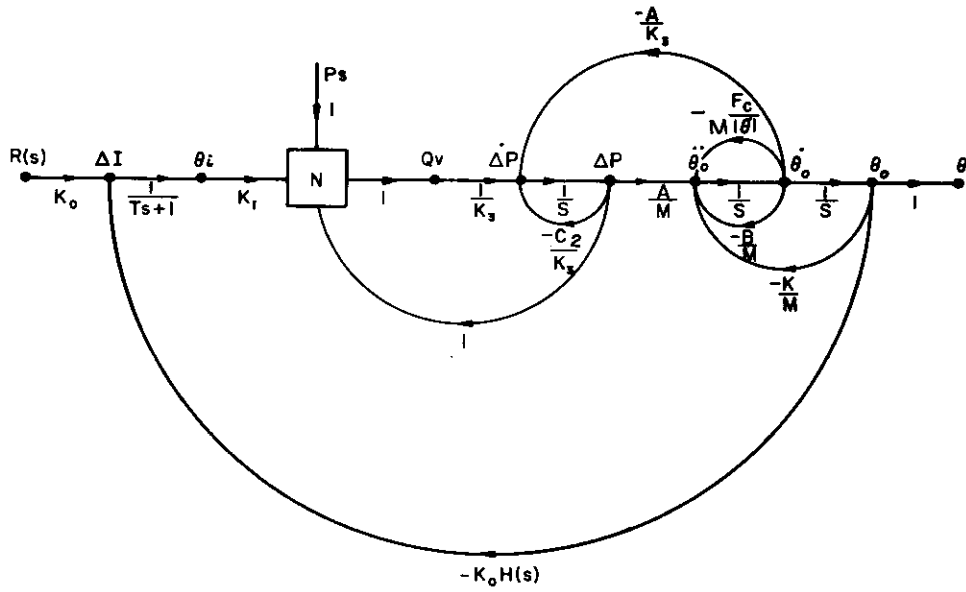
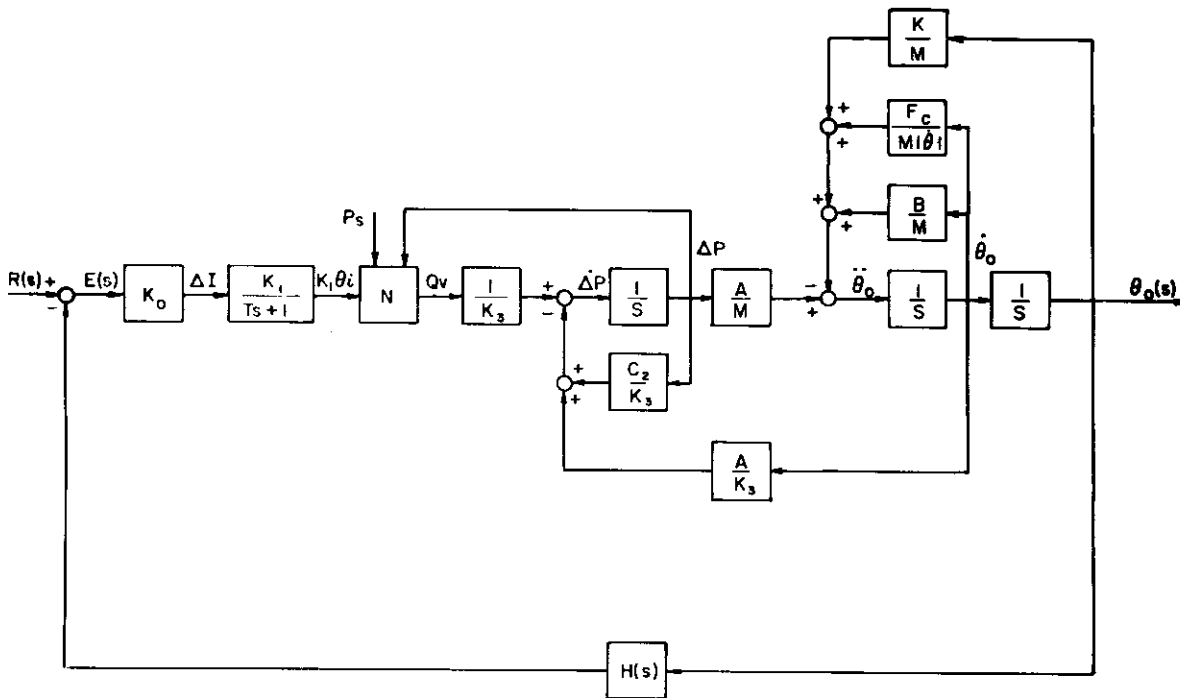Figure 33. Signal Flow Graph of Over-all System

Figure 34. Block Diagram of Over-all System

In both diagrams, N is a nonlinear element which generates Equation (1). These diagrams not only depict the relations between the variables of the equations, but also serve as a guide for the analog computer setup.

E. Mechanization of the System

Before the equations were actually mechanized, computer scale factors had to be taken into consideration. Although real-time operation of the computer was preferable, permitting direct simultaneous comparison with the system on the test stand, there were two considerations which required that a time-scale factor be used. First, the high natural frequencies and small time constants of the system elements exceeded the bandwidth of the available galvanometer-type recorders. Second, the relative magnitudes of the coefficients in Equations (3) and (4) differed considerably, indicating a disparity in gains. Both of these difficulties were removed by using a time scale change:

$$t = 0.002\tau$$

Amplitude scale factors were also required, because it was necessary to limit the output of the operational amplifiers to ± 100 volts. The equations relating computer variables to system variables are listed in Table 3, along with the maximum values of each.

TABLE 3 RELATIONS BETWEEN COMPUTER VARIABLES
AND SYSTEM VARIABLES

Variable	Symbol	Maximum Computer Variable	Maximum System Variable	Relating Equation
Pressure	Π	100 v	3000 psi	$P = 30\Pi$
Position	H	200 v	2 in.	$\theta = 0.01H$
Velocity	$\dfrac{dH}{d\tau}$	-	-	$\dot{\theta} = 5\dfrac{dH}{d\tau}$
Current	i	100 v	8 ma	$\Delta I = 0.08i$
Flow	ψ	100 v	40 in^3/sec	$Q = 0.4\psi$
Time	τ	-	-	$t = 0.002\tau$

After all scale factor changes were made and the resulting equations solved for the highest order derivative, Equations (1), (3), and (4) reduced to:

$$\psi = g(i, \pi_L) \tag{5}$$

$$0.1 \frac{d\pi_L}{d\tau} = 0.667\psi - 0.015\pi_L - 0.99\frac{dH}{d\tau} \tag{6}$$

$$\frac{d^2 H}{d\tau^2} = 0.194\pi_L - 0.386\frac{dH}{d\tau} - 0.0116H \tag{7}$$

Equations (6) and (7) were mechanized, using as a guide the circuits to the right of the nonlinear element in Fig. 32. Equation (2), when converted to computer time, reduced to:

$$\frac{H_i}{\Delta I} = \frac{1}{500\tau s + 1} \tag{8}$$

Figure 32, the interconnection diagram of the completed analog system, was used to set up the system on a GEDA L3 computer augmented by an N3A electronic Multiplier and an N3E function generator. Table 4 lists

TABLE 4 RESISTANCE VALUES USED IN ANALOG SIMULATION

	Input (volts rms)	R_1	R_2
FC-2	0.5	0.122	0.90
	1.0	0.122	0.90
	2.0	0.142	0.90
	3.0	0.142	0.90
1402C	0.5	0.234	1.00
	1.0	0.230	1.50
	2.0	0.44	2.20
	3.0	0.44	2.20

the various values of R_1 and R_2 used in the simulation of the system with both the FC-2 and the 1402C valves. The values of R_1 and R_2 were determined during the test phase of the analog study.

F.   Tests of the System

   1.   General Considerations

      Broadly speaking, dynamic-response tests of a system fall into two categories: transient response and frequency response. Transient response tests give an indication of the system's relative stability and provide a measure of the speed of response (rise time, settling time, etc.); frequency response tests directly yield the system bandwidth and permit rapid determination of the system transfer function.

      As far as the analog program was concerned, transient studies had three advantages:

         (1)   Step inputs could be easily applied to the system

         (2)   The resultant response could be easily recorded

         (3)   A complete test required only 2 or 3 minutes.

      However, because the analog system operated at 1/500 real time, direct simultaneous comparison of the analog response with the hydraulic system response was impossible.

      Frequency response tests, on the other hand, had three disadvantages:

         (1)   They were time consuming; a complete test, including data reduction, took about 45 minutes

         (2)   Accurate phase shift was difficult to obtain when using the curvilinear coordinate paper needed by the galvanometer-type recorder

         (3)   Output waveform was poor.

      Nevertheless, because frequency response tests did provide a better comparison of the characteristics of the two systems, they were chosen as the basis for making final parameter adjustments. Transient

tests were also conducted but for comparison purposes only.

2.   Tests Peculiar to the Hydraulic System

Open-loop frequency response tests (output velocity amplitude and phase) were run on the hydraulic system to see if it met the specified gain and phase characteristics. In addition, the open-loop gain was measured as a function of input differential current for various frequencies; the purpose of that test was to provide some guidance for setting the gain of the analog system at different operating points.

3.   Tests Common to the Hydraulic System and the Analog System

Closed-loop frequency response tests were run on both systems. Position amplitude and phase were measured on the hydraulic system for four different constant amplitude inputs - 0.5, 1.0, 2.0 and 3.0 volts rms. The valve gain and time constant of the analog system were then adjusted to match those responses as closely as possible.

After the best correspondence had been achieved, utilizing the frequency response tests as a comparison, closed-loop transient response tests were run. Oscilloscope recordings of the position, load pressure and differential current responses were taken for step inputs of 0.7, 1.4, 2.8 and 4.2 volts amplitude. The hydraulic system responses were photographed with a Fairchild Polaroid oscilloscope camera, whereas the analog system responses were portrayed on a Brush galvanometer-type recorder.

G.   Discussion of Test Results

1.   Frequency Response

The open-loop frequency responses of the reference system set up in the hydraulic laboratory are shown in Figs. 35 and 36 for the 1402C and FC-2 valves, respectively. These curves show the open-loop response, with and without the spring mass load. For the most part, the load had very little effect on the open-loop properties.

Figure 37 shows the open-loop amplitude response only for the reference system when driven by the FC-2 valve. The experiment verified the 250 cps calculated value of oil-mass resonance as correct. It is interesting to note that the amplitude curve did not begin

to decline until after the oil-mass resonant frequency. This was due to the fact that the FC-2 valve's response remained flat to a sufficiently high frequency that when its output flow amplitude did start to fall off, it was more than compensated for by the increasing amplitude characteristic of the oil-mass resonance. The curves for the 1402C (not shown) drop down considerably before resonance and then rise at resonance.

The above three curves were utilized to assist in setting up the open-loop transfer function of the analog system. They were particularly valuable since they were unaffected by loop gain settings.
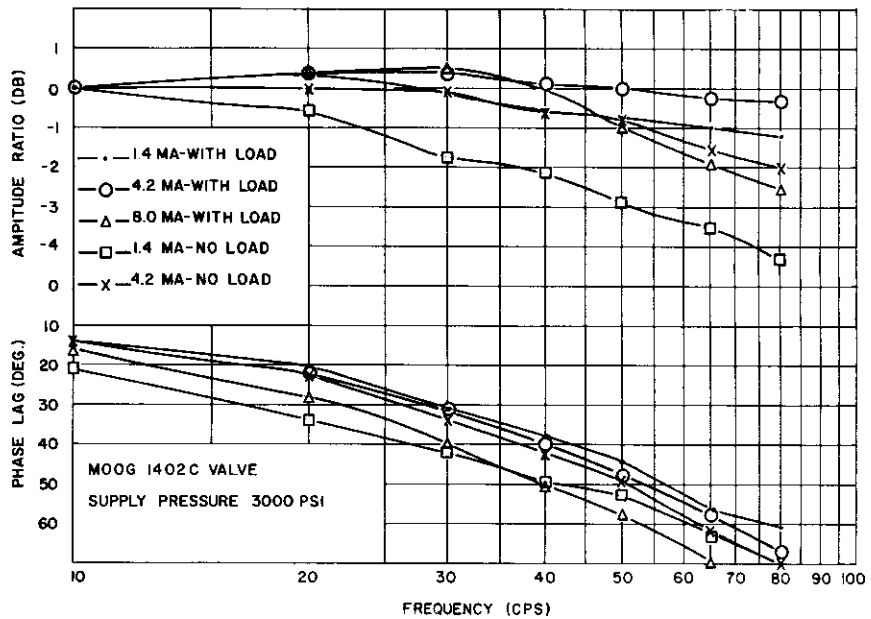
Figure 35. Open-Loop Frequency Response of Reference System - 1402C Valve
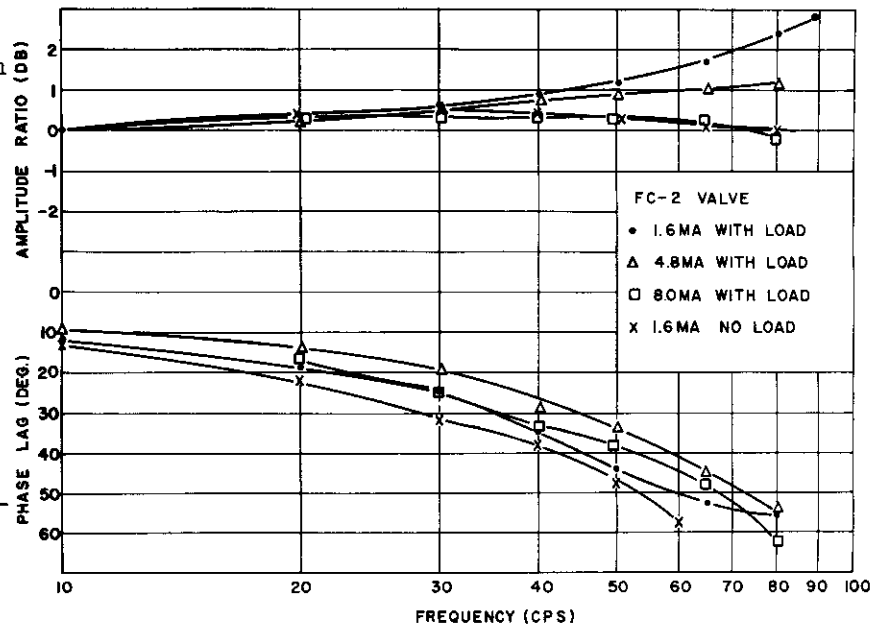
Figure 36. Open-Loop Frequency Response of Reference System - FC-2 Valve
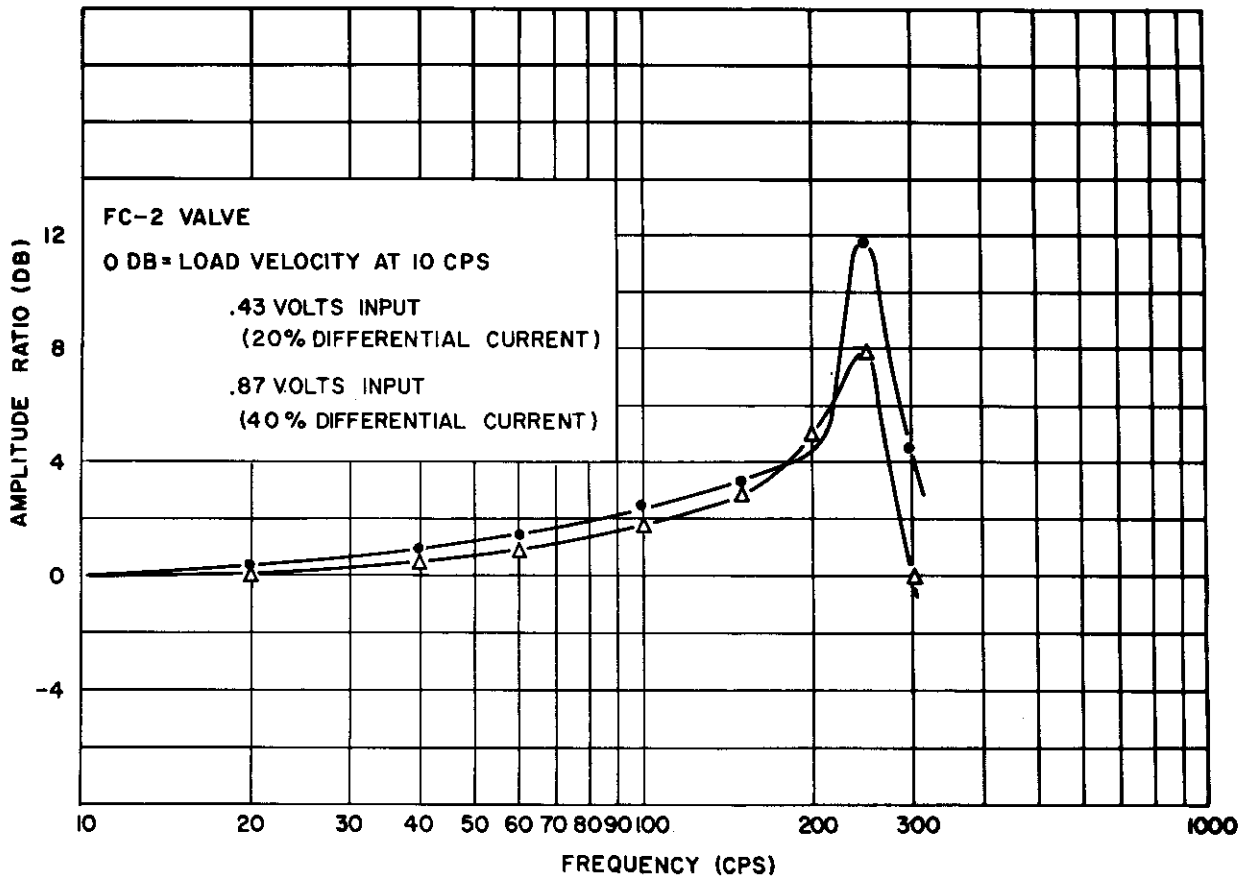
Figure 37. Open-Loop Amplitude Response
for Reference System FC-2 Valve

The closed loop frequency response of the reference control system set up in the hydraulic laboratory and the simulated system set up on the analog computer are shown in Figs. 38, 39, 40 and 41.

Figure 38 compares the 1402C reference system and the analog system for sine wave input magnitudes of 0.5 volt and 2.0 volts. The results compare quite closely in both phase and amplitude for the 0.5 volt input. For the 2.0 volt input, the resonant frequencies are the same; however, the shapes of the amplitude curves before resonance do not correspond closely, differing by as much as 1 db. Phase correspondence is fairly good to 30 cps, then deviates by more than 20 degrees at 60 cps.

Figure 39 compares the two 1402C systems for input amplitudes of 1.0 volt and 3.0 volts. As for the previous amplitudes discussed,
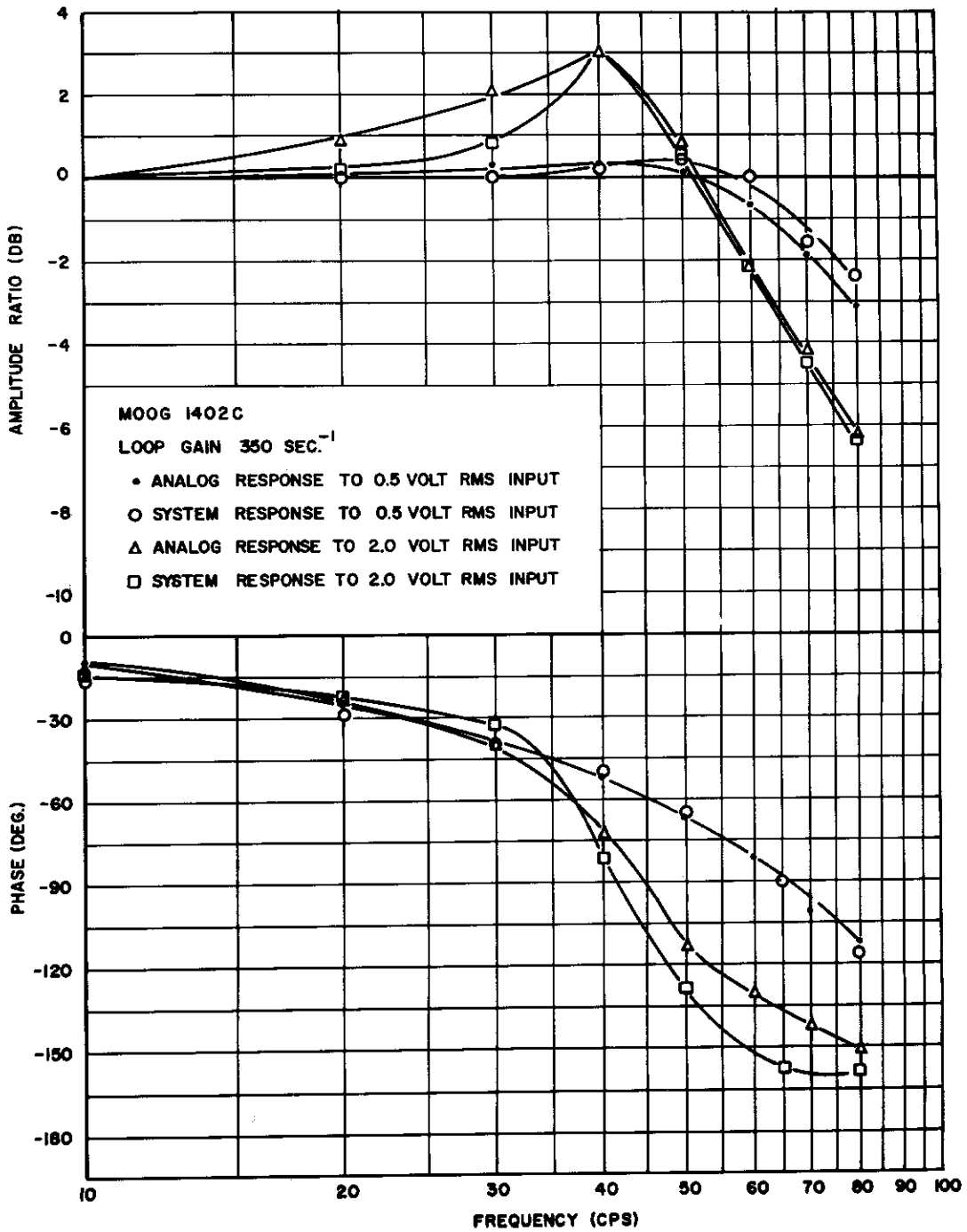
Figure 38. Closed-Loop Frequency Response of Analog and
Reference Systems - 1402C - 0.5 and 2.02 Input
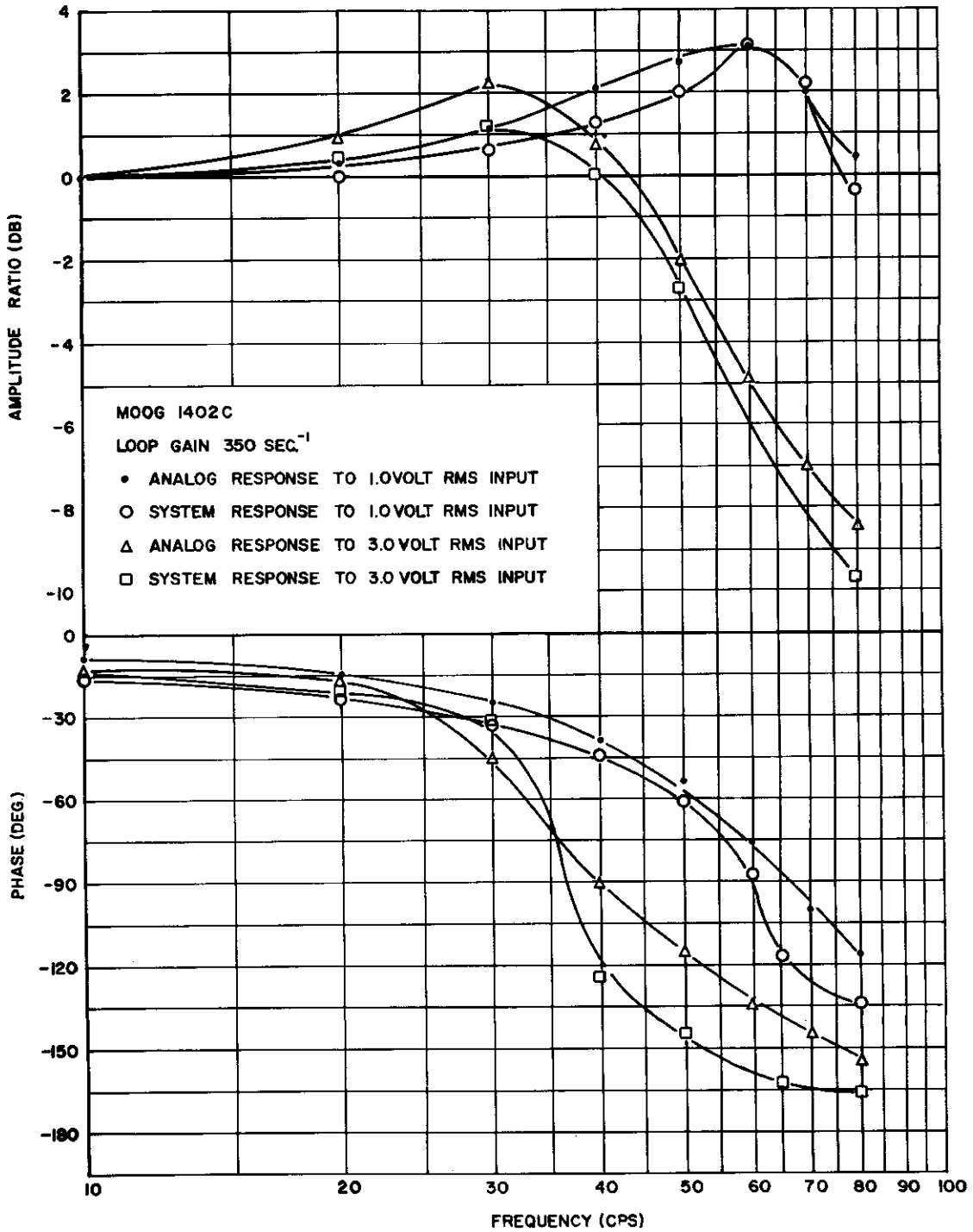
Figure 39. Closed-Loop Frequency Response of Analog and Reference Systems - 1402C - 1.0 and 3.0 Input
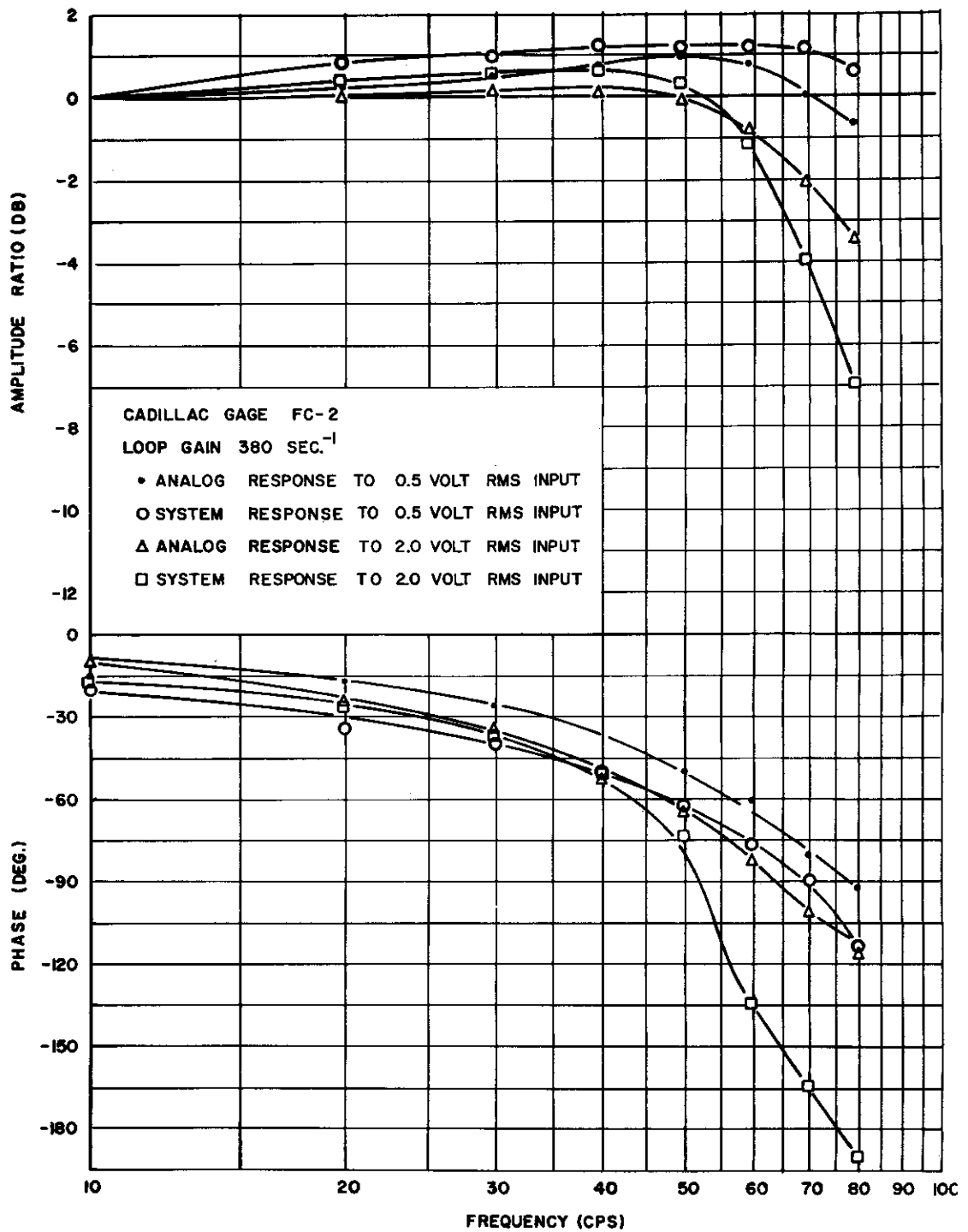
Figure 40. Closed-Loop Frequency Response of Analog and
Reference Systems - FC-2 - 0.5 and 2.0 Input
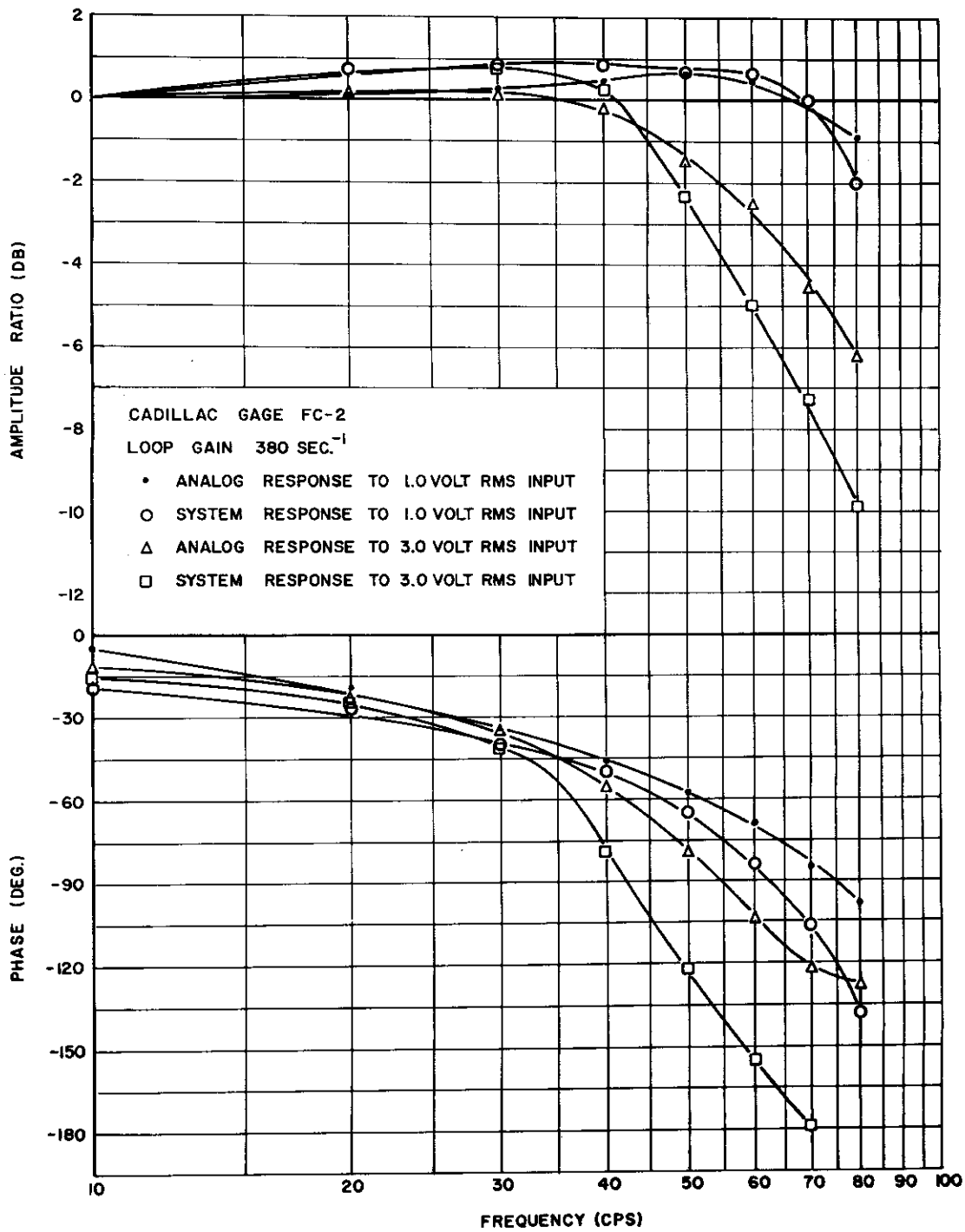
Figure 41. Closed-Loop Frequency Response of Analog and
Reference Systems - FC-2 - 1.0 and 3.0 Input

the resonant frequencies compare favorably, although the general shapes of the amplitude curves differ by a maximum of 1 db. Once again, the phase shows fairly good correspondence to 30 cps, and from there on, agrees only trendwise, differing by as much as 30 degrees.

It is interesting to note that the slopes of the amplitude curves correspond very well beyond resonance, the reason being that the valve has a very high pressure gain and is not influenced greatly by small amounts of coulomb friction. Since the valve's pressure gain was not simulated, the analog output amplitude is not influenced by coulomb friction either, except as damping.

Figure 40 shows the frequency response curves at 0.5 and 2.0 inputs for the two systems employing the FC-2 valve. Both the amplitude and phase curves show less correspondence than did the system using the 1402C valves. The amplitude curves show fair correspondence to approximately 50 cps, after which they deviate rapidly. The phase curves show that the analog system consistently exhibits less phase lag than does the reference system. From an examination of the no-load frequency response characteristics of the FC-2 (see WADC TR 55-29 and Fig. 78) it appears that the no-load characteristics of the valve could be simulated better as a second order lag. This was attempted but resulted in instability at the value of loop gain specified. The valve probably can be simulated better by a second order lag and a lead network. Since no lead compensation was employed in the physical system, this was not tried.

The 1 and 3 volt input curves in Fig. 41 for the FC-2 valve show poor correspondence except at frequencies below 30 cps. Converse to the results with 1402C valve, the slopes of the amplitude curves after the break point fall off much faster with the reference system than the analog system. This is attributed to the fact that the pressure gain of the FC-2 is relatively low and coulomb friction forces the output amplitude to decline rapidly.

From an over-all standpoint, the frequency response results show that the simulation of the system with the 1402C valve was much better than when the FC-2 valve was used.

2.   Transient Response

No attempt was made to obtain the same transient response in both the reference system and the simulated system. The transient responses listed in Figs. 42 through 49 are the transient response of
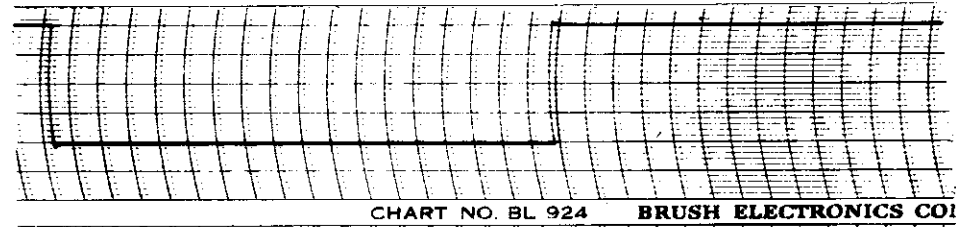
WADC TR 55-29 Pt IV   68

CHART NO. BL 924   **BRUSH ELECTRONICS COMPANY**

OUTPUT DISPLACEMENT

CHART NO. BL 924   **BRUSH ELECTRONICS CO**

DIFFERENTIAL LOAD PRESSURE   **30 PSI/LINE**

PRINTED IN U.S.A.   CHART NO. BL 924   **BRUSH El**

ERROR (DIFFERENTIAL CURRENT)

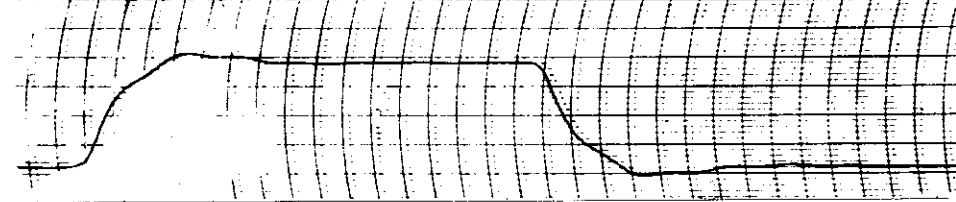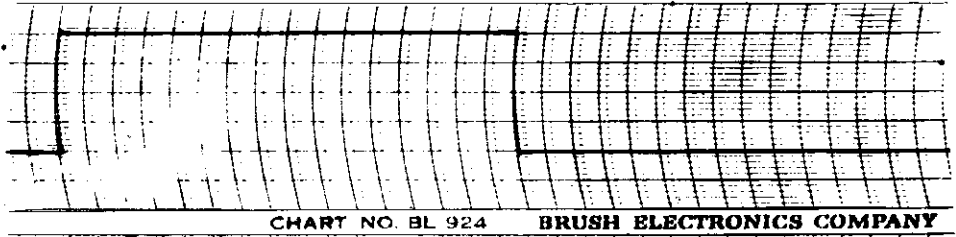**INPUT 0.5 VOLTS**   **LOOP GAIN 350 –**
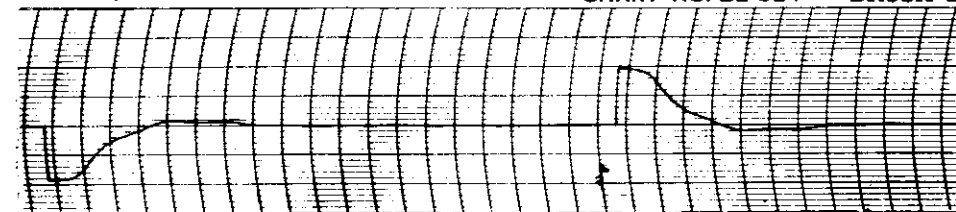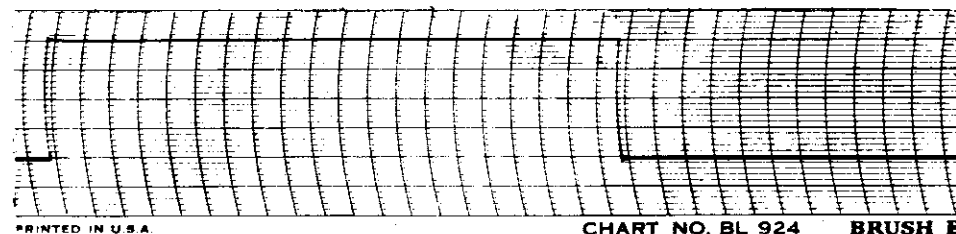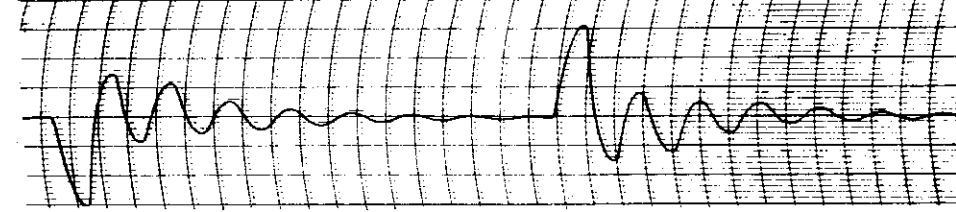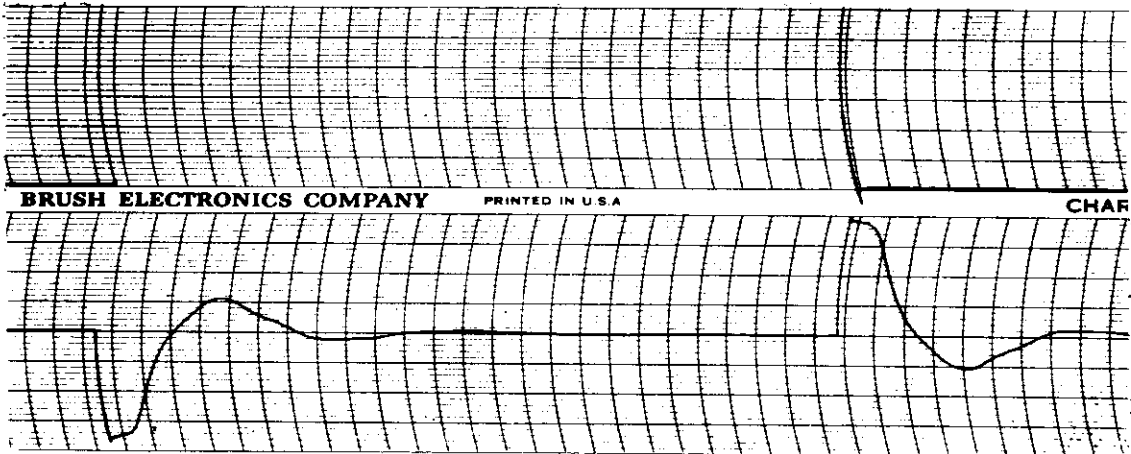
Figure 42.   Transient Response of Analog System - 1402C - 0.5 Input
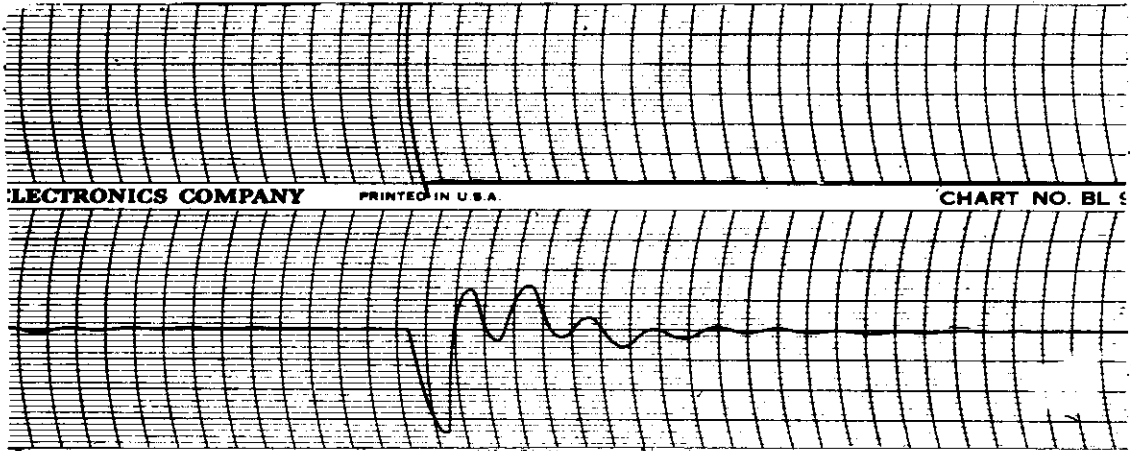
LECTRONICS COMPANY   PRINTED IN U.S.A.   CHART NO. BL S

OUTPUT DISPLACEMENT

LECTRONICS COMPANY   PRINTED IN U.S.A.   CHART NO. BL S

DIFFERENTIAL LOAD PRESSURE   **30 PSI/LINE**

BRUSH ELECTRONICS COMPANY   PRINTED IN U.S.A.   CHAR

ERROR (DIFFERENTIAL CURRENT)

INPUT 1.0 VOLTS   **GAIN 350**

Figure 43.   Transient Response of Analog System - 1402C - 1.0 Input
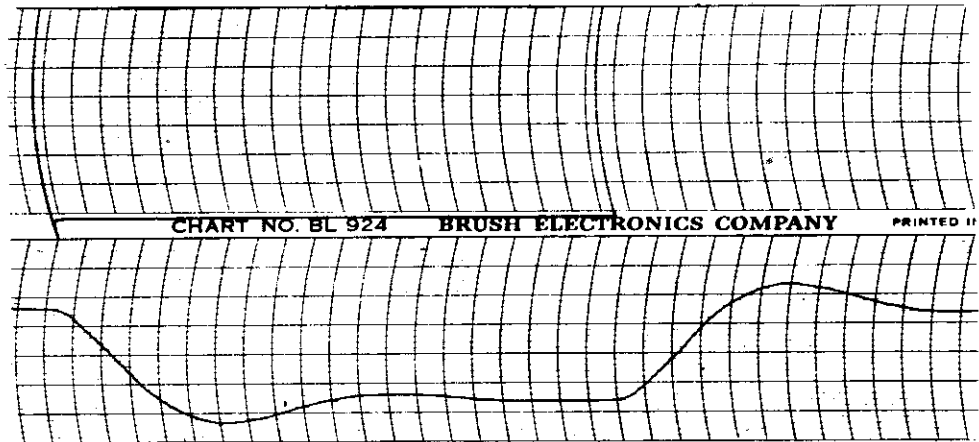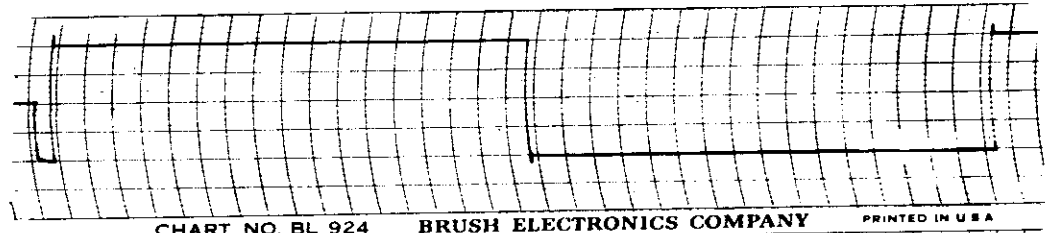
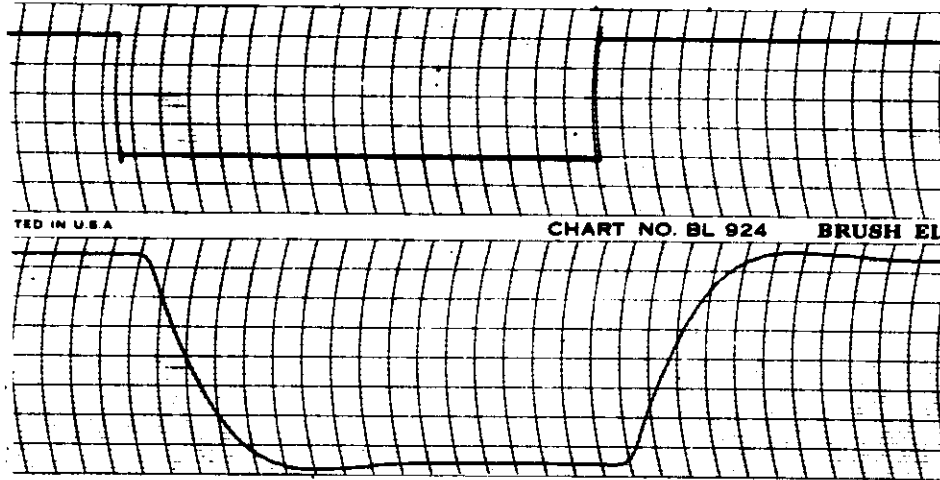OUTPUT DISPLACEMENT
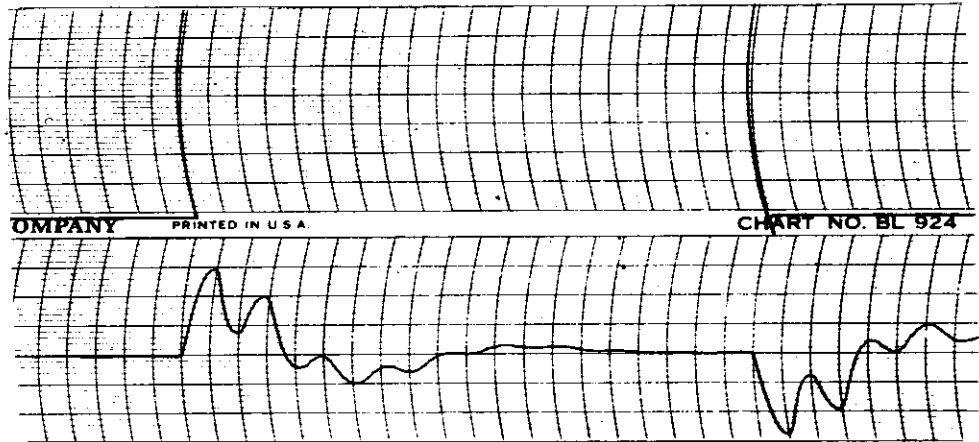
DIFFERENTIAL LOAD PRESSURE   60 PSI/LINE
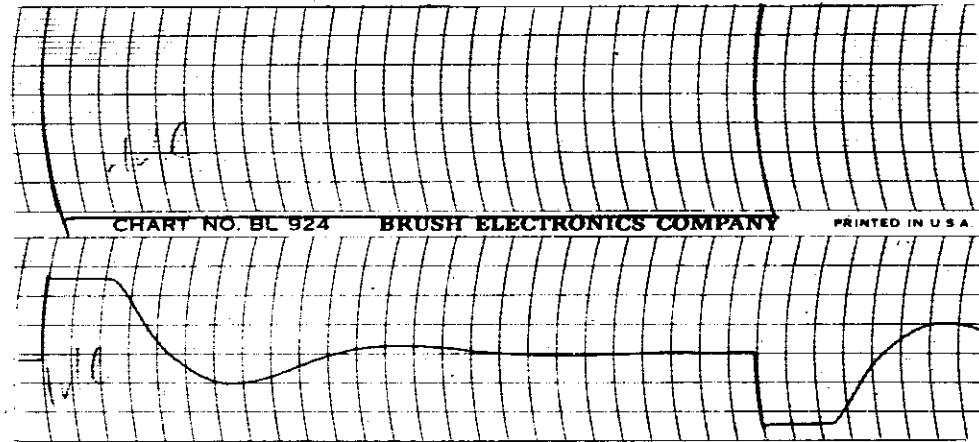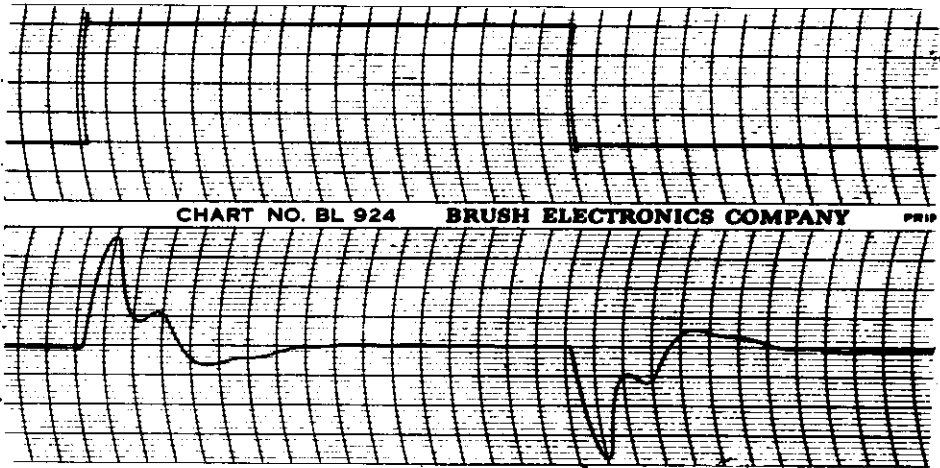
ERROR (DIFFERENTIAL CURRENT)

INPUT 2.0 VOLTS   LOOP GAIN 350

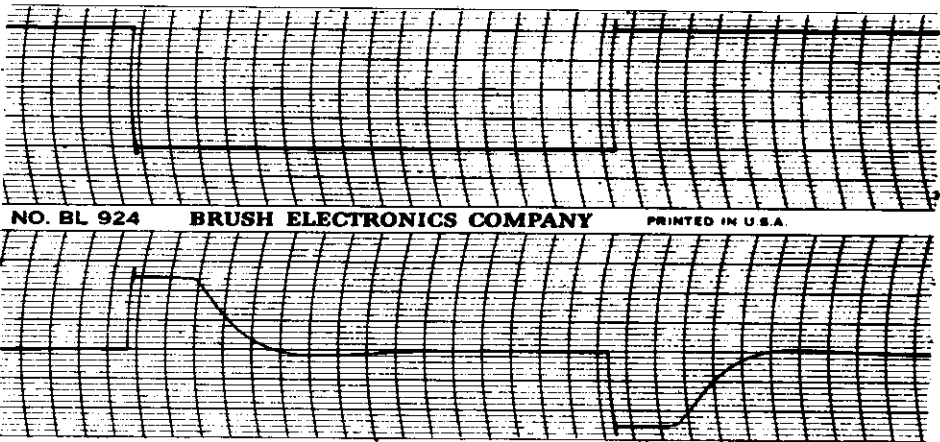Figure 44.   Transient Response of Analog System - 1402C - 2.0 Input

CHART NO. BL 924

OUTPUT DISPLACEMENT

ELECTRONICS COMPANY   PRINTED IN U.S.A.

DIFFERENTIAL LOAD PRESSURE   60 PSI/LINE

CHART NO. BL 924   BRUSH ELECTRO

INPUT 3.0 VOLTS   ERROR (DIFFERENTIAL CURRENT)   LOOP GAIN 350
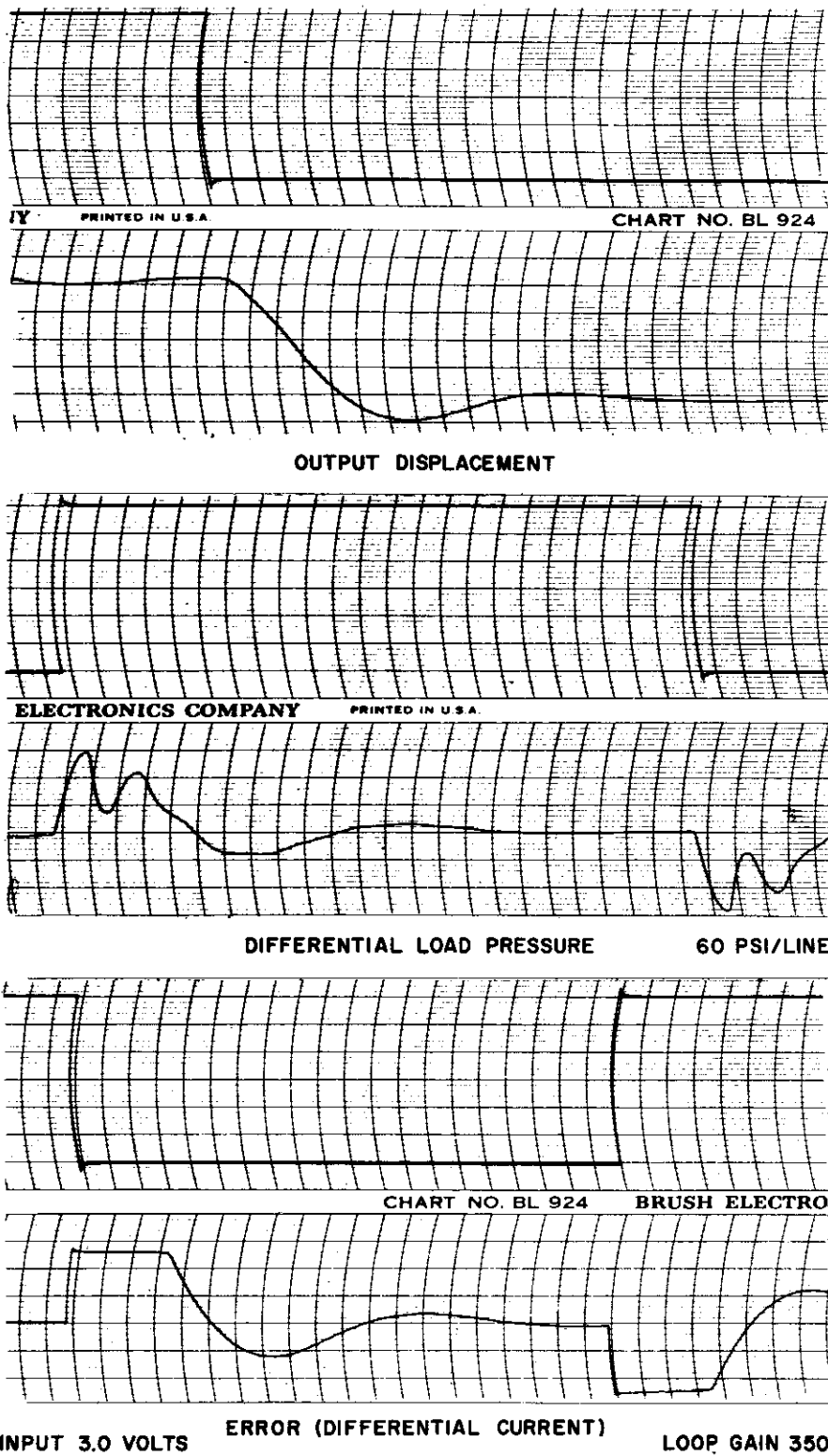
Figure 45.   Transient Response of Analog System - 1402C - 3.0 Input
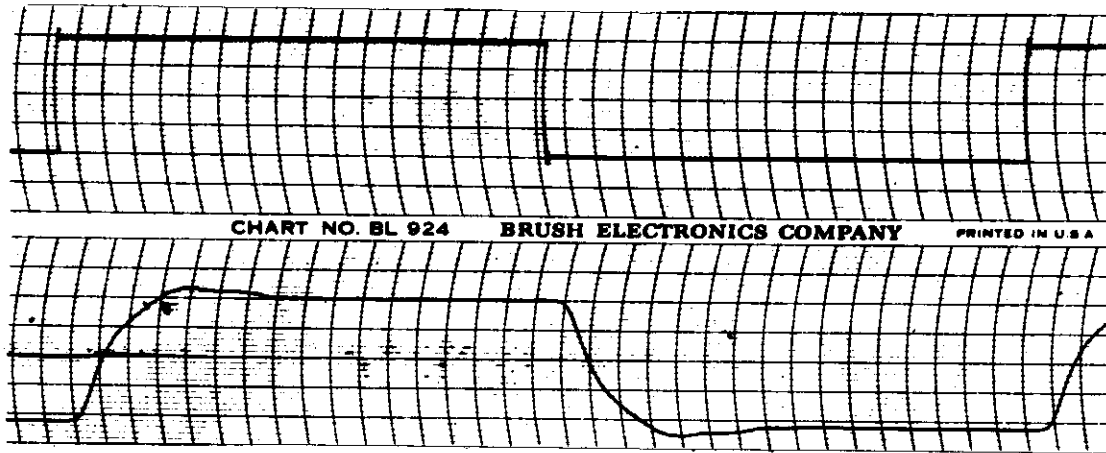
CHART NO. BL 924   BRUSH ELECTRONICS COMPANY   PRINTED IN U.S.A.

OUTPUT DISPLACEMENT
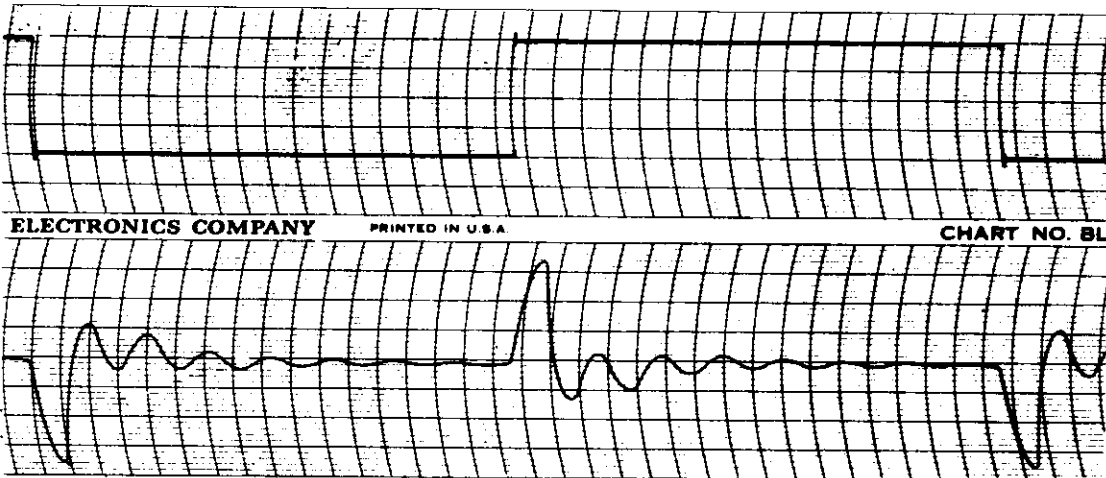
ELECTRONICS COMPANY   PRINTED IN U.S.A.   CHART NO. BL

DIFFERENTIAL LOAD PRESSURE   **30 PSI/LINE**
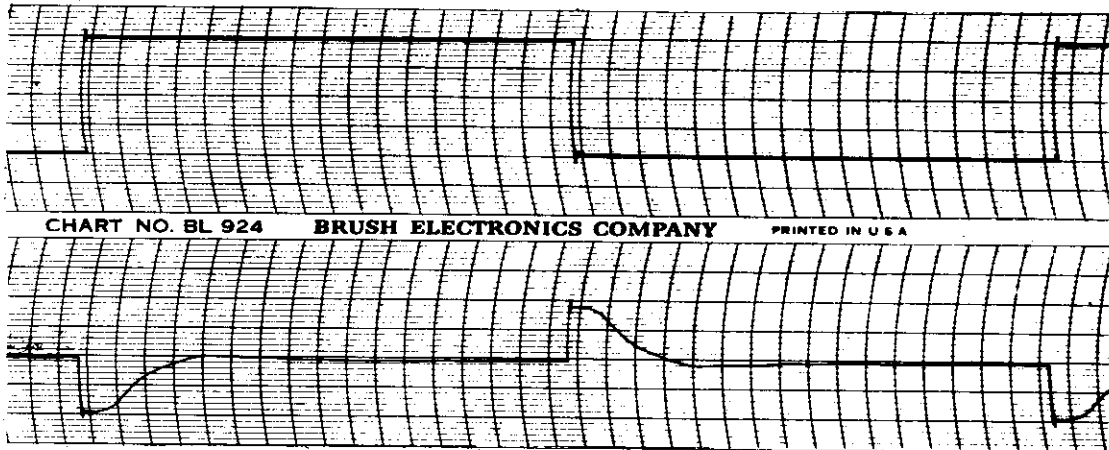
CHART NO. BL 924   BRUSH ELECTRONICS COMPANY   PRINTED IN U.S.A.

INPUT 0.5 VOLTS   **ERROR (DIFFERENTIAL CURRENT)**   **LOOP GAIN 300**

Figure 46.   Transient Response of Analog System - FC-2 - 0.5 Input

BRUSH ELECTRONICS COMPANY   PRINTED IN U S A   CH

OUTPUT DISPLACEMENT

S A   CHART NO. BL 924   BRUSH ELECTRONICS COM

DIFFERENTIAL LOAD PRESSURE   **60 PSI/LINE**

CHART NO. BL 924   BRUSH ELECTRONICS COMPANY   PRINTED IN U S A

ERROR (DIFFERENTIAL CURRENT)

INPUT 1.0 VOLTS   **LOOP GAIN 300**

Figure 47.   Transient Response of Analog System - FC-2 - 1.0 Input

WADC TR 55-29 Pt IV   74

OUTPUT DISPLACEMENT

CHART NO. BL 924   BRUSH ELECTRONICS COMPANY

DIFFERENTIAL LOAD PRESSURE   **60 PSI/LINE**

NO. BL 924   BRUSH ELECTRONICS COMPANY   PRINTED IN U.S.A.

INPUT 2 VOLTS   **ERROR (DIFFERENTIAL CURRENT)**   **GAIN 300**

Figure 48.   Transient Response of Analog System - FC-2 2.0 Input

PANY   PRINTED IN U.S.A.   CHART NO. BL 924   BRUSH E

OUTPUT DISPLACEMENT

S COMPANY   PRINTED IN U.S.A.   CHART NO. BL 924   B

DIFFERENTIAL LOAD PRESSURE   **60 PSI/LINE**

CHART NO. BL 924   **BRUSH ELECTRONICS COMPA**

ERROR (DIFFERENTIAL CURRENT)

INPUT 3 VOLTS   **GAIN 300 .**

Figure 49.   Transient Response of Analog System - FC-2 - 3.0 Input

the analog system with the same parameter values as used for the frequency response test, except for the loop gains. The latter came about because the transient responses had originally been measured at lower gain settings and there appeared to be no reason why the systems could not be compared transient-wise with this gain setting. The loop gain for the analog system had been increased to heighten the resonance amplitudes to facilitate the interpretation of test data.

The transient characteristics of the analog system, as illustrated by the curves in Figs. 42 through 49, correspond fairly closely to those of the reference laboratory system of Figs. 50 and 51. The overshoot amplitudes of the analog system are slightly lower, but damp out about as fast. It is a little difficult to compare the two because of the difference in time scales. While the time axis can be spread out on a brush recorder, which was used to record the analog results, as desired, the time axis of the oscilloscope display, which was employed to record the hydraulic system results, is quite limited. In addition, drift difficulties with the Dumont rack-mounted oscilloscope further complicated the recording and data reduction problem by making the acquisition of clear distinct waveforms difficult.

It is interesting to note from the analog test results, that the system exhibits a considerable amount of dead time (see both output amplitude and error). This is the result of simulating a fourth order system.

The instantaneous peak load pressures were greater for the analog system than for the reference system. The saturation effect shown by the analog error cannot be detected in the oscilloscope traces of the reference system error because of the compressed time scale.

The problem of exactly duplicating the reference system on the analog computer would be considerably more difficult if the transient tests were used as the basis for comparison. This is true since much the same transient response display can be obtained for two systems with different transfer functions by merely adjusting the gain and feedback compensation. The time scale is too short to permit the discerning of waveform differences.

H.   General Conclusions with Regard to Analog Simulation of Valve
Control System

It does not appear that the results of this analog investigation can
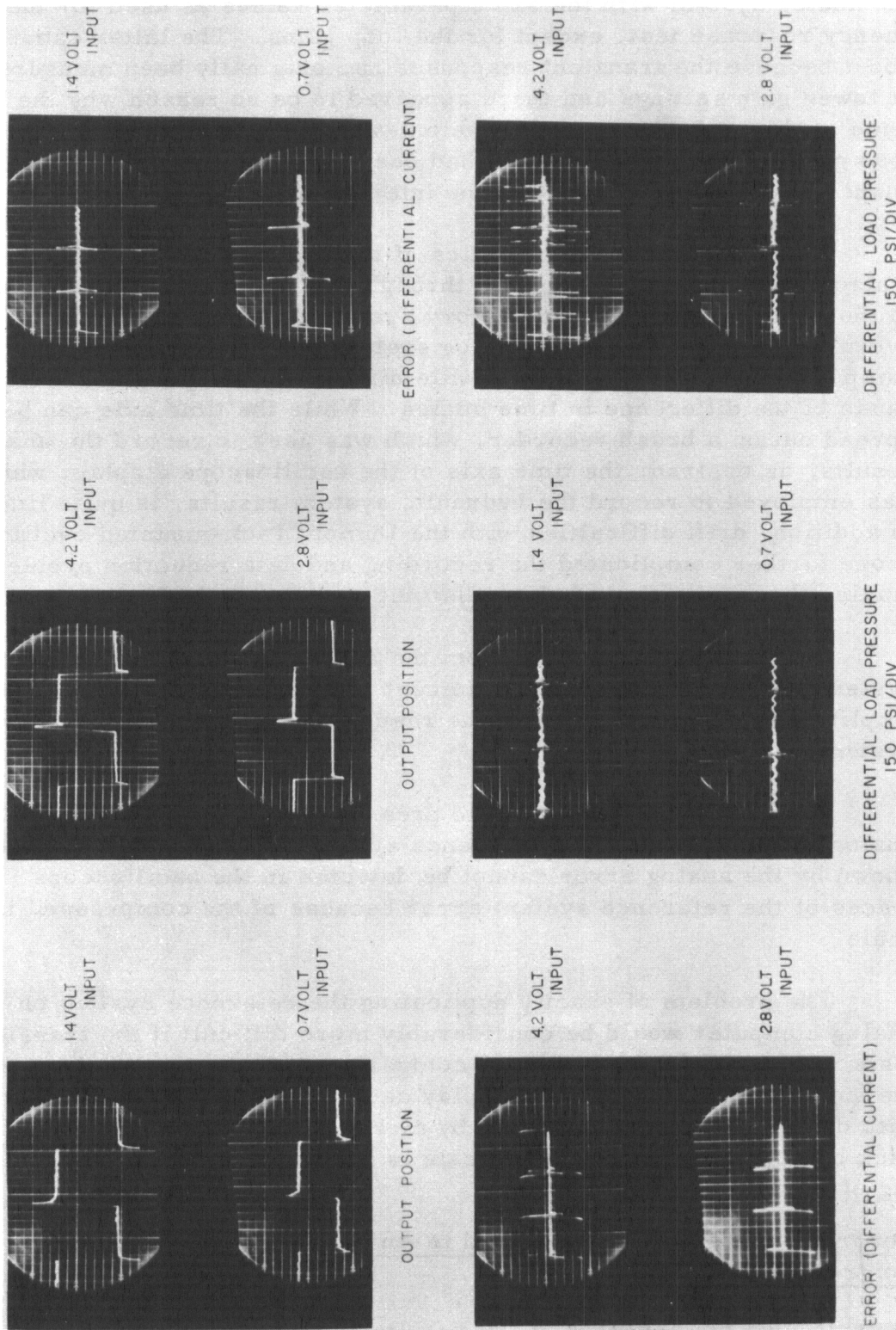
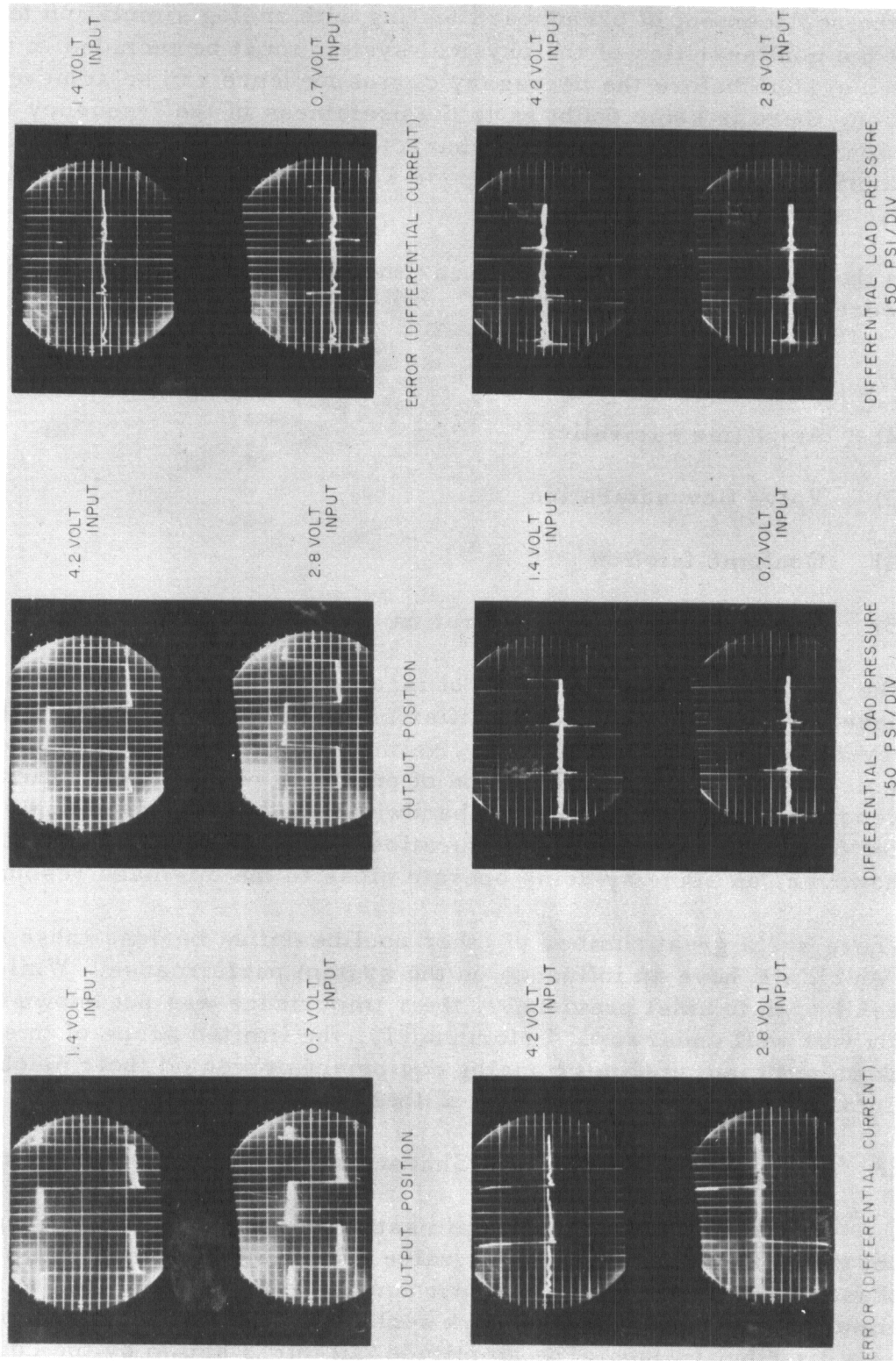Figure 50. Transient Response of Reference System 1402C

Figure 51. Transient Response of Reference System FC-2

justify the replacement of breadboard testing with analog simulation testing. More of the nonlinearities of the physical system must be included in the simulated system before the necessary correspondence can be achieved. In addition, there is some doubt as to the usefulness of the frequency response approach in ascertaining the characteristics of a system containing nonlinearities, primarily because of poor waveform problems and high amplitude sensitivity.

In the present study, five nonlinearities were originally mechanized. These were:

(1)   Pressure flow curves

(2)   Amplifier saturation

(3)   Valve flow saturation

(4)   Coulomb friction

(5)   Valve load pressure saturation.

The valve flow saturation was not incorporated in the final analog setup because it was found that the amplifier always saturated first and therefore prevented valve flow saturation. Neither was valve load pressure saturation mechanized because the region of oil-mass resonance at which this phenomenon occurs, was outside the bandwidth. (See linearized analysis phase for description of pressure saturation.) This will not always be the case, however, as some systems operate close to the oil-mass resonance.

There are a great number of other nonlinearities besides those included which will have an influence on the system performance. While these have been known to exist previously, their importance was not known until the study was well underway. Unfortunately, the limited scope of this study and lack of sufficient nonlinear analog equipment prevented their mechanization into the analog system. Some of these are discussed below.

1.   Variation in the No-load Characteristics with Input Amplitude

It was not possible to obtain satisfactory results utilizing one set time constant for the 1402C valve. Both the amplitude ratio and phase varied so greatly with input amplitude that they could not be simulated by any simple network such as a first or second order lag or a distribution lag. The amplitude fall-off is shown by the curve of

Fig. 52; both amplitude and phase are depicted in Fig. 35.

The FC-2 valve, on the other hand, showed very little output phase variation with input signal amplitude. However, the output flow amplitude fell off considerably at the higher input amplitudes (before amplifier saturation), especially at high frequencies (see Fig. 53). Difficulty was also experienced in duplicating the characteristics of this valve at any one amplitude adequately as discussed in the previous section.

2. Pressure Gain Nonlinearity

Every valve has a certain pressure gain which is related to the output spool orifice laps. Normally, this pressure gain or sensitivity is quite high (at least much higher than for equivalent electrical systems).

In this simulation, the two valves employed had radically different pressure gains, being 85,000 and 10,000 psi/ma, respectively, for the 1402C and FC-2. Now, coulomb friction was found to have only a damping influence on the analog system because pressure sensitivity of both valves as simulated were infinite. In other words, for an infinitesimally small signal, barely exceeding the noise region, the output could reach 3000 psi. This is not true of the physical system. Therefore, when coulomb friction is present, the output force on the load is limited, and for small inputs the output amplitude will fall off rapidly. The 1402C valve had a high enough pressure sensitivity so that the small amount of coulomb friction present in the system did not affect its response a great deal over the frequency range of the tests. Such was not the case for the FC-2 and this is the primary reason that the discrepancies in both phase and amplitude are considerable for the FC-2 at frequencies beyond the break point where output amplitudes are small.

3. Nonlinearity of Flow vs. Differential Current

As stated previously, it was not necessary to simulate valve flow saturation as the amplifier limited the input to the valve before it reached the saturation point. However, one effect which is very important at low amplitudes, and which could not be simulated, is the rounding off the flow vs. differential current curves in the vicinity of null. This reduces the gain at low input amplitudes and provides for slugglish operation. It was for this reason, that no comparison runs
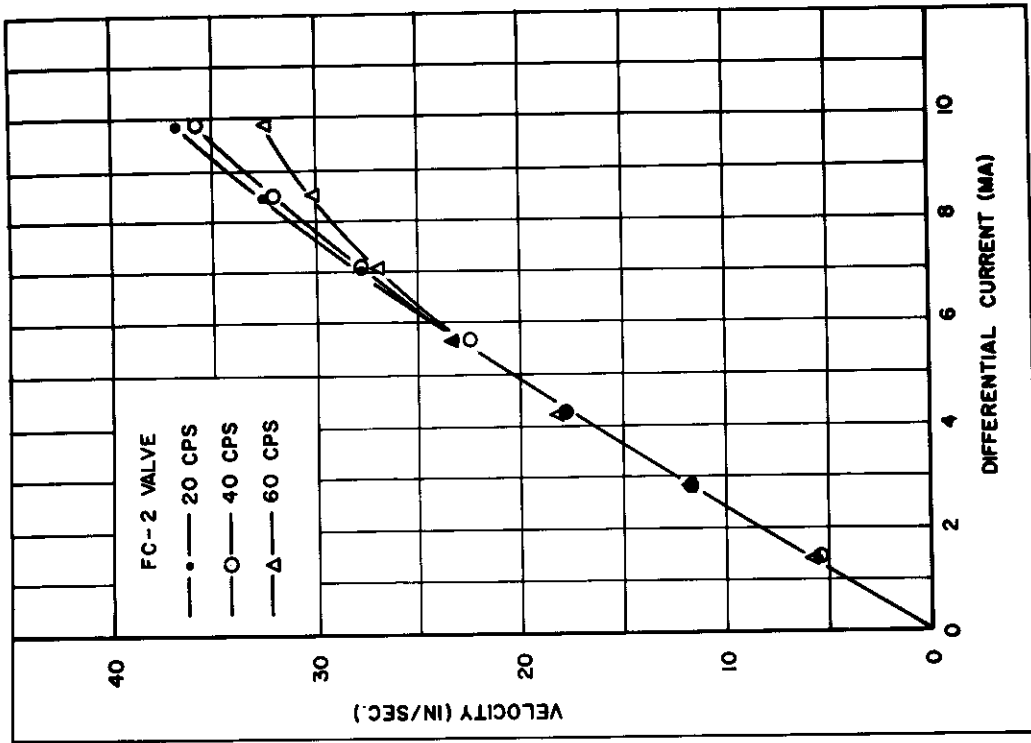
Figure 53. Open-Loop Gain vs. Input
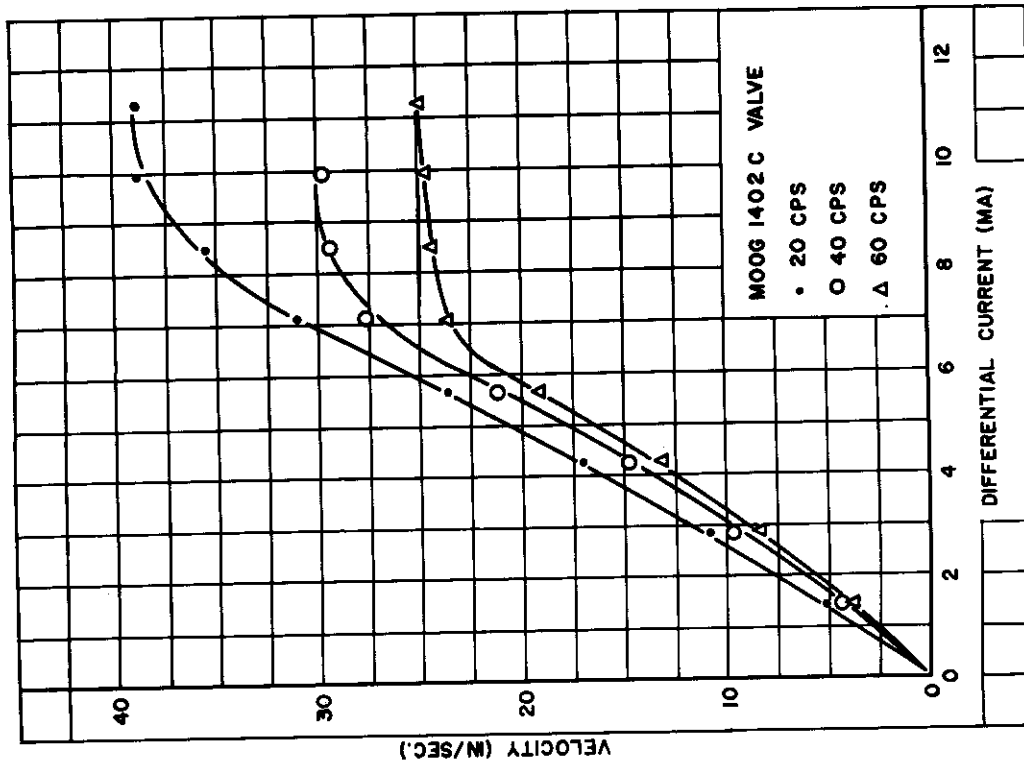Voltage FC-2

Figure 52. Open-Loop Gain vs. Input
Voltage 1402C

were made at very low amplitudes. Even at an amplitude of 0.5 volt runs, the simulated valve gain had to be reduced to take into account this loss in gain. Generally speaking, it is not believed that the non-linearities of the flow curves between the null region and rated current would necessitate their duplication in the simulation as the variance is generally less than 10 per cent.

4.   Variance in Valve Dynamics with Load

This is a nonlinear effect not investigated to date, although it is expected that its influence will not be negligible for large flow spring restrained valves where flow forces are appreciable. This characteristic should be more thoroughly understood when the valve simulation work scheduled for the next program has been completed.

5.   Second Order Nonlinearities

Other nonlinearities which have second order effects on performance are:

(1)   Variation in oil mass resonance due to temperature changes during runs, actuator shaft location, pressure changes, and valve short circuited pressure characteristics

(2)   Variation in viscous damping and leakage with temperature

(3)   Valve null shifts, hysteresis, threshold, etc. effects can be measurable if low loop gains are employed

(4)   In measurement, waveform asymmetry-giving both erroneous rms values and poor phase definition.

Pump piston pulsations were a continuous source of trouble during this study, and others, in which velocity measurements had to be made. While the pulsations did not affect the position waveform noticeably, they did distort the velocity waveforms. Not only did this distortion reduce the validity of rms voltage readings, but it rendered the use of velocity feedback for compensation networks practically useless. Forward compensation networks were also affected, although to a lesser degree. Fortunately, it was not necessary to employ compensation in any form in the reference system to obtain the specified performance.

The amplitude of the pressure pulsations, as measured by the dynamic pressure pickoffs was approximately 300 psi; their frequency was 140 cps. The employment of accumulators in various attitudes near the valve was unsuccessful in reducing the pulsations much below 300 psi. In actual system operations, the magnitude of these pulsations should be maintained well under 100 psi.

Noise emanating from the feedback potentiometers also presented some problems. The wear rate of the potentiometers was extremely rapid, especially for small amplitude inputs creating noise and causing gain variations. Three types were used, all giving unsatisfactory results; two of those were wire wound and one was made of conducting plastic. The latter was particularly noisy, even immediately after installation. These problems add further weight to the results of the survey phase, where it was found that pickoffs are one of the greatest sources of noise in control systems.

CHAPTER V

VALVE TEST PHASE

A. Purpose

The valve test phase represents a continuation of the valve tests initiated in the previous reports (WADC Technical Report 55-29, Parts I and II.) The purpose of the test phase of this project was to evaluate valves incorporating new and promising design concepts.

In general, the test procedures used in the evaluation of the valves selected were essentially those of WADC Report 55-29, Part II.

The following is a list of the tests conducted; a discussion of the purpose for these tests along with the actual procedures used is contained in the above referenced report.

(1)   Electrical tests

    (a)   DC resistance

    (b)   Inductance

    (c)   Q (quality factor)

(2)   Hysteresis test

(3)   Quiescent flow test

(4)   Load differential pressure vs. differential current at zero load flow test

(5)   Short circuited load pressure vs. differential current test

(6)   Servo valve load flow vs. differential current test (load pressure as a parameter)

(7)   Servo valve flow vs. differential current test (differential current as a parameter)

(8)   Null shift vs. supply pressure

(9)   Null shift vs. temperature test

(10)   Dynamic no-load frequency response test.

B.   Valves Selected

Many of the valves originally considered for test purposes were not purchased because they were not far enough along in their development to insure reliable or informative results. It is anticipated that at least some of those valves will be chosen for tests in the next valve test study program.

The following valves were selected for evaluation:

(1)   Moog 2074

(2)   Bendix Pacific HR-9

(3)   Weston Hydraulics, Ltd. 15690-1.

The Moog 2074 was selected because of its dry torque motor construction, which differentiates it from previous Moog valves.

The HR-9 was selected because of its unique first stage construction and the many favorable reports received on the valve from users.

The Weston was chosen at the request of WADC late in the program. It has a unique feedback arrangement.

Originally a Pegasus Servo Valve Model No. 20 had also been selected for evaluation. However, Pegasus was unable to deliver the valve in time and the status of the valve at the time of this writing is uncertain.

The tests results of the modified Bell SV-6C are also in this report, although the valve was tested during the last week of the previous program reported in Part II.

C.   Description of the Valves

The following is a description of each of the valves tested during this study and also a description of the Modified Bell SV-6C.

1.   Moog 2074

The Moog 2074 (see Fig. 54) is a two stage valve with a double
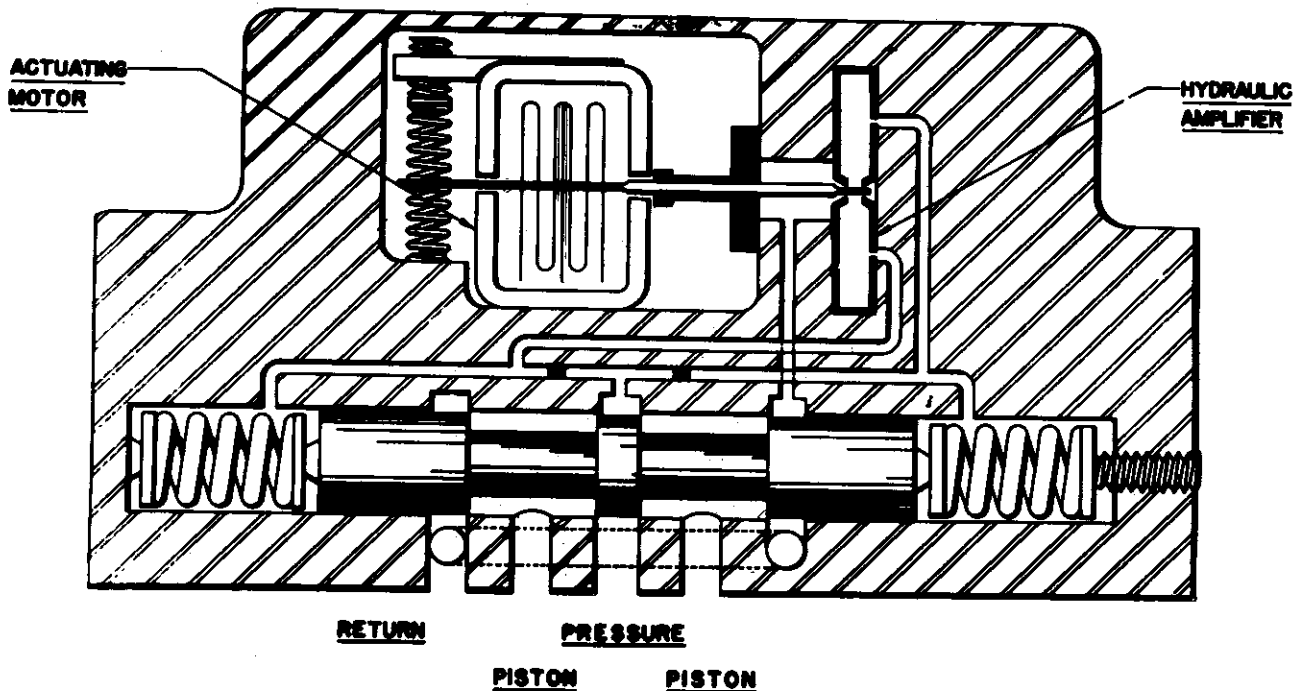
Figure 54.   Schematic of Moog 2074 Valve

nozzle flapper first stage driving a spring restrained spool output stage.   The second stage is similar to other model Moog valves. The first stage, however, is distinguishable from previous models because the coils are hydraulically isolated from the nozzles by a sealing tube.   This sealing tube acts as a flexure pivot for the armature flapper.   The dry torque motor design eliminates the requirement for magnetic traps.

2.   Bendix Pacific HR-9

The Bendix Pacific HR-9 (see Fig. 55) is a two stage servo valve utilizing a double nozzle flapper first stage to drive a spring restrained output stage.   The design of its first stage is unique in

that the two nozzles both face in the same direction (upward) rather than toward each other, and the flapper is positioned to float above them. According to theory, this construction permits the flapper to move a greater distance from the nozzles than in other designs, permitting larger particles of dirt to be washed to drain without clogging the valve.

Additional protection to aid in the prevention of dirt clogging is provided by a 5 micron filter ahead of each nozzle. The valve has an all steel body with hardened steel inserts. The torque motor is not isolated from the drain oil.
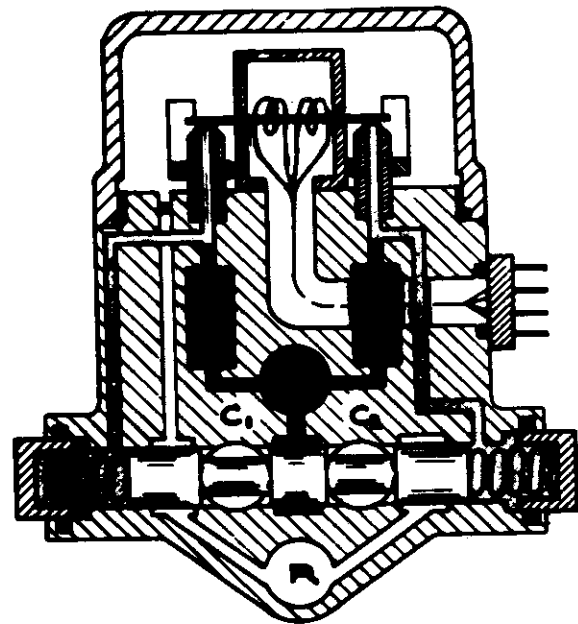
Figure 55. Schematic of Bendix Pacific HR-9 Valve

3. Weston Hydraulics, Ltd. 15690-1

The Weston Hydraulics, Ltd. 15690-1 (see Fig. 56) is a two stage, dual nozzle flapper, dry coil type valve with force feedback between stages. The force feedback is accomplished by effectively extending the flapper down to the spool where it is restrained by two springs attached to the spool. When a differential current is applied to the torque motor, the flapper is moved, creating a differential pressure across the spool. The spool moves
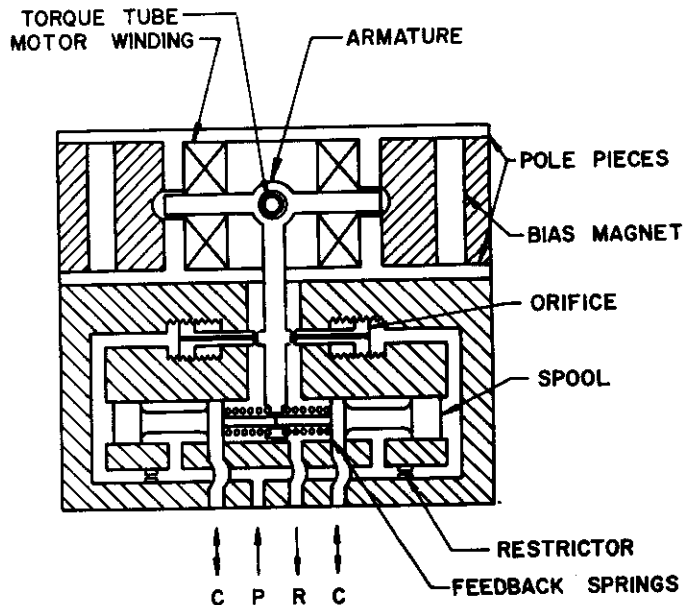
Figure 56. Schematic of Weston Hydraulics, Ltd. 15690-1 Valve

until a force is developed by the restraining springs on the flapper which is equal and opposite to the force applied by the torque motor, thus nulling the flapper. In this design, the spool movement is limited by a factor equal to the flapper displacement at the nozzles, times the ratio of the distance between the flapper pivot and the reaction point of the restraining springs to the distance between the pivot and the nozzle. Another interesting feature of this valve is that the nozzles consist of threaded inserts that are positioned in relation to each other, and to the flapper, by screwing them into the body of the valve.

4.   Bell SV-6C Modified

The Bell SV-6C valve (modified) (see Fig. 57) is a two stage valve with a nozzle flapper first stage driving a spring restrained output stage. The valve's torque motor is isolated from the oil flowing through the nozzles. The valve is constructed with hardened stainless steel sleeve, spool and centering springs. The sleeve is floated on O-rings in an aluminum body.

D.   Summary of Test Results

The four valves tested and described above are shown in Fig. 58. The test results are presented in graphical form in Appendix I. The data contained in these curves are summarized in Tables 5, 6 and 7 of this section. In these tables, average values are generally presented since most of the curves are unsymmetrical and nonlinear. Where a high degree of accuracy is required, the graphical presentations should be utilized.
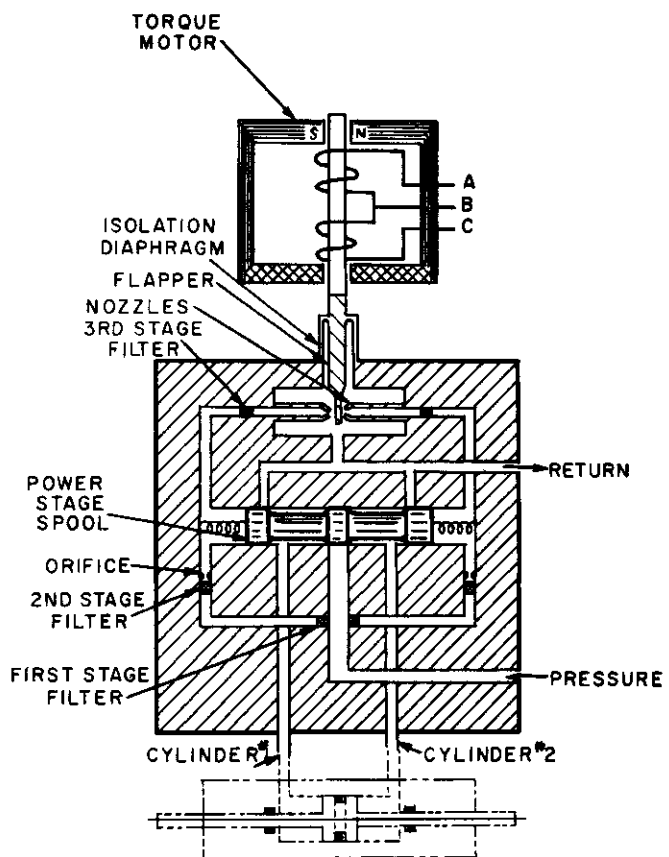
Figure 57.   Schematic of Bell SV-6C (Modified) Valve

Table 5 summarizes the static hydraulic tests. Table 6 presents the results of the dynamic no-load tests. Table 7 lists the electrical characteristics of the valves.

The following is a brief description of the column heading found in Table 5 where such headings are not self-explanatory.
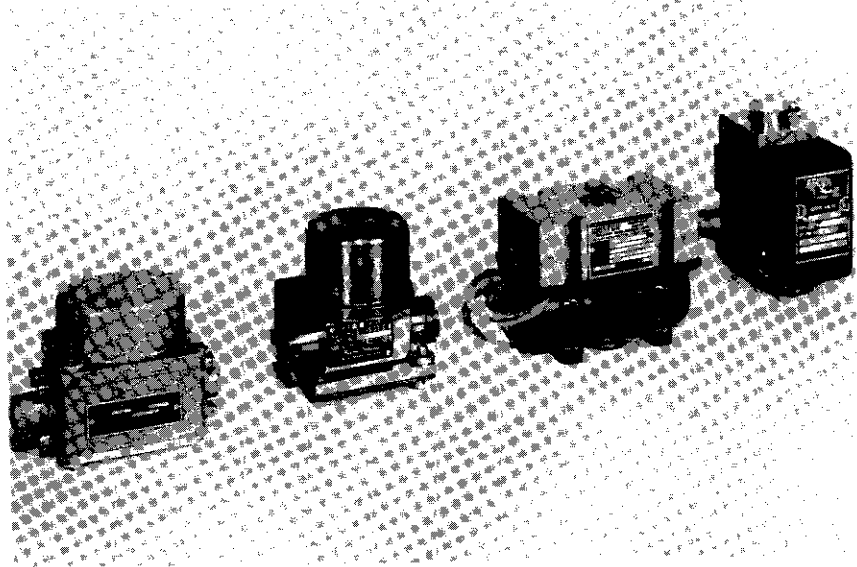
Figure 58. View of Valves Tested

1. Rated Flow

This represents the flow at rated current and supply pressures of 2000 psi and 3000 psi, with a load pressure drop of two-thirds supply pressure. These are the flows and pressures at which the valves are normally rated. The data were taken from the flow vs. differential current curves.

2. Maximum/Minimum Load Pressure

This was obtained from the short-circuited load pressure vs. differential current curves. It is the value of pressure at the pressure null (or antinull).

3. Range of Null Shift vs. Temperature

This represents the total extent of the null shift over the temperature range of 100°F to 200°F to 100°F.

4. Range of Null Shift vs. Pressure

This represents the total extent of the null shift over the pressure range of 3000 psi to 1500 psi to 3000 psi.

5. Per Cent Hysteresis

This represents the ratio of the envelope width along the

differential current axis to the total rated current.

6.   Flow Gain

This represents the average slope of the flow vs. differential current curves at a point in between the null zone and flow saturation zone.

7.   Pressure Gain

This is the slope of the load pressure vs. differential current (at zero load flow) curves. The slope is taken in the vicinity of minimum differential load pressure.

8.   Leakage, First Stage

This represents the asymptotes parallel to the differential current axis at the extremities of quiescent flow vs. differential current curves.

9.   Leakage, Total

This represents leakage at the null point of the quiescent flow vs. differential current curves. It is a composite of the first stage quiescent flow and the second stage leakage.

E.   Analysis of Test Results

In this section, each valve will be analyzed from the standpoint of the static test results, the dynamic test results, and general operating characteristics.

1.   Moog 2074

    a.   Static Test Results

As with other Moog valves previously tested, the hysteresis of this valve is very low, being less than 2 per cent. The valve is not gain compensated to any degree, being a low flow valve. As discussed in previous reports, low flow valves are not readily gain compensated because to have them so requires the reduction of the first stage gain to the point where stiction and null shift effects become detrimental.

TABLE 5 STATIC TEST RESULTS

	Rated Flow (gpm)		Mfrs. Rated Current (ma)	Min/Max Load Pressure psi	Range of Null Shift vs. Temp. (ma)		Range of Null Shift vs. Pressure (ma)		% Hysteresis 3000 psi	
	2000 psi	3000 psi			Dither	No Dither	Dither	No Dither	Dither	No Dither
Moog 2074	3.6	4.6	8	1100	0.78	1.02	0.43	0.52	0.93	1.7
Bendix HR-9	2.9	3.6	8	2300	0.054	0.095	0.02	0.23	1.45	1.7
Weston 15690-1	0.43	0.53	8	1900	0.050	0.091	0.007	0.011	7.0	9.0
Bell SV-6C	4.5	5.4	8	440	0.55	0.80	0.72	0.74	-	-

	Flow Gain (gpm/ma)						Pressure Gain psi/ma		Leakage (gpm)			
	3000 psi			2000 psi					First Stage		Total	
	No-Load	1000 psi Load	2000 psi Load	No-Load	1000 psi Load	1330 psi Load	3000	2000 psi	3000 psi	2000 psi	3000 psi	2000 psi
Moog 2074	0.90	0.81	0.62	0.66	0.53	0.48	400,000	25,000	0.056	0.044	0.320	0.22
Bendix HR-9	0.67	0.60	0.58	0.56	0.49	0.39	17,000	12,000	0.056	0.040	0.176	0.110
Weston 15690-1	0.10	0.069	0.047	0.070	0.050	0.041	12,500	8,000	0.13	0.098	0.16	0.12
Bell SV-6C	1.06	0.87	0.72	0.84	0.69	0.53	5,000	2,700	0.10	0.08	0.32	0.22

TABLE 6 DYNAMIC TEST RESULTS - NO LOAD

NO-LOAD FREQUENCY RESPONSE

Servo Valve Model and Manufacturer	20% Rated Diff. Current			60% Rated Diff. Current			100% Rated Diff. Current		
	Freq at -3 db (cps)	Freq at 90° (cps)	Phase Shift at -3 db (degrees)	Freq at -3 db (cps)	Freq at 90° (cps)	Phase Shift at -3 db (degrees)	Freq at -3 db (cps)	Freq at 90° (cps)	Phase Shift at -3 db (degrees)
Moog 2074	100	100	90	78	90	84	47	75	72
Bendix HR-9	>300	>100	>60	120	>100	>60	77	>100	48
Weston 15690-1	35	81	47	50	100	50	55	100	55
Bell SV-6C (Mod.)				60	180	35			

TABLE 7 ELECTRICAL CHARACTERISTICS

Valve Type & Rated Differential Current		Inductance & Q at 1000 cps With Designated Percentages & Polarities of Differential Current in Each Coil										Inductance, Resistance With No Quiescent Current		Resistance to Case from Electrical Input Terminals			
		0%		100%		-100%		+50%		-50%				A	B	C	D
		L	Q	L	Q	L	Q	L	Q	L	Q	L	R				
Moog 2074	Coil 1	0.183	2.5	0.242	1.71	0.170	1.52	0.255	1.81	0.199	1.67	0.197	234.5				
	Coil 2	0.173	2.7	0.234	1.70	0.180	1.50	0.252	1.80	0.185	1.62	0.185	163.5				
Bendix HR-9	Coil 1	0.599	1.97	0.837	2.93	0.432	1.88	0.698	2.24	0.515	1.80	1.16	880	All resistances measured at least 10^9
	Coil 2	0.611	2.02	0.856	2.88	0.465	1.75	0.718	2.32	0.518	1.82	1.18	875				
Weston 15690-1	Coil 1	3.01	2.9	3.05	3.1	2.80	2.2	3.05	3.0	2.85	2.8	4.45	1220				
	Coil 2	5.09	3.35	4.40	4.7	4.48	2.01	4.83	4.0	4.7	3.1	11.5	1220				

Note: Resistance to Case from Electrical Input Terminals (A B C D) — All resistances measured at least 10^9

The output flow vs. differential current characteristics of the Moog 2074 are peculiar in that the slope of the curves is increasing at rated current rather than tapering off. While this characteristic is not particularly undesirable, Moog has experienced some difficulty in attaining more linearity, without compromising response.

The quiescent flow of the first stage is comparatively low (0.05 gpm) while the total leakage is high. It is believed that the relatively large leakage of the output spool may have been included for stabilizing purposes.

This valve exhibited relatively large null shifts when the oil temperature was varied. This has been the characteristic of all dry torque motors tested and is one of the disadvantages of employing the dry torque motors designed to date. These null shifts result from the condition when the environment is different on the two sides of the isolating flexture pivot, thus creating unbalanced forces on the seal and flapper at different temperatures.

As with previous Moog valves tested, this valve exhibited a greater pressure drop at the load inlet orifices than at the load drain orifices. The minimum no-load pressure was of the same order as previous Moog valves tested. The pressure gain was exceptionally high, being 400,000 psi/ma.

b.   Dynamic Test Results

The Model 2074 valve exhibited poorer dynamic response than the standard "wet" torque motor Moog valves tested previously, even though this was a lower flow valve, once again illustrating the problems of using dry torque motors. This valve exhibited the best dynamic characteristics at low values of differential current inputs. At 20 per cent of rated differential current input, the -3 db point occurred at a frequency of 100 cps and a phase shift of 90 degrees.

c.   General Operation

When the valve was originally received from Moog Valve Company it exhibited a very nonlinear flow vs. differential current characteristics, and in addition exhibited a low

frequency oscillation. The nonlinearity of the flow curve resulted from a condition where the first stage null had drifted (or had not been adjusted properly during manufacture) so far from the electrical null that adjustment of the output stage null could not compensate for it. The valve was returned to the factory where these conditions were corrected.

The valve exhibited a relatively unstable null condition which made the leakage and pressure gain tests difficult to perform. In general, its operational characteristics were inferior to those of the standard types of Moog valves, although still acceptable for most applications.

2.   Bendix HR-9

a.   Static Test Results

This valve had a very low amount of hysteresis, being less than 2 per cent. It exhibits very little gain compensation.

The valve exhibits a very linear flow vs. differential current characteristic, having no flow saturation at 3000 psi and very little at 2000 psi supply pressure. In addition, the curves are very symmetrical. The quiescent flow of the first stage and leakage of the output spool are relatively low, being approximately 0.05 gpm and 0.12 gpm, respectively.

The pressure gain of the valve is about average. This, in conjunction with the low leakage, indicates that the spool orifices are slightly overlapped.

The stability of the valve around null is very good, being comparable to the standard Moog valves. It also exhibits low null shifts when both supply pressure and oil temperatures are varied. In this particular model, the load orifices on the drain side were more closely lapped than those on the supply side.

b.   Dynamic

The no-load frequency response of the valve was the best of any valve tested to date, although only slightly better than the Moog 942 valve tested previously. Because of difficulties with waveform and the TIC phase meter, no phase measurements

could be made beyond 100 cps. The -3 db point of the gain curve occurred at a frequency of 300 cps. The phase shift at 100 cps was less than -45 degrees for both the 20 per cent and 60 per cent rated inputs.

c.   General Operation

The Bendix HR-9 performed exceptionally well in every respect and gave no difficulty during testing. As mentioned earlier, the null was quite stable, facilitating the performance of leakage and pressure gain tests.

The valve was received with the spool positioning screws tied with lockwire. It was the laboratory's policy not to break any lockwire seals on the valve until all tests had been completed. Therefore, no null adjustments were made on this valve. Consequently, the valve was operated in a somewhat unbalanced manner as can be seen by inspecting the flow vs. differential current curves.

3.   Weston 15690-1

a.   Static Test Results

The Weston valve exhibits an extremely large amount of hysteresis. It is of the order of four to five times greater than the hysteresis of the other valves. It is doubtful that this much hysteresis could be tolerated in a high response control system.

The output flow of the valve is quite low, being of the order of only five times greater than the total leakage flow. The latter is rather high for this size of valve.

The flow vs. differential current characteristic of this valve is quite symmetrical and exhibits no saturation. The low gain null region consumes a sizeable portion of the total operating range because of the relatively high leakage compared to the output flow.

This valve employs force feedback between the output stage and first stage and therefore, should have good null shift characteristics. The test results confirmed this; the null shifts for both supply pressure and temperature variations

were lowest of all the valves tested. The pressure gain of the valve is about average being around 12,500 psi/ma.

In this particular valve, the load drain orifices have a larger pressure drop than the pressure input orifices. The short circuited pressure at pressure null is 1900 psi.

b. Dynamic Test Results

The valve exhibits its best dynamic response when the input signal amplitude is 60 per cent rated differential current. At this input, the -3 db point occurs at 58 cps. The 20 per cent and 100 per cent amplitude curves reach the -3 db point at 35 cps and 48 cps respectively. This response is considerably lower than that of the other valves tested. It appears that the torque motor is the limiting element in the valve performance, as the high hysteresis and low dynamic performance are to a large extent a function of the torque motor characteristics. Response curves provided by Weston for this valve when tested at the factory showed slightly better dynamic performance than was attained in our tests.

c. General Operation

There is no readily available method of adjusting the null of this valve, and, therefore, the nulls on the graphs do not correspond exactly to the zero differential current point.

This valve was designed primarily for a stabilization augmentation system wherein only a small amount of load flow is required. The valve exhibited quite stable operational characteristics and presented no difficulty during test.

4. Bell SV-6C (Mod.)

a. Static Test Results

As the name implies, this valve is the SV-6C valve tested during the previous program which was modified by Bell to conform to a later design. This valve exhibits a more linear flow vs. differential current characteristic than the original version and has very little flow saturation at full rated current input.

The null of the valve is quite broad and flat, indicating that the output spool is overlapped. It is our understanding that this valve has the same output spool as the original unit. However, this valve exhibits much greater leakage, possibly indicating wear of the pressure and drain control orifices during the modification.

The pressure gain of this valve is very low, probably due to the high leakage rate in conjunction with the overlapped orificies. This valve might present problems in controlling a load with an appreciable amount of friction.

The valve exhibits large null shifts when both oil temperature and supply pressure are varied, probably because of its dry torque motor design. None of the valves employing dry torque motors that have been tested to date have exhibited stable null characteristics.

On this particular valve, the pressure drop is greater on the supply orifices than the drain orifices, providing a low load pressure at null. This could present oil compressibility problems. The pressure-flow characteristics of the valve are nearly parabolic.

b.   Dynamic Test Results

The valve exhibited very good no-load frequency response. Only one run was made at 60 per cent. The 3 db point occurred at a frequency of 60 cps and a phase shift of 35 degrees. The dynamic performance of this valve was improved over that of the previous version by changes in the torque motor, indicating once again that most dynamic limitations occur there.

c.   General Operation

The valve operated very satisfactorily until after the null shift tests, when the flapper developed a permanent set. Since all the tests except the hysteresis test had been completed, the valve was not returned for repair. The problem of flapper offset also occurred with the previous version; no similar incident has been experienced with any other valve.

Before it became defective, the valve operated in a very stable manner.

F. Conclusions

Generally speaking, the Bendix HR series valve performed as well and in some instances better than the standard Moog valves tested during the previous contract. Of course, this is only one valve against a considerable number of Moog valves that have been tested at this laboratory with comparable performance.

The dry torque motor valves tested to date have not been able to match performance either statically or dynamically, with the "wet torque motor" valves. It is possible that many of the future designs will utilize the "stale" (stagnant oil) torque motor feature where the environment on either side of the seal is more nearly matched to minimize null shift problems. To our knowledge, none of these valves are available commercially as yet, although several companies are working on development of this type of valve.

The Weston valve, which employs feedback between the output and first stages, exhibited lower null shifts than did the three valves with spring restrained output stages. However, its performance did not match theirs in most other respects. It is, of course, realized that the valve is still undergoing development.

One aspect which has not been covered in this report is the variance in dynamic test results with different test equipment and different mounts. The no-load frequency response of the valves tested with the new rigid test stand was considerably superior to that of the valves tested on the old test setup.

This can be seen by comparing the no-load frequency responses of the Moog 1402C and 1402X valves and the Cadillac Gage FC-2 and PC-2 valves when tested on the present test stand, Fig. 78 and the no-load frequency response curves listed for the same valves in WADC TR 55-29, Part II. The low amplitude input responses are more greatly affected than the high amplitude responses. (This is not illustrated in Fig. 78.)

The question then arises, what type of test stand should be chosen as a standard. The chances are that the test results of the old, less rigid test stand will conform more closely with the valve responses in actual aircraft operation. This is a question that must be answered in future studies.

APPENDIX I
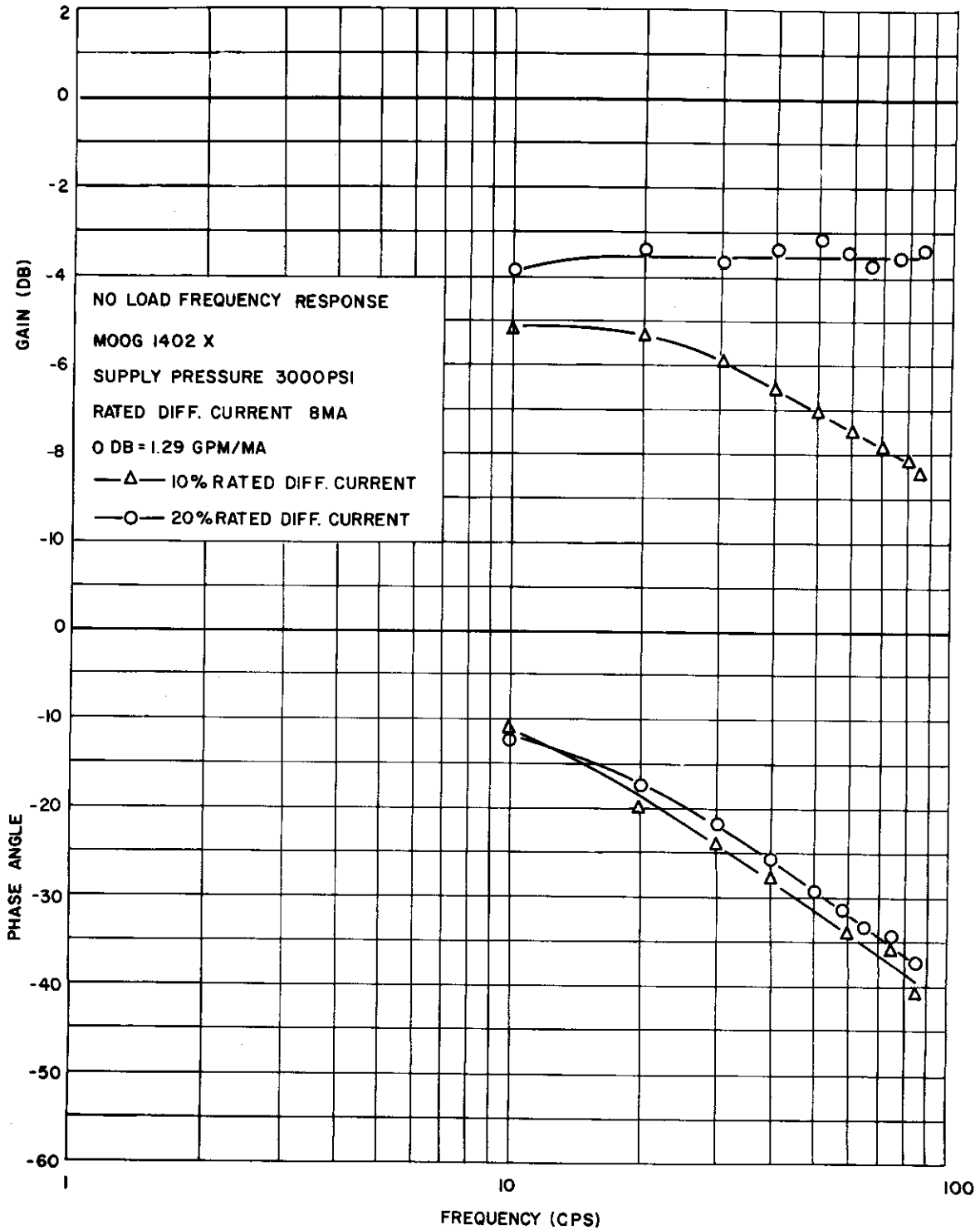
Figure 59. Moog 1402X No-Load Frequency Response
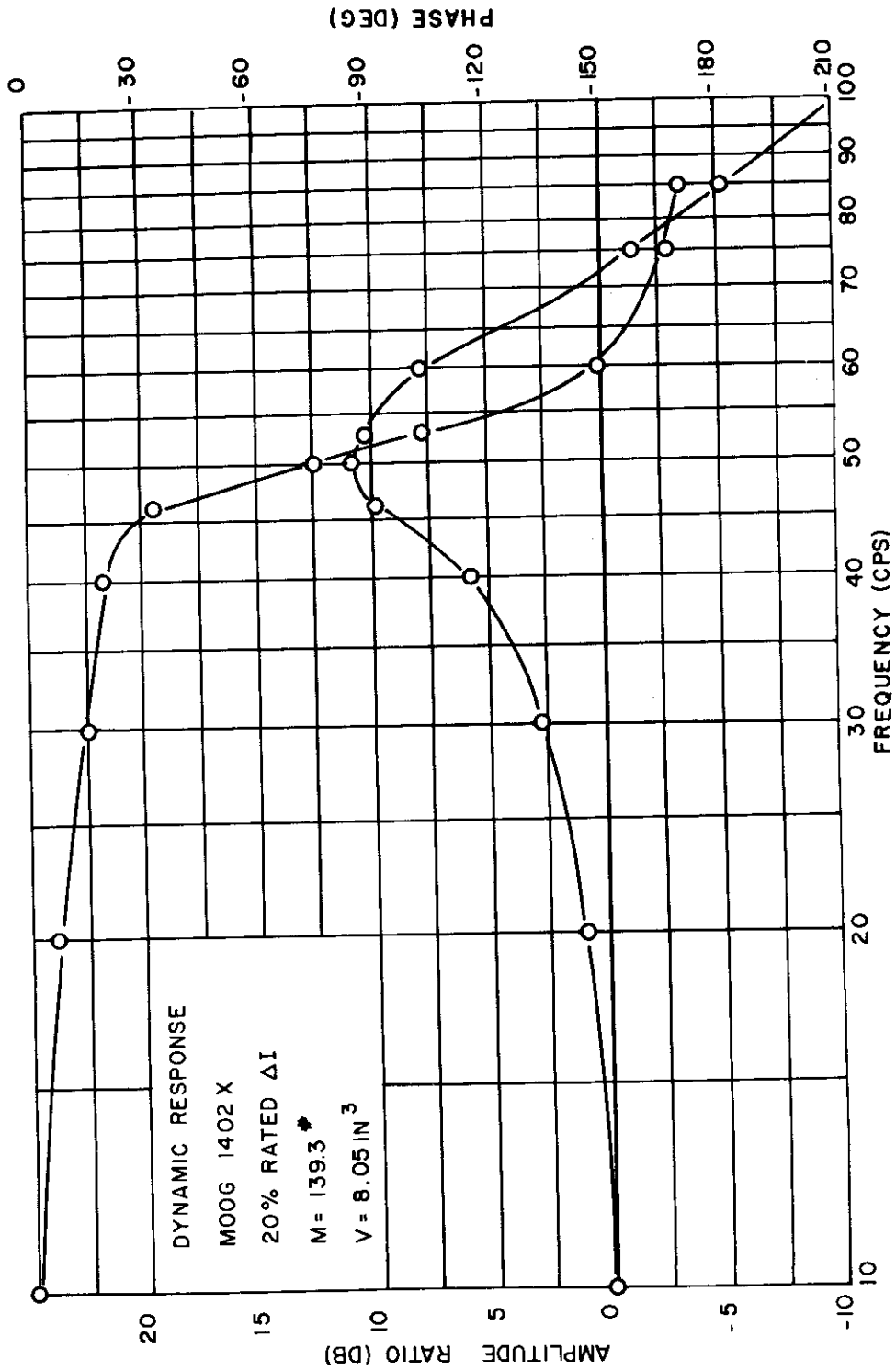
Figure 60. Moog 1402X Frequency Response Under Load of Run No. 1

The figure shows a graph with the following elements:

PHASE (DEG) axis: 0, -30, -60, -90, -120, -150, -180, -210
AMPLITUDE RATIO (DB) axis: 20, 15, 10, 5, 0, -5, -10
FREQUENCY (CPS) axis: 10, 20, 30, 40, 50, 60, 70, 80, 90, 100

DYNAMIC RESPONSE
MOOG 1402 X
20% RATED ΔI
M= 139.3
V = 8.05 IN^3
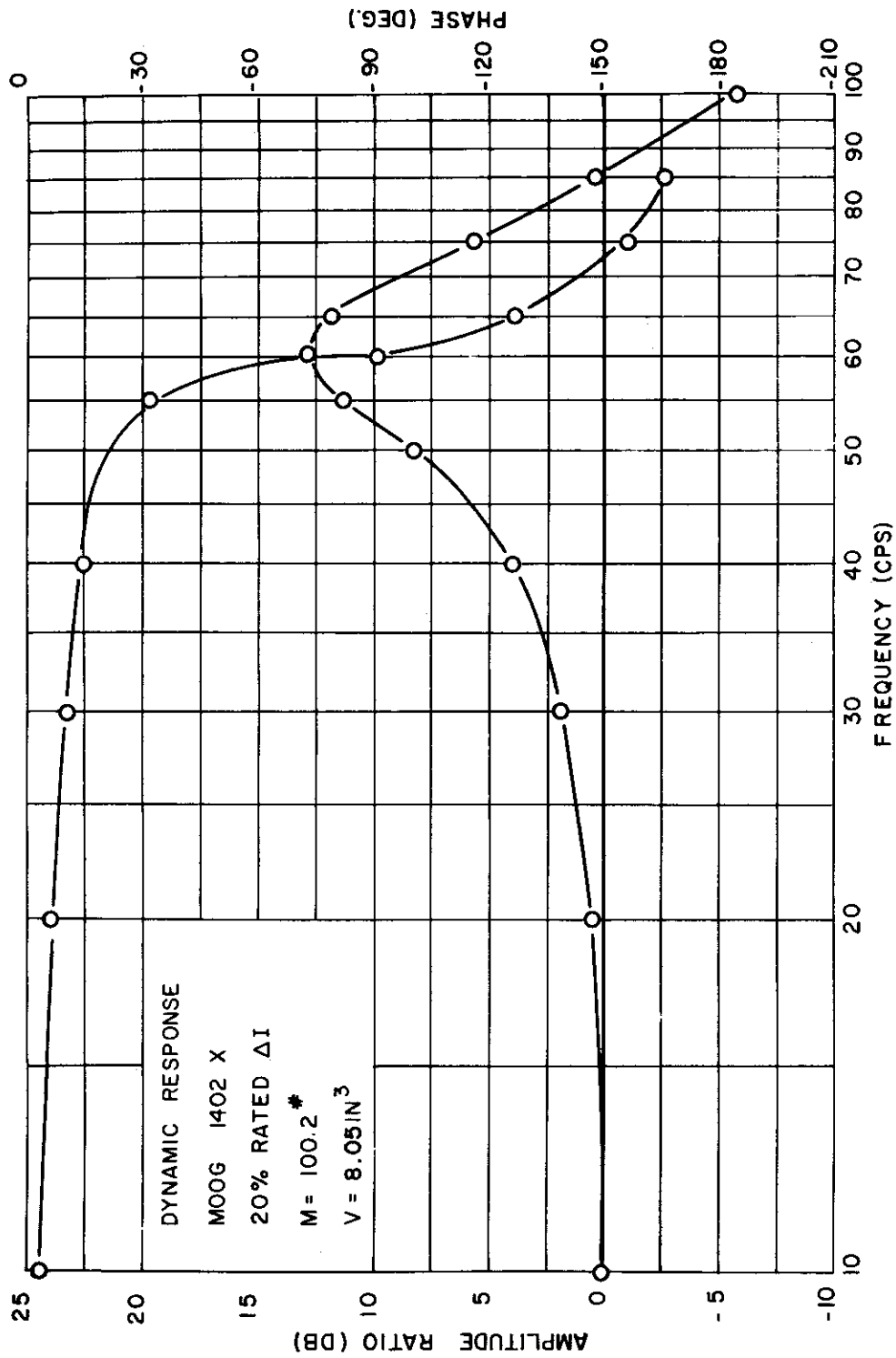
Figure 61. Moog 1402X Frequency Response Under Load of Run No. 2

DYNAMIC RESPONSE

MOOG 1402 X

20% RATED ΔI

M = 100.2 #

V = 8.05 IN^3
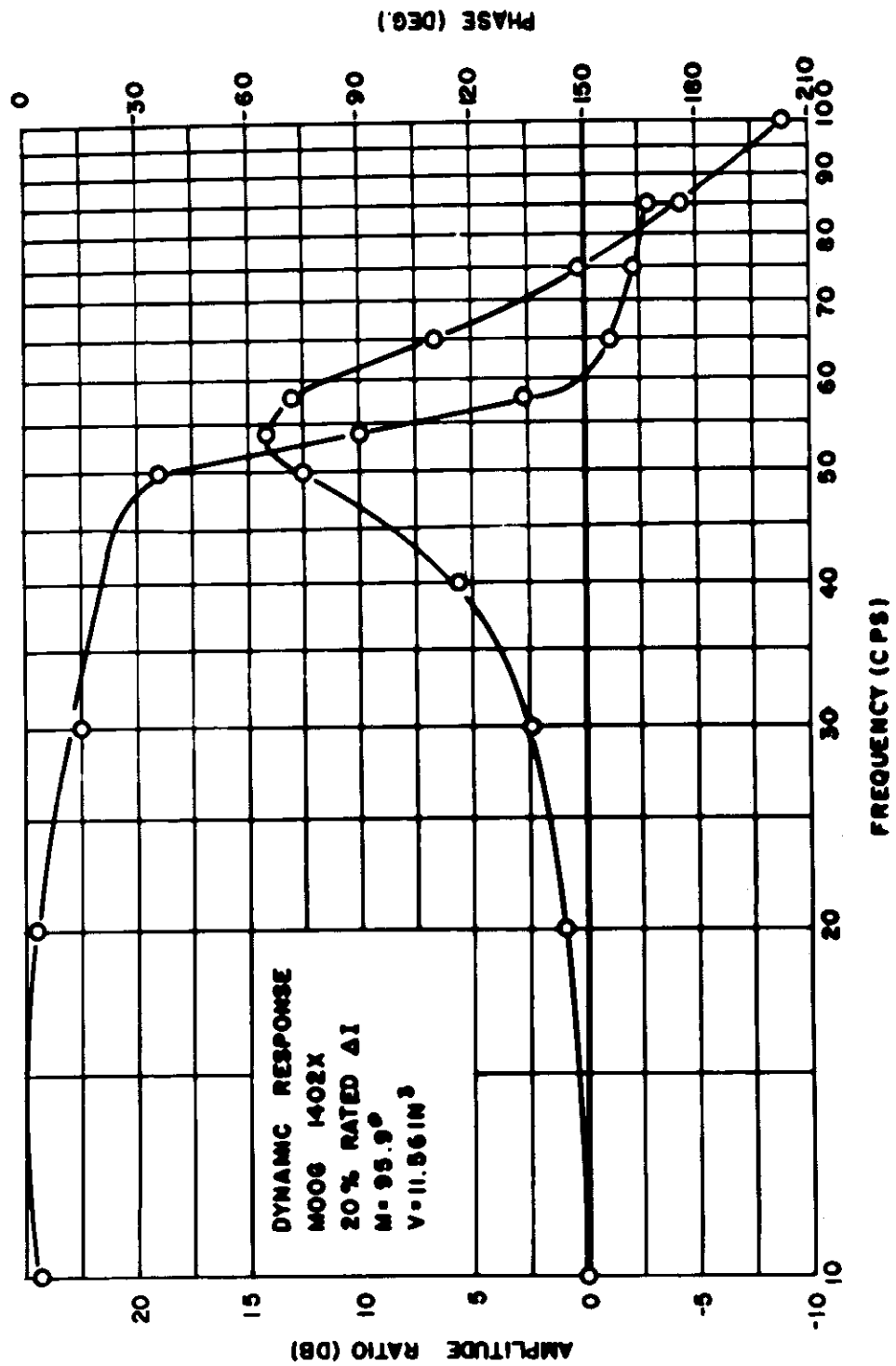
Figure 62. Moog 1402X Frequency Response Under Load of Run No. 3
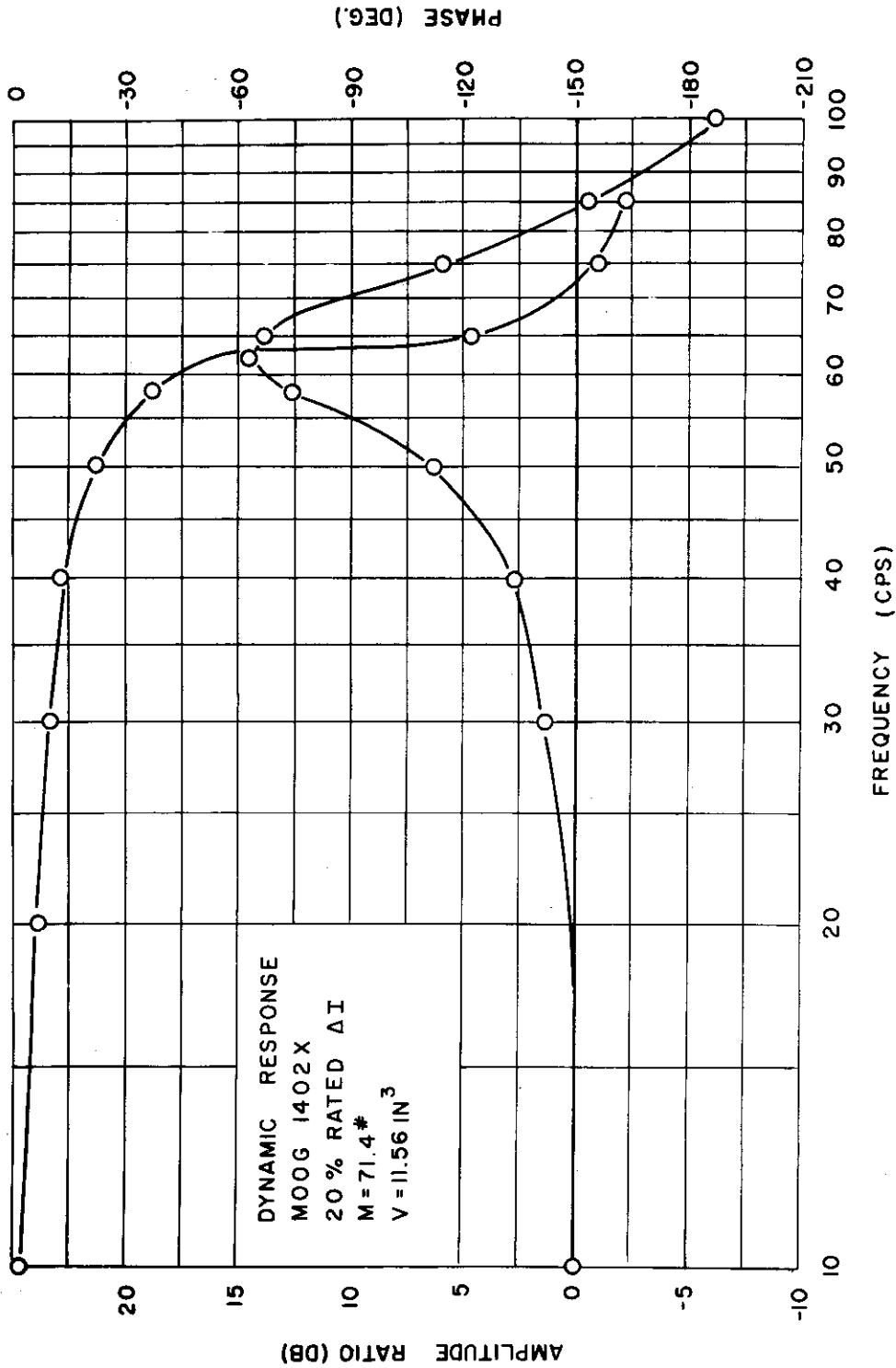
Figure 63. Moog 1402X Frequency Response Under Load of Run No. 4

PHASE (DEG.)

FREQUENCY (CPS)

AMPLITUDE RATIO (DB)

DYNAMIC RESPONSE
MOOG 1402X
20% RATED ΔI
M = 71.4*
V = 11.56 IN^3
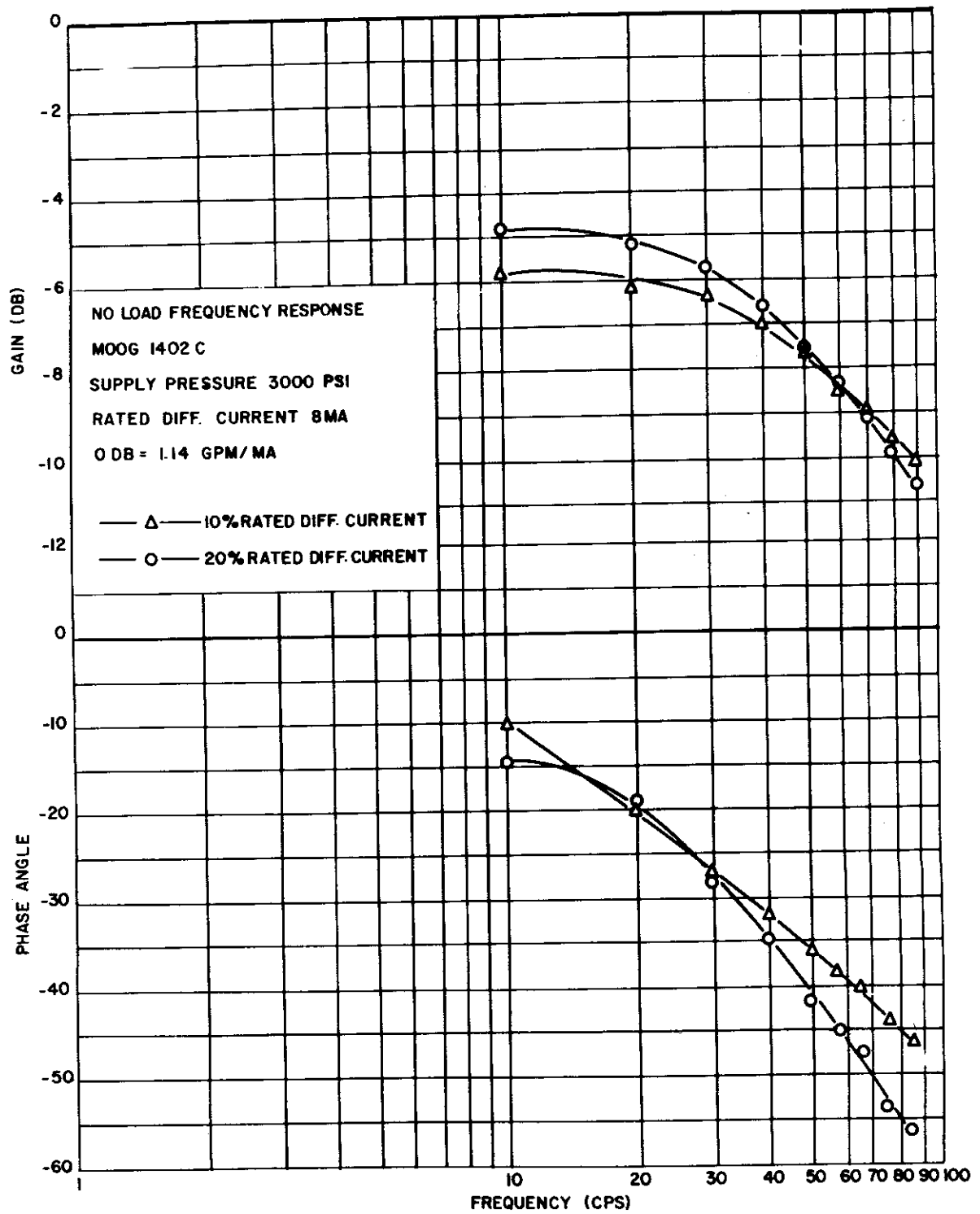
Figure 64.   Moog 1402C No-Load Frequency Response
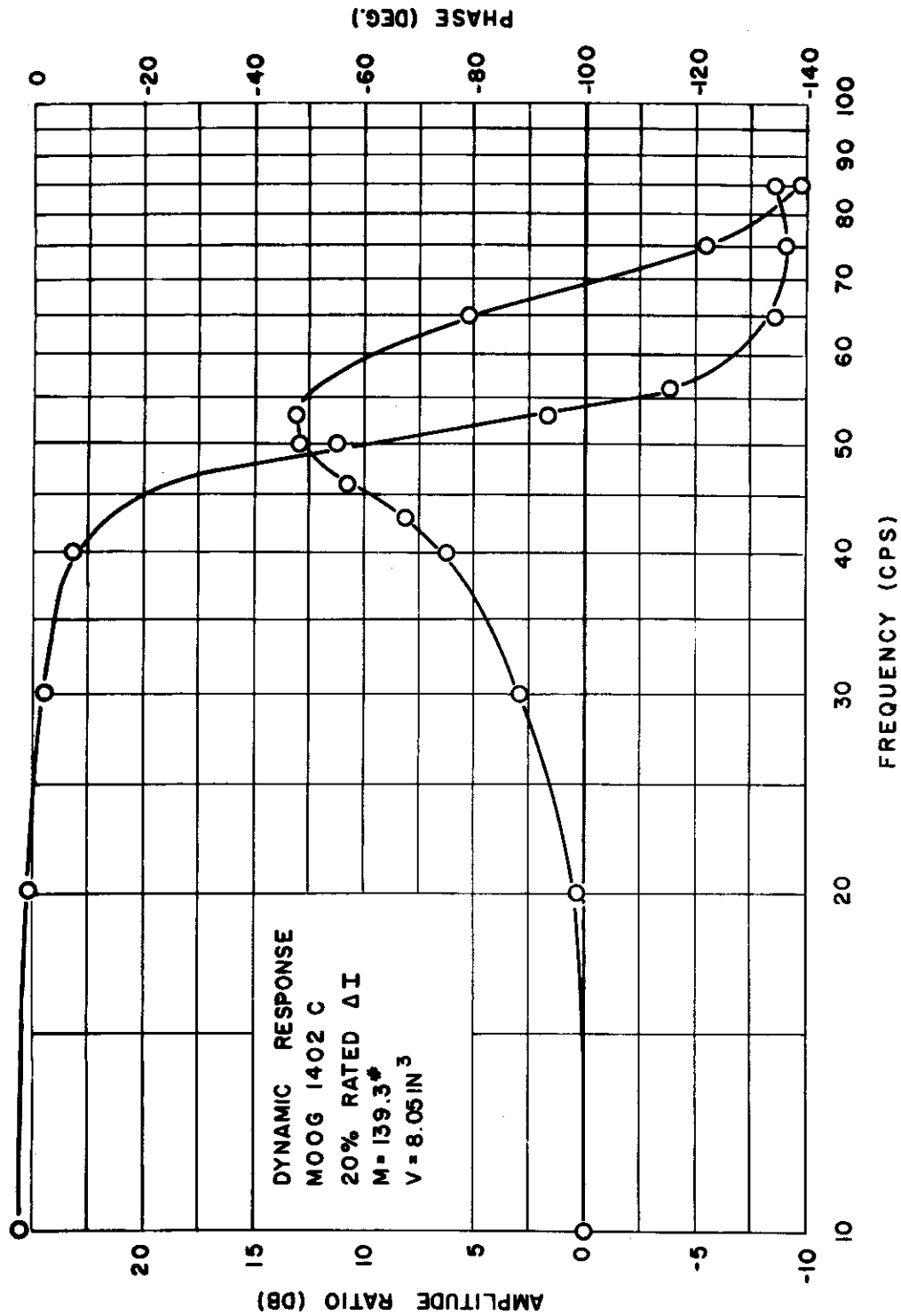
Figure 65. Moog 1402C Frequency Response Under Load of Run No. 1
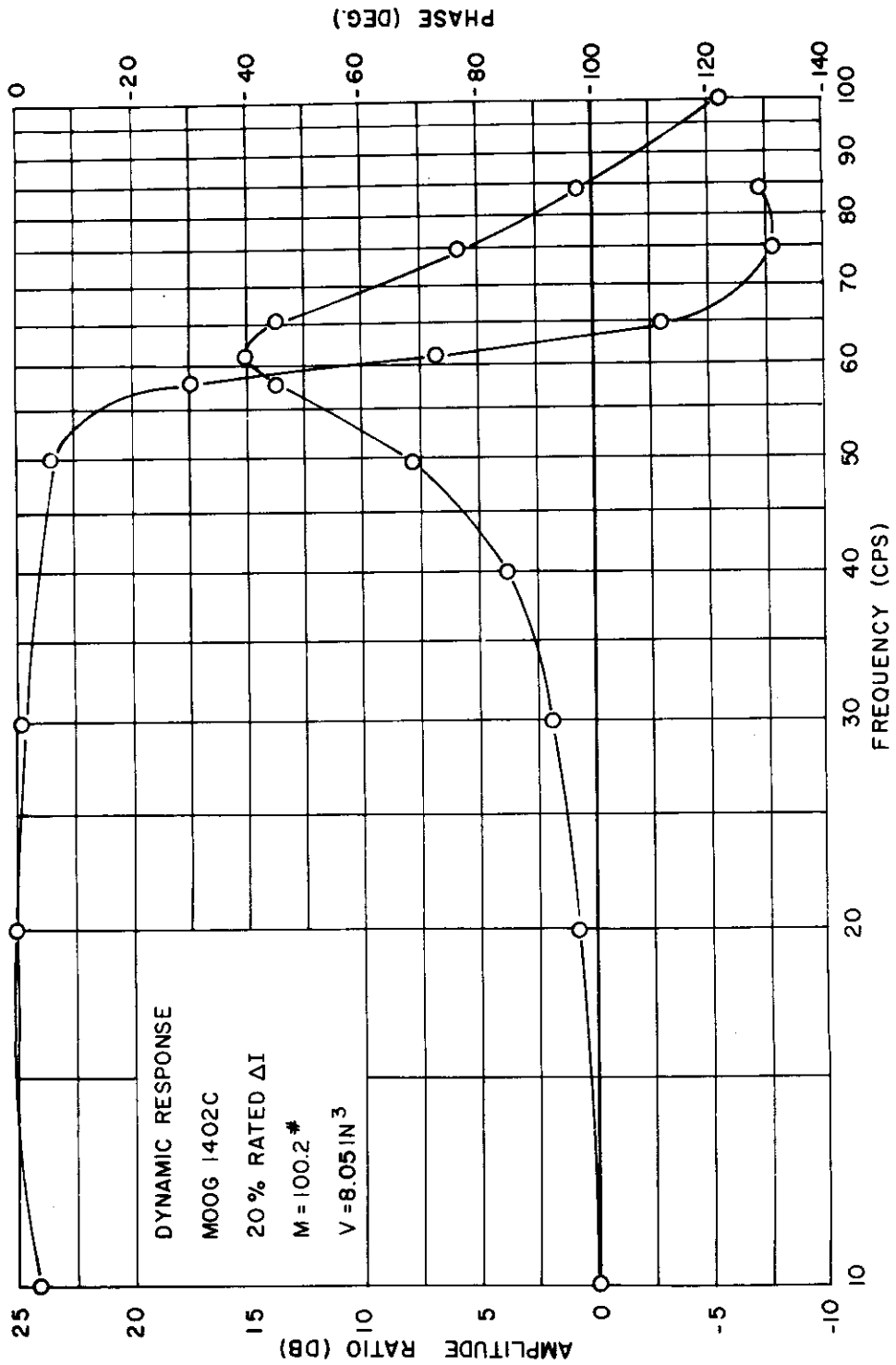
Figure 66. Moog 1402C Frequency Response Under Load of Run No. 2

DYNAMIC RESPONSE

MOOG 1402C

20% RATED ΔI

M = 100.2 #

V = 8.05 IN^3
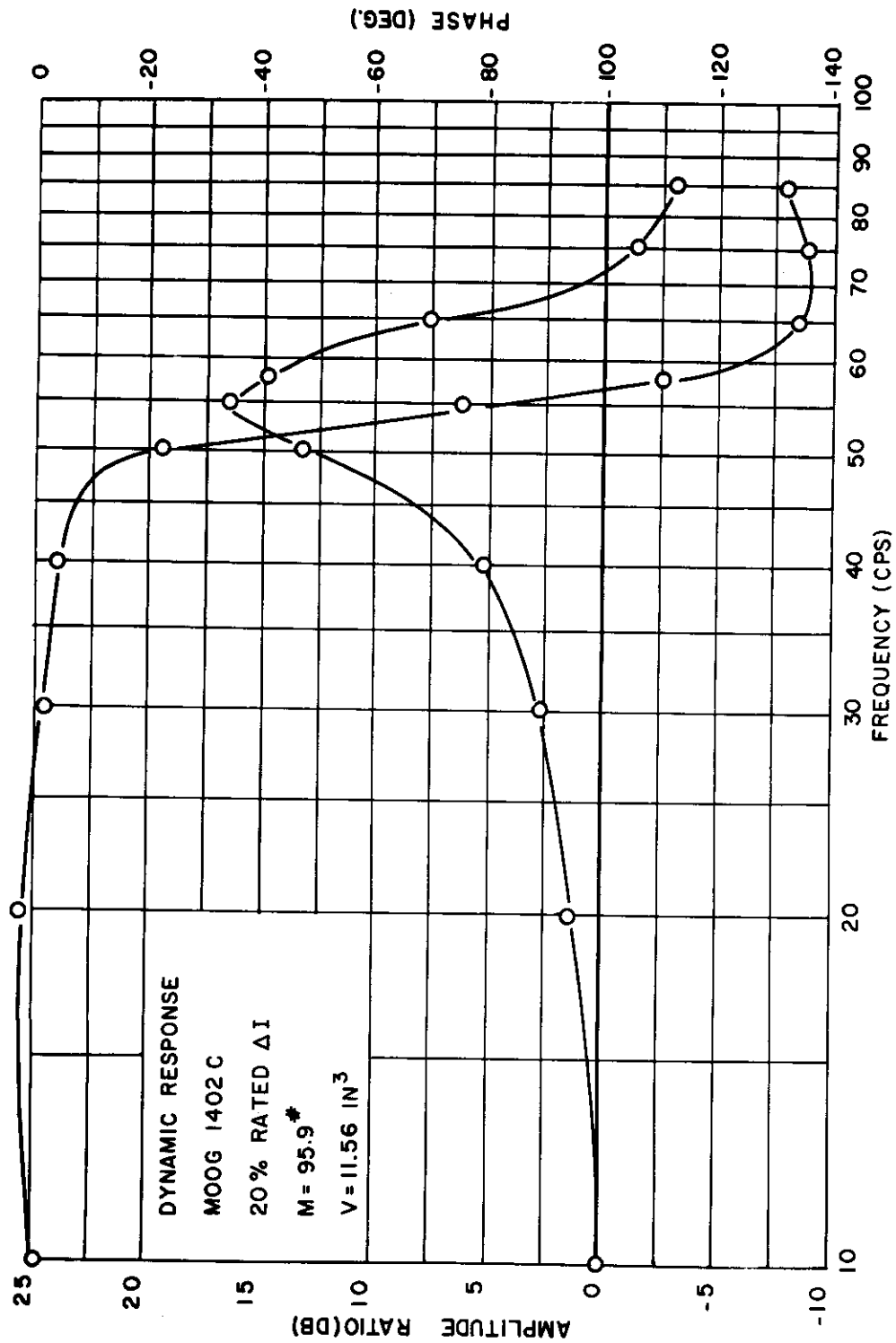
Figure 67. Moog 1402C Frequency Response Under Load of Run No. 3

DYNAMIC RESPONSE

MOOG 1402 C

20 % RATED ΔI

M = 95.9 $^{\#}$

V = 11.56 IN^3
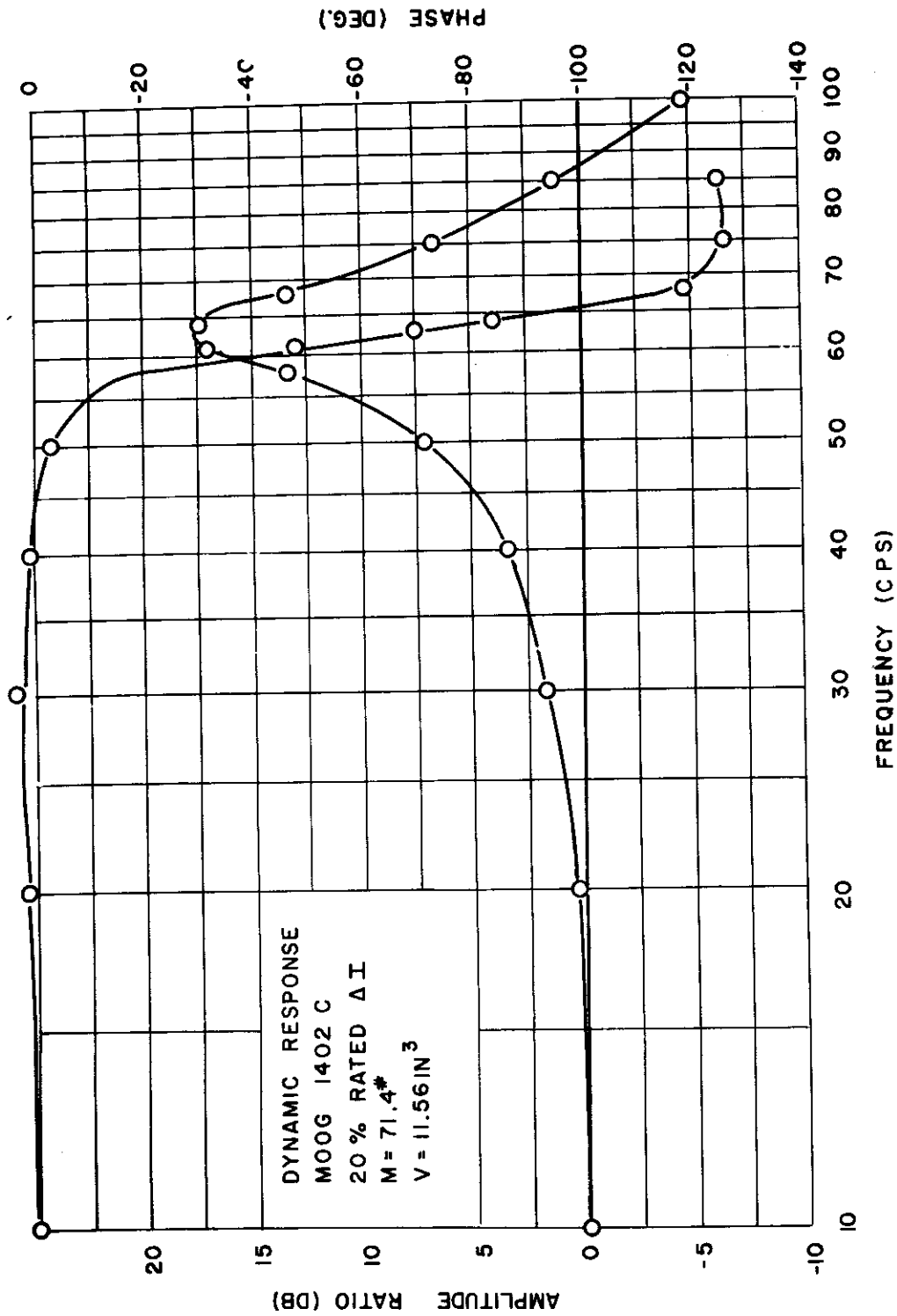
Figure 68. Moog 1402C Frequency Response Under Load of Run No. 4
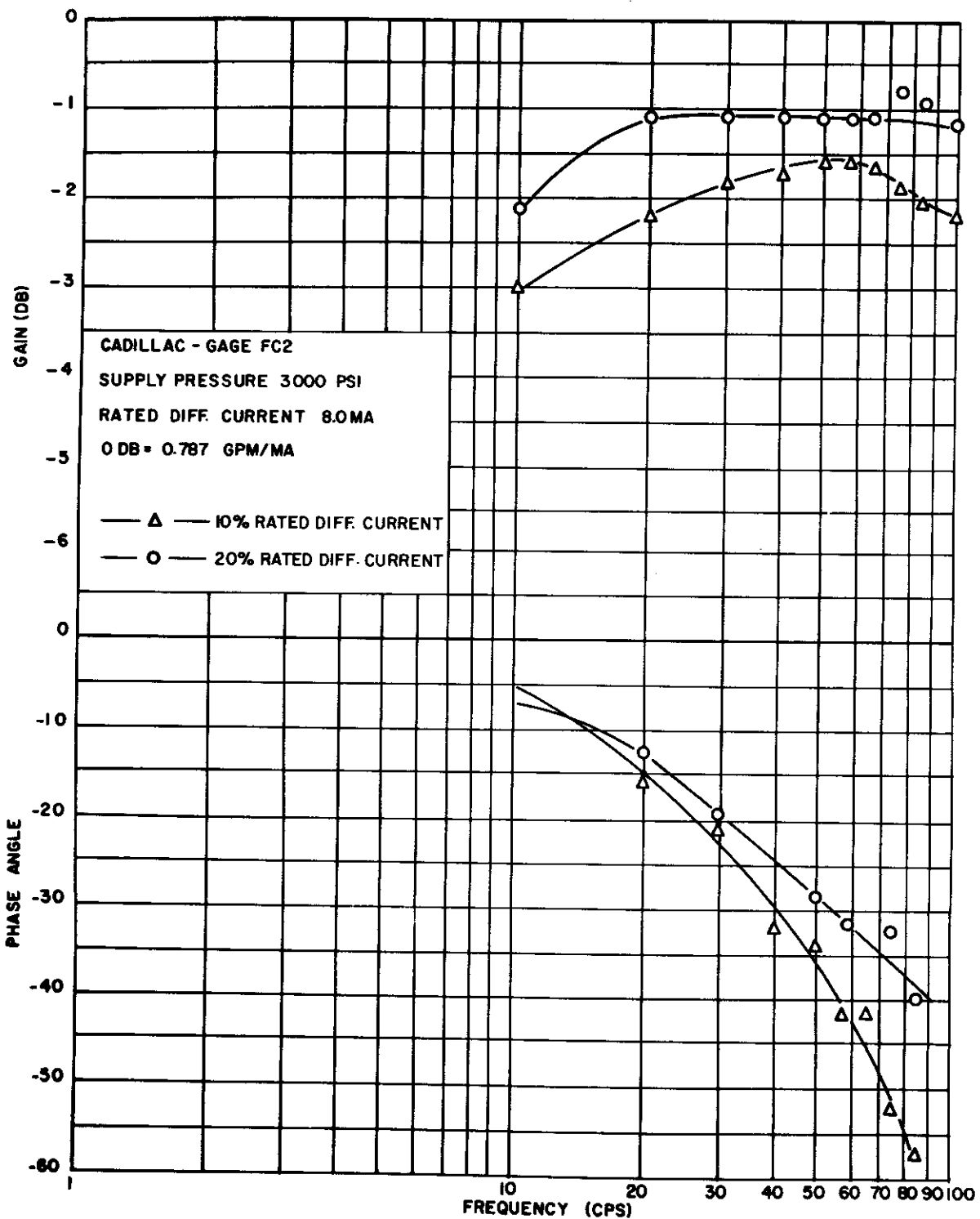
Figure 69. Cadillac Gage FC-2 No-Load Frequency Response
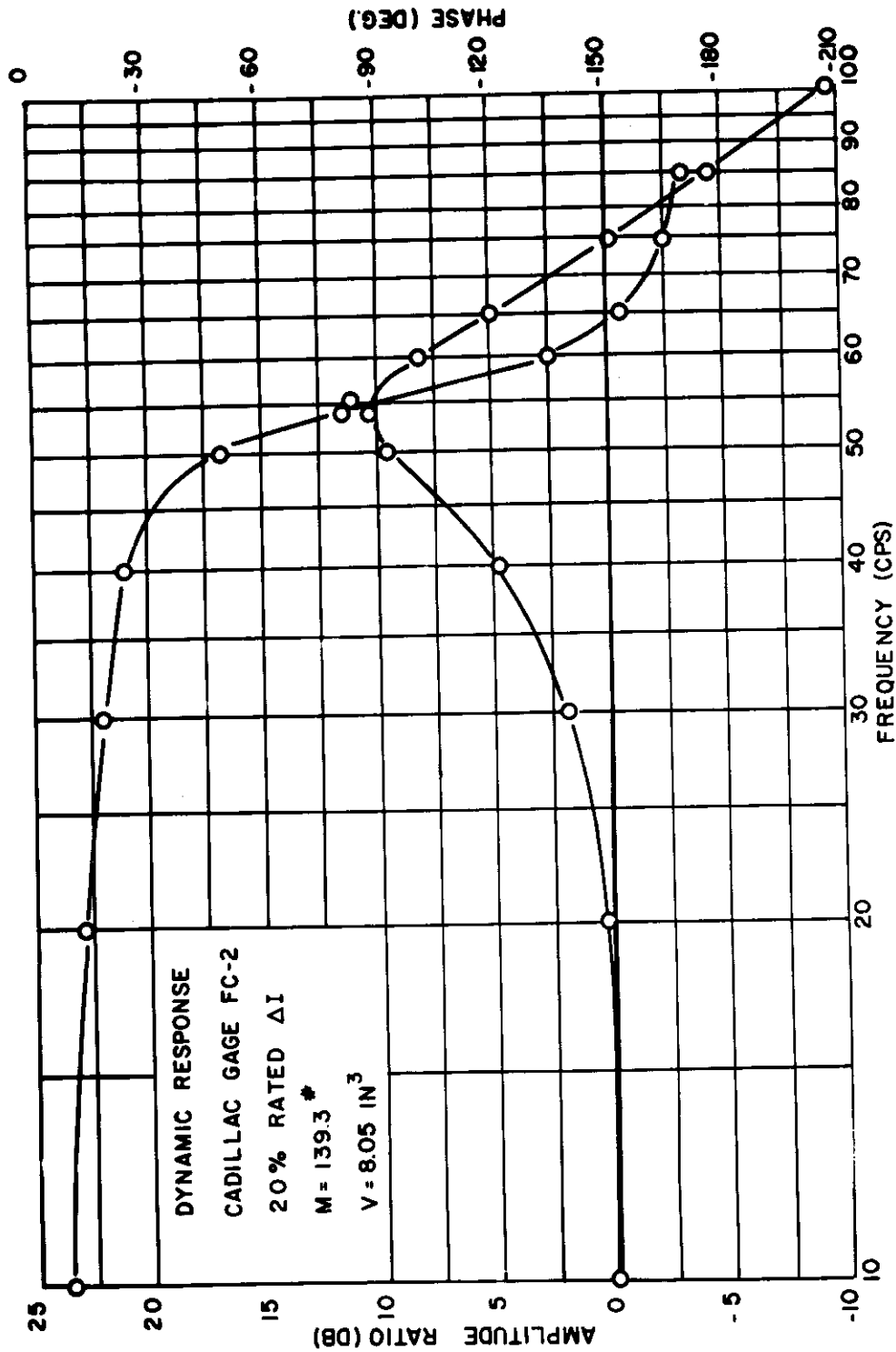
Figure 70.   Cadillac Gage FC-2 Frequency Response Under Load of Run No. 1

DYNAMIC RESPONSE

CADILLAC GAGE FC-2

20% RATED ΔI

M = 139.3 *

V = 8.05 IN^3
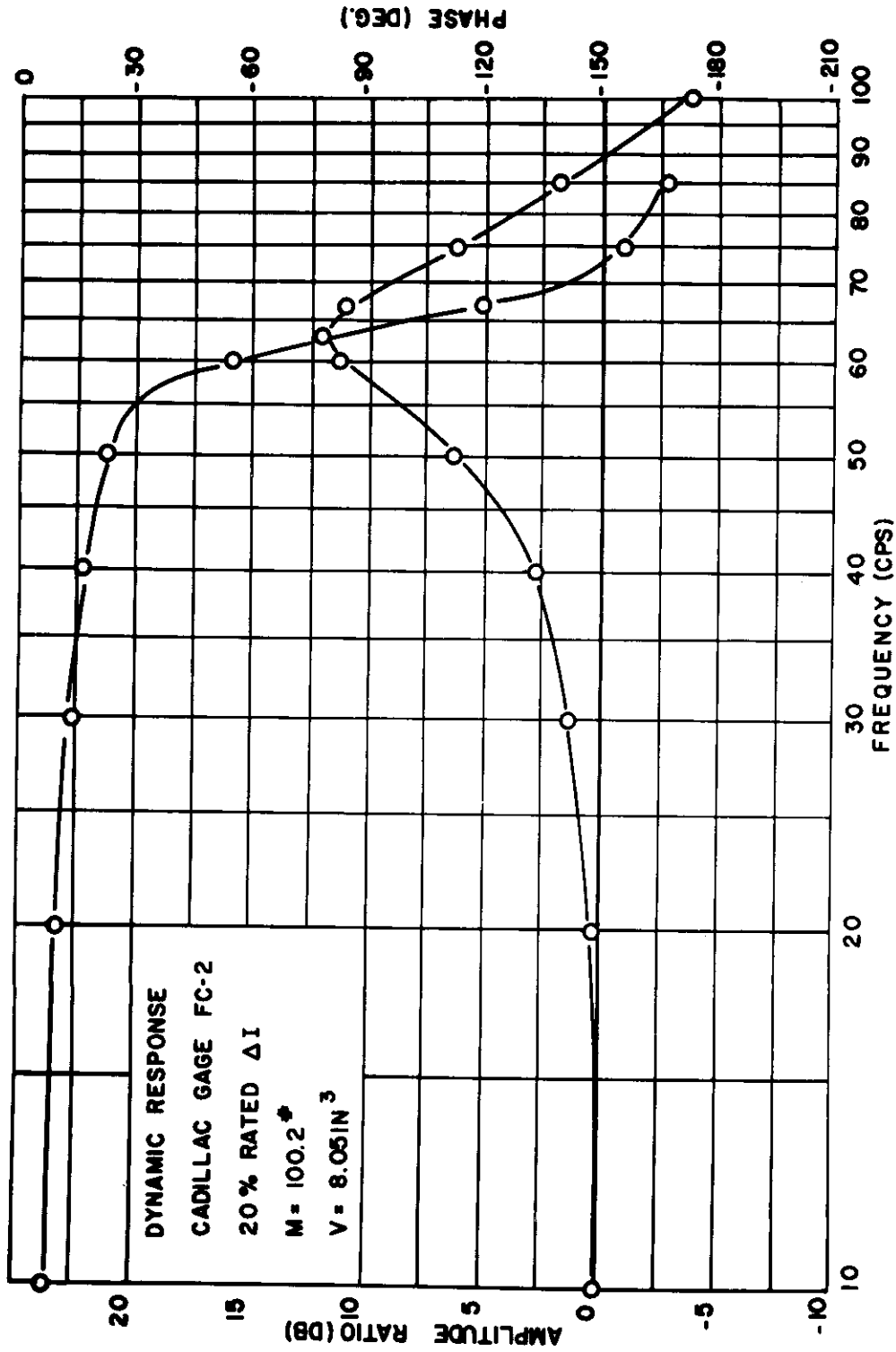
Figure 71. Cadillac Gage FC-2 Frequency Response Under Load of Run No. 2

DYNAMIC RESPONSE

CADILLAC GAGE FC-2

20% RATED ΔI

M = 100.2*

V = 8.05IN^3
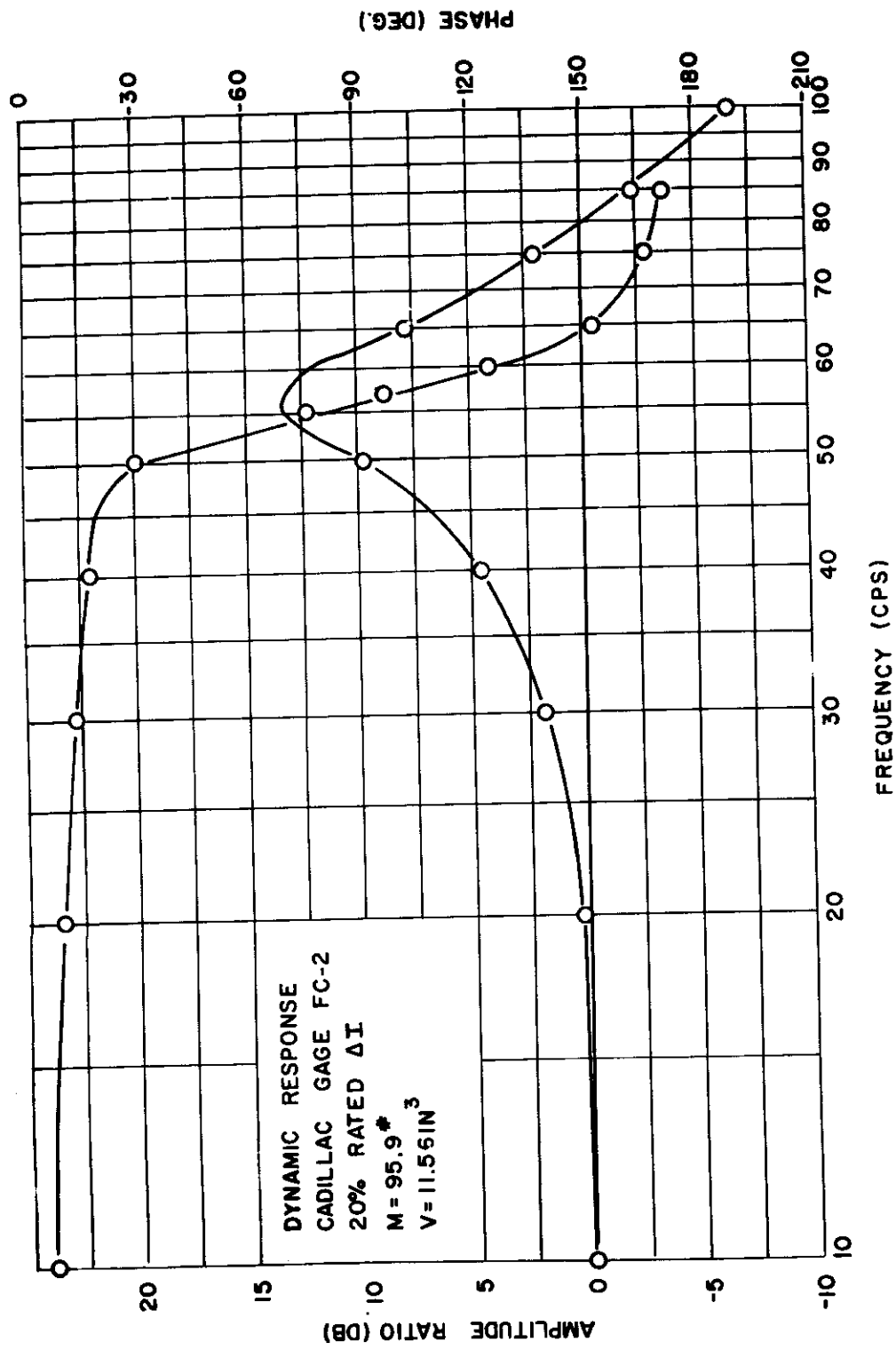
Figure 72. Cadillac Gage FC-2 Frequency Response Under Load of Run No. 3
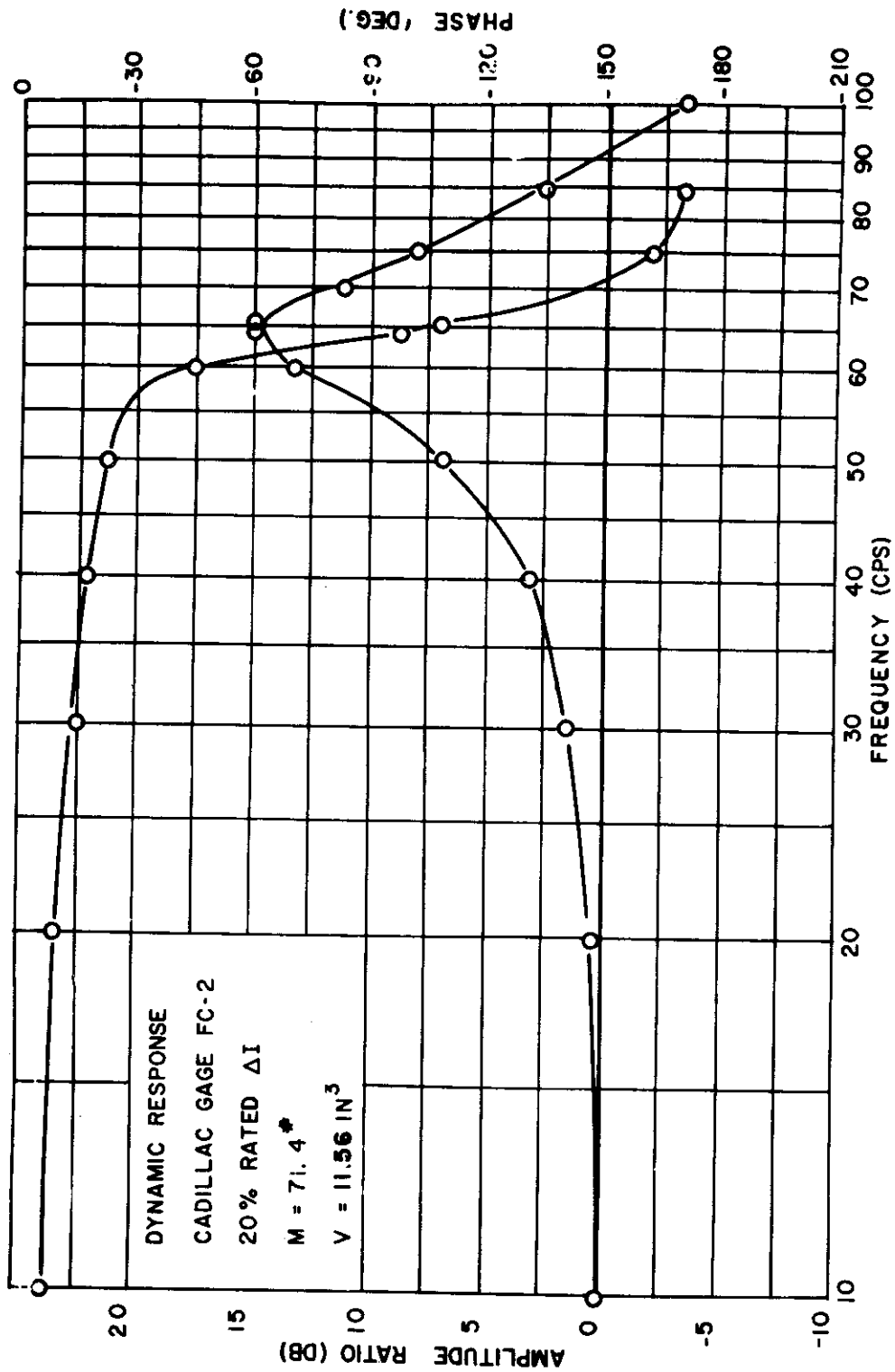
Figure 73. Cadillac Gage FC-2 Frequency Response Under Load of Run No. 4

DYNAMIC RESPONSE
CADILLAC GAGE FC-2
20% RATED ΔI
$M = 71.4^{\#}$
$V = 11.56 IN^3$
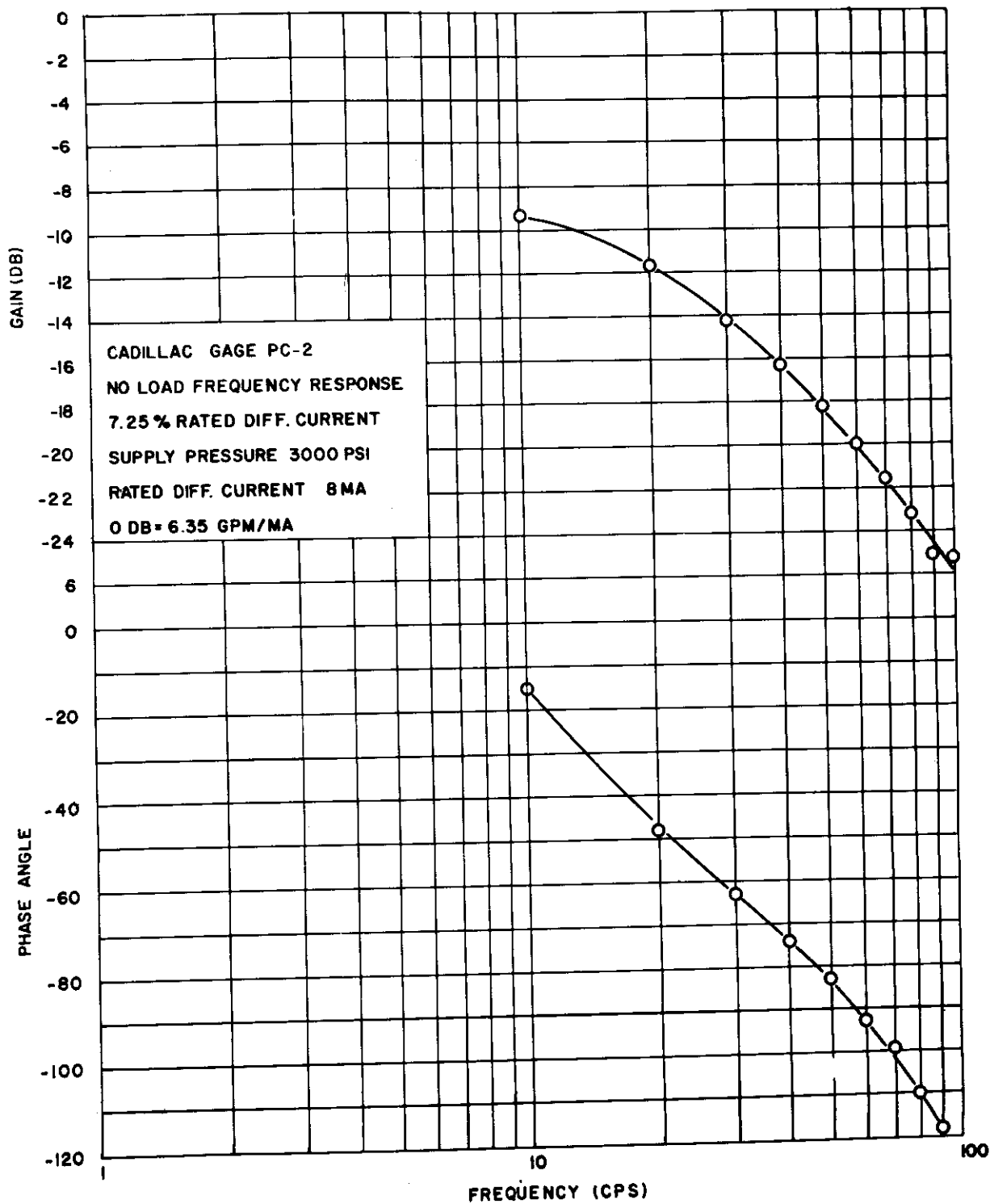
Figure 74.   Cadillac Gage PC-2 No-Load Frequency Response
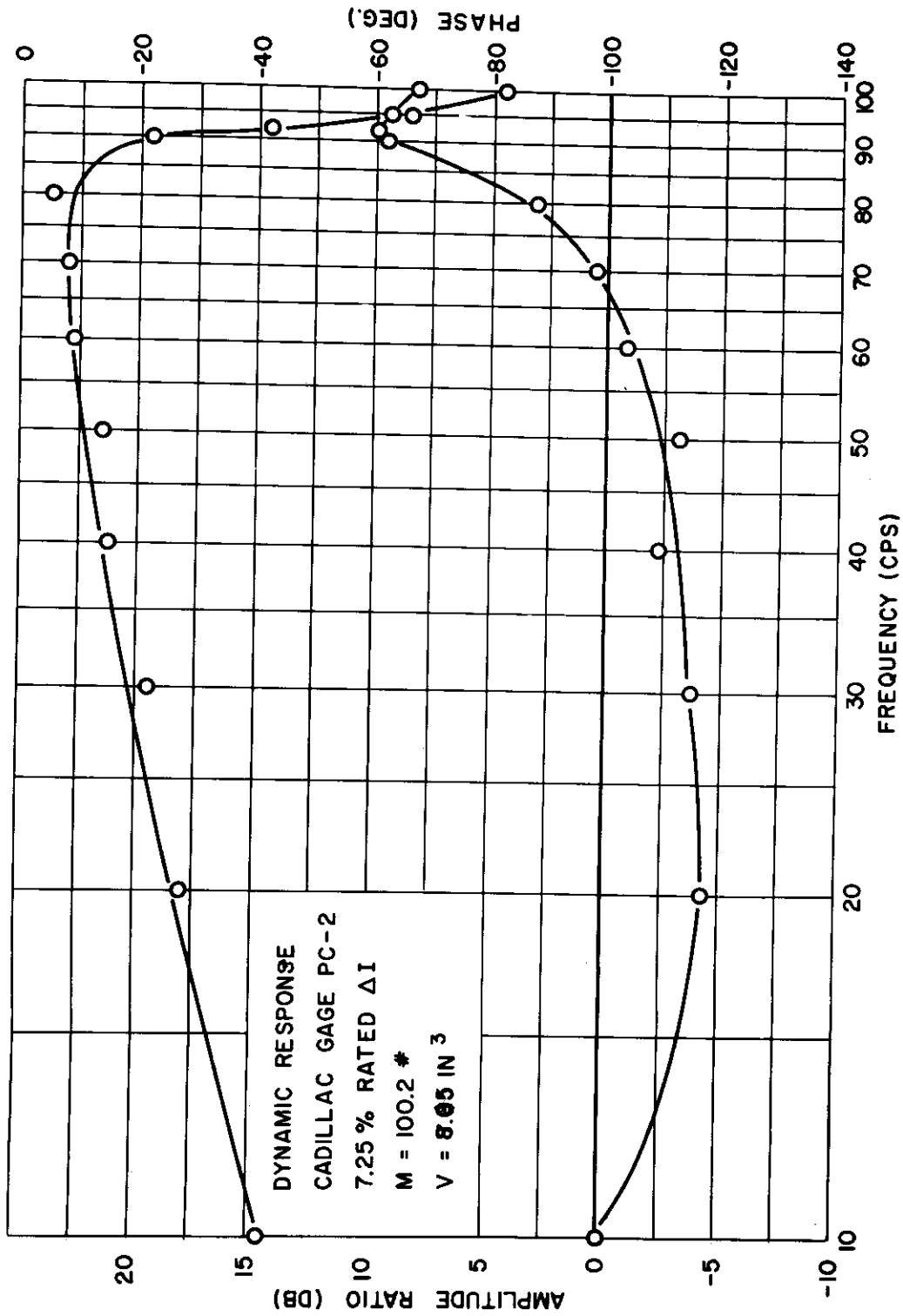
Figure 75. Cadillac Gage PC-2 Frequency Response Under Load of Run No. 2
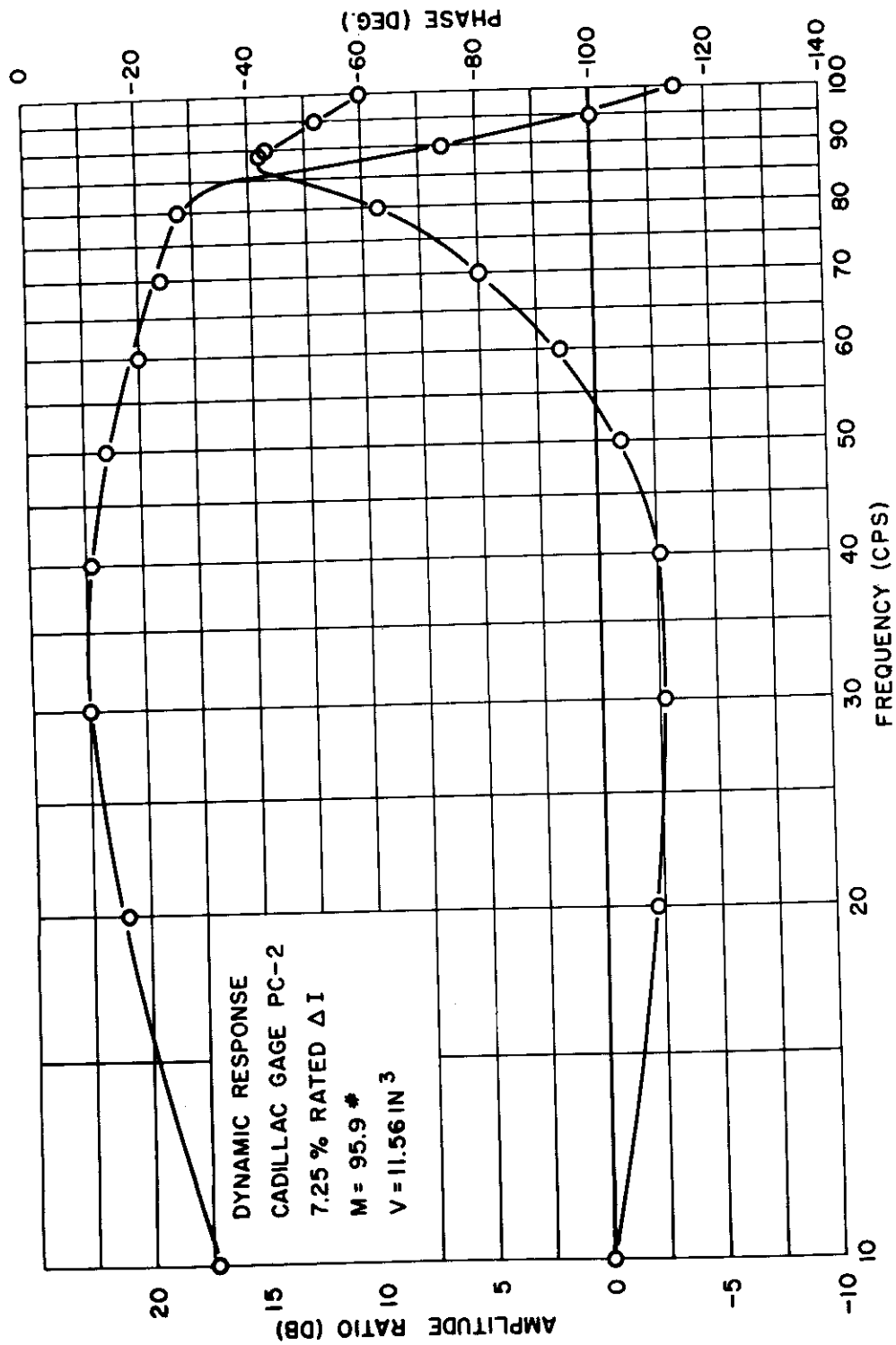
Figure 76. Cadillac Gage PC-2 Frequency Response Under Load of Run No. 3

PHASE (DEG.)

AMPLITUDE RATIO (DB)

FREQUENCY (CPS)

DYNAMIC RESPONSE
CADILLAC GAGE PC-2
7.25 % RATED Δ I
M = 95.9 #
V = 11.56 IN^3
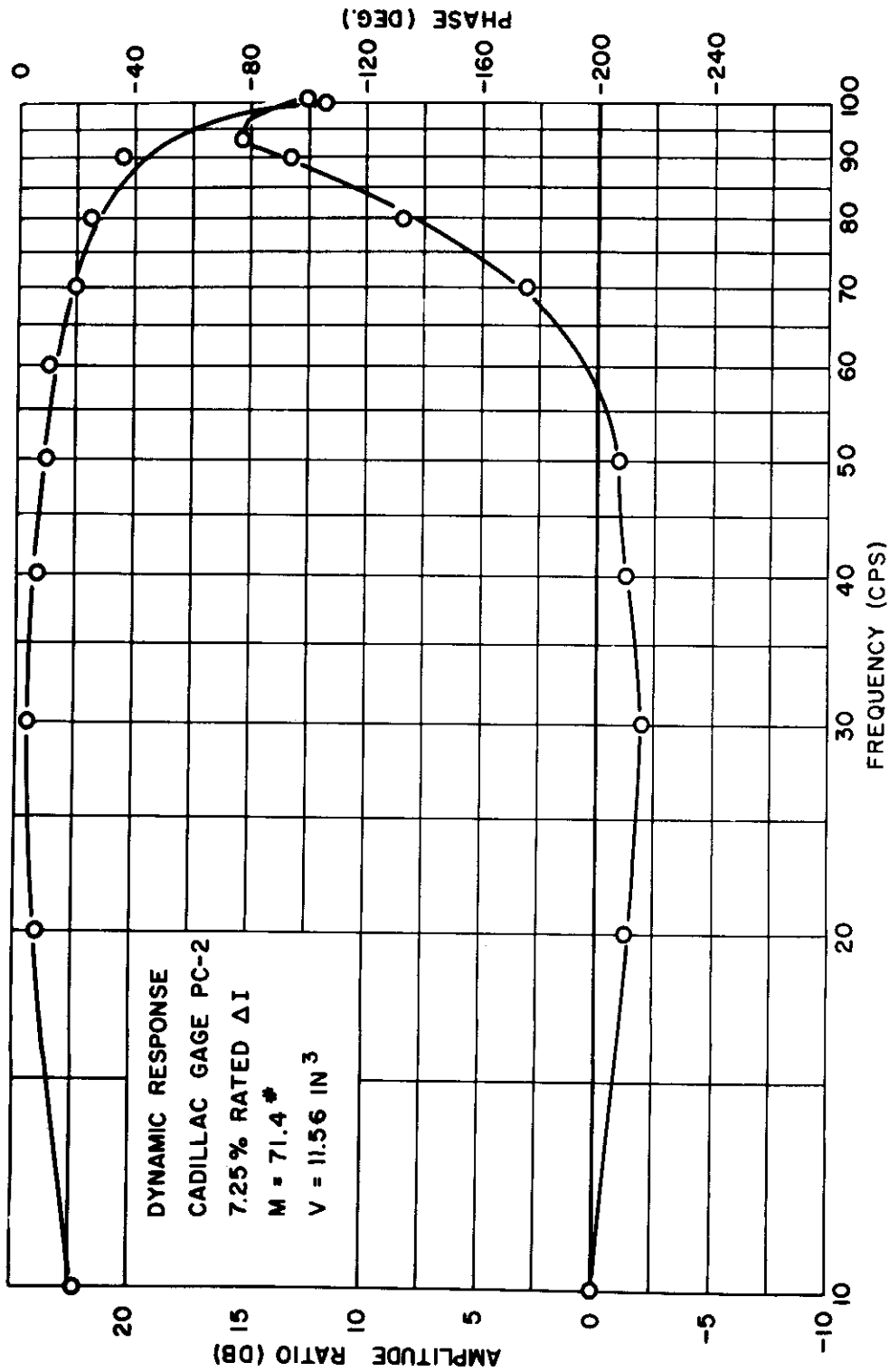
Figure 77. Cadillac Gage PC-2 Frequency Response Under Load of Run No. 4
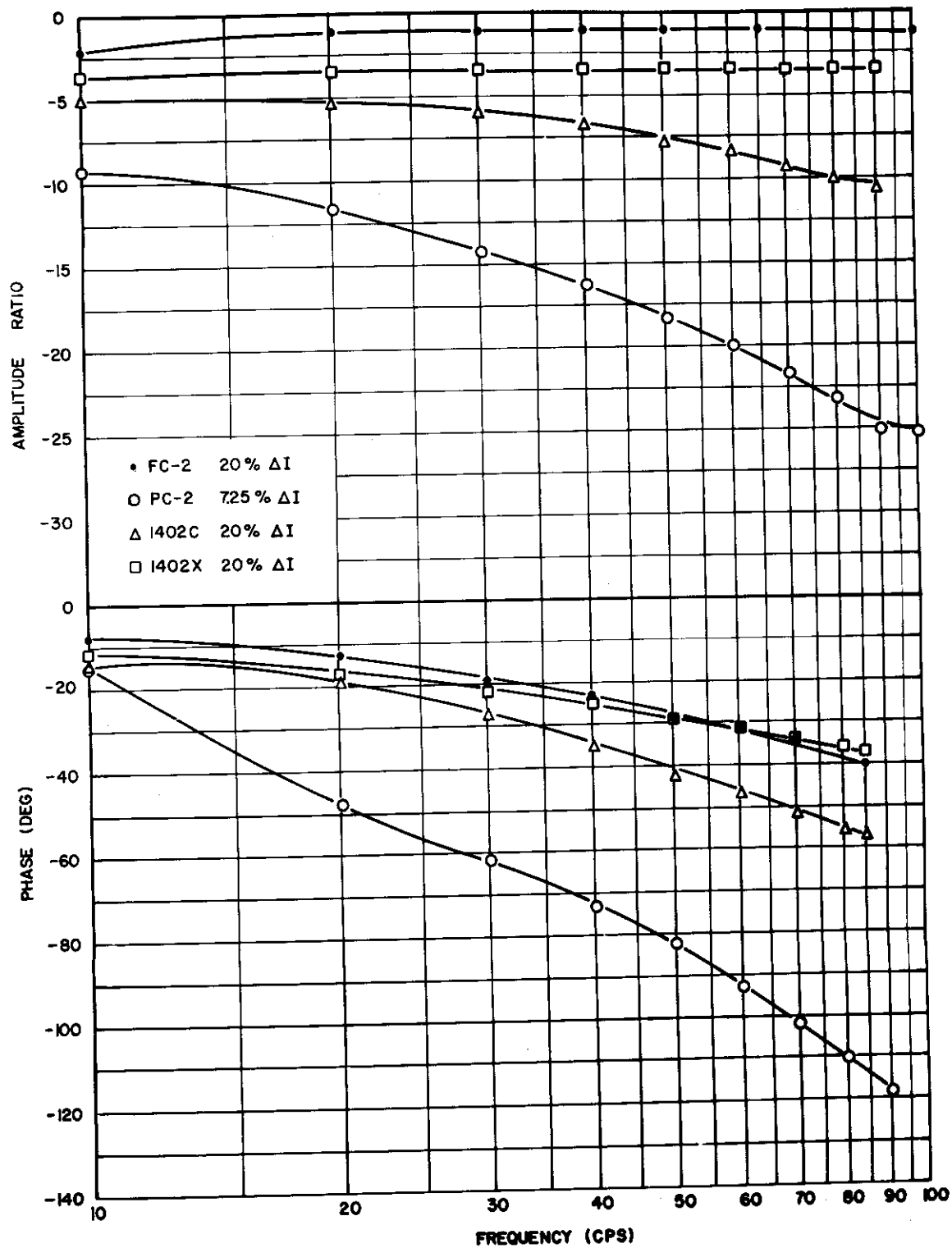
Figure 78.   Comparison of No-Load Responses of Four Valves

APPENDIX II
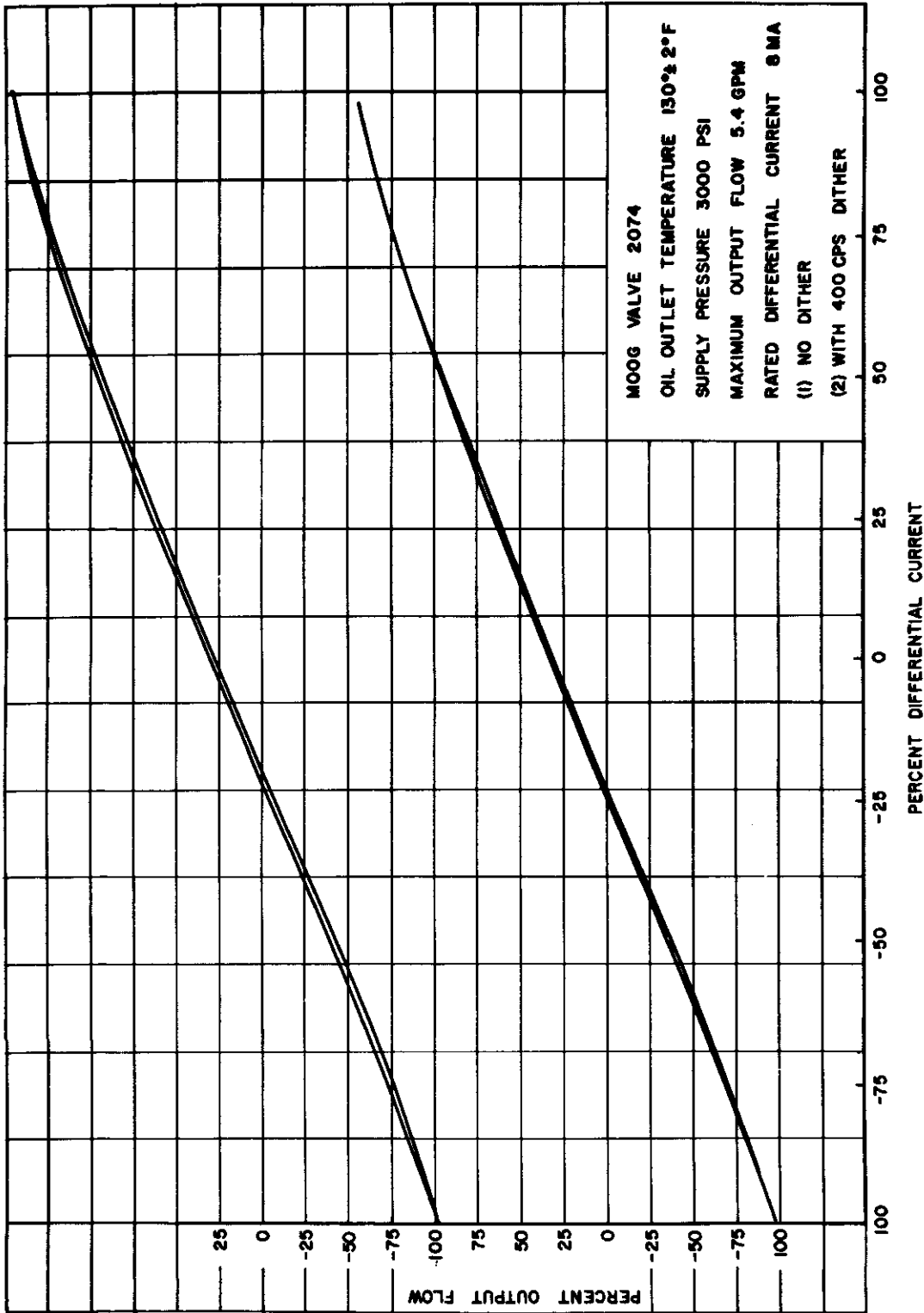
Figure 79. Moog 2074 Hysteresis - Rated Current
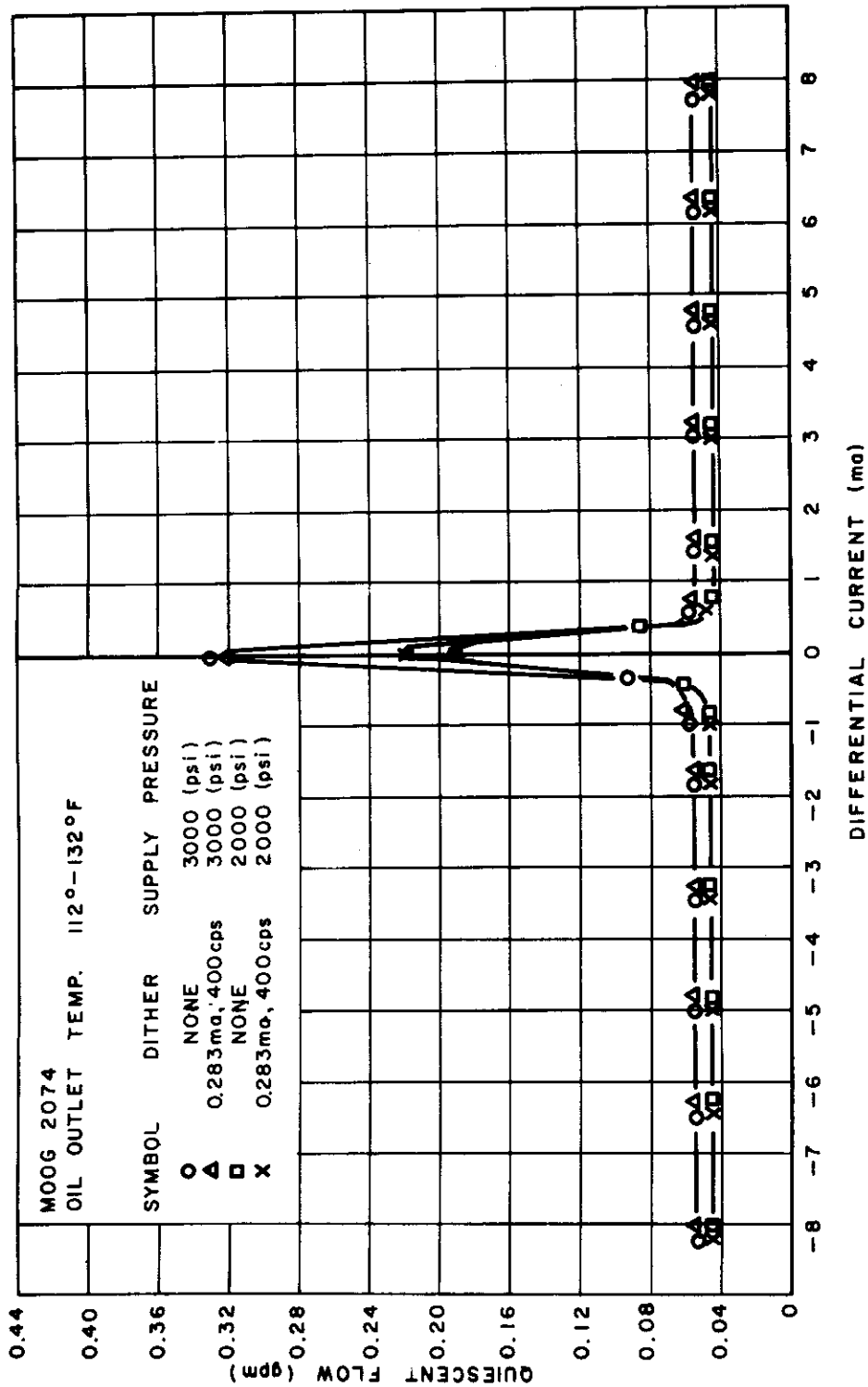
Figure 80. Moog 2074 Quiescent Flow vs. Differential Current
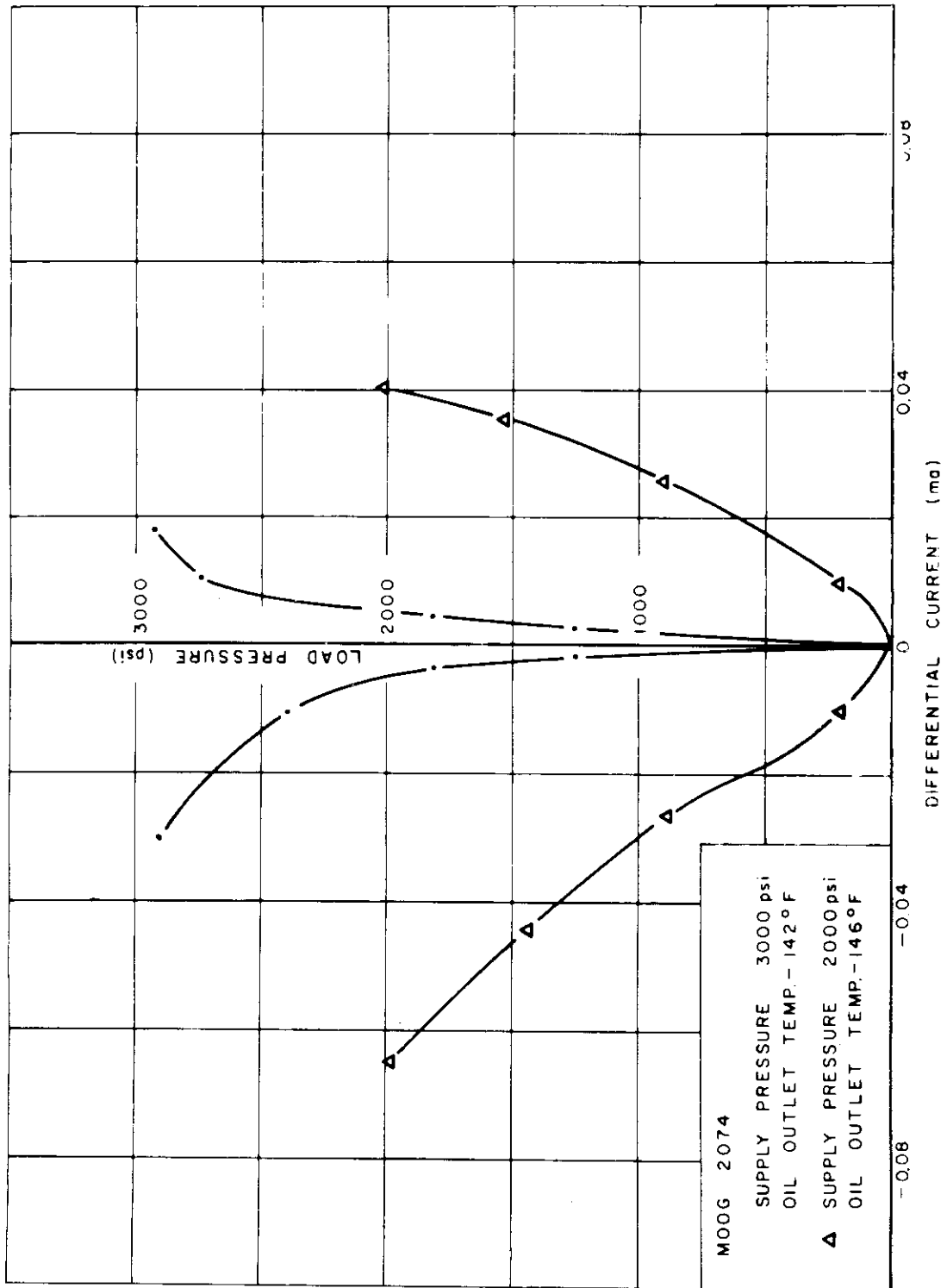
Figure 81. Moog 2074 Load Pressure vs. Differential Current at Zero Load Flow

MOOG 2074

SUPPLY PRESSURE 3000 psi
OIL OUTLET TEMP.- 142°F

△ SUPPLY PRESSURE 2000 psi
OIL OUTLET TEMP.-146°F
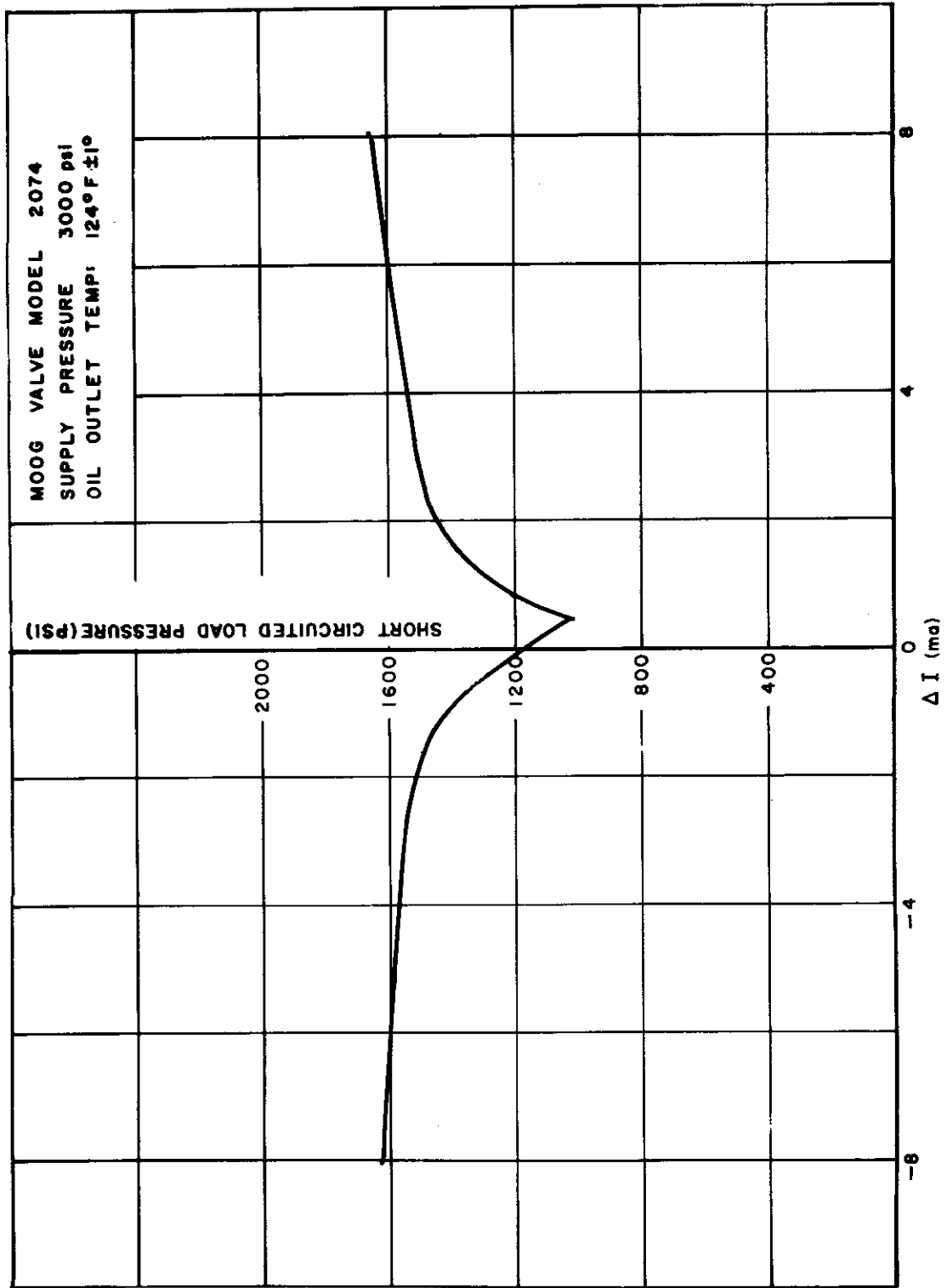
Figure 82. Moog 2074 Short Circuited Load Pressure vs. Differential Current
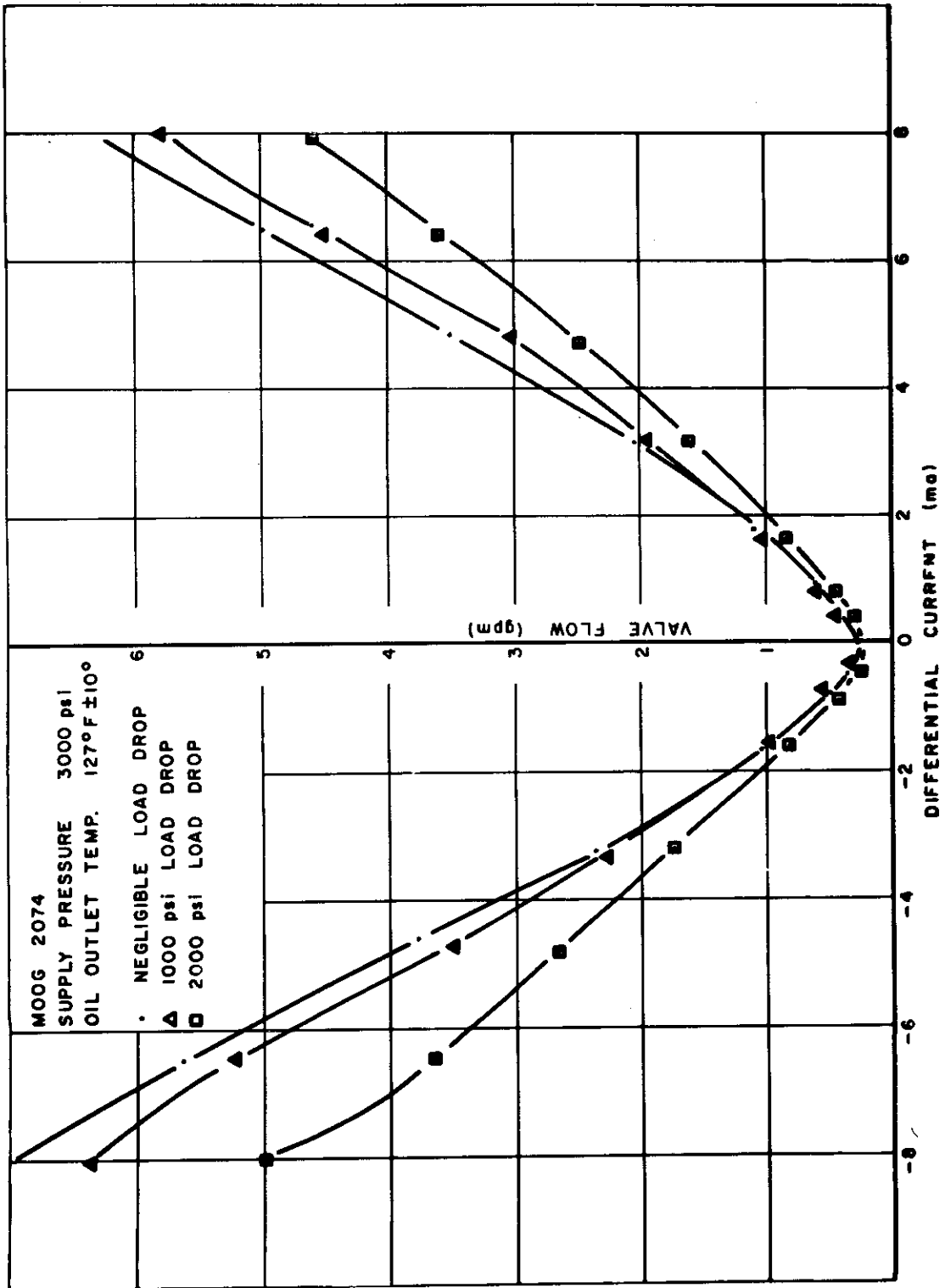
Figure 83. Moog 2074 Valve Flow vs. Differential Current – 3000 psi Supply Pressure

MOOG 2074
SUPPLY PRESSURE   3000 psi
OIL OUTLET TEMP. 127°F ±10°

· NEGLIGIBLE LOAD DROP
▲ 1000 psi LOAD DROP
◼ 2000 psi LOAD DROP

VALVE FLOW (gpm)

DIFFERENTIAL CURRENT (ma)
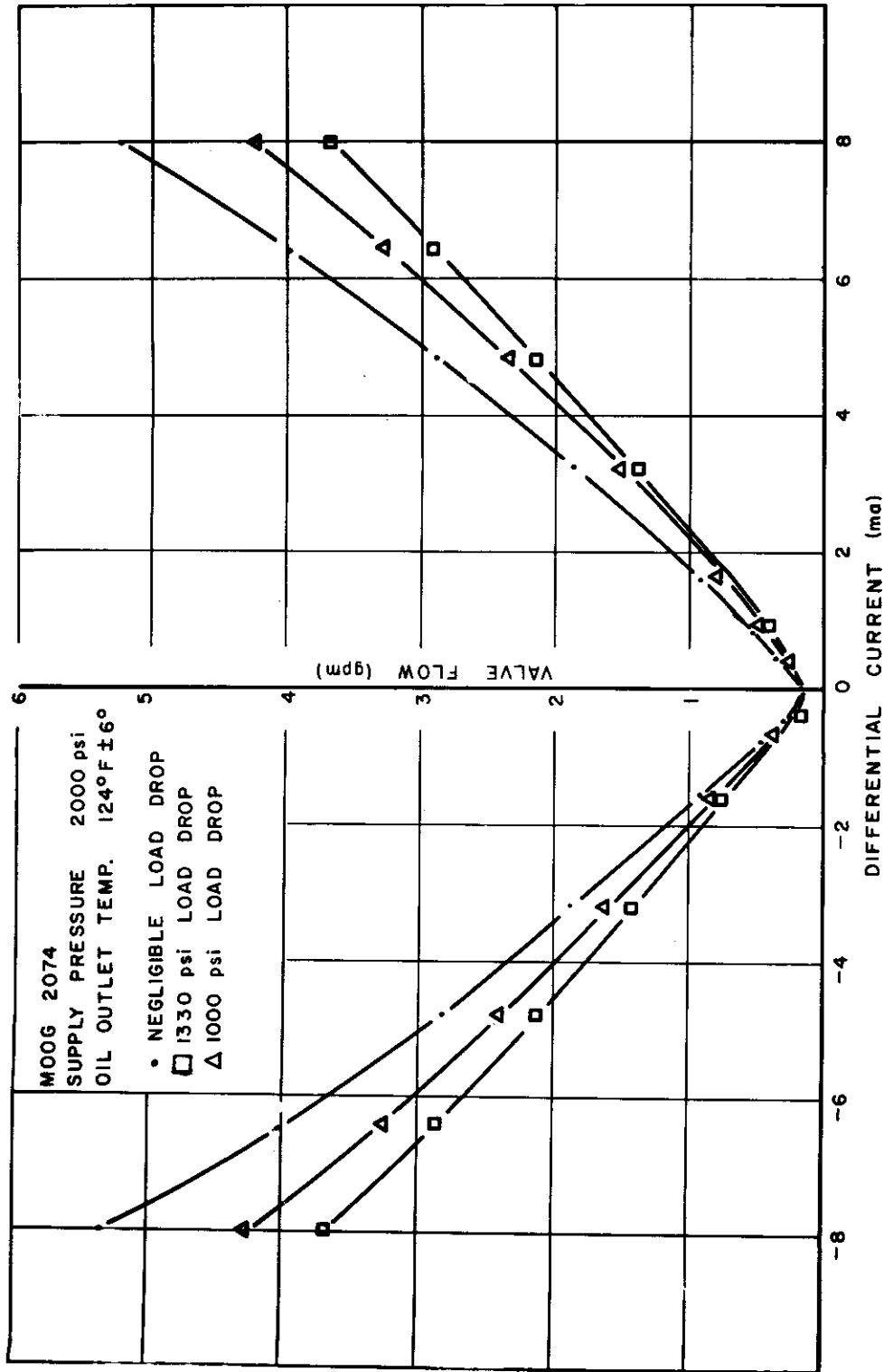
Figure 84. Moog 2074 Valve Flow vs. Differential Current – 2000 psi Supply Pressure

The chart contains the following labels:

MOOG 2074
SUPPLY PRESSURE   2000 psi
OIL OUTLET TEMP.   124°F ±6°

• NEGLIGIBLE LOAD DROP
□ 1330 psi LOAD DROP
△ 1000 psi LOAD DROP

VALVE FLOW (gpm)

DIFFERENTIAL CURRENT (ma)
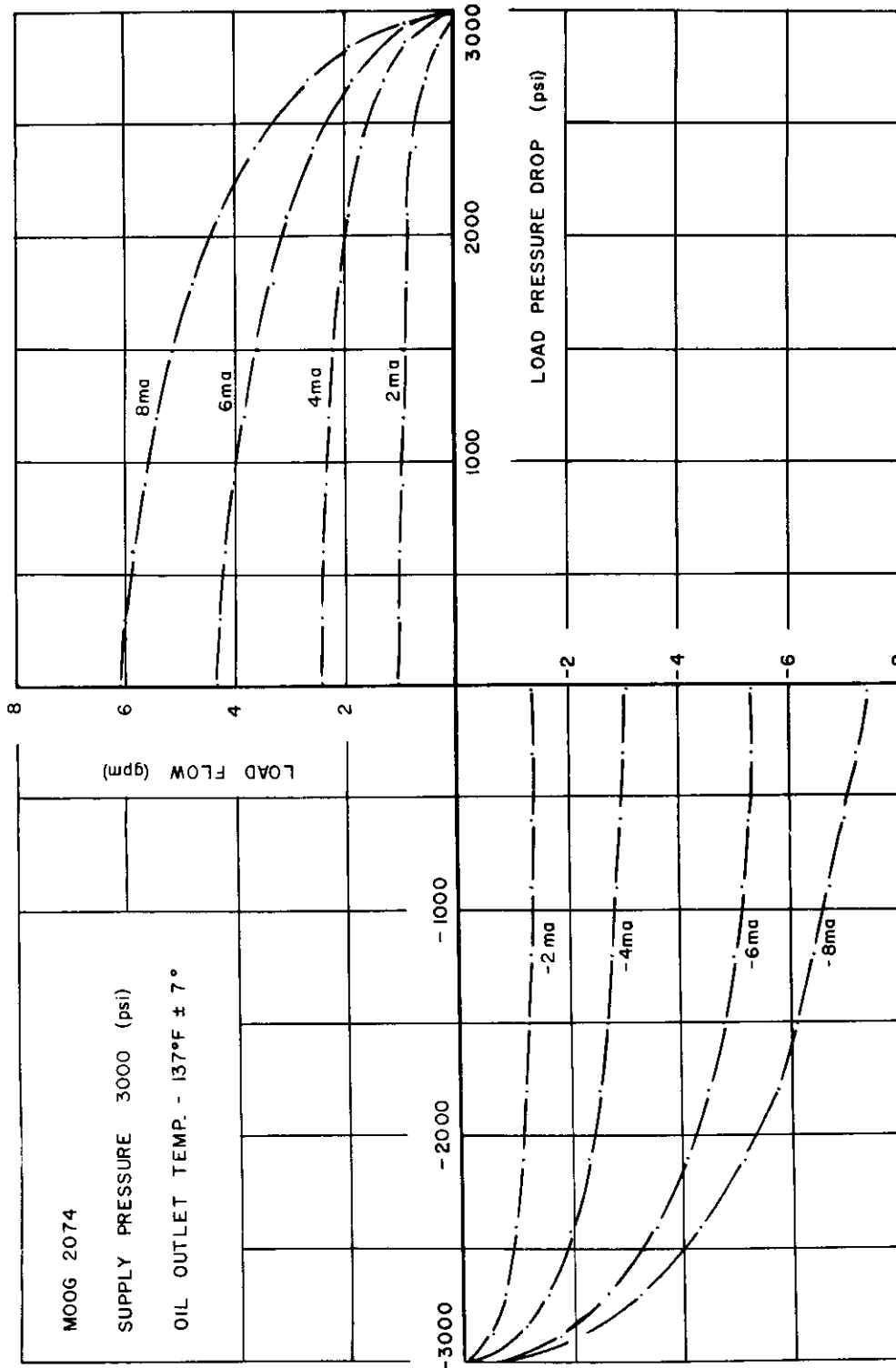
Figure 85. Moog 2074 Load Flow vs. Load Pressure - 3000 psi Supply Pressure

MOOG 2074

SUPPLY PRESSURE 3000 (psi)

OIL OUTLET TEMP. - 137°F ± 7°
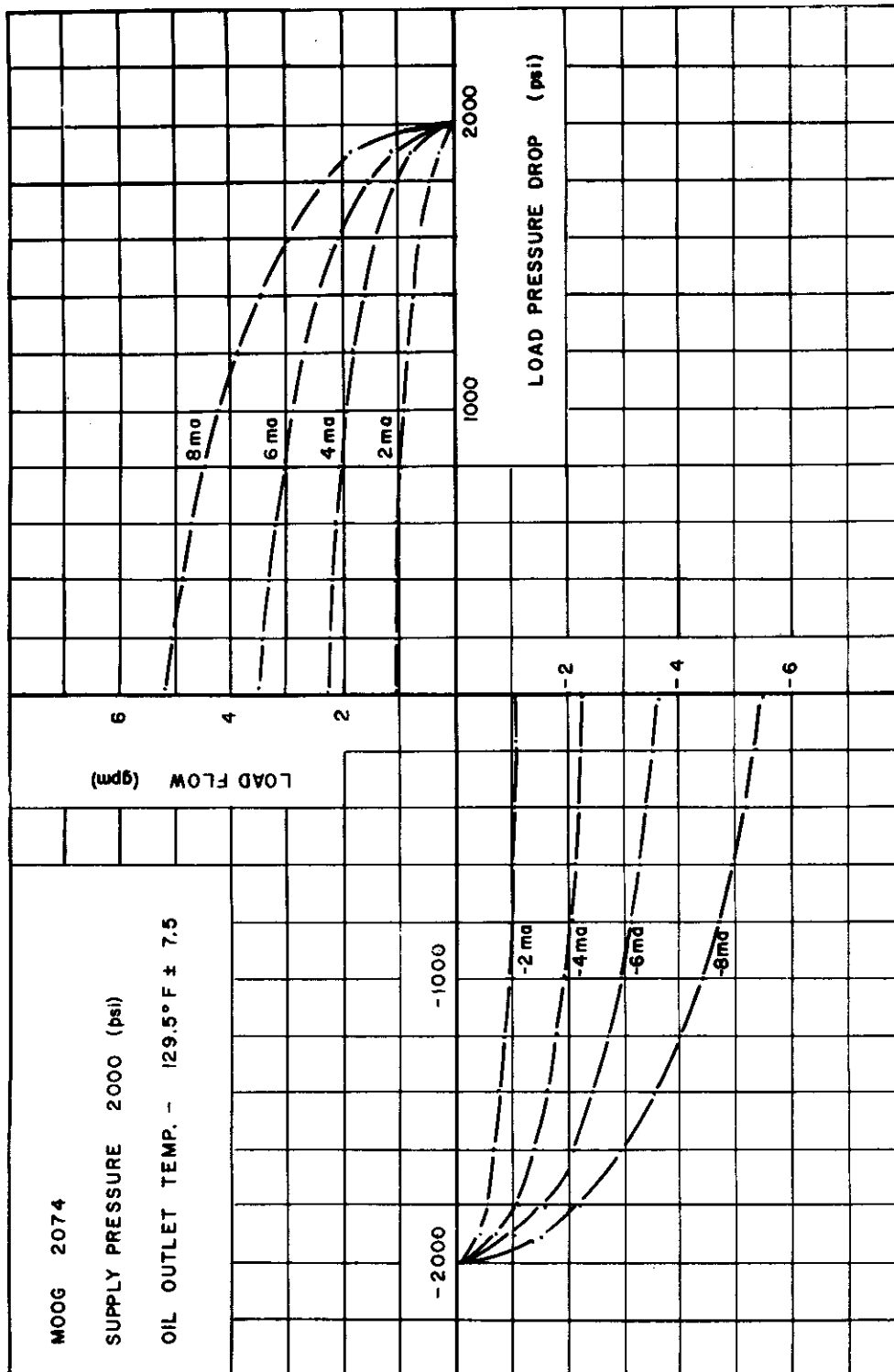
Figure 86. Moog 2074 Load Flow vs. Load Pressure - 2000 psi Supply Pressure
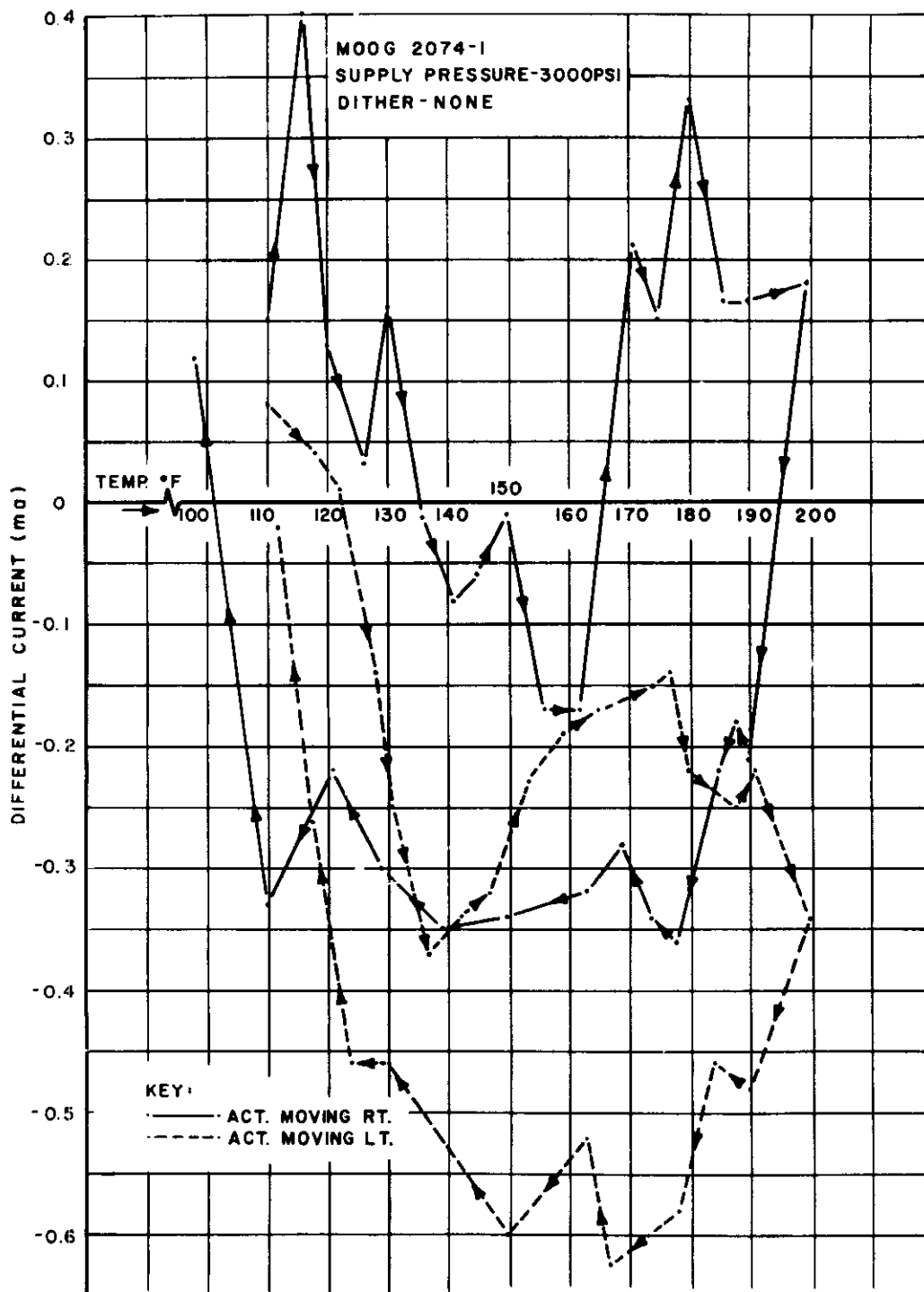
Figure 87. Moog 2074 Null Shift vs. Oil Temperature -
No Dither
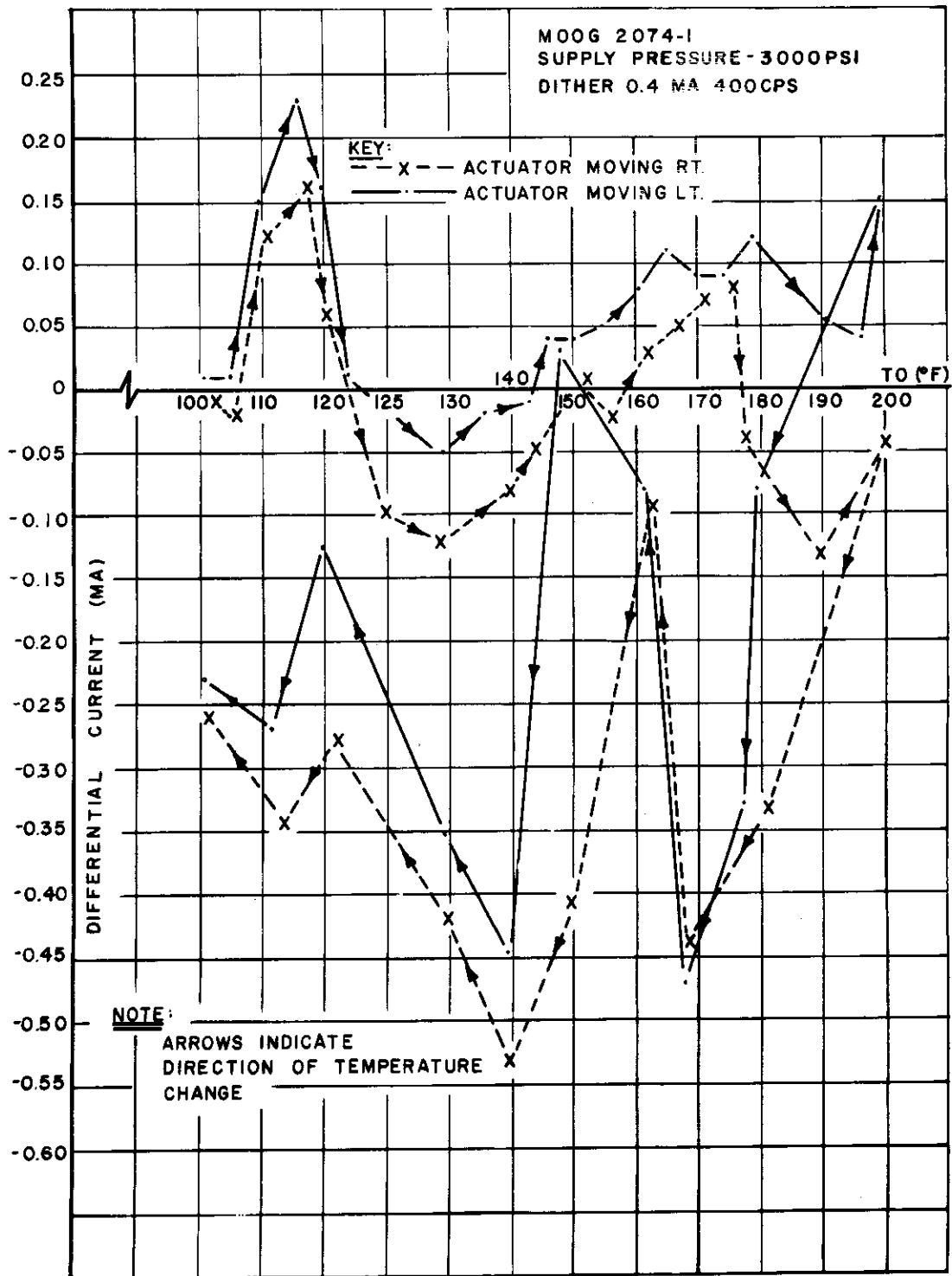
Figure 88. Moog 2074 Null Shift vs. Oil Temperature -
Dither
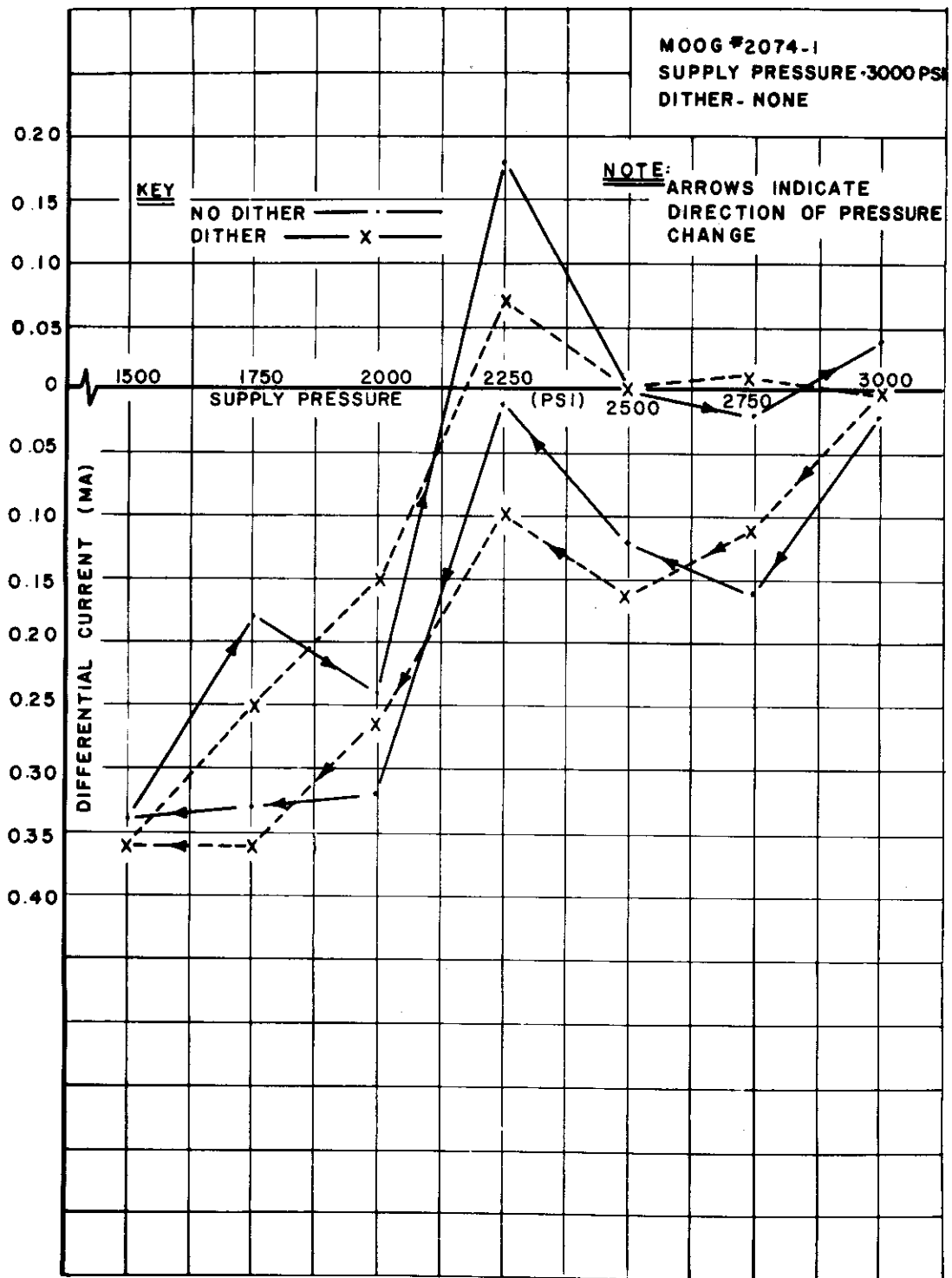
Figure 89. Moog 2074 Null Shift vs. Supply Pressure
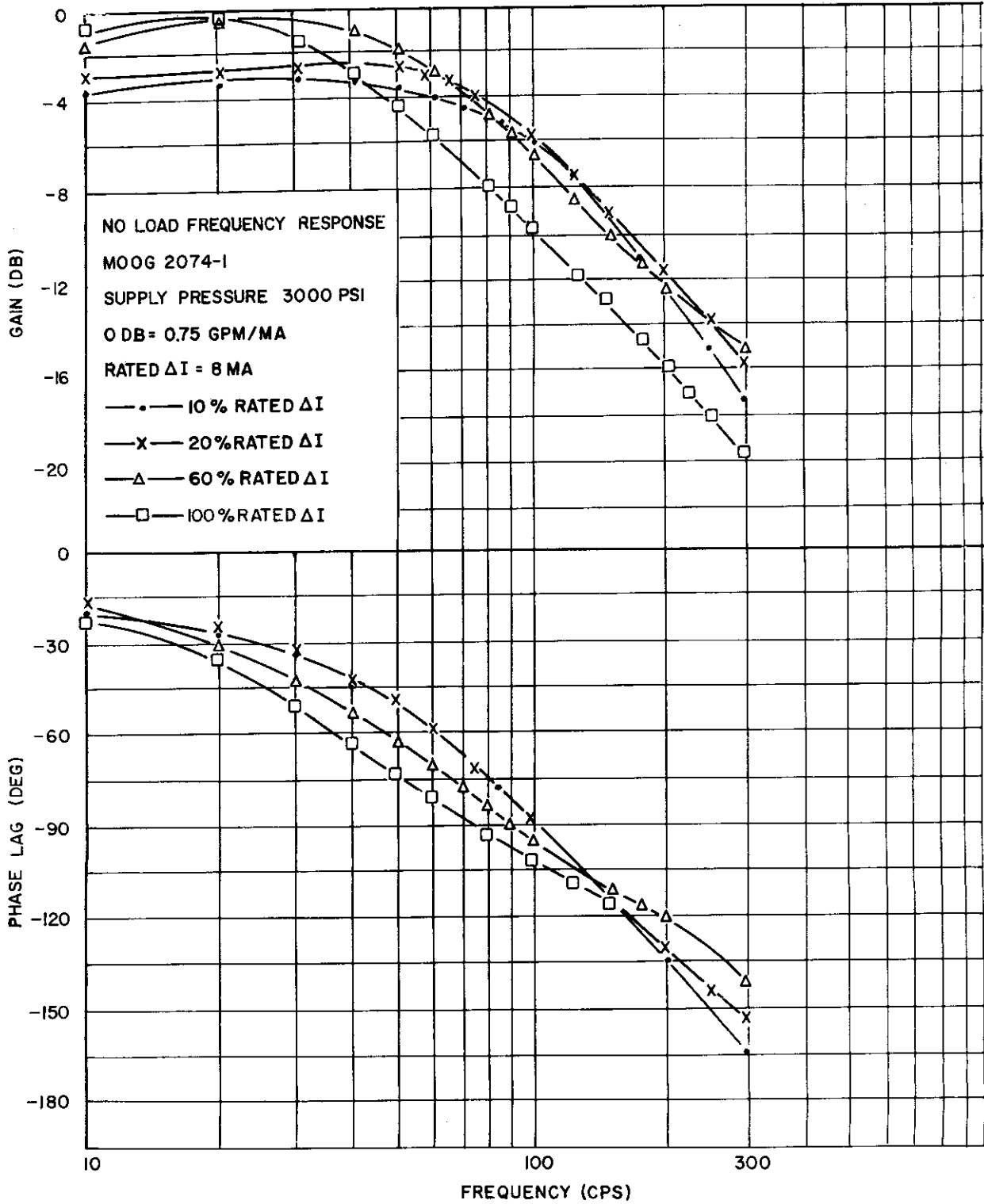
Figure 90. Moog 2074 No-Load Frequency Response
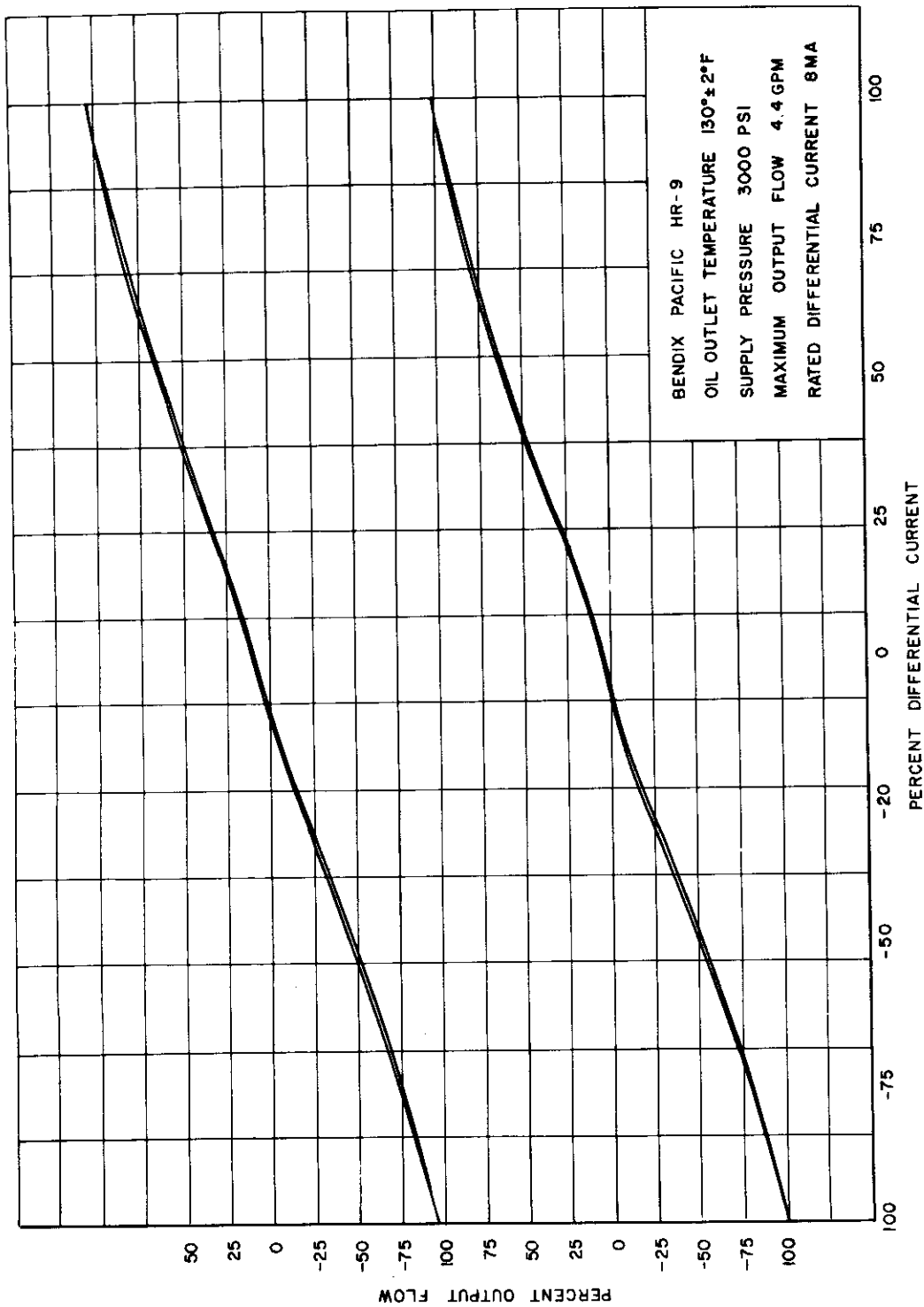
Figure 91. Bendix Pacific HR-9 Hysteresis - Rated Current

BENDIX PACIFIC HR-9

OIL OUTLET TEMPERATURE 130°±2°F

SUPPLY PRESSURE 3000 PSI

MAXIMUM OUTPUT FLOW 4.4 GPM

RATED DIFFERENTIAL CURRENT 8 MA

PERCENT DIFFERENTIAL CURRENT

PERCENT OUTPUT FLOW
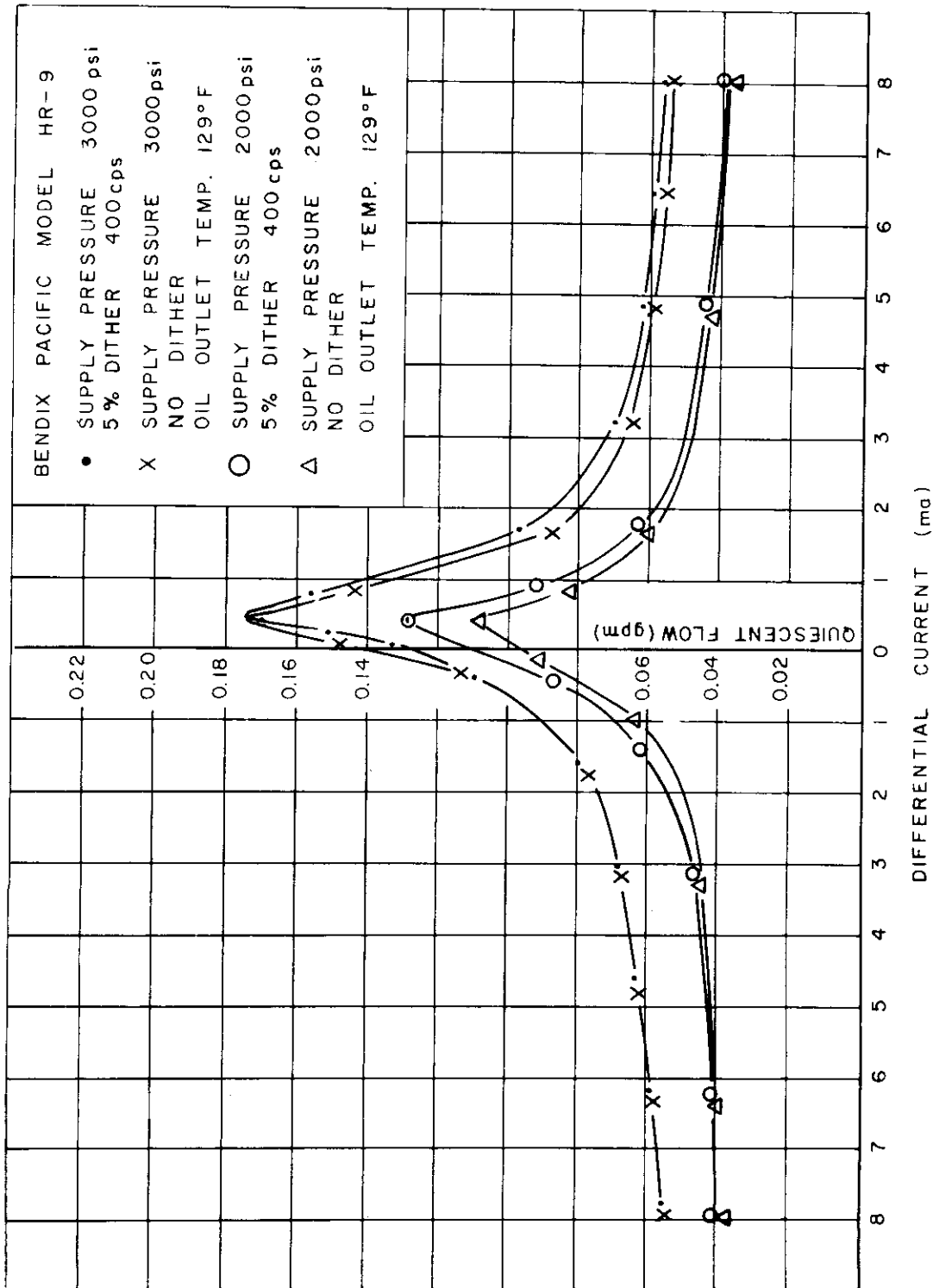
Figure 92. Bendix Pacific HR-9 Quiescent Flow vs. Differential Current
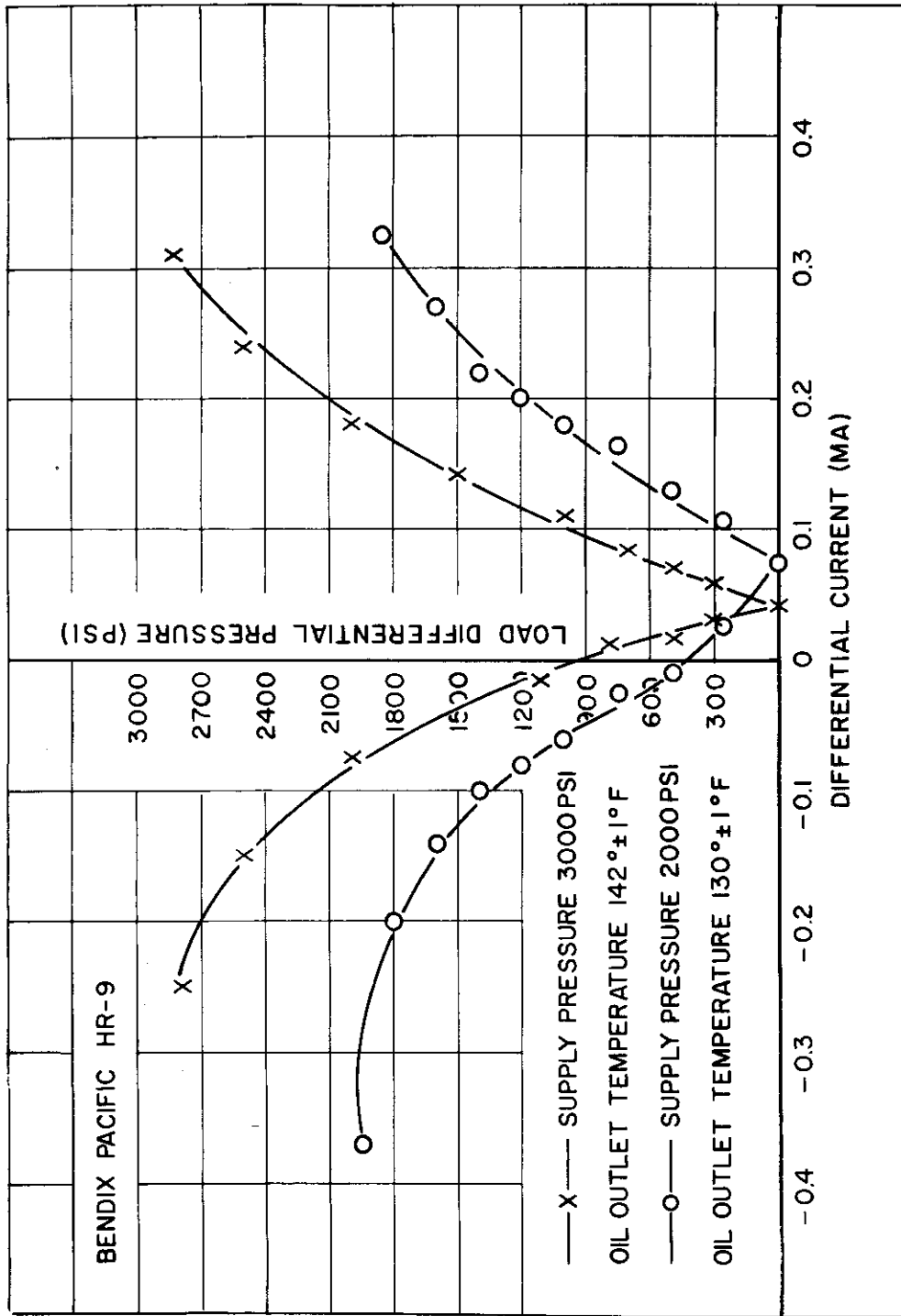
Figure 93. Bendix Pacific HR-9 Load Pressure vs. Differential Current at Zero Load Flow
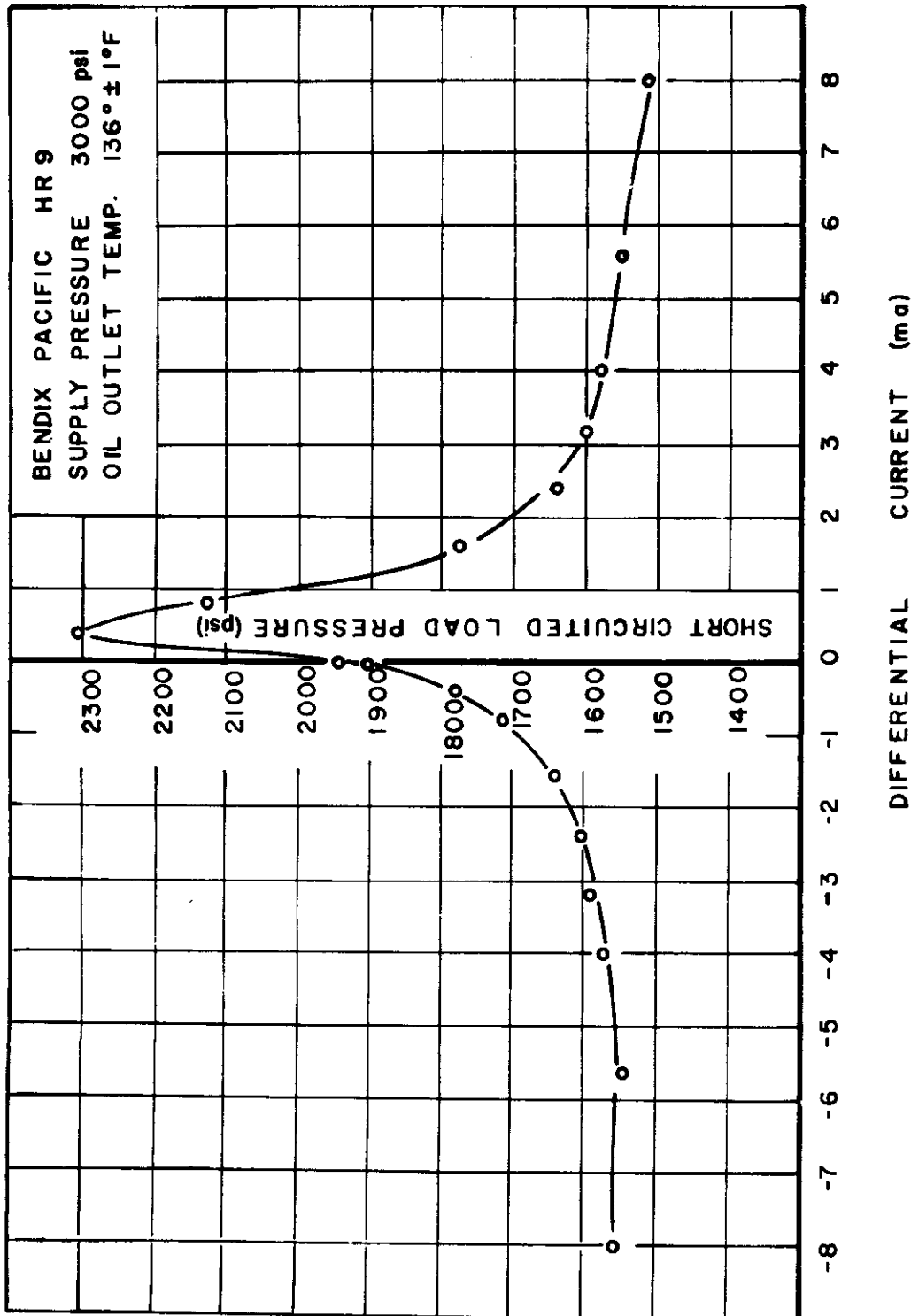
Figure 94. Bendix Pacific HR-9 Short Circuited Load Pressure vs. Differential Current

The graph contains the following labels:

BENDIX PACIFIC HR 9
SUPPLY PRESSURE 3000 psi
OIL OUTLET TEMP. 135° ± 1°F

o — NEGLIGIBLE LOAD DROP
□ — 1000 psi LOAD DROP
x — 2 000psi LOAD DROP

TOTAL VALVE FLOW (gpm)

DIFFERENTIAL CURRENT (ma)
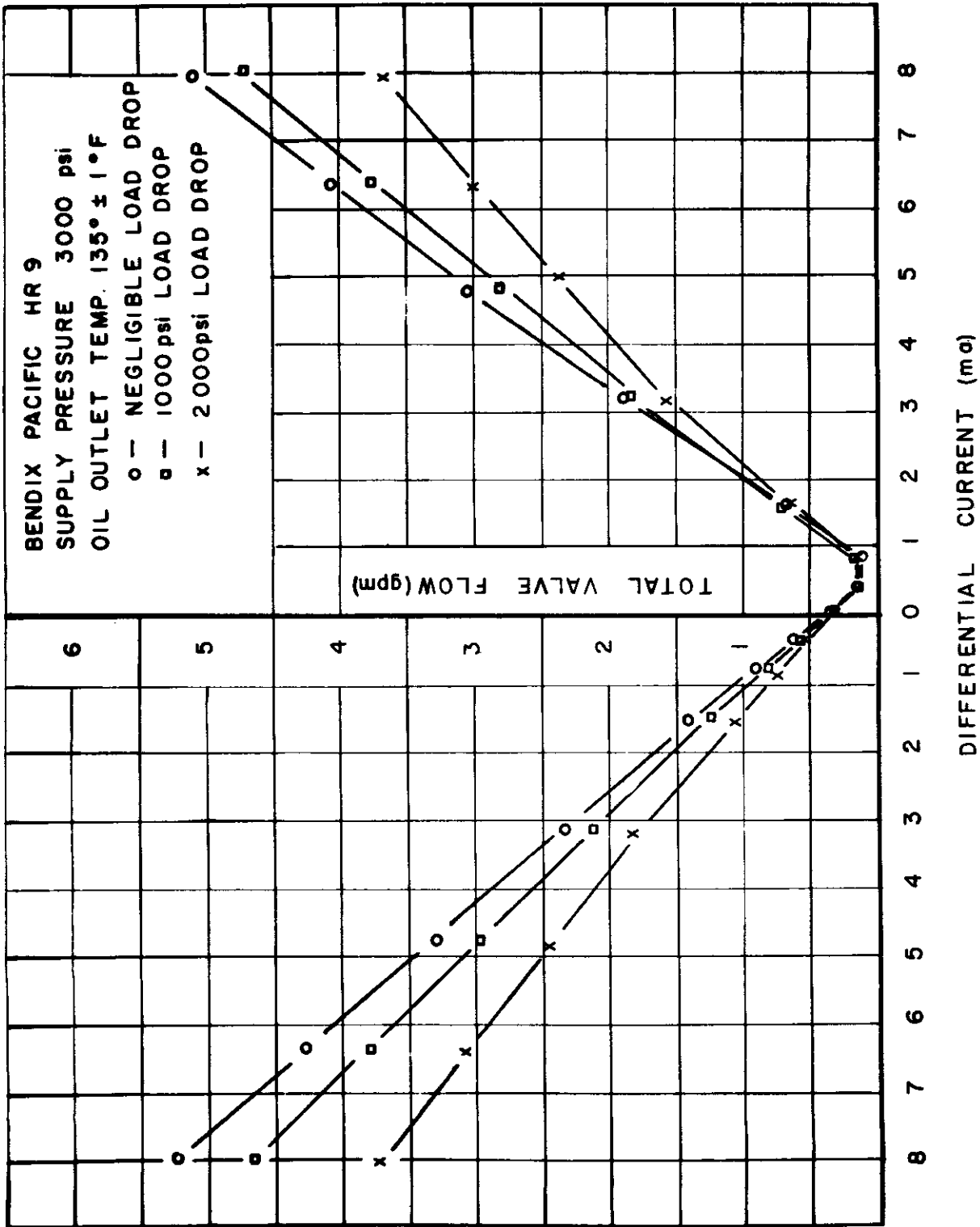
Figure 95. Bendix Pacific HR-9 Valve Flow vs. Differential Current - 3000 psi Supply Pressure
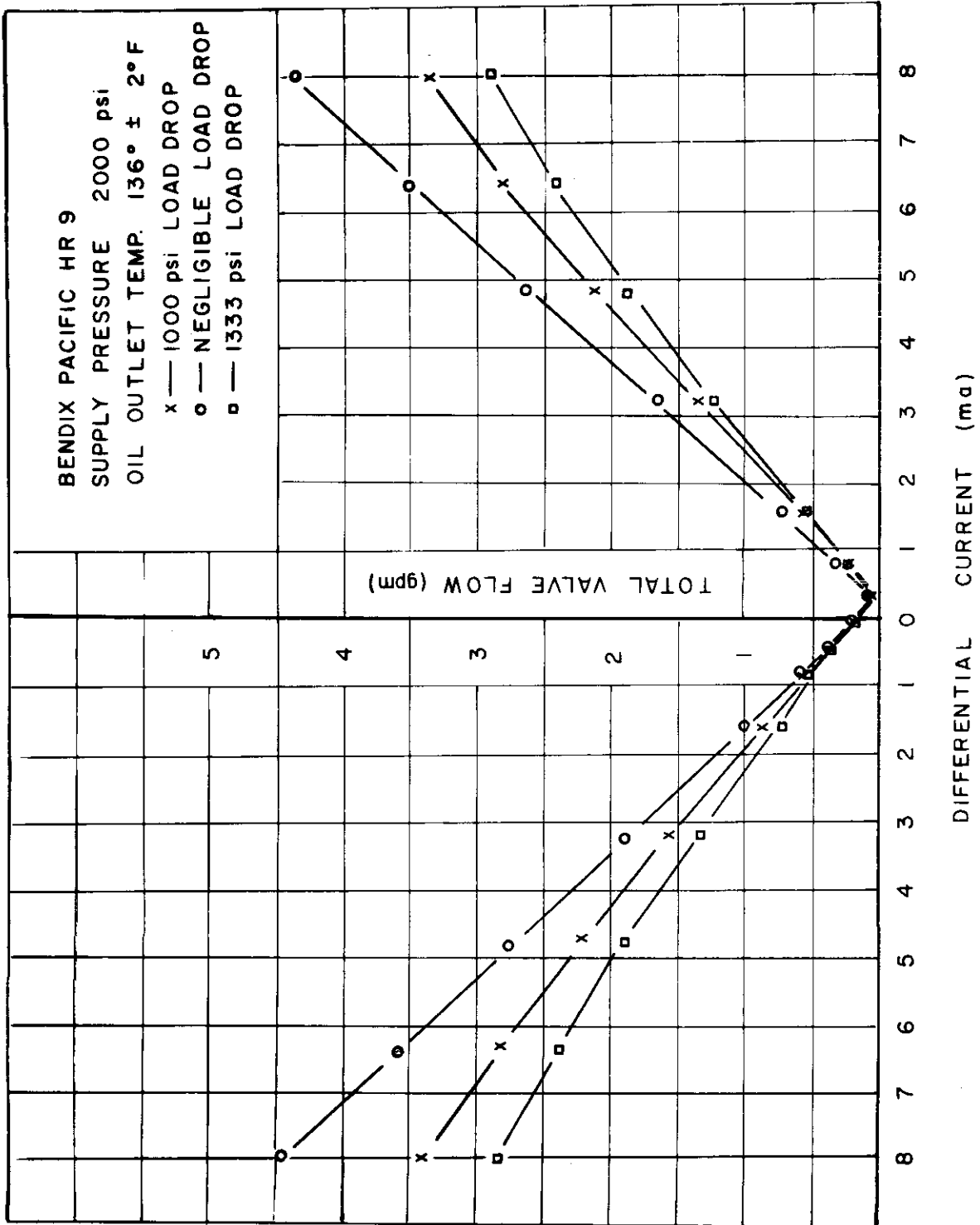
Figure 96. Bendix Pacific HR-9 Valve Flow vs. Differential Current - 2000 psi Supply Pressure
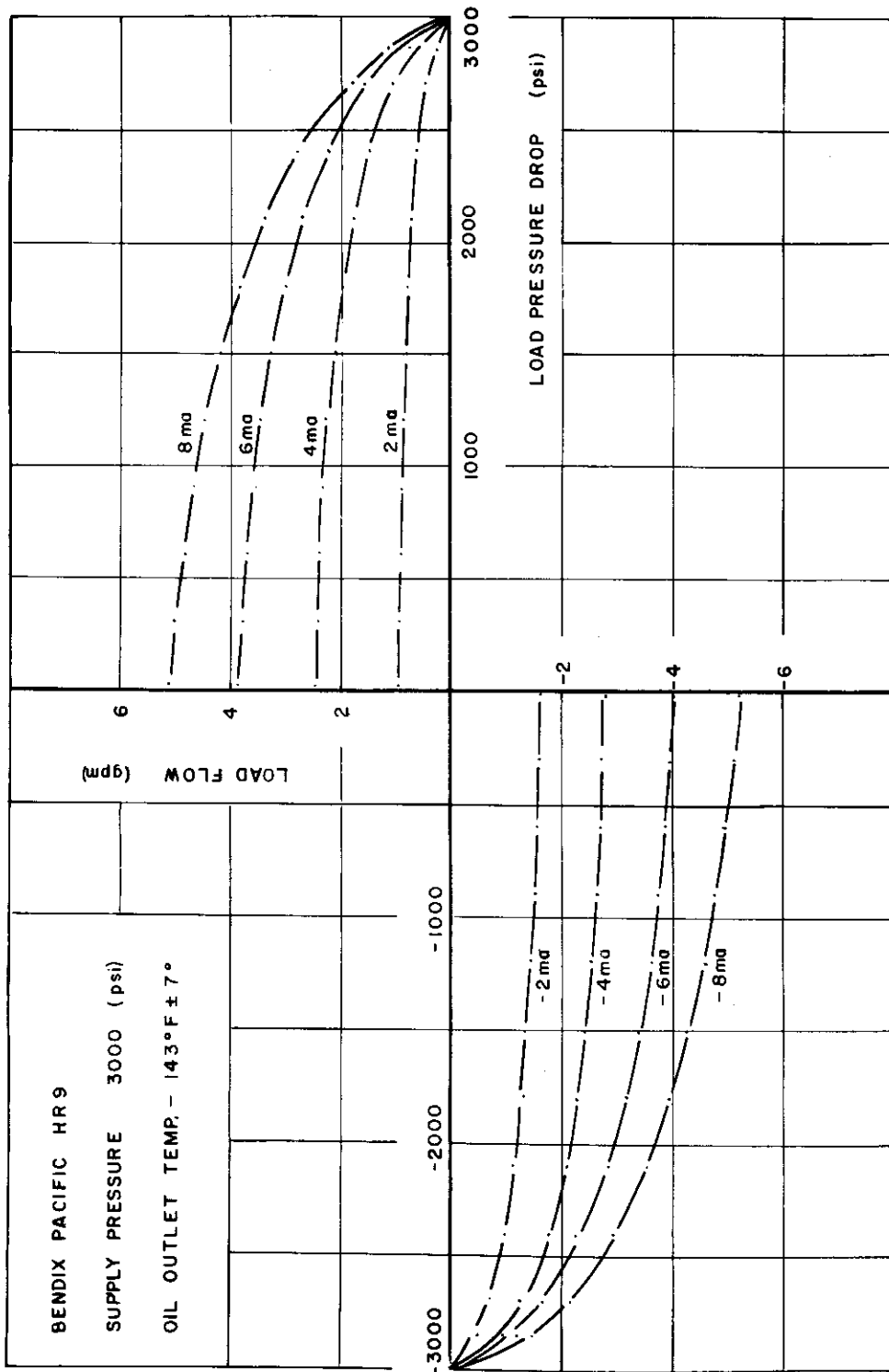
Figure 97. Bendix Pacific HR-9 Load Flow vs. Load Pressure - 3000 psi Supply Pressure
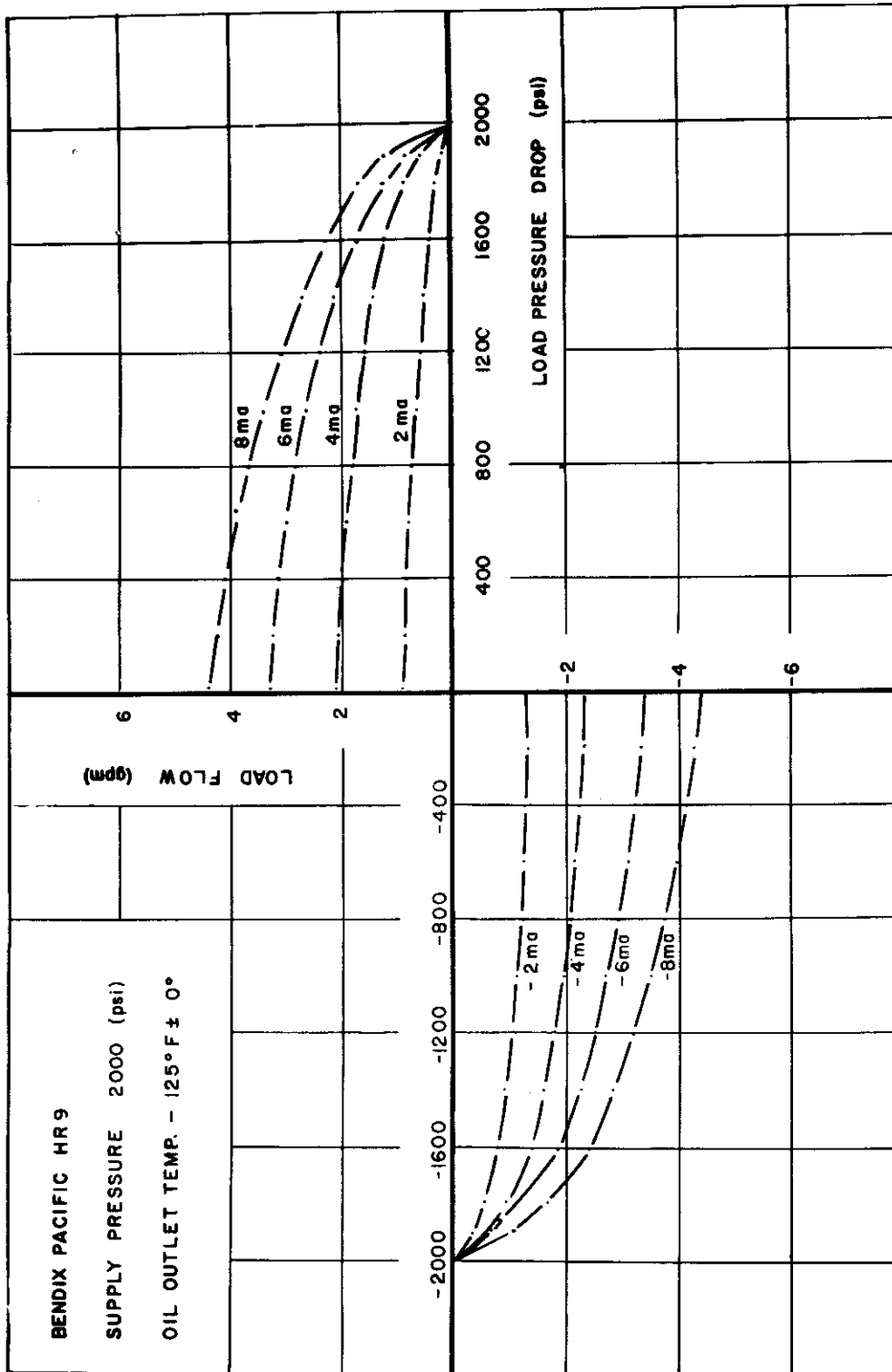
Figure 98. Bendix Pacific HR-9 Load Flow vs. Load Pressure - 2000 psi Supply Pressure
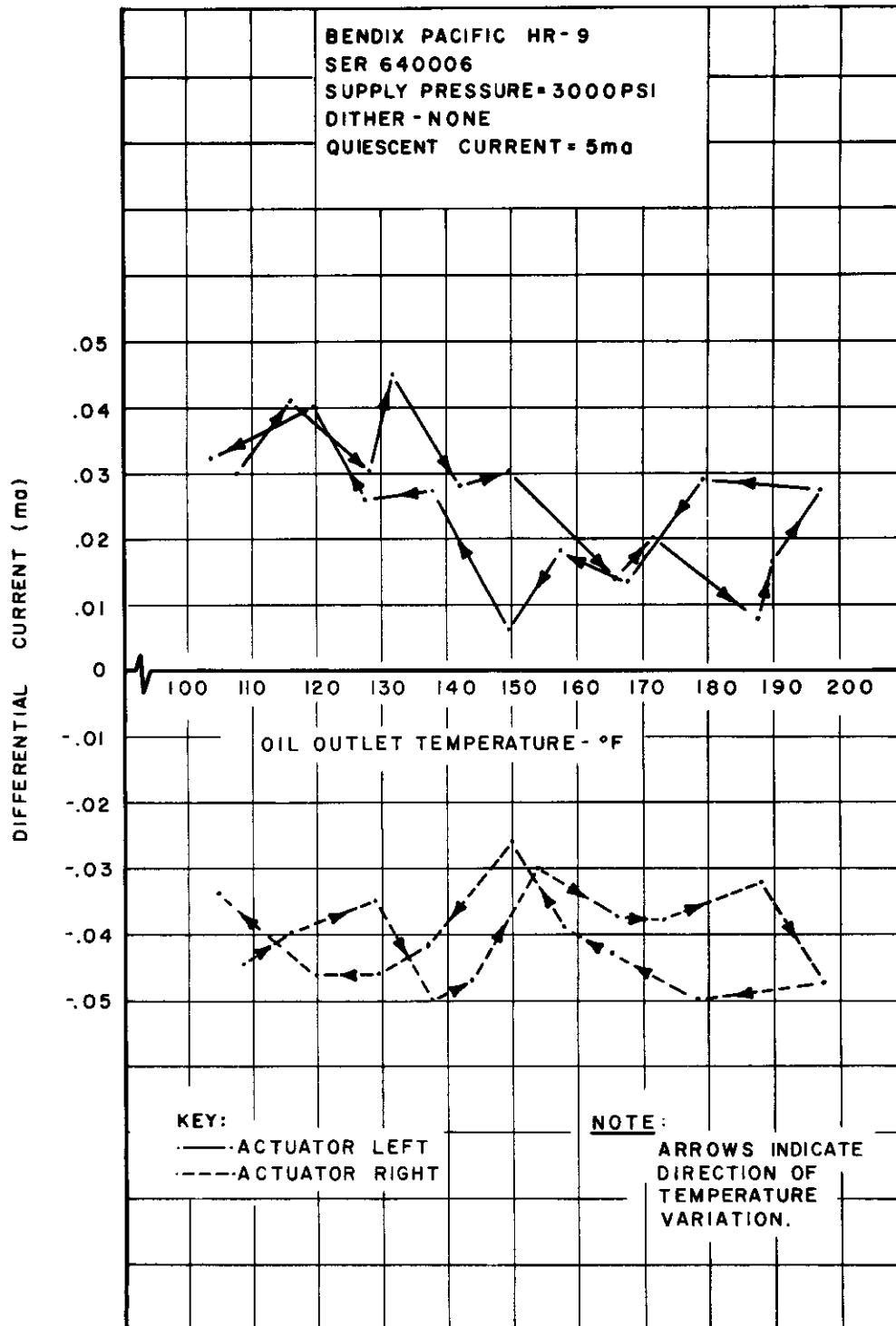
Figure 99.   Bendix Pacific HR-9 Null Shift vs. Oil Temperature -
No Dither
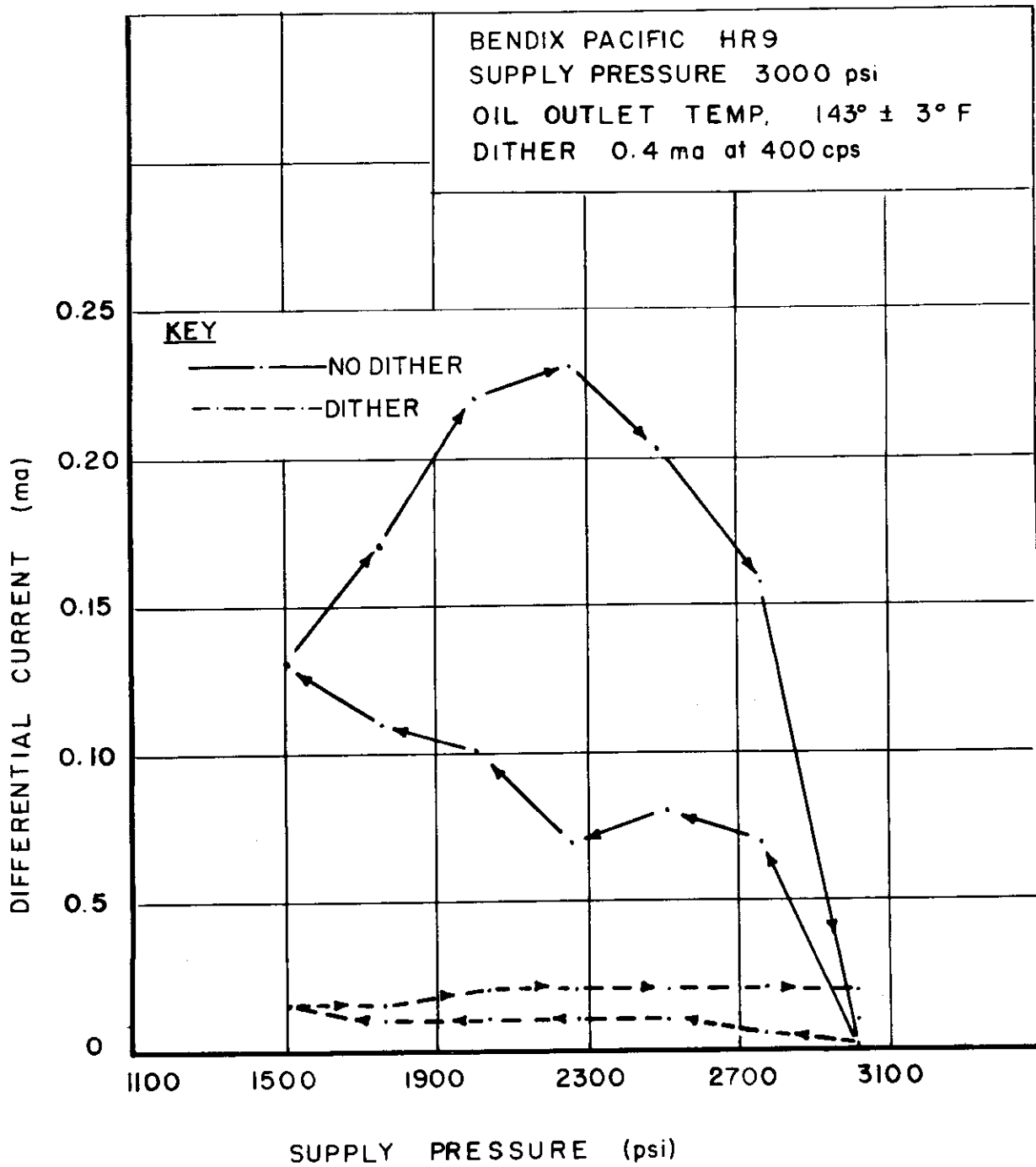
Figure 100. Bendix Pacific HR-9 Null Shift vs. Oil Temperature -
Dither
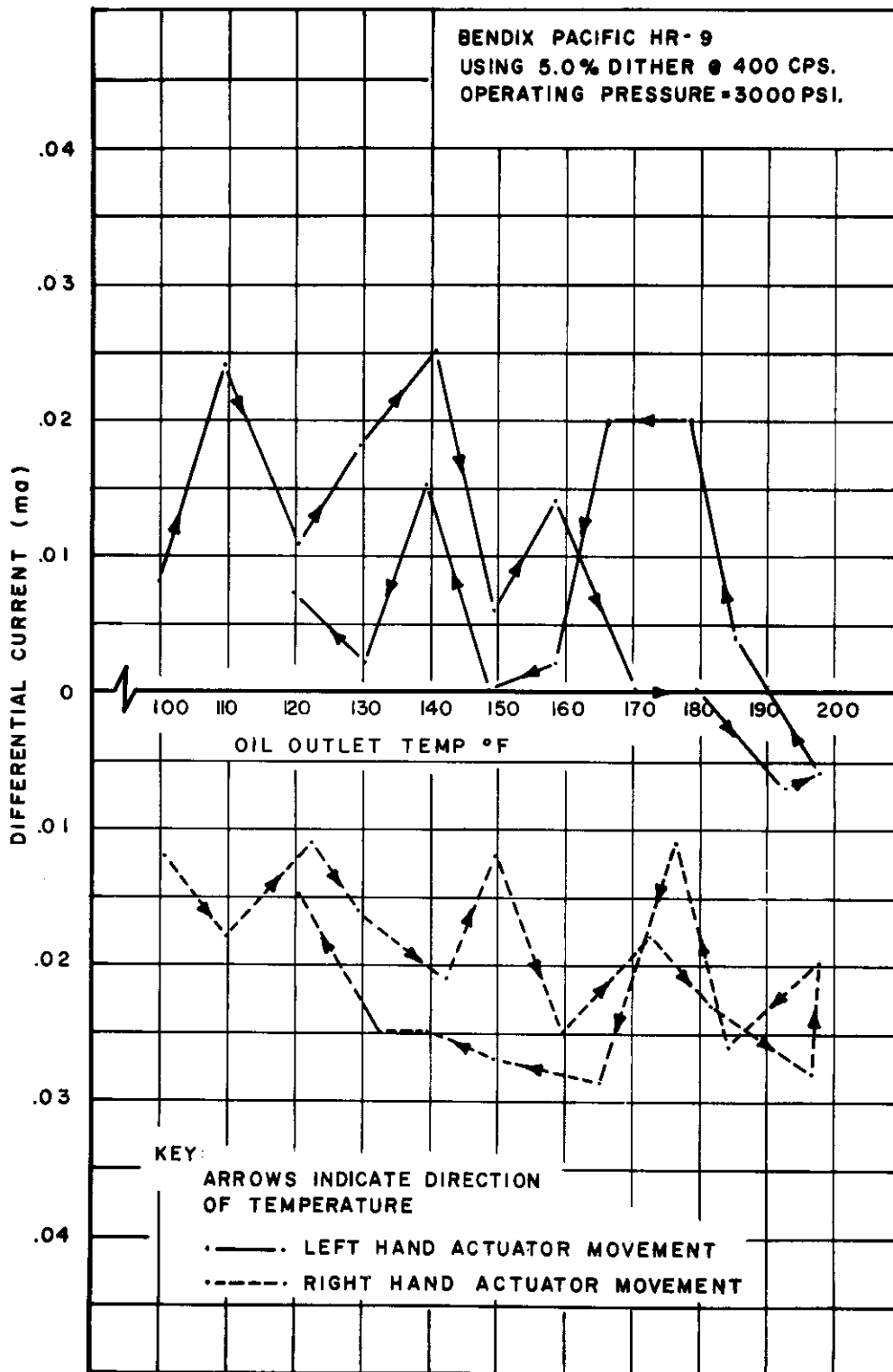
Figure 101. Bendix Pacific HR-9 Null Shift vs. Supply Pressure
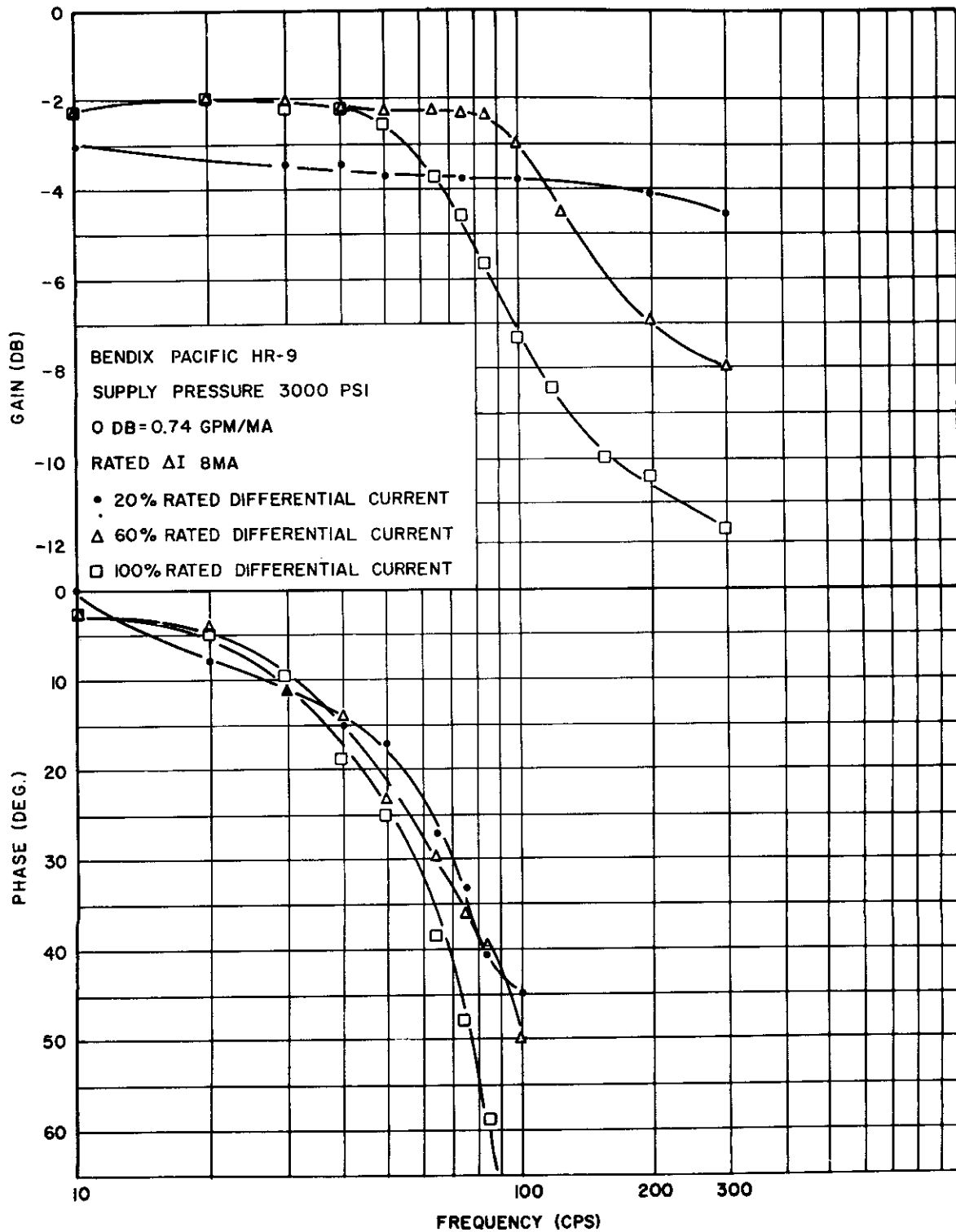
Figure 102. Bendix Pacific HR-9 No-Load Frequency Response
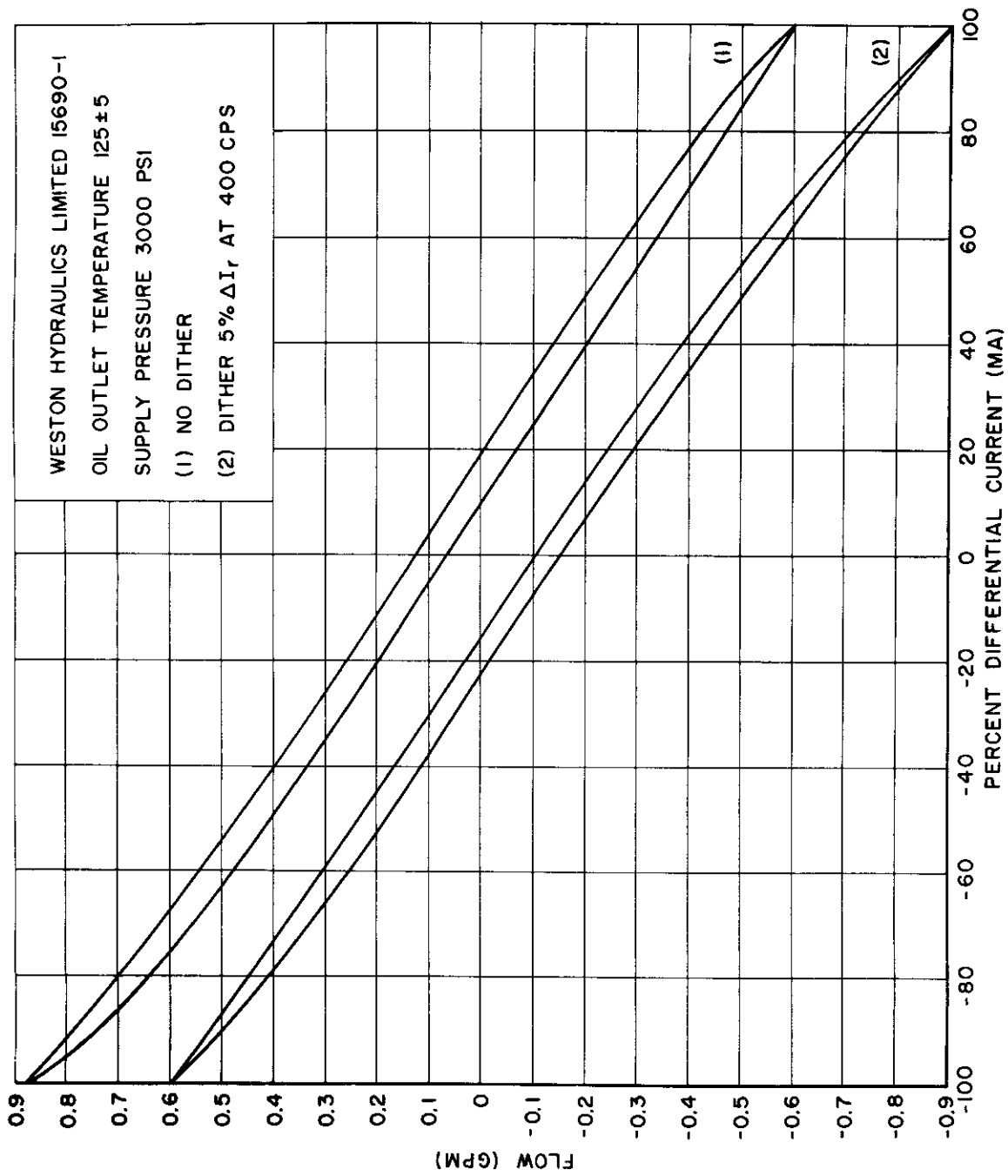
Figure 103. Weston Hydraulics Ltd. 15690 - 1 Hysteresis - Rated Current

149
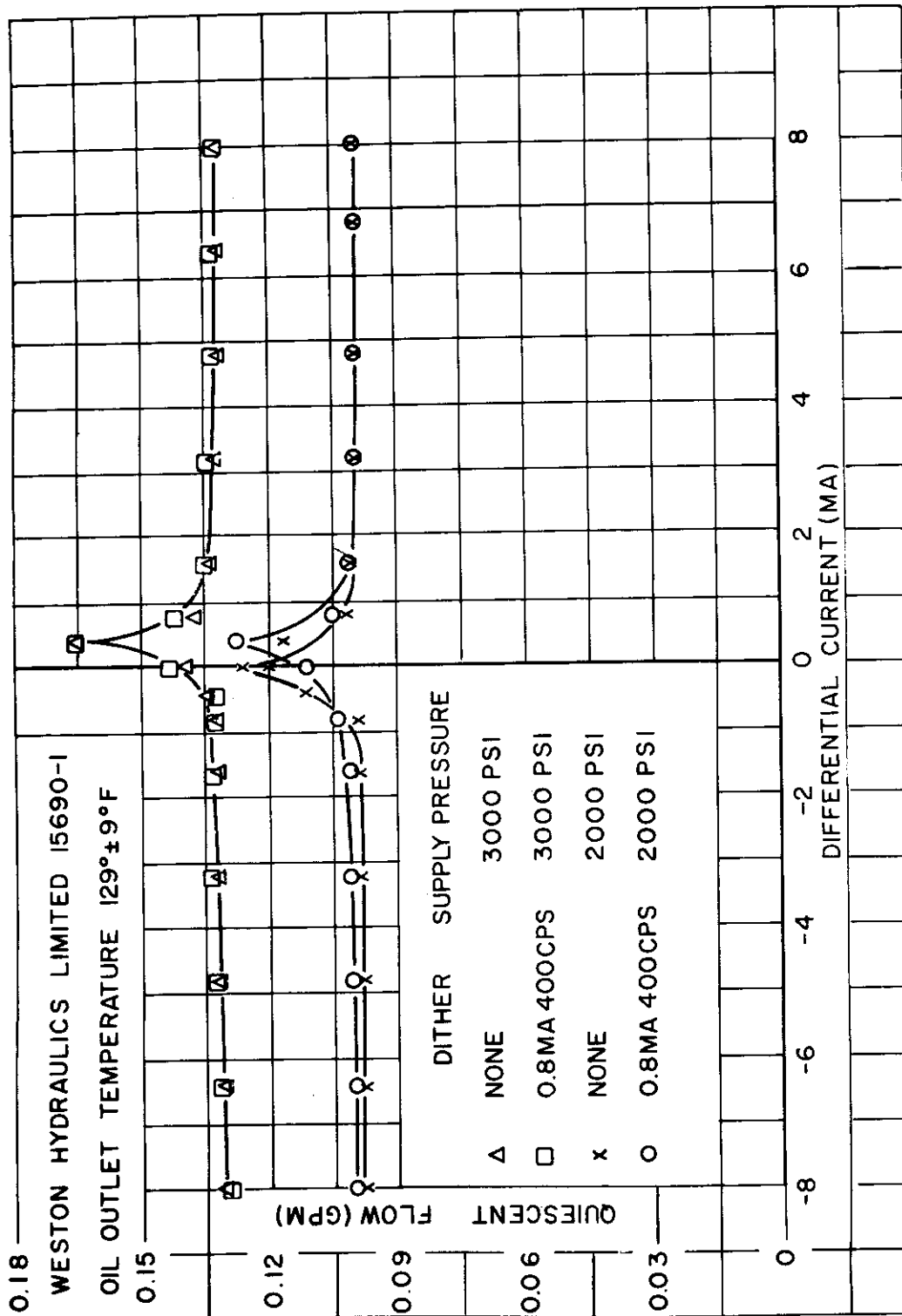
Figure 104. Weston Hydraulics Ltd. 15690 - 1 Quiescent Flow vs. Differential Current
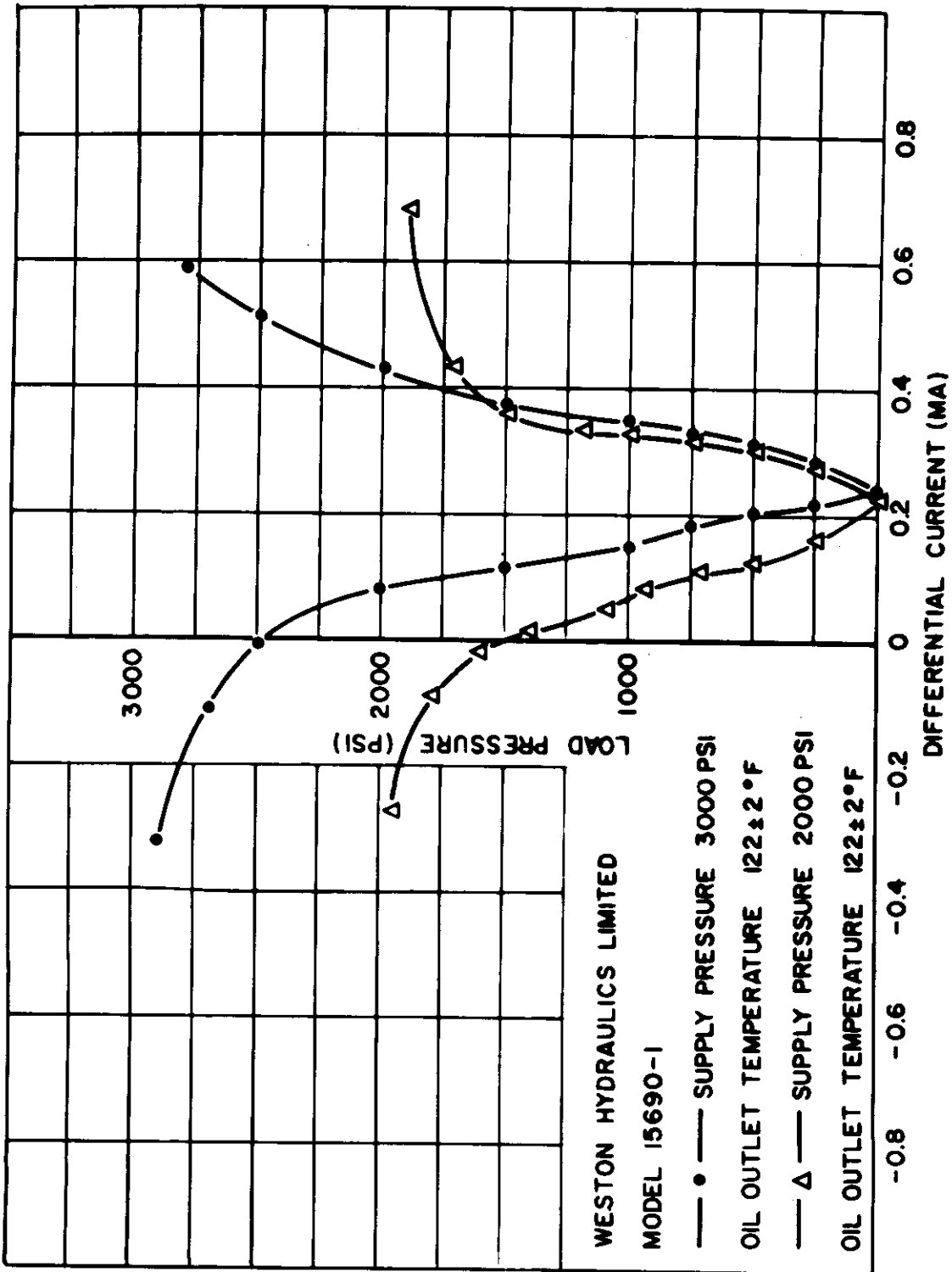
Figure 105. Weston Hydraulics Ltd. 15690 - 1 Load Pressure vs. Differential Current at Zero Load Flow
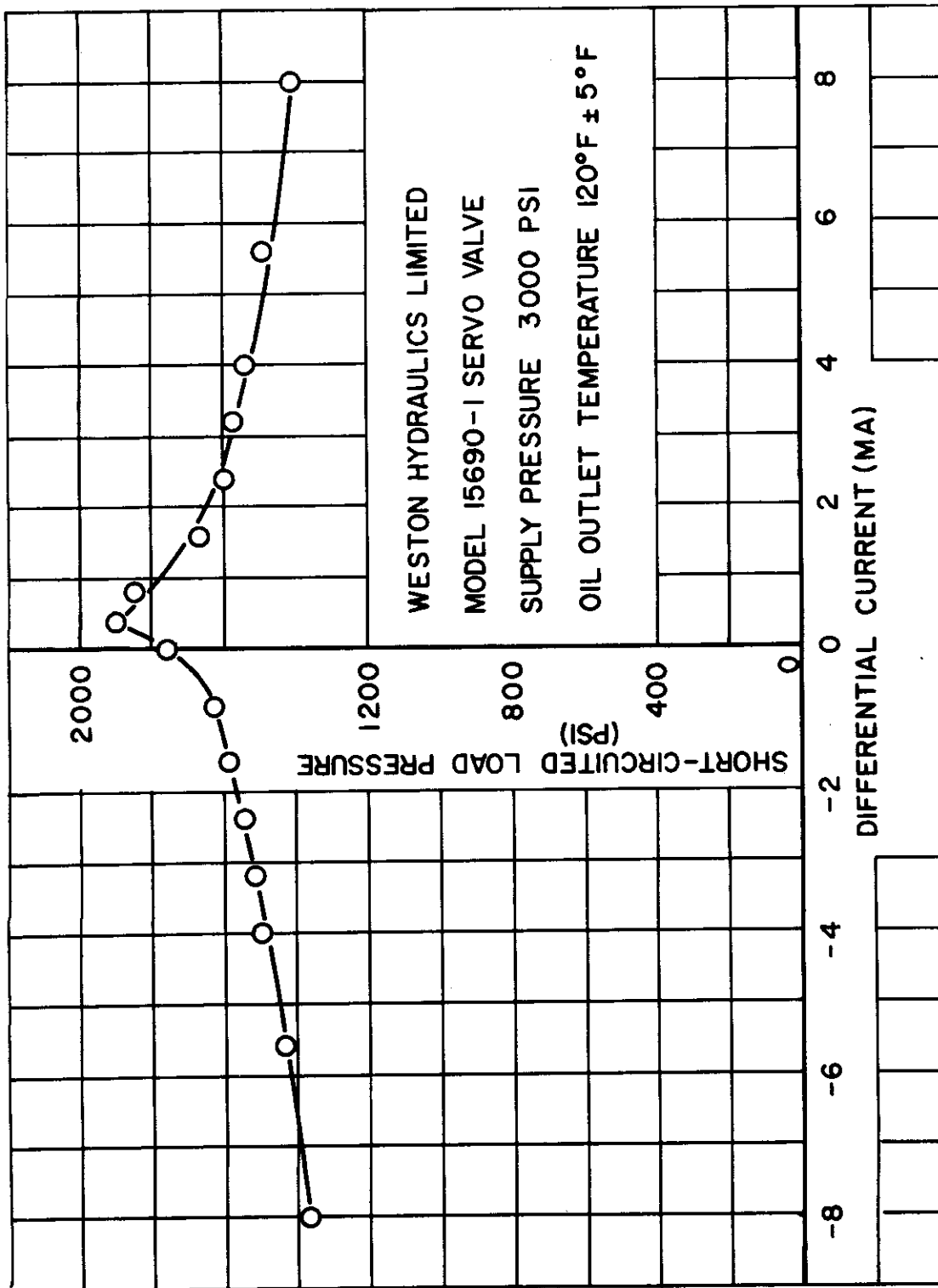
Figure 106. Weston Hydraulics Ltd. 15690 - 1 Short Circuited
Load Pressure vs. Differential Current
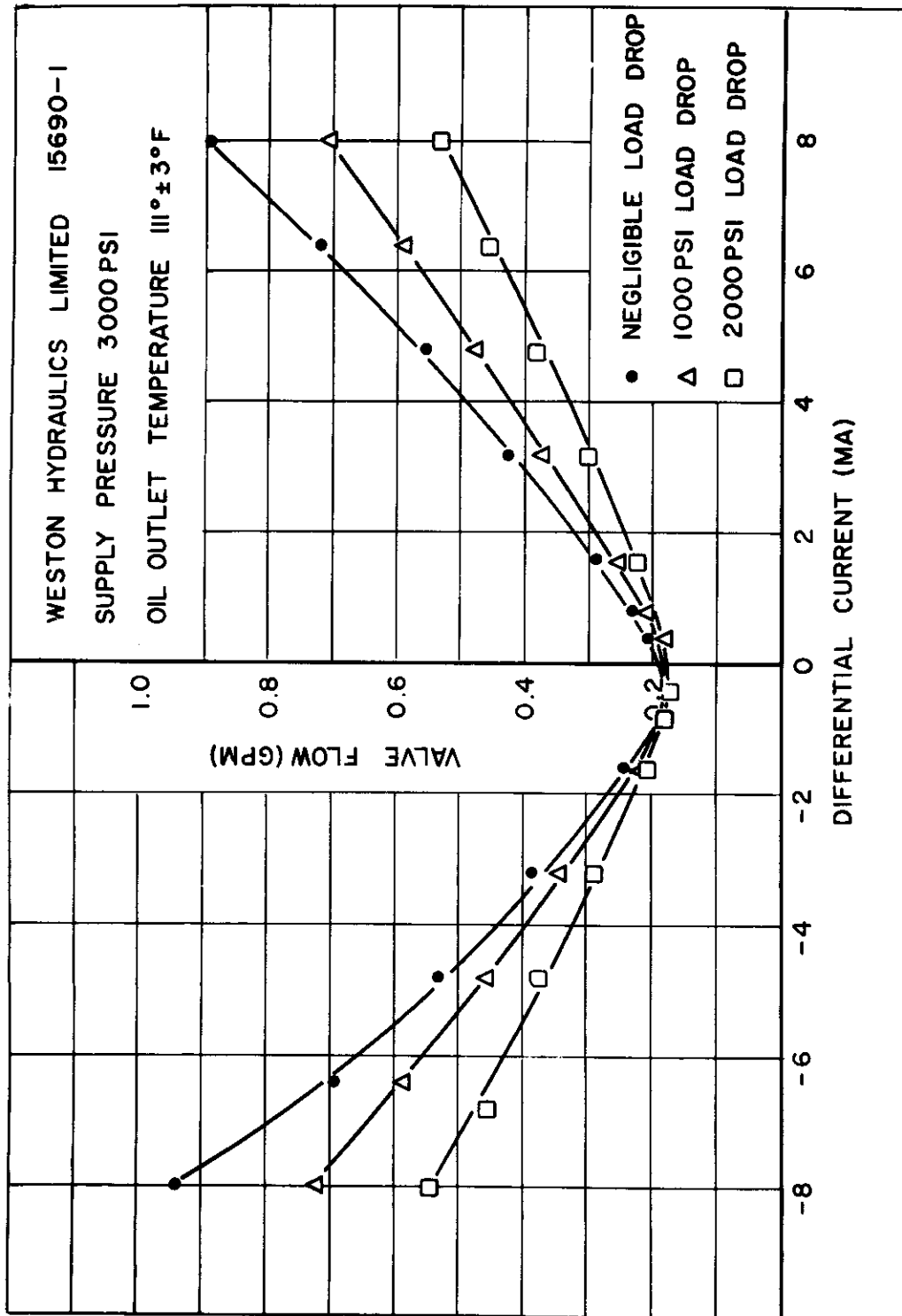
Figure 107. Weston Hydraulic Ltd. 15690 - 1 Valve Flow vs.
Differential Current – 3000 psi Supply Pressure
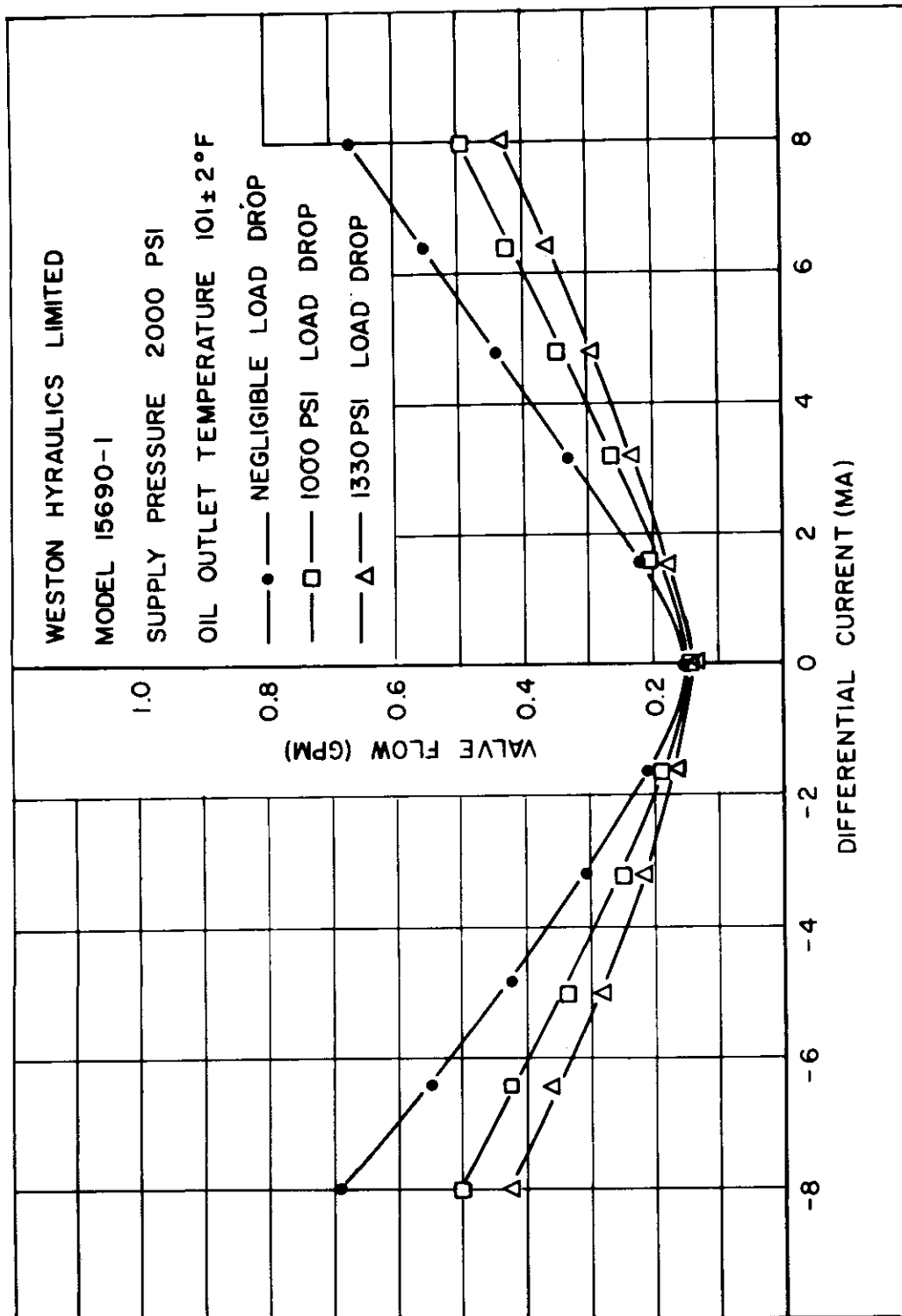
Figure 108. Weston Hydraulic Ltd. 15690 - 1 Valve Flow vs. Differential Current - 2000 psi Supply Pressure
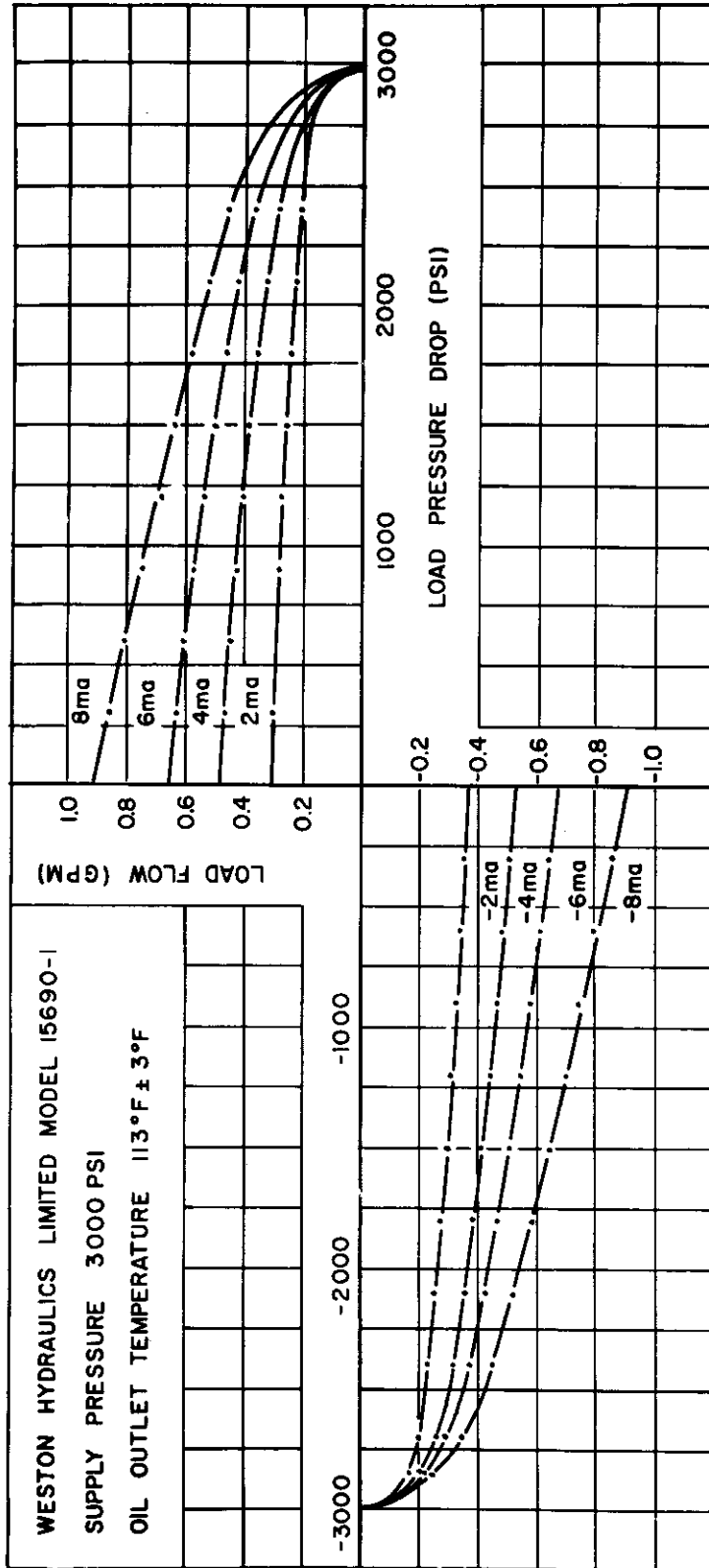
Figure 109. Weston Hydraulic Ltd. 15690 - 1 Load Flow vs. Load Pressure - 3000 psi Supply Pressure

WESTON HYDRAULICS LIMITED #15690-1
SUPPLY PRESSURE 2000 PSI
OIL OUTLET TEMPERATURE 114°F ± 4°F

LOAD FLOW (GPM)

LOAD PRESSURE DROP (PSI)
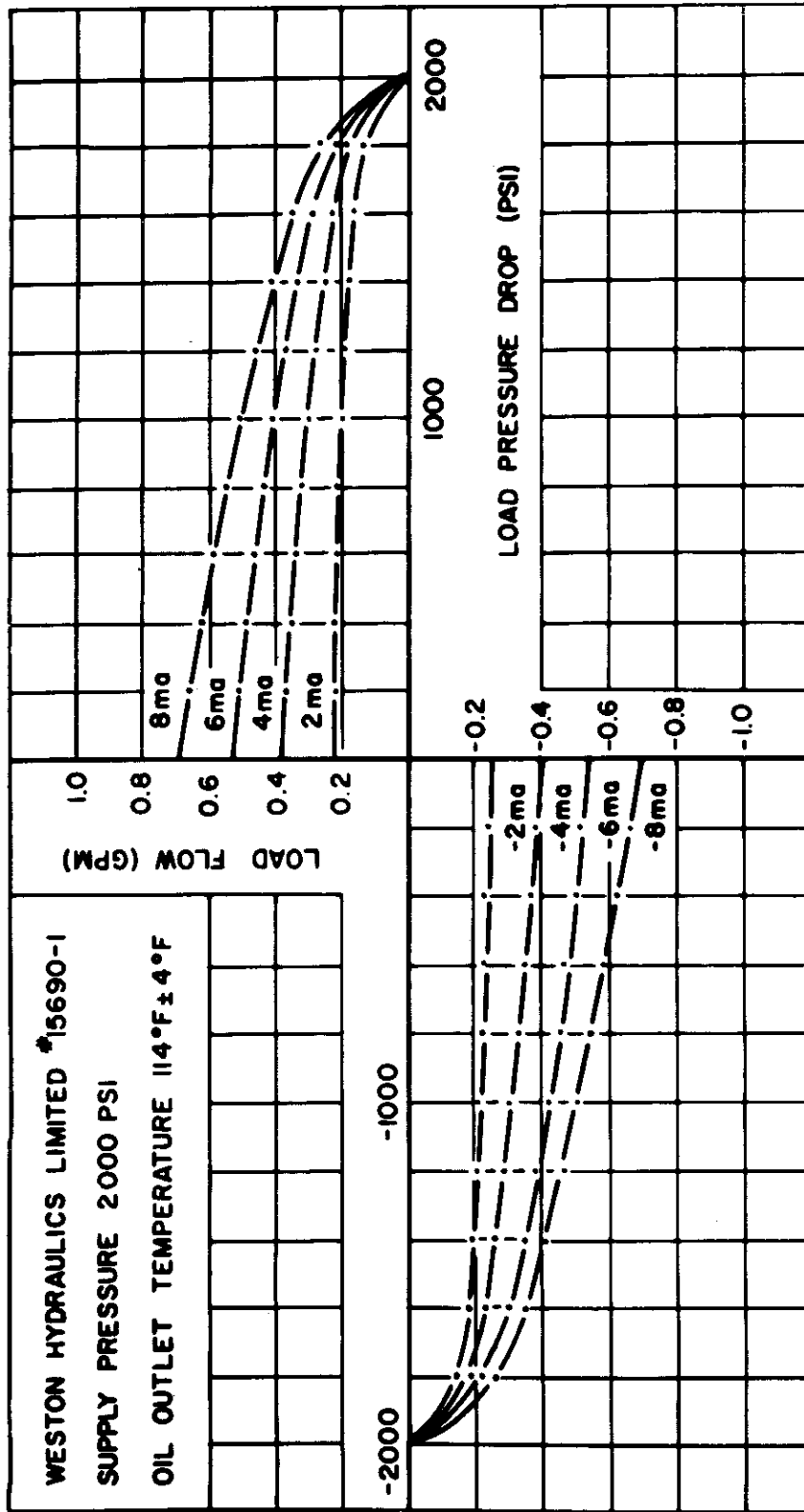
Figure 110. Weston Hydraulic Ltd. 15690 - 1 Load Flow vs.
Load Pressure - 2000 psi Supply Pressure
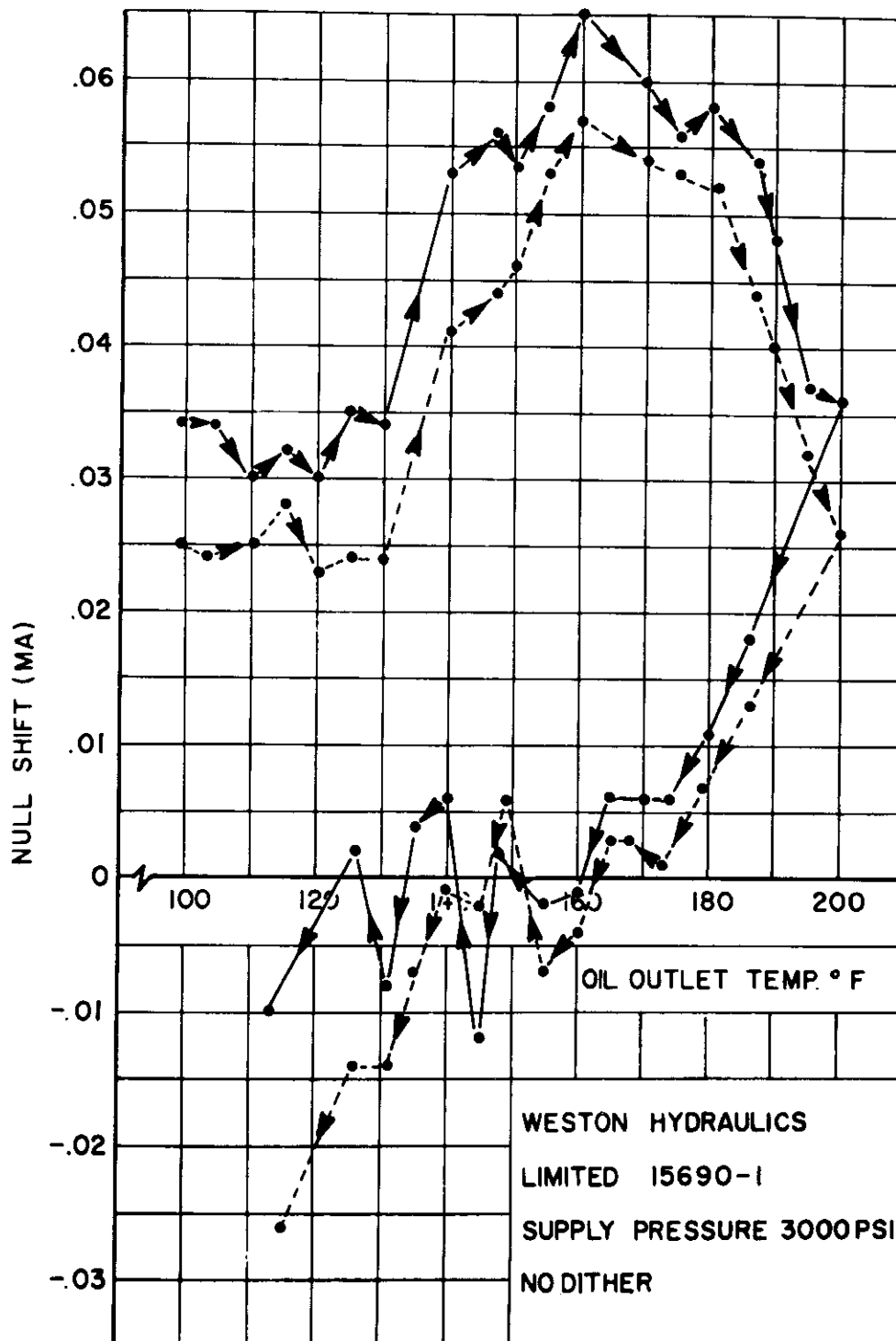
Figure 111. Weston Hydraulic Ltd. 15690 - 1 Null Shift vs.
Oil Temperature - No Dither
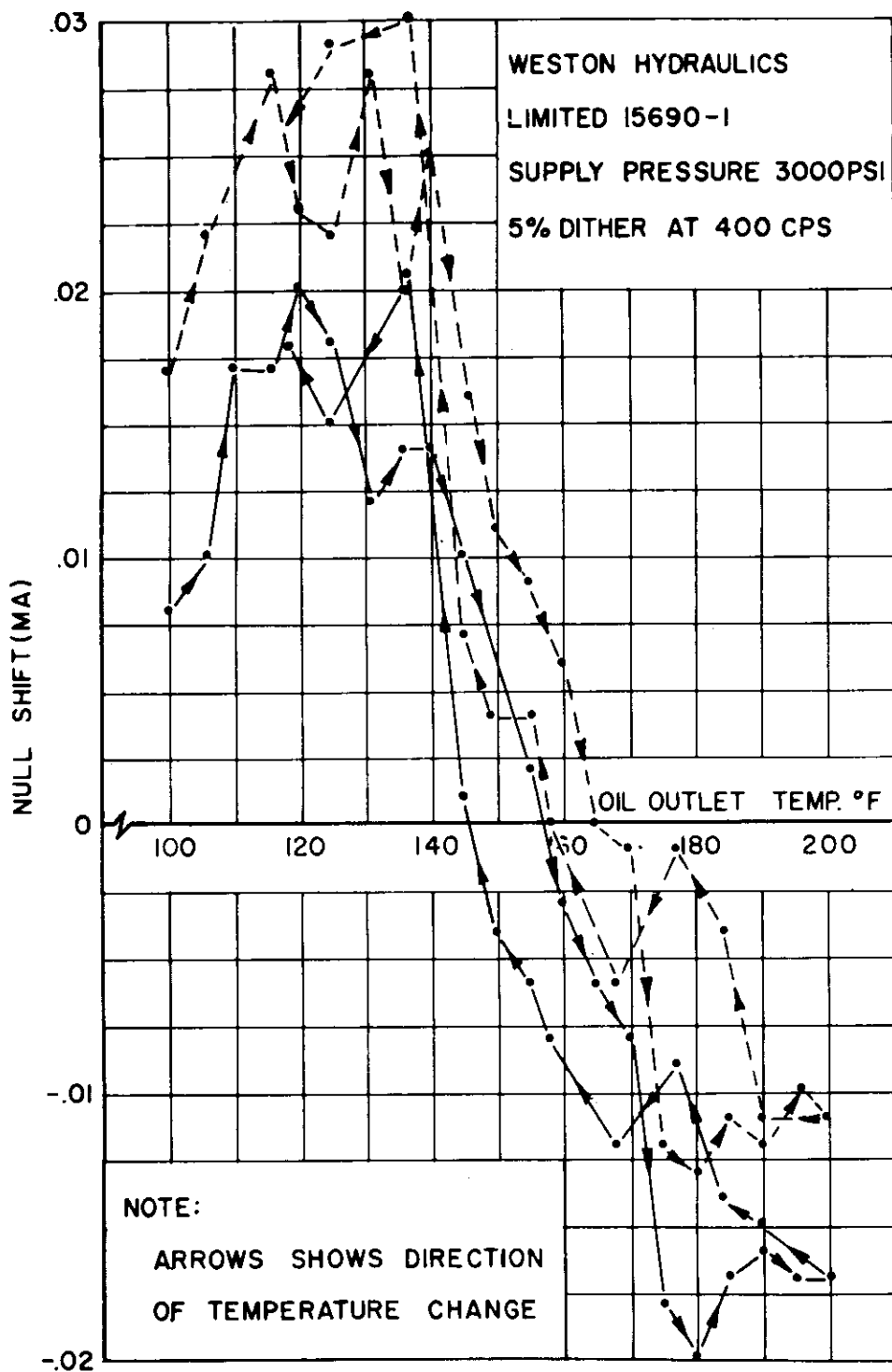
Figure 112.   Weston Hydraulic Ltd. 15690 - 1 Null Shift vs.
Oil Temperature - Dither
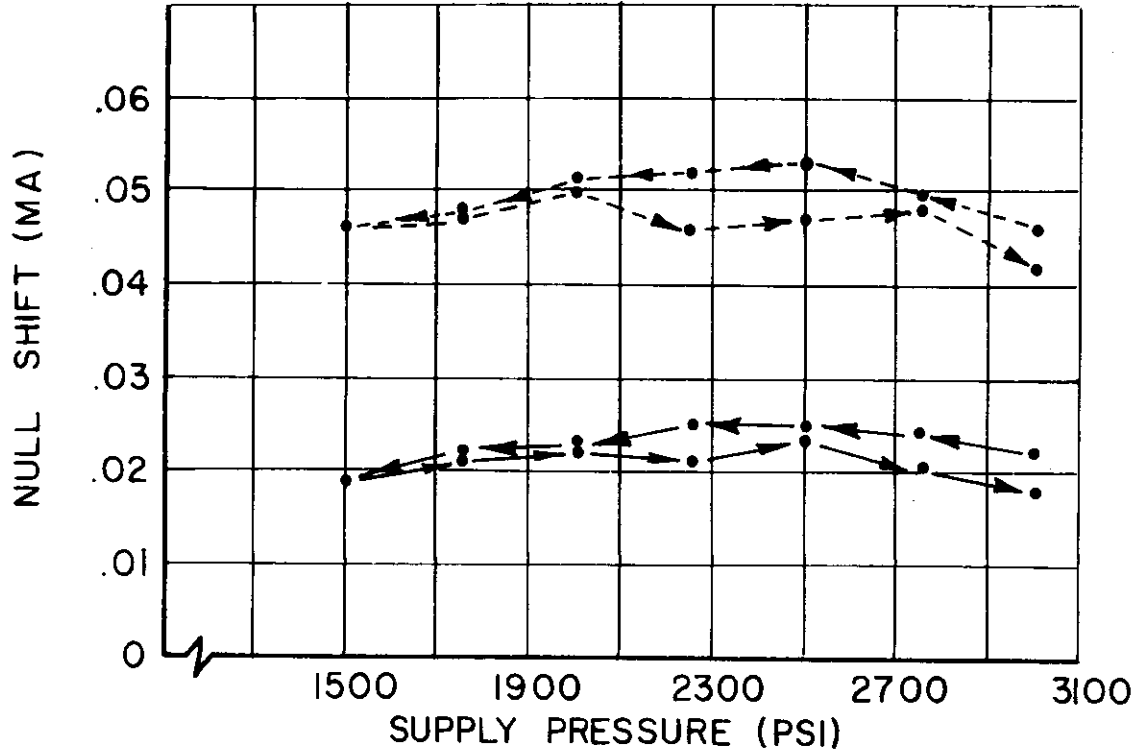
WESTON HYDRAULICS LIMITED 15690-1

OIL OUTLET TEMPERATURE 136.5°±3.5°F

———•——— NO DITHER

———•——— 5% ΔI_r AT 400 CPS

NOTE:

ARROWS SHOW DIRECTION

OF PRESSURE CHANGE

Figure 113. Weston Hydraulic Ltd. 15690 - 1 Null Shift vs. Supply Pressure
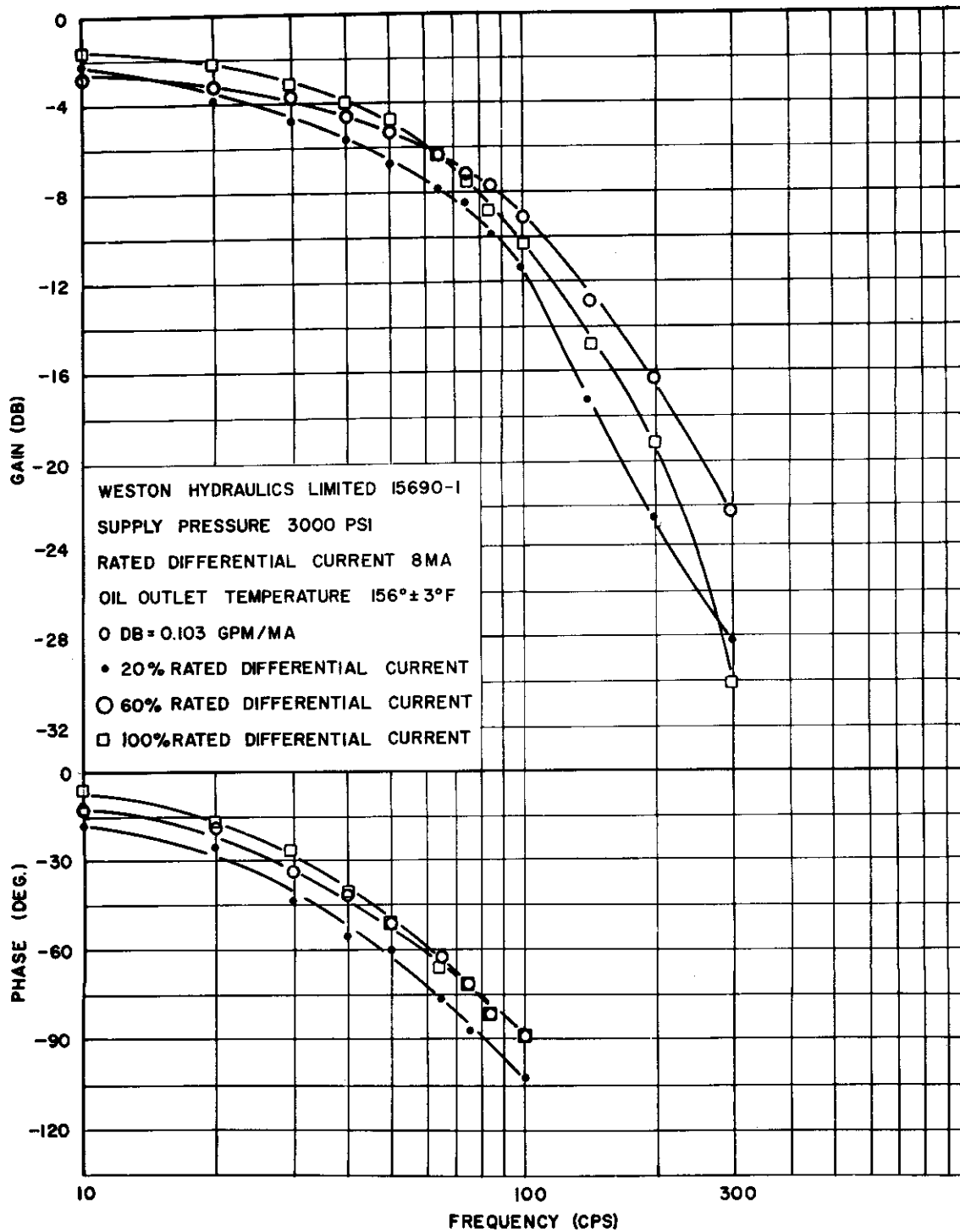
Figure 114.   Weston Hydraulic Ltd. 15690-1 No-Load
Frequency Response
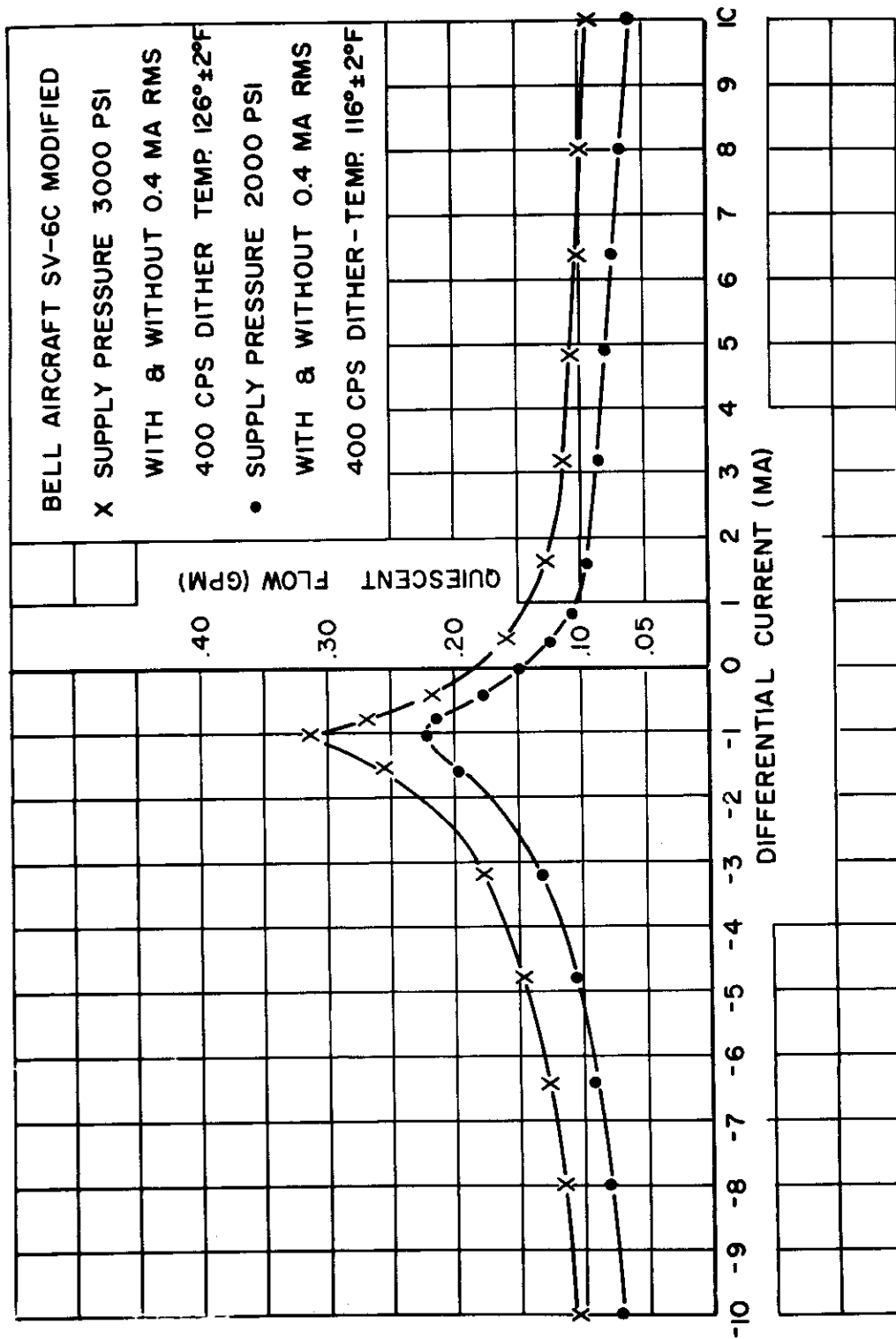
Figure 115. Bell SV-6C (Mod.) Quiescent Flow vs. Differential Current
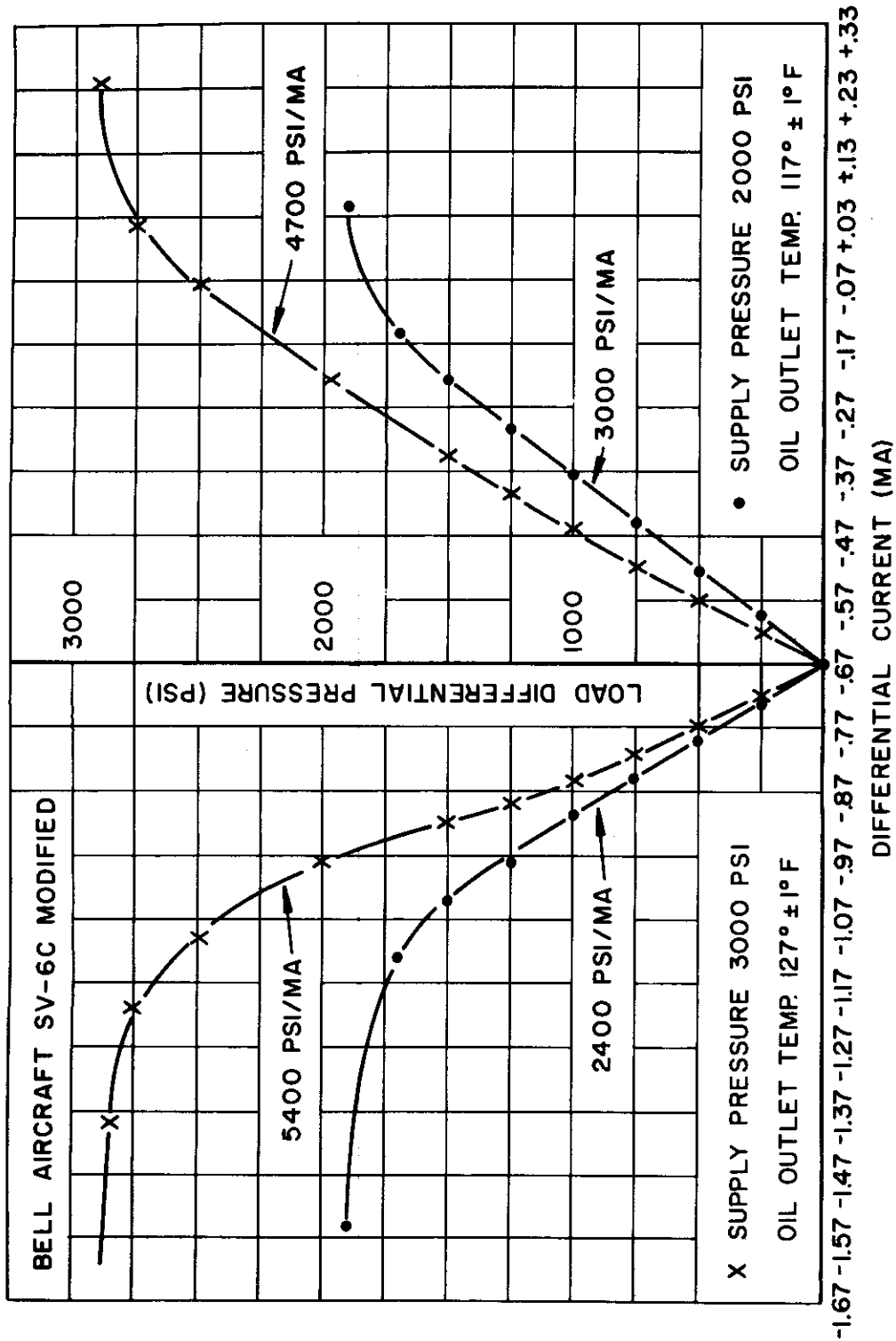
Figure 116. Bell SV-6C (Mod.) Load Pressure vs. Differential Current at Zero Load Flow
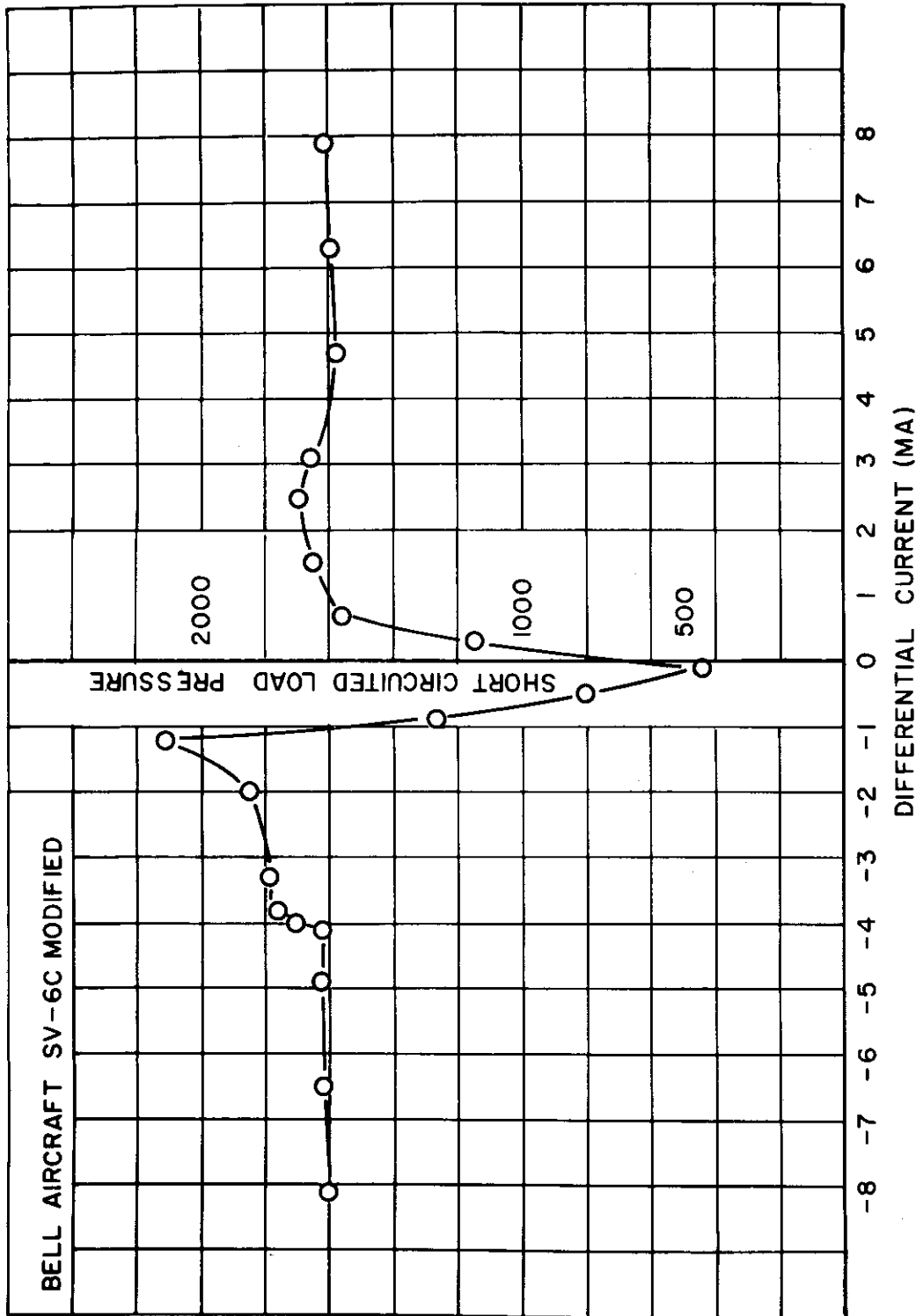
Figure 117. Bell SV-6C (Mod.) Short Circuited Load Pressure
vs. Differential Current
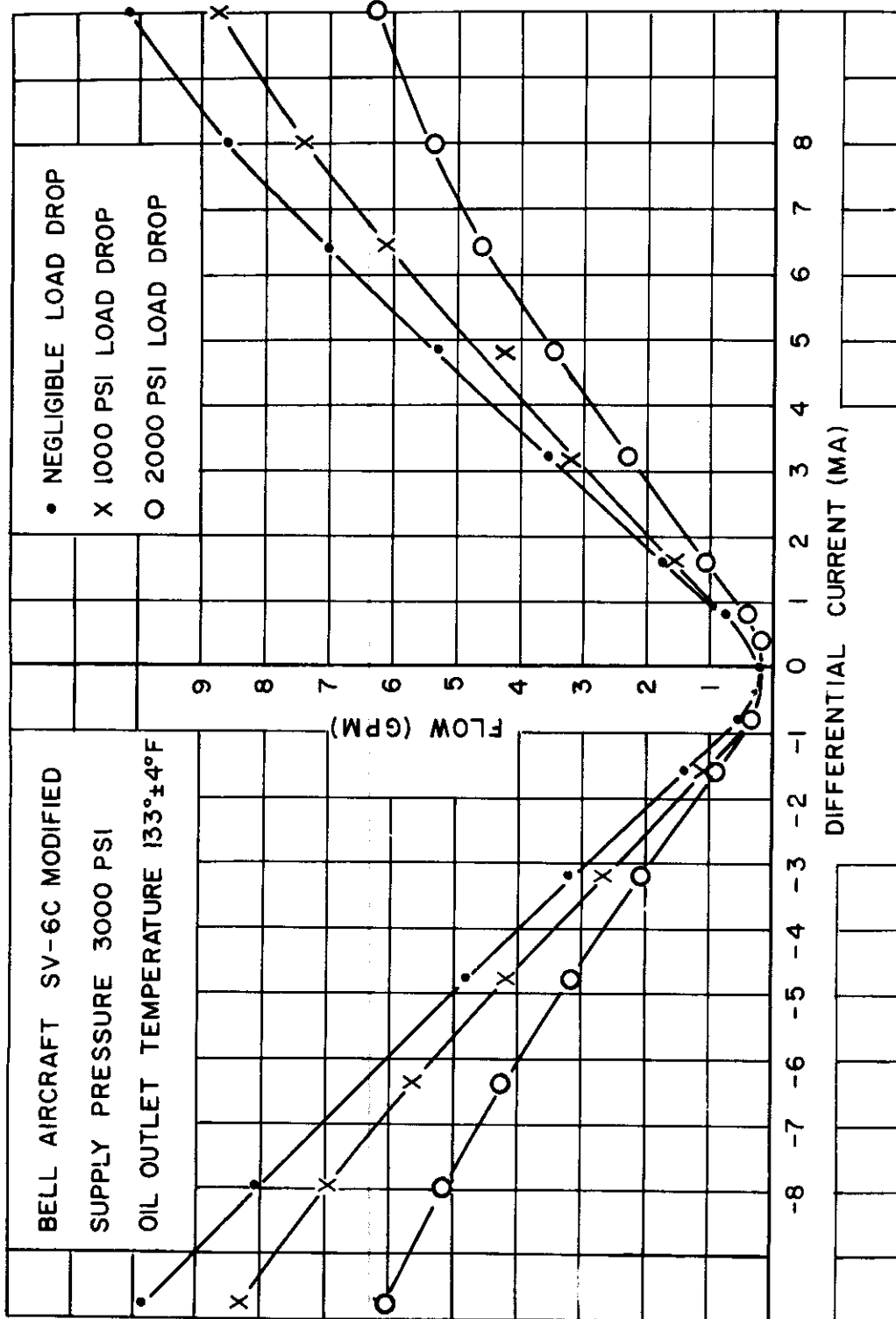
Figure 118. Bell SV-6C (Mod.) Valve Flow vs. Differential Current - 3000 psi Supply Pressure
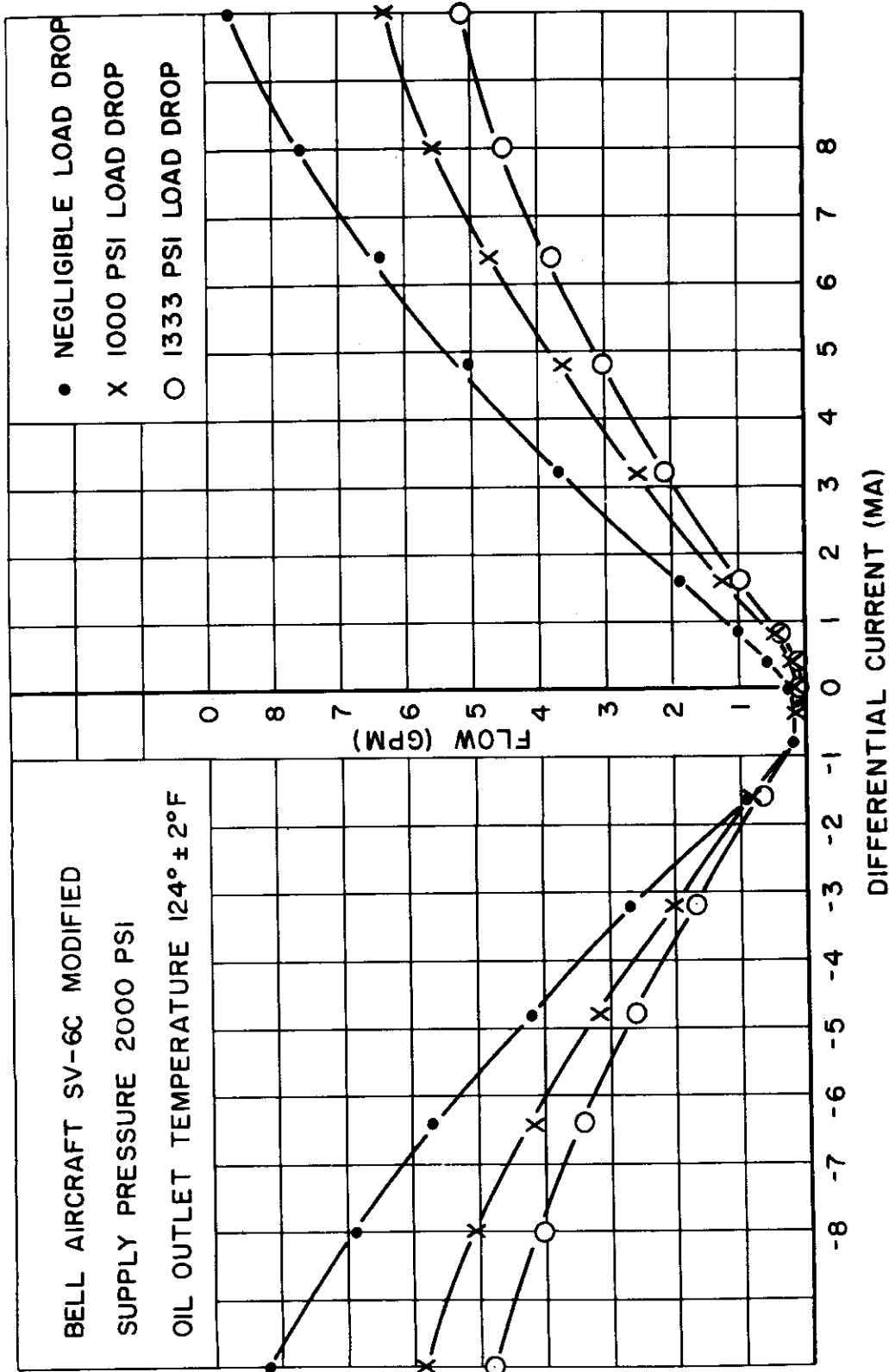
Figure 119. Bell SV-6C (Mod.) Valve Flow vs. Differential Current –
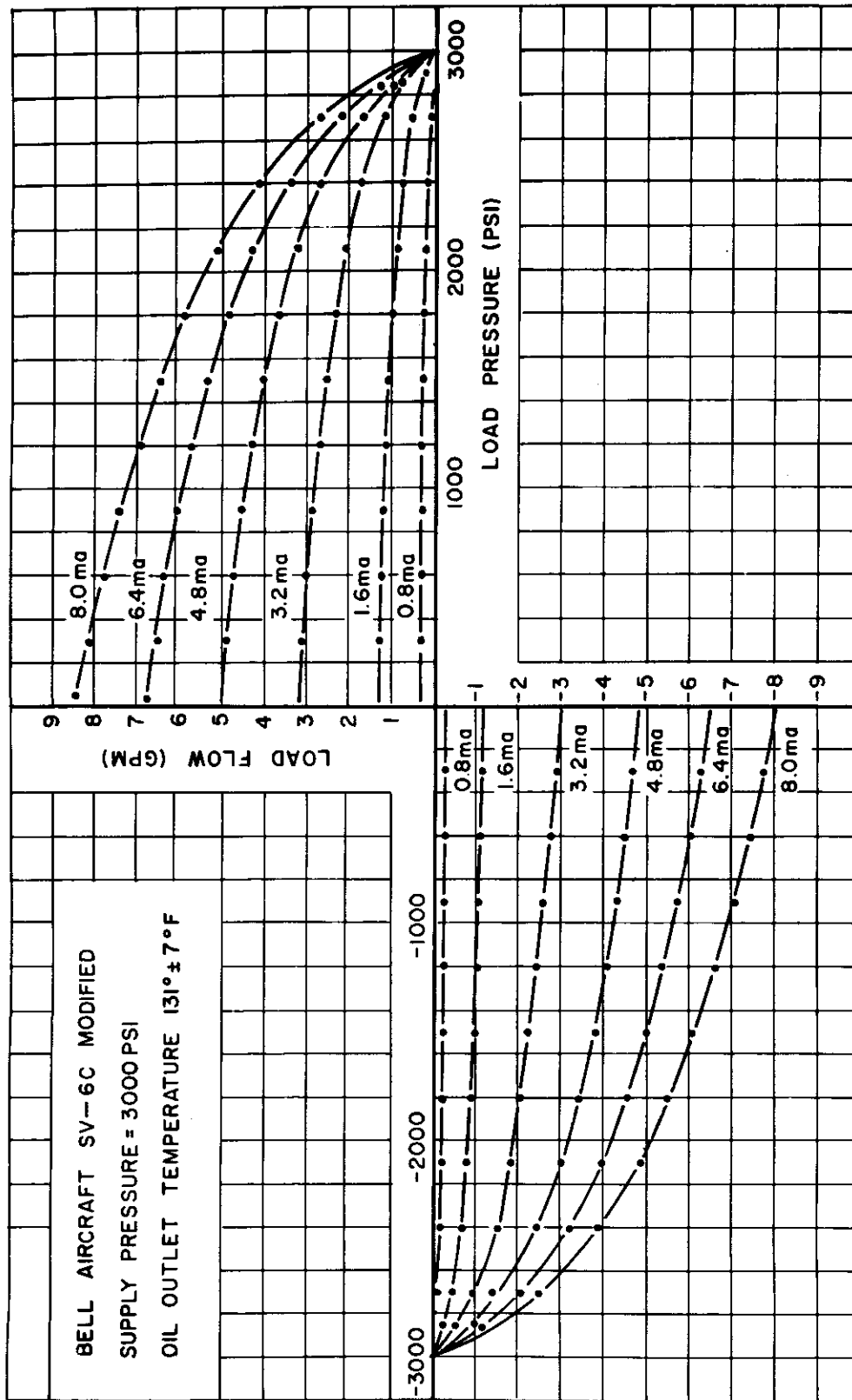2000 psi Supply Pressure

Figure 120. Bell SV-6C (Mod.) Load Flow vs. Load Pressure - 3000 psi Supply Pressure
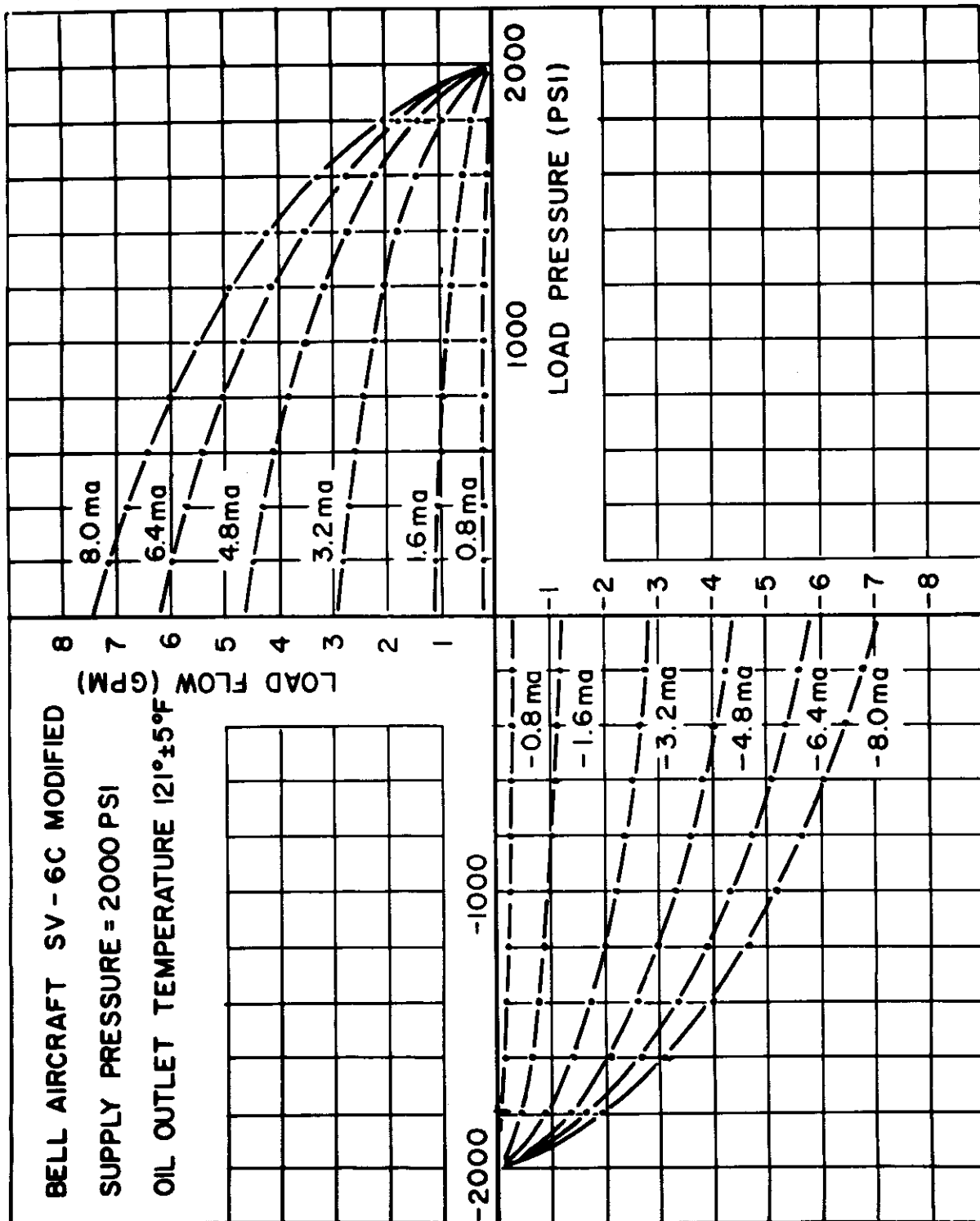
Figure 121. Bell SV-6C (Mod.) Load Flow vs. Load Pressure - 2000 psi Supply Pressure
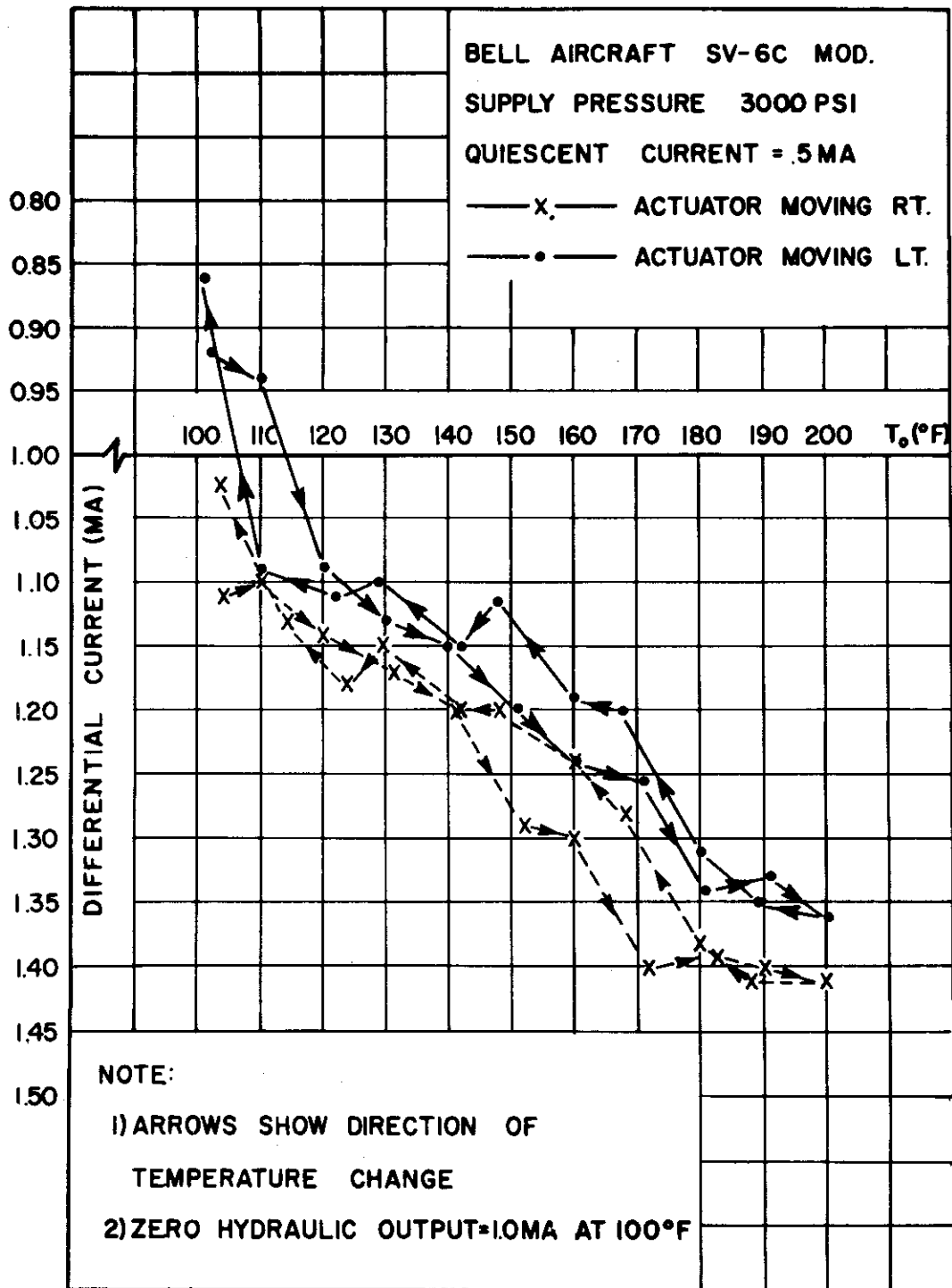
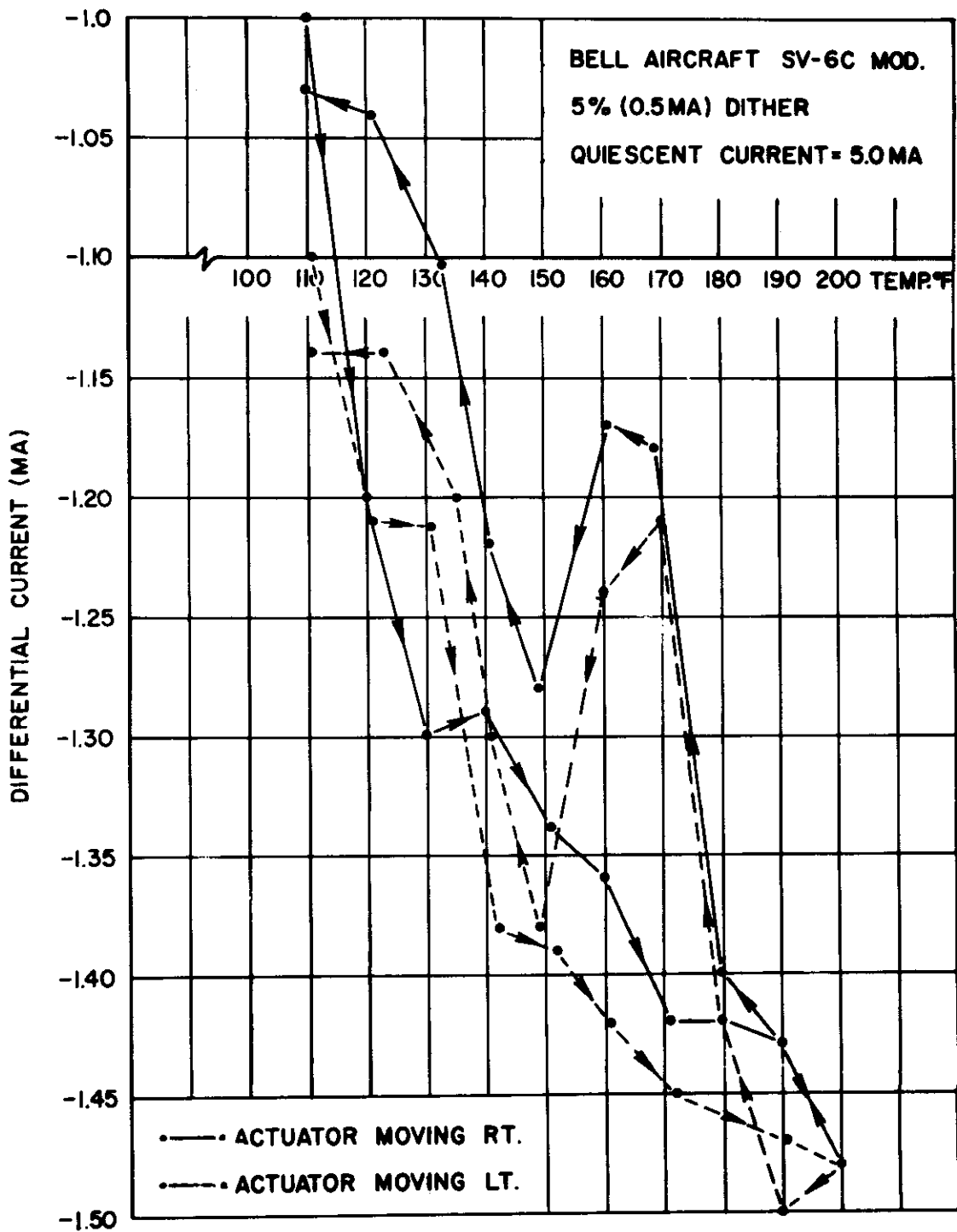Figure 122.   Bell SV-6C (Mod.) Null Shift vs. Oil
Temperature - No Dither

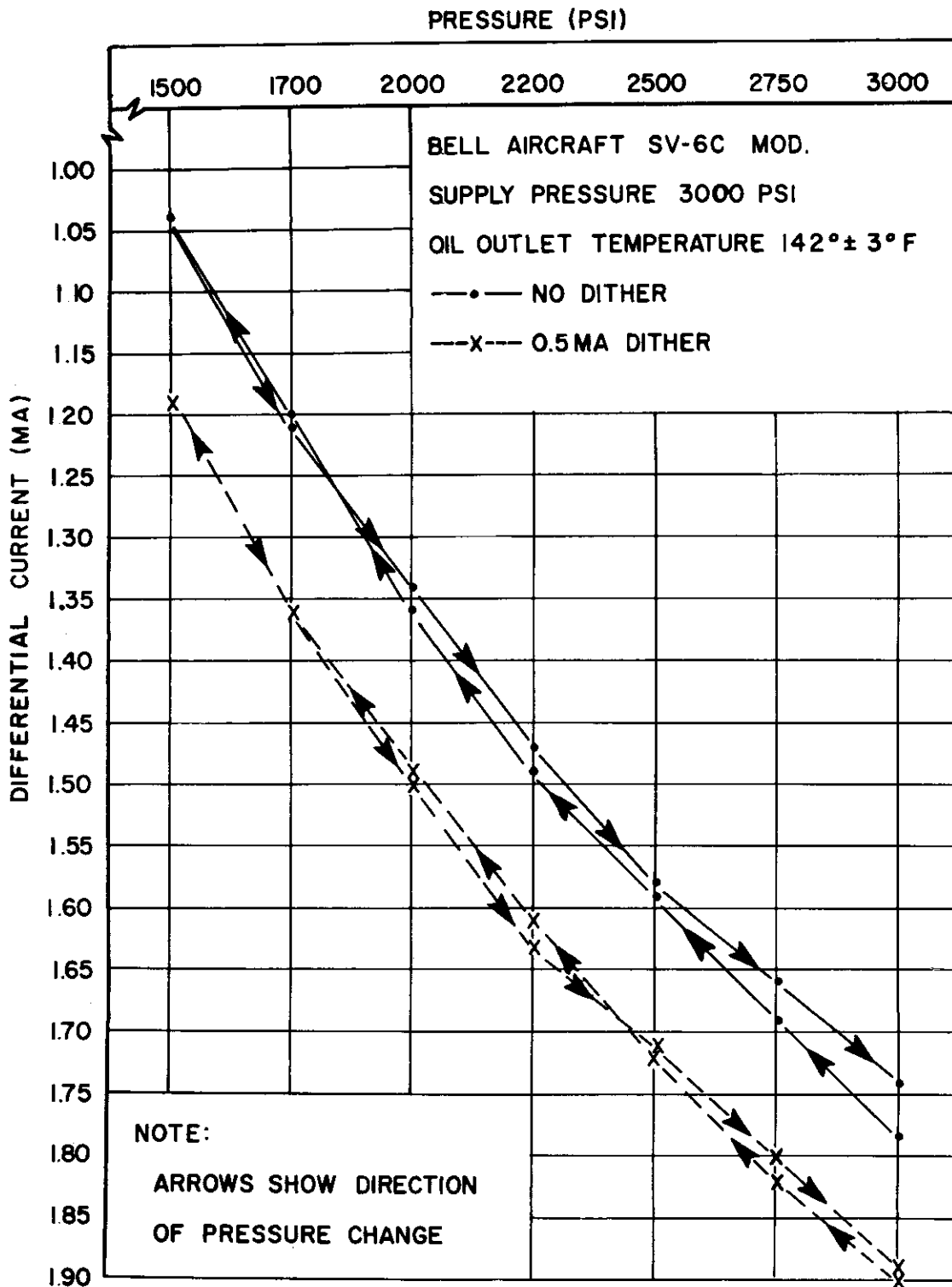Figure 123. Bell SV-6C (Mod.) Null Shift vs. Oil Temperature - Dither

PRESSURE (PSI)

Figure 124. Bell SV-6C (Mod.) Null Shift vs. Supply Pressure

The chart plots GAIN (DB) and PHASE (DEG.) versus FREQUENCY (CPS).

Text box on chart:

BELL AIRCRAFT SV-6C MOD.
SUPPLY PRESSURE 3000 PSI
RATED DIFFERENTIAL CURRENT 8 MA
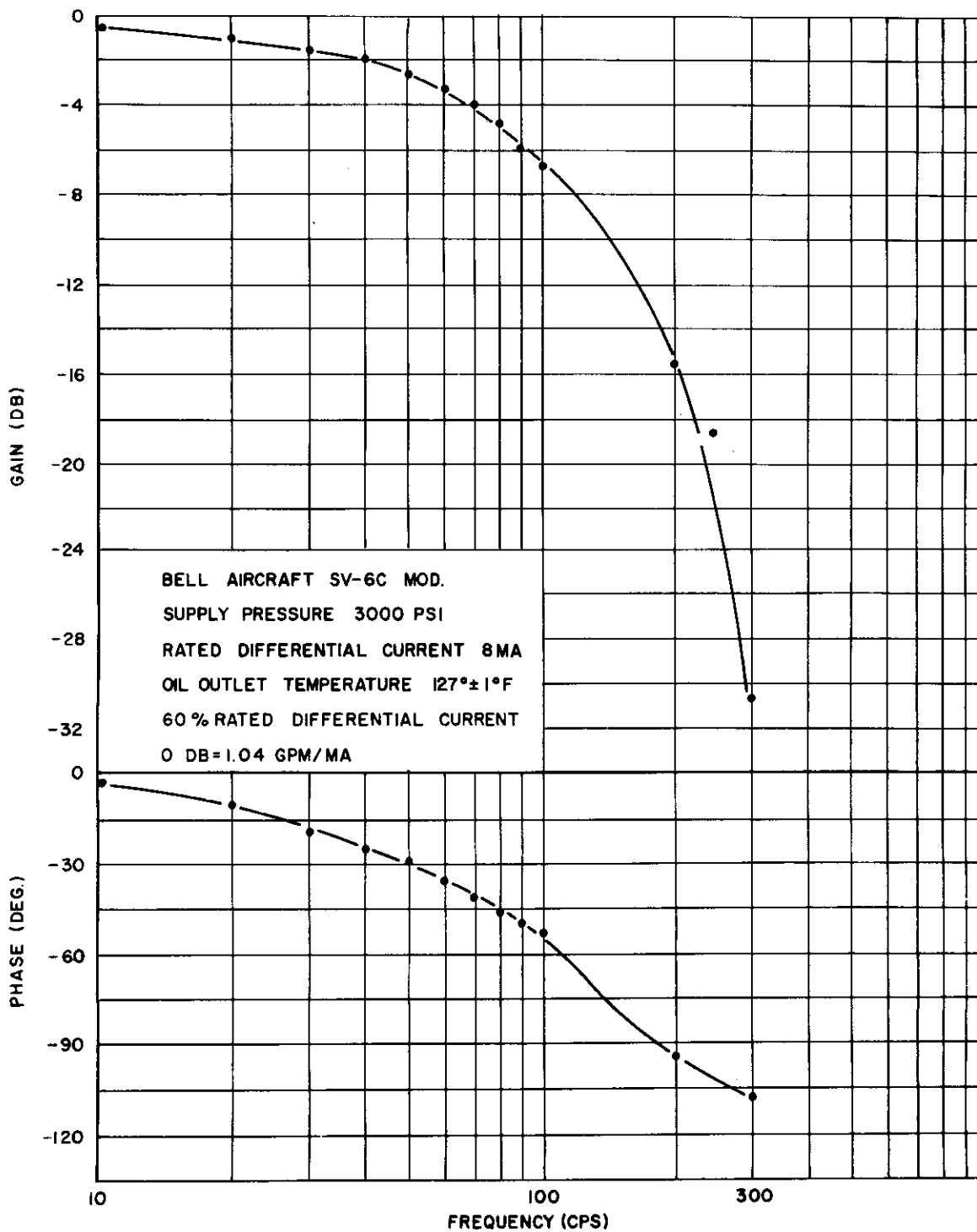OIL OUTLET TEMPERATURE 127°±1°F
60 % RATED DIFFERENTIAL CURRENT
O DB=1.04 GPM/MA

Figure 125. Bell SV-6C (Mod.) No-Load Frequency Response

WADC TR 55-29 Pt IV   171